Molecularly Imprinted Core-Shell Nanoparticles by Surface Initiated RAFT Polymerization

A thesis submitted to the
Faculty of Chemistry and Chemical Biology at the
Technical University of Dortmund

for the degree of
Doctor of Philosophy in Chemistry

by
Reza Mohammadi

Supervisors:
Prof. Dr. Börje Sellergren
Prof. Dr. Ralf Weberskirch

June 2014

Declaration

The work presented in this thesis was carried out in the Institute of Environmental Research of the Faculty of Chemistry and Chemical Biology, at Technical University of Dortmund (Germany) and is a result of the original work of the author, except where acknowledged in the text. The thesis was composed by the author and was not submitted to any other degree or professional qualification.

Reza Mohammadi
Institute of Environmental Research of the
Faculty of Chemistry and Chemical Biology,
Technical University of Dortmund
Germany

Molecularly Imprinted Core-Shell Nanoparticles by Surface Initiated RAFT Polymerization

Dissertation

zur Erlangung des akademischen Grades

Doktor der Naturwissenschaften

(Dr. rer. nat.)

der Fakultät für Chemie und Chemische Biologie

Technische Universität Dortmund

vorgelegt von

Dipl.-Chem. Reza Mohammadi

aus Naghadeh, Iran

Dortmund 2014

Die vorliegende Doktorarbeit wurde am Institut für Umweltforschung angefertigt und eingereicht an der Fakultät für Chemie und Chemische Biologie der Technischen Universität Dortmund.

Gutachter der Dissertation:
1. Gutachter: Prof. Dr. Börje Sellergren
2. Gutachter: Prof. Dr. Ralf Weberskirch

Tag des öffentlichen Promotionskolloquiums:

Erklärung

Hiermit erkläre ich, dass ich die vorliegende Dissertation selbständig und nur mit den angegebenen Hilfsmitteln angefertigt habe. Die Arbeit wurde bisher in gleicher oder ähnlicher Form keiner anderen Prüfungskommission vorgelegt und auch nicht veröffentlicht.

Dortmund, den date

_____

Reza Mohammadi

Acknowledgment

I would never have been able to finish my dissertation without the grace of Allah, guidance of my supervisor, help from friends, and support from my family and wife.

First and foremost, I would like to express my sincere gratitude to my supervisor Prof. Dr. Börje Sellergren for the continuous support of my PhD study and research, for his patience, motivation, enthusiasm, and immense knowledge. I am deeply grateful for all the meetings and discussions, which served as a constant source of motivation for me. His guidance helped me in all the time of research and writing of this thesis. I could not have imagined having a better advisor and mentor for my PhD study.

I would also like to thank Prof. Dr. Ralf Weberskirch for so kindly agreeing to be the second evaluator for my PhD defense. I would like to thank to Prof. Dr. Michael Spiteller for welcoming in the INFU and for providing all professional resources.

My deep appreciation to all my colleagues during my PhD studies for being always supportive and friendly, for providing a nice and international working environment, in particular: Abed Abdel Qader, Dr. Mahadeo Halhalli, Melanie Berghaus, Dr. Farid Ramezany, Patrick Lindemann, Dr. Sudhir Shinde, Dr. Eric Schillinger, Dr. Fatemeh Ghorbani, Dr. Annabell Tenboll, Emelie Fritz, Dr. Rosaria Anna Picca, Dr. Javier Urraca, Dr. Wei Sun, Dr. Carla Aureliano, Dr. Ricarda Wagner, Dr. Porkodi Kadhirvel, Dr. Ali Nematollahzadeh, Celina Wirzbicka, Dr. Rüstem Kecili, Dr. Gyoergy Szekely, Dr. Robert Sulc, Mohamad Wasim Almozaik, Deppak Chandrasekaran, Malak Boutrus, Zhiqi Wang, Raj Schneider.

I would like to thank Dr. Mahadeo Halhalli who helped at the beginning of the project and for his valuable suggestion during the project for sharing his knowledge and being of great help during my first year. Also, thanks to Melanie Berghaus for her fruitful discussion about work, sharing her magnetic nanoparticles with me and critical suggestion and for the summary translation in German language.

I express my sincere and deepest gratitude to Abed Abdel Qader for his good advices and valuable knowledge in analytical chemistry, for being there to support me in many aspects of my life. May Allah bless you and your family.

My sincere thanks also goes to Dr. Farid Ramezani for all his scientific advices, for his useful and technical suggestions during the rebinding study.

I would also like to thank Dr. Annabell Tenboll for trying to teach me ellipsometry and for her guidance in the laboratory. Also, thanks to Patrick Lindemann for his software skills, for being helpful for me whenever I needed any help. I would like to thank Dr. Sudhir Shinde, for being supportive throughout my time here and for helping me to solve some of organic synthesis problems. I am thankful to Emelie Fritz and Dr. Ricarda Wagner for their kindness, friendship and support. I also would like to thank Dr. Eric Schillinger, for all his help, encouragement and suggestions.

I would also like to acknowledge the work of Monika Meuris from the department of chemical and biochemical engineering at TU Dortmund, who recorded the SEM and TEM pictures. I would like to thank all the INFU co-workers specially Dr. Lamshöft, Dr. Zühlke, Jürgen, Mrs. Apitius, Jana, Uli for always being kind and helpful.

My most sincere appreciation goes to Prof. Dr. Ali Akbar Entezami from university of Tabriz, who brought me to the world of polymer chemistry, for his constant guidance, motivation, great support and encouragement during my master and PhD thesis. Also, thanks to Assoc. Prof. Dr. Nasser Arsalani for helping me in my master study and research. I would like to say thank you to all my colleagues and friends in the old college the polymer research laboratory, university of Tabriz, for their kindness and help during my master thesis.

I would like to acknowledge the financial support of the Ministry of Science, Research and Technology of the Islamic Republic of Iran, particularly in the award of a scholarship that provided the necessary financial support for this research.

Last but not least, I would like to extend my immense gratitude, appreciation and love to my parents, brother, sisters, my darling wife, Seddigheh and to my lovely son, Mohammadhossein, for filling my life with happiness, for their understanding and support on this wonderful journey. Without them my life would not be as full. If this work has sometimes prevented us from sharing important moments of life, know that I never stopped thinking about you.

Table of Contents

Abbreviations list 14

List of Figures 17

List of Tables 24

Summary..... 27

Zusammenfassung..... 29

Objectives of the Thesis 32

Chapter 1: Background and State of the Art 34

1.1 Molecularly imprinted polymers 34

1.2 Imprinting approaches 36

1.2.1 Covalent imprinting 37

1.2.2 Non-covalent imprinting 37

1.2.3 Semi-covalent imprinting 38

1.2.4 Metal ion imprinting 39

1.3 Molecularly imprinted polymer syntheses 40

1.3.1 Template 40

1.3.2 Functional monomers 42

1.3.3 Cross-linkers 43

1.3.4 Solvents (porogens) 44

1.3.5 Initiators 45

1.3.6 General polymerization procedures 46

1.4 Living radical polymerization and MIPs 47

1.4.1 MIPs synthesis by free radical polymerization 48

1.4.2 Limitation of free radical polymerization at MIPs 49

1.4.3 MIPs synthesis by controlled radical polymerization 50

1.4.3.1 Iniferter polymerization 50

1.4.3.2 Nitroxide mediated polymerization (NMP) 52

1.4.3.3 Atom transfer radical polymerization (ATRP) 53

1.4.3.4 Reversible addition fragmentation chain transfer polymerization (RAFT) 54

1.4.4 Surface-initiated controlled radical polymerization and MIPs 58

1.4.4.1 MIPs via surface-initiated iniferter polymerization 61

1.4.4.2 MIPs via surface-initiated atom transfer radical polymerization (SI-ATRP) 63

1.4.4.3 MIPs via surface-initiated reversible addition fragmentation chain transfer polymerization (SI-RAFT) 65
1.4.4.3.1 Grafting-from surface-anchored initiators 65
1.4.4.3.2 Grafting-from surface-anchored CTAs 67
1.5 Molecularly imprinted nanoparticles 71
1.5.1 Imprinted nanofibers, nanowires and nanotubes 72
1.5.2 Imprinted nanofilms 73
1.5.3 Imprinted microgel/nanogel 73
1.5.4 Molecularly imprinted core-shell nanoparticles 75
1.6 Proteins and peptides imprinting 77
1.6.1 Bulk imprinting 78
1.6.2 Surface imprinting 79
1.6.3 Epitope imprinting 81
Chapter 2: Characterization Techniques 85
2.1 Thermogravimetric analysis (TGA) 85
2.2 Scanning electron microscopy (SEM) 87
2.3 Transmission electron microscopy (TEM) 87
2.4 Fourier transform infrared spectroscopy (FTIR) 87
2.5 Solution NMR 88
2.6 Dynamic light scattering (DLS) 88
2.7 Elemental analysis (EA) 88
2.8 Nitrogen adsorption 90
2.9 Binding experiments 90
2.9.1 Single point rebinding 90
2.9.2 Binding isotherm 91
Chapter 3: MIP Core-Shell NPs for Chiral Recognition 95
3.1 Introduction 95
3.2 Results and Discussions 96
3.2.1 Silica nanoparticles 96
3.2.2 Amino modified silica nanoparticles 97
3.2.3 Immobilization of dithiobenzoate RAFT agent onto silica nanoparticles 98
3.2.4 Characterization of the resulting silica core nanoparticles 100
3.2.5 Synthesis of trithiocarbonate RAFT agent 108
3.2.6 Immobilization of trithiocarbonate RAFT agent onto silica nanoparticles 108
3.2.7 Characterization of surface-modified silica nanoparticles 109

3.2.8 Optimization for the grafted linear polymers from silica support 112
3.2.8.1 Methyl methacrylate graft polymerization from RAFT-modified silica nanoparticles (SiO_2-g-PMMA) 113
3.2.8.2 Styrene graft polymerization from RAFT-modified silica nanoparticles (SiO_2-g-PSt) 113
3.2.8.3 Methacrylamide graft polymerization from RAFT-modified silica nanoparticles (SiO_2-g-PMAAM) 114
3.2.9 Characterization of grafted linear polymers 114
3.2.10 Grafting of molecularly imprinted polymer shells via RAFT- modified silica core nanoparticles 120
3.2.11 Characterization of grafted imprinted polymer shells 121
3.2.12 Binding isotherms of the imprinted polymers 126
3.3 Conclusions.....131
3.4 Experimental.....131
3.4.1 Synthesis of monodisperse SiO_2 nanoparticles.....131
3.4.2 Synthesis of amino modified silica nanoparticles.....132
3.4.3 Synthesis of dithiobenzoate modified silica core particles.....133
3.4.4 Synthesis of S,S′-Bis(α,α′-dimethyl-α′′-acetic acid)- trithiocarbonate 134
3.4.5 Synthesis of trithiocarbonate modified silica core particles 135
3.4.6 Preparation of methyl methacrylate grafted polymer from RAFT-modified silica nanoparticles.....136
3.4.7 Preparation of styrene grafted polymer from RAFT-modified silica nanoparticles 136
3.4.8 Preparation of methacrylamide grafted polymer from RAFT-modified silica nanoparticles.....137
3.4.9 Synthesis of core-shell MIPs using a soluble L-PA.....138
3.4.10 Template synthesis.....140
3.4.10.1 Synthesis of BOC-L/D-phenylalanine anilide.....140
3.4.10.2 Synthesis of L/D-phenylalanine anylide.....140
3.4.11 Batch binding tests of NPs for their affinity for L-PA and D-PA. 141
Chapter 4: Solid-Phase Synthesis of MIP Core-Shell NPs using Magnetic Template 144
4.1 Introduction 144
4.2 Results and Discussions.....146
4.2.1 Synthesis of magnetic core-silica shell nanoparticles (magNP@SiO_2).....146
4.2.2 Aminofunctionalization of magnetic silica nanoparticles (magNP-NH_2) 147
4.2.3 Immobilization of L-phenylalanine on magNP-NH_2 (magNP-L-Phe) 147

4.2.4 Grafting imprinted polymer nanoshell onto surface of RAFT- modified silica nanoparticles 150
4.2.5 Polymer characterization 151
4.2.6 Binding isotherms of the imprinted polymers 154
4.3 Conclusions 158
4.4 Experimental 158
4.4.1 Synthesis of magnetic core nanoparticles (magNP) 158
4.4.2 Silica coating on the surface of magnetic nanoparticles (magNP@SiO_2) 159
4.4.3 Aminofunctionalization of magnetic silica nanoparticles (magNP-NH_2) 159
4.4.4 Immobilization of L-phenylalanine on magNP-NH_2 (magNP-L-Phe) 159
4.4.5 Synthesis of core-shell MIPs using magNP-L-Phe as template (SiNP-MIP) 160
4.4.6 Batch binding tests of NPs for their affinity for L-PA and D-PA. 160

Chapter 5: Epitope Imprinted Core-Shell Nanoparticles Targeting β-Amyloid 163

5.1 Introduction 163
5.1.1 Choice of the amyloid peptide epitopes 163
5.2 Results and Discussions 164
5.2.1 Template synthesis 164
5.2.2 Grafting of beta-amyloid imprinted polymers from RAFT-modified silica nanoparticles 165
5.2.3 Polymer characterization 167
5.2.4 Binding isotherms 171
5.3 Conclusions 173
5.4 Experimental 173
5.4.1 Acetylation of $A\beta_{37-42}$ 173
5.4.2 Tetrabutylammonium salt preparation of acetylated $A\beta_{37-42}$ 174
5.4.3 Preparation of beta-amyloid imprinted polymers from RAFT-modified silica nanoparticles 174
5.4.4 Batch rebinding 176

Chapter 6: Nano-Sized Core-Shell Particles by Grafting of Thin Films Imprinted with a Hydrophilic Peptide from Nonporous Silica Cores 178

6.1 Introduction 178
6.1.1 Selection of the functional and crosslinking monomers 179
6.2 Results and Discussions 180

6.2.1 Grafting of T10 and R10 imprinted polymers from dithiobenzoate-modified silica nanoparticles 180
6.2.2 Polymer characterization 181
6.2.3 The reductive aminolysis of grafting polymers 183
6.2.4 Binding study via BCA assay 184
6.2.5 Grafting of T10 imprinted polymer onto silica nanoparticles via RAFT polymerization in organic media 185
6.2.6 Grafting of T10 imprinted polymer onto silica nanoparticles via aqueous RAFT polymerization 186
6.2.7 Polymer characterization 189
6.2.8 Binding isotherms 193
6.3 Conclusions 198
6.4 Experimental 199
6.4.1 Aminolysis of the dithioester end groups in the RAFT polymers 199
6.4.2 BCA protein assay 199
6.4.3 Synthesis of 5-(methacryloylamido)-m-xylylene bisphosphonic acid dimethylester dilithium salt 199
6.4.4 Synthesis of PEG-TTC macro chain transfer agent 200
6.4.5 Preparation of T10 imprinted core-shell MIPs in organic media 201
6.4.6 Preparation of T10 imprinted core-shell MIPs using MAA in aqueous media 202
6.4.7 Preparation of T10 imprinted core-shell MIPs using BPA in aqueous media 202
6.4.8 Binding experiments 203
Conclusions and Perspectives 205
Chemicals 209
References 213
Curriculum Vitae 229

Abbreviations list

ABDV	Azo-bis-dimethylvaleronitrile
Aβ	Beta amyloid peptide
ACN	Acetonitrile
AD	Alzheimer's disease
AIBN	Azo-bis isobutyronitrile
APS	Ammonium persulfate
APTES	3-Aminopropyltriethoxysilane
APDMES	3-Aminopropyldimethylethoxysilane
ATRP	Atom transfer radical polymerization
CL	Crosslinker
CPDB	4-cyanopentanoic acid dithiobenzoate
CRP	Controlled radical polymerization
CTA	Chain transfer agent
DCC	Dicyclohexyl carbodiimide
DCM	Dichloromethane
DLS	Dynamic light scattering
D-PA	D-phenylalanine anilide
DMF	Dimethylformamide
DMSO	Dimethylsulphoxide
DSC	Differential scanning colorimeter
DTG	Derivative thermogravimetric tnalysis
DVB	Divinylbenzene
EA	Elemental analysis
EAMA	Ethyl ammonium methacrylate
EBA	N,N′- ethylenebisacrylamide
EDC	N-(3-dimethylaminopropyl)-N′-ethylcarbodiimide
EDMA	Ethyleneglycol dimethacrylate
FA	Formic acid
FM	Functional monomer
Fmoc-Phe-OH	N-(9-Fluorenylmethoxycarbonyl)-L-phenylalanine
FRP	Free radical polymerization
FT-IR	Fourier transform infrared spectroscopy
GuHCl	Guanidine hydrochloride

HOBt	1-Hydroxybenzotriazole
HEPES	2-[4-(2-hydroxyethyl)piperazin-1-yl]ethanesulfonic acid
HOBt	1-Hydroxybenzotriazole
HPLC	High performance liquid chromatography
IF	Imprinting factor
IgG	Immunoglobulin G
Iniferter	Initiator-transfer agent-terminator
LPA	L-phenylalanine anilide
MAA	Methacrylic acid
MAAM	Methacrylamide
MEK-ST	Colloidal silica particles
MeOH	Methanol
MeCN	Acetonitrile
MIP	Molecularly imprinted polymer
MMA	Methyl methacrylate
NHS	N-hydroxysuccinimide
NIP	Non-imprinted polymer
NMP	Nitroxide mediated polymerization
RP-HPLC	Reversed phase HPLC
RT	Room temperature
RAFT	Reversible addition fragmentation chain transfer polymerization
S_A	Surface area
SEM	Scanning electron microscopy
SPE	Solid phase extraction
St	Styrene
TEA	Triethylamine
TEMED	Tetramethylethylenediamine
TEM	Transmission electron microscopy
TEOS	Tetraethyl orthosilicate
TFA	Trifluoroacetic acid
TGA	Thermogravimetric analysis
THF	Tetrahydrofuran
TTC	Trithiocarbonate
T10	Decapeptide

The following three-letter code and one-letter code abbreviations were used for amino acids:

Ala	A	Alanine	Met	M	Methionine
Cys	C	Cysteine	Asn	N	Asparagine
Asp	D	Aspartic acid	Pro	P	Proline
Glu	E	Glutamic acid	Gln	Q	Glutamine
Phe	F	Phenylalanine	Arg	R	Arginine
Gly	G	Glycine	Ser	S	Serine
His	H	Histidine	Thr	T	Threonine
Ile	I	Isoleucine	Val	V	Valine
Lys	K	Lysine	Trp	W	Tryptophan
Leu	L	Leucine	Tyr	Y	Tyrosine

List of Figures

Figure 1.1. Principle of molecular imprinting.....34
Figure 1.2. Steps involved in MIP design. (adapted from [6]) 35
Figure 1.3. Scheme outlining the main applications envisaged for MIPs.(adapted from[20]) 36
Figure1.4. Covalent imprinting of 4-nitrophenyl-a-d-mannopyranoside-2,3:4,6-di-O-(4vinylphenylboronate). (adapted from[22]) 37
Figure 1.5. Non-covalent imprinting of a dipeptide derivative by multiple non-covalent interactions with methacrylic acid. (adapted from[25]).....38
Figure 1.6. Semi-covalent imprinting for L-p-aminophenylalanine ethyl ester. (adapted from[27]).....39
Figure 1.7. Structure of the most common monomers used for molecular imprinting.....43
Figure 1.8. Structure of the most common cross-linkers used for molecular imprinting. 44
Figure 1.9. Chemical structure of common initiators used in molecular imprinting. 46
Figure 1.10. Schematic representation of free radical polymerization. 49
Figure 1.11. Irregularly shaped particles resulting from mechanical grinding of a "traditional" molecularly imprinted polymer (MIP-FRP). 50
Figure 1.12. General mechanism of iniferter polymerization.....51
Figure 1.13. Mechanism of Nitroxide Mediated Polymerization (NMP).....52
Figure 1.14. Mechanism of ATRP.....53
Figure 1.15. General form of RAFT chain transfer agents. 55
Figure 1.16. The overall outcome of the RAFT process.....56
Figure 1.17. Mechanism of RAFT polymerization. (adapted from[125]) 57
Figure 1.18. Schematic illustrations of (a) "grafting to" and (b) "grafting from" methodologies. (adapted from[136]).....59
Figure 1.19. Surface-grafting of MIP layers on the spherical particles by photo-iniferter-induced living radical polymerization.(adapted from[91]).....62
Figure 1.20. A general process of surface-initiated RAFT polymerizations from a surface-anchored azo initiator. (adapted from[159]) 66
Figure 1.21. The grafting of L-phenylalanine anilide (L-PA) imprinted polymer films from porous silica supports controlled by addition of RAFT agent.(adapted from[126]) 67

Figure 1.22. Two different approaches of surface attachment where RAFT agent attached to the surface via its Z or R group.(adapted from[160]) 68
Figure 1.23. Synthesis route of multiwalled carbon nanotubes.(adapted from[197]).....72
Figure 1.24. Schematic illustration of the preparation of thermo-responsive lysozyme-imprinted nanogels via aqueous precipitation polymerization and their shrinking/swelling behavior around the volume phase transition temperature (VPTT). (adapted from[192]) 74
Figure 1.25. Schematic representation of the possible preparation process of magnetic MIPs. (adapted from[212]) 76
Figure 1.26. Schematic of preparation of MIP for bovine hemoglobin(BHb) recognition. (adapted from[220]) 80
Figure 1.27. The surface-bound epitope approach employed by the group of Shea using C-terminal nonapeptides as templates for protein imprinting. (adapted from[224]) 82
Figure 3.1. Schematic representation of the Stöber process. 97
Figure 3.2. Amino modification of silica surface with APTES. 98
Figure 3.3. Immobilization of RAFT agent on silica surface. 99
Figure 3.4. a) SiNP2 (A), SiNP2-NH_2 (B) and SiNP2-CPDB (C) dispersed in THF b) SiNP2-CPDB dispersed in acetone (A), toluene (B) and methanol (C). 99
Figure 3.5. Thermal gravimetric analysis of SiNP1 (pink), SiNP1-NH_2 (green) and SiNP1-CPDB (blue) (A), SiNP2 (pink), SiNP2-NH_2 (green) and SiNP2-CPDB (blue) (B). 101
Figure 3.6. TEM images of SiNP1 (A, B), SiNP1-NH_2 (C, D), and SiNP1-CPDB (E, F). The scale bar is 100 nm in the case of (A, D); 500 nm for (C) and 200 nm for (B, E, F). 103
Figure 3.7. TEM images of SiNP2 (A,B), SiNP2-NH_2 (C,D), and SiNP2-CPDB (E,F). The scale bar is 20 nm in the case of (A), (B), (C), (D), (F); and 50 nm for (E). 104
Figure 3.8. DLS analysis of SiNP1 (A), SiNP1-NH_2 (B) and SiNP1-CPDB (C). 106
Figure 3.9. DLS analysis of SiNP2 (A), SiNP2-NH_2 (B) and SiNP2-CPDB (C). 107
Figure 3.10. Chemical structure of trithiocarbonate RAFT agent used to create MIPs. 108
Figure 3.11. Immobilization of RAFT agent on silica surface. 109
Figure 3.12. Thermal gravimetric analysis of SiNP (pink), SiNP-NH_2 (green) and SiNP-TTC (blue). 110

Figure 3.13. TEM images of SiNP-NH_2 (A), SiNP-TTC (B). The scale bar is 20 nm in the case of (A) and 100 nm for (B). 112

Figure 3.14. Schematic representation of graft polymerization from RAFT-modified silica nanoparticles. 113

Figure 3.15. Thermal gravimetric analysis of SiO_2-g-PMMA-2 (A), SiO_2-g-PSt-3 SiO_2-g-PMAAM-4 (C). 117

Figure 3.16. TEM images of bare silica NPs (A, B); SiO_2-g-PMMA (C, D, E); SiO_2-g-PSt (F, G); SiO_2-g-PMAAM (H, I). The polymer shells are indicated by arrows. The scale bar is 50 nm in the case of (A, D, H) 100 nm for (B, C) 20 nm for(E, F, G) and 10 nm for (I). 118

Figure 3.17. SEM images of bare silica NPs (A); SiO_2-g-MMA (B, C, D); SiO_2-g-MAAM(E); SiO_2-g-PSt (F). The polymer shells are indicated by arrows. 119

Figure 3.18. Procedure used to synthesise silica core-MIP shell nanoparticles. 120

Figure 3.19. Thermal gravimetric analysis of the L-PA imprinted and nonimprinted core shell nanoparticles; TGA of SiNP1-MIP and SiNP1-NIP (A), DTG of SiNP1-MIP and SiNP1-NIP (B), TGA of SiNP2-MIP and SiNP2-NIP (C), DTG of SiNP2-MIP and SiNP2-NIP (D). 123

Figure 3.20. TEM images of the L-PA imprinted and nonimprinted core-shell nanoparticles SiNP1-MIP and SiNP1-NIP (A, B), SiNP2-MIP and SiNP2-NIP (C, D). The polymer shells are indicated by arrows. The scale bar is 100 nm in the case of (A) 50 nm for (B) and (C) and 20 nm for (D). 124

Figure 3.21. DLS analysis of the L-PA imprinted core-shell nanoparticles SiNP1-MIP (A) and SiNP2-MIP (B). 125

Figure 3.22. FTIR spectra of SiNP-RAFT(a) SiNP-MIP(b), SiNP-NIP(c). Curves were shifted for clarity. 125

Figure 3.23. Equilibrium binding isotherms of L-PA (circles) and D-PA (squares) on imprinted and nonimprinted core-shell particles in acetonitrile. A) L-PA imprinted SiNP1-MIP, B) L-PA imprinted SiNP1-MIP (red circles) and SiNP1-NIP (green circles), C) L-PA imprinted SiNP2-MIP, D) L-PA imprinted SiNP2-MIP (red circles) and SiNP2-NIP (green circles). 128

Figure 3.24. Fisher values obtained by fitting the L/D-PA binding curves in Figure 3.23 to mono-Langmuir, bi-Langmuir and Freundlich isotherm models (see Table 3.11 to Table 3.13). 130

Figure 3.25. Synthesis of carboxyl-terminated trithiocarbonate RAFT agent. 135
Figure 3.26. Synthesis of BOC-L /D phenylalanine aniline. 140
Figure 3.27. Synthesis of L /D- phenylalanine anilide. 141
Figure 4.1. Principle of using magnetic templates for synthesis, affinity enrichment and purification of surface imprinted core-shell nanoparticles. (1) Polymerization of monomers in presence of the binary particle suspension, (2) Separating the magnetic template and polymers adhering to the template from the crude reaction mixture. (3) Washing off loosely bound unreacted monomers and oligomers, (4) Gradually releasing the polymer adhering to the magnetic template by physical or chemical means thereby enriching high affinity MIP particles. (5) Reuse of the magnetic template repeating steps 1-4 [268] 145
Figure 4.2. Schematic illustration of the synthesis of magnetic core-silica shell nanoparticles. 146
Figure 4.3. FTIR spectra of magNP (blue line), magNP@SiO_2 (red line). The Fe-O-Fe band of the core is accompanied by the Si-O-Si band at ca 1100 cm^{-1} in the IR-spectra of the magnetite particles after the application of the silica shell. 146
Figure 4.4. Aminomodification of magnetic-silica core-shell nanoparticles. 147
Figure 4.5. Synthesis route of template immobilization on the surface of magNP-NH_2. 148
Figure 4.6. FTIR spectra of of aminofunctionalized magNP@SiO_2 prior to (A) and after (B) coupling of Fmoc-L-Phe. In (B) the amide I and II bands have been indicated by arrows. 149
Figure 4.7. TEM images of magNP@SiO_2 (A) and magNP-L-Phe (B).The scale bar is 10 nm in the case of (A) and 20 nm for (B). 149
Figure 4.8. Procedure used to synthesize silica core-MIP shell nanoparticles using magnetic template. 150
Figure 4.9. Thermal gravimetric analysis of the L-Phe imprinted core-shell nanoparticles using magnetic template; TGA (A), DTG (B); crude magNP-L-Phe/SiNP-MIP prior to washing (red), magNP-L-Phe/SiNP-MIP after washing (blue) and released SiNP-MIP (green). 152
Figure 4.10. TEM (A, B) and SEM (C, D) images of the L-Phe imprinted core-shell nanoparticles using magnetic template. The scale bar is 50 nm in the case of (A) 20 nm for (B) 400 nm in the case of (C) and 300 nm for (D). 153
Figure 4.11. FTIR spectra of SiNP-RAFT(a) and SiNP-MIP (b). 154

Figure 4.12. DLS results of the magnetic L-Phe imprinted nanoparticles. 154

Figure 4.13. Equilibrium binding isotherms of L-PA (circles) and D-PA (triangle) on imprinted core-shell particles in acetonitrile. The MIPs were synthesized using the magnetic template. 156

Figure 4.14. Fisher values obtained by fitting the L/D-PA binding curves in Figure 4.13 to mono-Langmuir, bi-Langmuir and Freundlich isotherm models (see Table 4.4 to Table 4.6). 157

Figure 5.1. Schematic representation of the amyloid precursor protein (APP) and the location of the Aβ peptide(up) and the 42 amino acid sequence of $A\beta_{1-42}$ (down). 164

Figure 5.2. Chemical structure of the template used for the synthesis of the imprinted polymers (Ac-Gly-Gly-Val-Val-Ile-Ala-O^-TBA^+, Ac-$A\beta_{37-42}$-TBA). 165

Figure 5.3. Procedure for preparing beta-amyloid imprinted polymers from RAFT-modified silica nanoparticles for binding of the C-terminus of $A\beta_{33-42}$. 166

Figure 5.4. Thermal gravimetric analysis of the beta-amyloid imprinted and nonimprinted core-shell nanoparticles; TGA and DTG of SiNP-MIP-1 and SiNP-NIP-1 (A), TGA and DTG of SiNP-MIP-2 and SiNP-NIP-2 (B), TGA and DTG of SiNP-MIP-3 and SiNP-NIP-3 (C), TGA and DTG of SiNP-MIP-4 and SiNP-NIP-4 (D). 169

Figure 5.5. TEM images of SiNP-MIP-1 and SiNP-NIP-1 (A, B); SiNP-MIP-2 and SiNP-NIP-2 (C, D); SiNP-MIP-3 and SiNP-NIP-3 (E, F). The polymer shells are indicated by arrows. The scale bar is 200 nm in the case of (A) 100 nm for (B) 20 nm for(C, E) 50 nm for (D) and 10 nm for (F). 170

Figure 5.6. Equilibrium binding isotherms of Ab_{33-42} on imprinted (circles) and nonimprinted (triangles) core-shell particles in GuHCl (4M)/ACN: 90/10 (v/v). A) SiNP-MIP-1(red circles) and SiNP-NIP-1(blue triangles), B) SiNP-MIP-2(red circles) and SiNP-NIP-2(blue triangles), C) SiNP-MIP-3 (red circles) and SiNP-NIP-3 (blue triangles), D) SiNP-MIP-4 (red circles) and SiNP-NIP-4 (blue triangles). 172

Figure 6.1. Structure of the selected C-terminal epitope decapeptide (T10) and its reference decapeptide (R10). 178

Figure 6.2. Functional monomers and cross-linker used to create decapeptide MIPs, (1): Methacrylamide (MAAM), (2): Methacrylic acid (MAA), (3): 5-(methacryloylamido)-m-xylylene bisphosphonic acid dimethylester dilithium salt, (4): N,N′-ethylenebisacrylamide (EBA). 180

Figure 6.3. Thermal gravimetric analysis of the T10 and R10 imprinted and nonimprinted core-shell nanoparticles; TGA of SiNP-MIP-A and SiNP-NIP-A (A), TGA of SiNP-MIP-B and SiNP-NIP-B (B). 182

Figure 6.4. TEM images of the T10 and R10 imprinted and nonimprinted core-shell nanoparticles SiNP-MIP-A and SiNP-NIP-A (A), SiNP-MIP-B and SiNP-NIP-B (B). The scale bar is 20 nm. 183

Figure 6.5. Aminolysis of grafting polymers. 183

Figure 6.6. UV spectra of RAFT modified particles prior to (red trace) and after (blue trace) aminolysis. The inset shows the particle appearance prior to (left vial) and after (right vial) aminolysis. 184

Figure 6.7. Photograph of BCA protein and peptide assay. Solution of supernatant of imprinted and non-imprinted polymers with BCA reagent(a-d), solution of T10 with BCA reagent(e,f) (A); solution of BCA reagent and IgG(a), BCA reagent(b), solution of non-aminolysed and aminolysed particles with BCA reagent(c,d) (B). 185

Figure 6.8. Procedure used to synthesis silica core-MIP shell nanoparticles for decapeptide in aqueous media. 187

Figure 6.9. Thermal gravimetric analysis of the T10 imprinted and nonimprinted core-shell nanoparticles; TGA of SiNP-MIP1 and SiNP-NIP1 (A), DTG of SiNP-MIP1 and SiNP-NIP1(B), TGA of SiNP-MIP2 and SiNP-NIP2 (C), DTG of SiNP-MIP2 and SiNP-NIP2 (D), TGA of SiNP-MIP3 and SiNP-NIP3 (E), DTG of SiNP-MIP3 and SiNP-NIP3 (F).....191

Figure 6.10. TEM images of the T10 imprinted and nonimprinted core-shell nanoparticles SiNP-MIP1 (A), SiNP-NIP1 (B), SiNP-MIP2 (C), SiNP-NIP2 (D), SiNP-MIP3 (E) and SiNP-NIP3 (F). The scale bar is 20 nm in the case of (A), (B), (C), (E), (F) and 10 nm for (D).....192

Figure 6.11. FTIR spectra of SiNP-TTC (a), SiNP-MIP (b), SiNP-NIP (c). 193

Figure 6.12. Equilibrium binding isotherms of T10 on imprinted (circles) and nonimprinted (triangles) core-shell particles in buffer. A) SiNP-MIP1(red circles) and SiNP-NIP1(blue triangles), B) SiNP-MIP2(red circles) and SiNP-NIP2(blue triangles), C) SiNP-MIP3 (red circles) and SiNP-NIP3 (blue triangles). 196

Figure 6.13. Fisher values obtained by fitting the T10 binding curves in Figure 6.12 to mono-Langmuir, bi- Langmuir and Freundlich isotherm models (see Table 6.7 to Table 6.9). 198
Figure 6.14. Synthesis of 5-(methacryloylamido)-m-xylylene bisphosphonic acid dimethylester dilithium salt.....200
Figure 6.15. Synthesis of PEG-TTC macro chain transfer agent.....201
Figure 6.16. Picture of TTC modified silica, imprinted and nonimprinted particles; A) SiNP-TTC, B) SiNP-MIP and NIP (before drying), C) SiNP-MIP and NIP (after drying). 203

List of Tables

Table 1.1. Examples of various templates used in molecular imprinting. 41

Table1.2. MIPs prepared by the surface-initiated controlled radical polymerization techniques.....60

Table 1.3. Typical characteristics of antibodies and MIPs. (adapted from[215]).....78

Table 3.1. Properties of the silica bead supports.....97

Table 3.2. Characterisation of modified silica supports by TGA.....100

Table 3.3. Results from the characterisation of modified silica beads by elemental analysis. 102

Table 3.4. Number average particle size and polydispersity from DLS of nanoparticles used in the study. 105

Table 3.5. Characterisation of modified silica supports by TGA.....110

Table 3.6. Results from the characterisation of modified silica beads by elemental analysis. 111

Table 3.7. Results from the characterization of grafted linear polymers. 115

Table 3.8. Amount of ungrafted free polymers in the wash fractions.....116

Table 3.9. Procedure for the preparation of core-shell L-PA imprinted nanoparticles. 121

Table 3.10. Results from the characterization of imprinted and nonimprinted core shell beads.....122

Table 3.11. Mono-Langmuir isotherm fitting parameters obtained by nonlinear regression of data shown in Figure 3.23. 129

Table 3.12. Bi-Langmuir Isotherm fitting parameters obtained by nonlinear regression of data shown in Figure 3.23. 129

Table 3.13. Freundlich isotherms fitting parameters obtained by nonlinear regression of data shown in Figure 3.23.....130

Table 3.14. Reaction conditions for the preparation of silica NPs of various sizes. 132

Table 3.15. Reaction conditions for the amino modification of silica NPs of various sizes.133

Table 3.16. Reaction conditions for the RAFT modification of silica NPs of various sizes.134

Table 3.17. Polymerization procedure for the methyl methacrylate graft polymerization. ..136

Table 3.18. Polymerization procedure for the styrene graft polymerization. 137

Table 3.19. Polymerization procedure for the methacrylamide graft polymerization. 138

Table 3.20. Polymerization procedure for the preparation of L-PA imprinted core-shell NPs. 139
Table 4.1. Results from the characterisation of modified silica beads by elemental analysis. 148
Table 4.2. Procedure for the preparation of core-shell L-PA imprinted nanoparticles. 151
Table 4.3. Results from the characterisation of imprinted core-shell beads. 152
Table 4.4. Mono-Langmuir isotherm fitting parameters obtained by nonlinear regression of data shown in Figure 4.13. 156
Table 4.5. Bi-Langmuir isotherm fitting parameters obtained by nonlinear regression of data shown in Figure 4.13. 157
Table 4.6. Freundlich isotherms fitting parameters obtained by nonlinear regression of data shown in Figure 4.13. 157
Table 5.1. Procedure for the preparation of core-shell beta-amyloid imprinted nanoparticles. 167
Table 5.2. Results from the characterisation of imprinted and nonimprinted core-shell beads. 168
Table 5.3. Polymerization procedure for the beta-amyloid imprinted polymers. 175
Table 6.1. Procedure for the preparation of T10 and R10 imprinted core-shell nanoparticles. 181
Table 6.2. Results from the characterisation of R10 and T10 imprinted and nonimprinted core-shell beads. 182
Table 6.3. Procedure for the preparation of core-shell T10 imprinted nanoparticles in organic media. 186
Table 6.4. Procedure for the preparation of core-shell T10 imprinted nanoparticles in aqueous media. 188
Table 6.5. Amount of the resultant template from the T10 MIPs in the different wash fractions. 188
Table 6.6. Results from the characterisation of T10 imprinted and nonimprinted core-shell beads 190
Table 6.7. Mono-Langmuir isotherm fitting parameters obtained by nonlinear regression of data shown in Figure 6.12. 196
Table 6.8. Bi-Langmuir isotherm fitting parameters obtained by nonlinear regression of data shown in Figure 6.12. 197

Table 6.9. Freundlich isotherms fitting parameters obtained by nonlinear regression of data shown in Figure 6.12.....197

Summary

Molecularly imprinted polymers (MIP) are perceived to have several shortcomings such as heterogeneous binding site, template occlusion, and difficulties in template recovery and in upscaling for commercial exploitation. This thesis describes the development of novel methods to overcome these drawbacks, combining surface imprinting on nanoparticles with Reversible Addition Fragmentation chain Transfer polymerization (RAFT) to prepare well-defined MIP composites.

The first part of this thesis describes the use of R-immobilized RAFT technique from silica core to generate tunable core-shell structured cross-linked MIP nanoparticles for chiral discrimination. Before creating the cross-linked polymers, the grafting of linear polymers from RAFT modified silica nanoparticles was optimized. Imprinted copolymers of methacrylic acid (MAA) and ethyleneglycol dimethacrylate (EGDMA) were grafted from the supports in presence of L-phenylalanine anilide (L-PA) as chiral template. The relatively low ABDV/CPDB ratio reduced the amount of free polymer derived from the initiator and yet maintained a moderate polymerization rate. Silica nanoparticles with two different sizes, ca 20 nm and ca 200 nm, were used as a support material to investigate the effect of core size in binding properties of MIP particles. The resulting beads were subsequently characterised by FTIR, TEM, SEM, DLS, TGA and elemental analysis. In binding tests using reversed phase HPLC, the imprinted nanoparticles exhibited a much-higher binding affinity for the template molecule than the non-imprinted particles. In addition, the imprinted nanoparticles were able to discriminate the template L-PA and its optical antipode D-PA. Furthermore, core-shell particles with smaller core size displayed a higher binding affinity than those with larger cores.

In the second part of this thesis, the previously established, optimized synthesis route for core-shell nanoparticles imprinted with L-PA was applied in a solid-phase synthesis approach to prepare molecularly imprinted core-shell nanoparticles (MIPNPs) in template free form towards L-phenylalanine (L-Phe) immobilized on magnetic placeholder templates. The latter was achieved by grafting poly (MAA-co-EDMA) on RAFT-modified silica nanoparticles. To the best of my knowledge, this thesis presents the first artificial receptor that has successfully been produced using magnetic placeholder templates. All the materials were characterized using elemental microanalysis, FT-IR, TGA, SEM, TEM and DLS. In order to evaluate the

binding properties, the particles were subsequently tested for their affinity towards the template L-PA and D-PA in acetonitrile. The results demonstrated that the MIPNPs prepared via this method had highly accessible binding sites and good discrimination towards the template L-PA and D-PA.

The third part of this thesis illustrates engineering of epitope imprinted core-shell nanoparticles towards beta-amyloid template. The "epitope imprinting" consists of using only a short and exposed peptide sequences as a surrogate template for the whole protein. Beta-amyloid contains a pool of peptidic fragments in varying length, which are important biomarkers involved in the pathology of Alzheimer's disease. With the aim of developing polymeric complements to one of these biomarkers, the peptide $A\beta_{37-42}$ was used as template to generate an artificial receptor. The MIPs were prepared in organic media by using diarylurea as comonomer, ethyl ammonium methacrylate as a functional monomer and divinylbenzene as a crosslinker. The adsorption capacity of the resulting MIPs was examined by reversed phase HPLC.

The last part of this thesis had the aim to develop an artificial receptor for the human immunoglobulin G (IgG). The decapeptide fragment (T10) from the C-terminus of its heavy chain was used as template. Epitope imprinted nanoparticles were prepared by grafting of poly-(methacrylicacid-co-methacrylamide-co-ethylbisacrylamide) and/or poly-(bisphosphonicacid-co-methacrylamide-co-ethylbisacrylamide) in presence of the T10 template from a RAFT modified colloidal silica core. The resultant MIPs were characterised by FT-IR, TEM, TGA and elemental analysis. The polymers were examined by equilibrium rebinding for their affinity towards the template T10 in aqueous media by reversed phase HPLC. For polymers prepared in organic media, the resulting imprinted and nonimprinted particles revealed a similar adsorption capacity towards T10 template. When the synthesis was performed in aqueous media, the imprinted particles displayed a higher adsorption capacity than the nonimprinted particles. Compared to polymer grafted using the bisphosphonic acid monomer, polymer obtained via methacrylic acid as functional monomer showed better imprinting performance. Our results provide a new potential for peptide and protein imprinting in aqueous media using SI-RAFT technique and it might also be transferred to epitopes of other proteins. We believe that such synthetic MIP nanoparticles are highly promising alternatives to biological receptors with great potential in many analytical applications and other areas.

Zusammenfassung

Molekular geprägte Polymere (MIP) weisen diverse Mängel wie heterogene Bindungsstellen, Einschluss der Template und Schwierigkeiten bei der Rückgewinnung der Template und der Hochskalierung zur kommerziellen Nutzung auf. Diese Arbeit beschreibt die Entwicklung neuer Methoden, um diese Nachteile zu überwinden. Dabei kombiniert sie die Oberflächenprägung auf Nanopartikeln mit der Reversible-Addition-Fragmentation-Chain-Transfer-Polymerisation (RAFT), um klar definierte MIP Komposite herzustellen.

Der erste Teil der Arbeit beschreibt die Anwendung von R-immobilisierter RAFT-Polymerisation auf Silica-Kernen, um vernetzte MIP-Nanopartikel mit wohldefinierter Kern-Schale-Struktur für die chirale Unterscheidung von Analyten herzustellen. Vor der Herstellung der vernetzten Polymeren wurde zunächst die Pfropfung von linearen Polymeren mit Silica-Nanopartikeln, die mit RAFT-Reagenzioen modifiziert waren, optimiert. Geprägte Copolymere von Methacrylsäure (MAA) und Ethylenglycoldimethacrylat (EGDMA) wurden auf das Trägermaterial in Gegenwart von L-Phenylalanin anilid (L-PA) als chiralem Templat gepfropft. Das relativ geringe ABDV/CPDB Verhältnis reduzierte die Menge des durch den Initiator gebildeten freien Polymers und führte dennoch zu einer moderaten Polymerisationsrate. Silica-Nanopartikel mit zwei verschiedenen Größen , ca. 20 nm und ca. 200 nm, wurden als Trägermaterial verwendet, um die Auswirkung der Kerngröße auf die Bindungseigenschaften der MIP-Teilchen zu untersuchen. Die resultierenden Partikel wurden dann durch FTIR, TEM, SEM, DLS, TGA und Elementaranalyse charakterisiert. In Bindungstests unter Verwendung von Umkehrphasen-HPLC zeigten die geprägten Nanopartikel eine viel höhere Bindungsaffinität für das Templat-Molekül als die nicht geprägten Teilchen. Darüber hinaus wurden die Template L-PA und sein Spiegelbildisomer D-PA von den geprägten Nanopartikel unterschiedlich stark gebunden. Des Weiteren zeigte sich, dass Kern-Schale-Teilchen mit kleineren Kerngrößen eine höhere eine höhere Bindunsgaffinität aufweisen, als Partikel mit größerem Silicakern.

Im zweiten Teil dieser Arbeit wurde die zuvor entwickelte, optimierte Syntheseroute für die mit L-PA geprägten Kern-Schale-Nanopartikel in einem Festphasen-Synthese-Ansatz angewandt. Durch die Immobilisierung von L-Phenylalanin (L-Phe) auf magnetischen Platzhalter-Templaten wurden molekular geprägte Kern-Schale-Nanopartikel (MIPNPs) in templatfreier Form synthetisiert. Dieses wurde durch Pfropfung von Poly(MAA-co-EDMA)

auf RAFT -modifizierten Siliciumdioxid-Nanoteilchen erreicht. Nach meinem besten Wissen stellt diese Arbeit den ersten künstlichen Rezeptor vor, der erfolgreich unter Verwendung von magnetischen Platzhalter-Templaten hergestellt wurde. Alle Materialien wurden unter Verwendung von Mikroelementaranalyse, FT-IR, TGA, SEM, TEM und DLS charakterisiert. Um die Bindungseigenschaften zu studieren, wurden die Teilchen anschließend bezüglich ihrer Affinität gegenüber der Template L-PA und D-PA in Acetonitril getestet. Die Ergebnisse zeigten, dass die mit dieser Methode hergestellten MIP-Nanopartikel gut zugängliche Bindungsstellen hatten und L-PA gegenüber D-PA bevorzugt gebunden wurde.

Der dritte Teil der Arbeit veranschaulicht die Konstruktion von Epitop-geprägten Kern-Schale-Nanopartikeln zur Bindung eines Beta-Amyloid-Templats. Das "Epitop-Imprinting" beinhaltet die Verwendung einer kurzen, an der Oberfläche exponierten Peptidsequenzen als Surrogat-Templat für ein ganzes Protein. Beta-Amyloid besteht aus unterschiedlich langen Peptidfragmenten, diese sind wichtige Biomarker, die an der Pathologie der Alzheimer-Krankheit beteiligt sind. Mit dem Ziel einen künstlichen Rezeptor zu einem dieser Biomarker zu entwickeln wurde das Peptid $A\beta_{37\text{-}42}$ als Templat zur MIP-Synthee verwendet. Die MIPs wurden mit Diarylharnstoff als Comonomer sowie Ethyl-Ammonium-Methacrylat als funktionelles Monomer und Divinylbenzol als Vernetzer in organischem Lösungsmittel synthetisiert. Die Adsorptionskapazität der erhaltenen MIPs wurde durch Umkehrphasen-HPLC untersucht.

Der letzte Teil der Arbeit hatte das Ziel, einen künstlichen Rezeptor für das humane Immunglobulin G (IgG) zu entwickeln. Das Dekapeptid-Fragment (T10) aus dem C-Terminus seiner schweren Kette wurde als Matrize verwendet. Epitop-geprägte Nanopartikel wurden durch Grafting von Poly(Methacrylsäure-co-Methacrylamid-co-Ethylbisacrylamide) und/oder Poly(Bisphosphonsäure-co-Methacrylamid-co-Ethylbisacrylamid) in Gegenwart des T10 Templats aus RAFT-modifizierten, kolloidalen Siliciumdioxid-Kernen hergestellt. Die resultierenden MIPs wurden durch FT-IR, TEM, TGA und Elementaranalyse charakterisiert. Die Polymere wurden unter Verwendung von Umkehrphasen-HPLC durch Gleichgewichts-Rebinding auf ihre Affinität gegenüber des Templats T10 in wässrigen Medien untersucht. Bei Polymeren, die in organischen Medien hergestellt wurden, zeigten die resultierenden geprägten und nicht-geprägtem Polymere ähnliche Aufnahmekapazität gegenüber dem T10-Templat. Bei der Synthese in wässrigem Medium zeigten die geprägten Partikel eine höhere Aufnahmekapazität als die nicht geprägten Partikel. Im Vergleich zu den gepfropften

Polymeren mit dem Bisphosphonsäure-Monomer zeigten die Polymere mit Methacrylsäure als funktionellem Monomer eine bessere Prägeeffektivität.

Unsere Ergebnisse liefern einen neuen Ansatz zur Prägung von Polymeren mit Peptiden und Proteinen in wässrigen Medien unter Verwendung der SI-RAFT-Technik, die auch auf Epitope anderer Proteine übertragen werden könnte. Wir sind davon überzeugt, dass diese synthetischen MIP Nanopartikel vielversprechende Alternativen zu biologischen Rezeptoren mit großem Potenzial in vielen analytischen Anwendungen und auch in anderen Bereichen sind.

Objectives of the Thesis

The main objective of this work is to develop novel molecularly imprinted core-shell nanoparticles (MIP NPs) by using surface initiated RAFT polymerization showing high affinity and good selectivity for target molecules. Novel recognitive polymer networks have been designed with considerations of the complex interactions taking place between the templates and ligands at the molecular level. Chapter 2 briefly describes the characterization techniques used to analysis prepared polymers in this thesis. Grafting imprinted polymers from the RAFT modified silica supports towards the template L-PA and its optical antipode D-PA have been studied in chapter 3. This grafting procedure consists of R-group immobilization of RAFT agent onto silica nanoparticles and coplymerization of methacrylic acid (MAA) and ethyleneglycol dimethacrylate (EDMA). In chapter 4, solid- phase synthesis of MIPs core-shell nanoparticles using magnetic template has been investigated. In this method the protected L-phenylalanine (Fomc-L-Phe) template was immobilized on the surface of magnetic-silica nanoparticles. Subsequently the magnetic placeholder template was added to prepolymerization mixture (i.e. MAA, EDMA, RAFT-SiO_2 and toluene) to yield the L-Phe imprinted MIP NPs.

The engineering of epitope imprinted core-shell nanoparticles towards beta-amyloid template for the pathology of Alzheimer's disease has been investigated in chapter 5. The C-terminal sequence $A\beta_{37\text{-}42}$ was selected as template and transformed into its acetylated tetrabutylammonium salt (Ac-$A\beta_{37\text{-}42}$-TBA) to enhance the template solubility. The MIPs were synthesized using divinylbenzene as hydrophobic crosslinker in organic media. In chapter 6, nano-sized core-shell particles by grafting of thin films imprinted with a hydrophilic peptide from nonporous silica cores have been reported. In this chapter decapeptide fragment (T10) from the C-terminus of IgG heavy chain was selected as template and polymerization was carried out using hydrophilic acrylamide based monomers in aqueous media. The resulting beads were subsequently characterised by FTIR, TEM, DLS, TGA and elemental analysis. In each chapter the polymers were tested for their affinity towards the target molecules by reversed phase HPLC.

Chapter 1: Background and State of the Art

1.1 Molecularly imprinted polymers

Robust molecular recognition elements with antibody-like ability to bind and discriminate between molecules can today be synthesized using various forms of molecular imprinting (Figure 1.1) [1-5]. The most common form of imprinting entails the synthesis of reticulated polymers in the presence of templates (T) which, widely defined, may range from being individual ions, small molecules, or biological macromolecules to microorganisms or crystal particles. Functional monomers act as anchors, interacting with the template (1) and holding it in place during the subsequent polymerization (2). Removal of the template from the formed polymer liberates binding sites (3) complementary in shape and binding groups to the template structure. Hence, these molecularly imprinted polymers (MIPs) are functional in the sense that they exhibit a memory for the template and can selectively bind it or related structures with high affinity, not unlike the way antibodies bind their antigens. In spite of this advanced function, and in contrast to the biological recognition elements, MIPs are remarkably stable against mechanical stresses, high temperatures and pressures, and intense radiation. They are also resistant to treatment with acid, base or metal ions, and stable in a wide range of solvents. The storage endurance of the polymers is also very high. Furthermore, the polymers can be used repeatedly without loss of their "memory effect." This, in addition to the relative ease of producing MIPs, has led to a boom in the research and industrial interest in this fascinating class of materials, particularly with the aim of finding alternatives or substitutes for the labile biologically derived recognition elements [6].

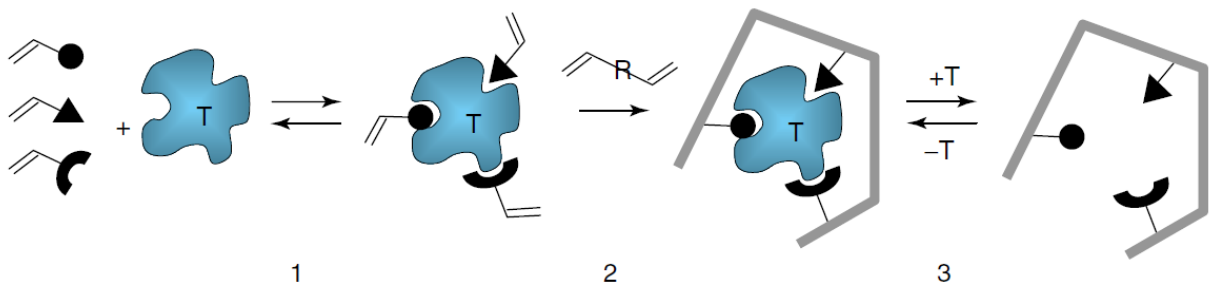

Figure 1.1. Principle of molecular imprinting.

The main appeal of molecular imprinting lies in its simplicity in terms of the required ingredients, equipment, and unit operations. The majority of the reported examples are based on MIPs formed by free radical polymerization in the presence of the template by operations requiring only simple equipment. Hence, MIPs can be produced in essentially any moderately equipped laboratory.

The design of a MIP receptor can be divided into three steps, distinguished by the type of chemistry involved and the length scales of the designed features (Figure 1.2) [6]. The construction of a binding site for a low-molecular-weight target aims to place functional groups at 1-nm length scale, in complementary positions to the target. This design starts with an examination of the structural and functional features of the target molecule for which an MIP is needed, while also considering the context in which the MIP should operate (solvent, temperature, target concentration, static or dynamic mode, etc.) and whether the binding event should trigger an associated function. The template can be either covalently or noncovalently linked to the functional monomer and the same distinction can be made with respect to the interactions occurring between the target molecule and the resulting binding site.

Binding site design	Scaffold design	Morphology design
* Template molecule - Target imprinting - Fragment imprinting - Analog imprinting * Functional monomers - Computational methods - Combinatorial methods - Host-guest chemistry - Covalent imprinting	* Organic polymers - Polymethacrylics, polyacrylics, and polystyrens * Inorganic polymers - For example, SiO_2, TiO_2, etc. * Polymerization techniques - Noncontrolled - Controlled - Type of initiator * Crosslinking - During polymerization - After polymerization - Degree of cross-linking - Covalent or noncovalent	* Crushed monoliths * Beaded MIPs * Hierarchical MIPs * Composites * Thin films * Fibers and tubes * Membranes * Perfusive monoliths * Nanostructured MIPs

Figure 1.2. Steps involved in MIP design. (adapted from [6])

MIPs have attracted great interest during recent years because they have certain advantages over immunosorbents, such as mechanical robustness, resistance to elevated temperatures and pressures, an improved inertness to strong acids, bases and organic solvents, as well as low cost, ease of preparation, long shelf-life and reproducibility. Consequently, MIPs have been widely used in applications based on specific molecular recognition, namely as recognition elements in sensors [7-9], as substitutes of antibodies in binding immunoassays [10], for directed synthesis and catalysis [11], for drug delivery [12], as drugs [13, 14], chiral recognition [15, 16] and, in particular, in purification and separation techniques [17-19].

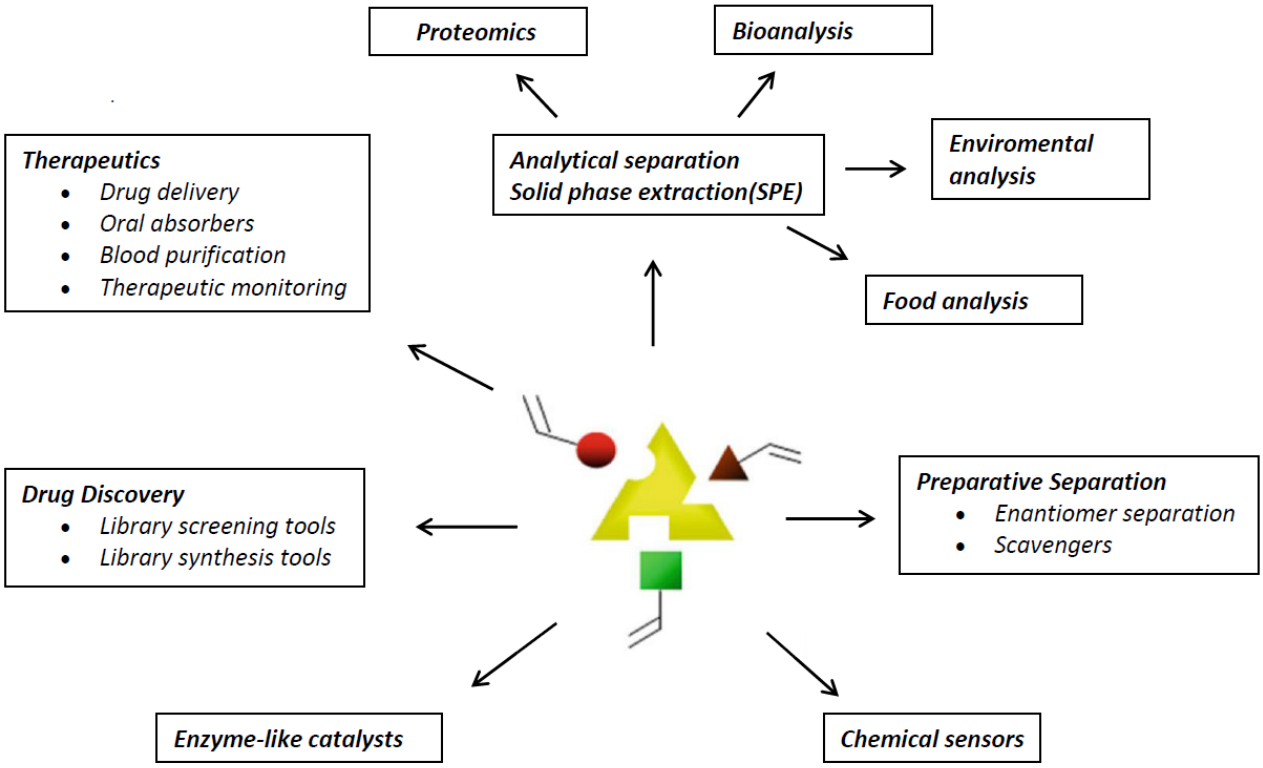

Figure 1.3. Scheme outlining the main applications envisaged for MIPs.(adapted from[20])

1.2 Imprinting approaches

The approaches to produce MIPs can be generally divided into a few categories, based on the type of interactions between the template and the functional monomer, which are covalent molecular, non-covalent, semi-covalent and metal-coordinating molecular imprinting.

1.2.1 Covalent imprinting

Covalent imprinting is where the template is bound to one or several polymerization groups covalently. Once the template-MIP complex is formed (after synthesis), the covalent bonds must be cleaved. After the template is removed, the target molecule can rebind due to covalent bonds being formed in the same locations, with the main advantages being that the functional groups are associated with the template only, and the stability of covalent bonding yields more homogeneous binding sites. Only certain compounds can be imprinted in this way, including diols, aldehydes, ketones, amines, and carboxylic acids [2]. Covalent imprinting methods have historically been the more prevalent (until recently) where it was first developed by Wulff et al.[21]

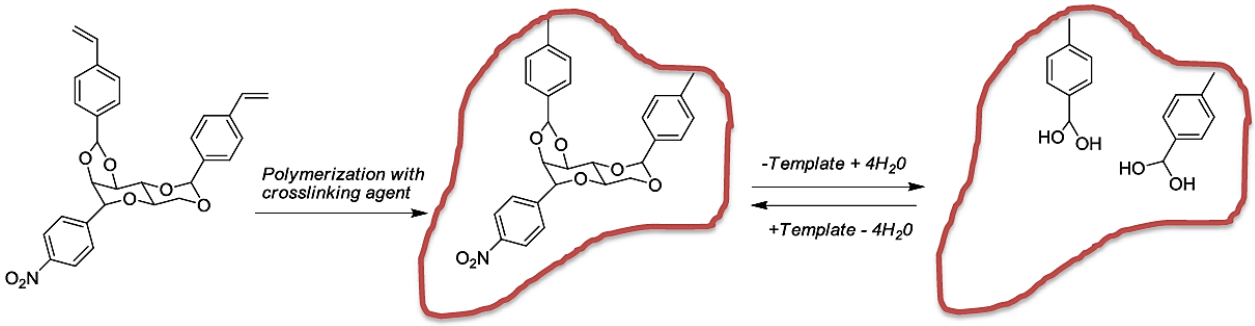

Figure1.4. Covalent imprinting of 4-nitrophenyl-a-d-mannopyranoside-2,3:4,6-di-O-(4vinylphenylboronate). (adapted from[22])

1.2.2 Non-covalent imprinting

Non-covalent imprinting adducts, which are formed between the template and functional monomer, are based on non-covalent interactions, such as hydrogen bonding, ion pairing, dipole-dipole interactions, and Van der Waals forces. Unlike covalent imprinting these adducts are unstable and rearrange in relation to the imprinting process [2, 22]. After production the template is removed by washing with a solvent or a mixture of solvents. The non-covalent approach is the most popular method of MIP synthesis [20] and was introduced in the early 1980s [23].

Non-covalent imprinting is usually based on commodity acrylics or methacrylic monomers (e.g., methacrylic acid (MAA)) which are then cross-linked with ethylene glycol

dimethacrylate (EGDMA). Hydrogen bonding or acid-base interactions between the template and functional groups (of low molecular weight compounds) are desirable [24].

The non-covalent approach has been used more extensively due to follow three reasons:

(i) Non-covalent methodology is easier because it does not require synthetic steps toward the prepolymer complex; interactions between monomers and template are easily obtained when all components are mixed in solution.
(ii) Removal of the template is generally much easier, usually accomplished by continuous extraction.
(iii) A greater variety of functionality can be introduced into the MIP binding site using noncovalent methods.

Therefore, investigations into the behavior of MIPs have dealt more frequently with non-covalent systems.

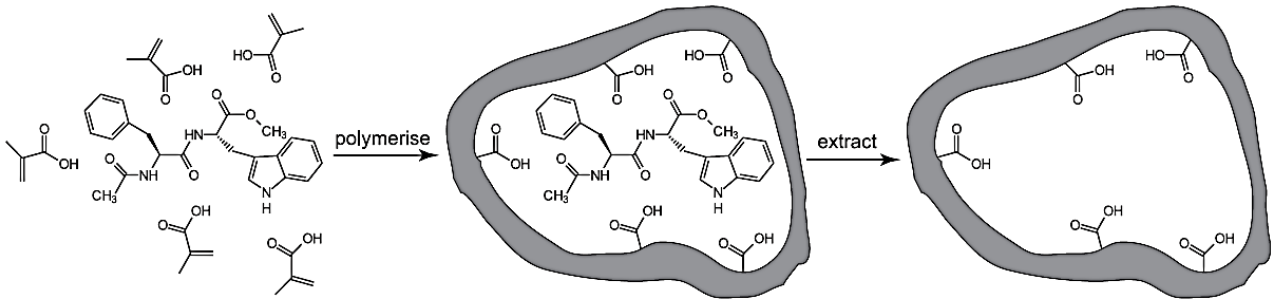

Figure 1.5. Non-covalent imprinting of a dipeptide derivative by multiple non-covalent interactions with methacrylic acid. (adapted from[25])

1.2.3 Semi-covalent imprinting

Semi-covalent imprinting attempts to combine the advantages of the covalent and the non-covalent approach. As the template is covalently bound to a polymerizable group, the functionality which is recovered after cleavage of the template should only be found in the binding site. This also results in a more uniform distribution in binding site affinities [26]. Semi-covalent imprinting is also possible and refers to the method which utilizes a covalent or partly covalent template structure in the polymerization step but is distinct from covalent

imprinting in that the rebinding step is non-covalent [22], and this was pioneered by Sellergren and Andersson [27].

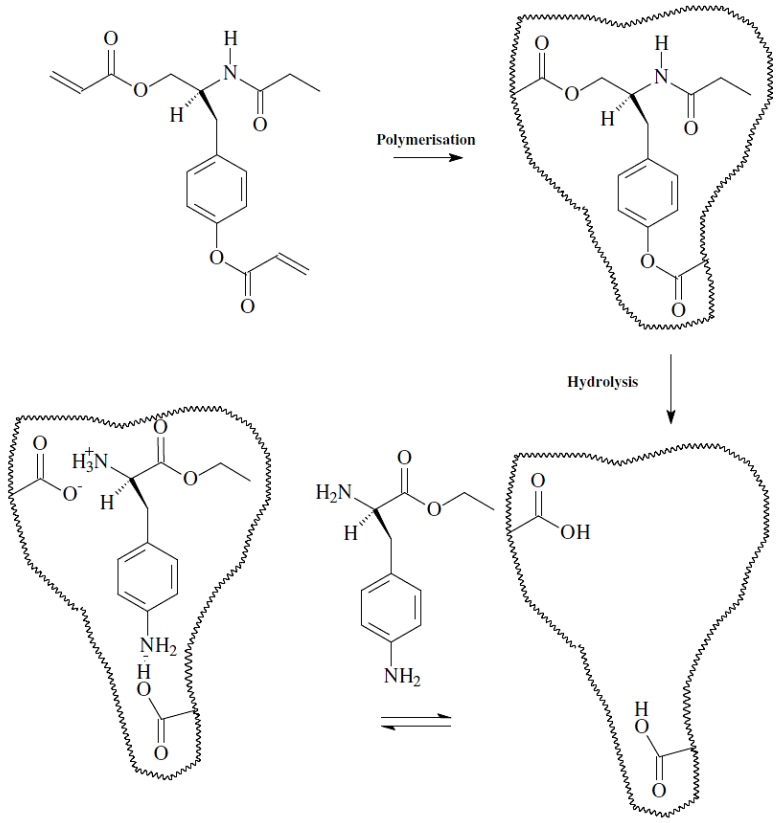

Figure 1.6. Semi-covalent imprinting for L-p-aminophenylalanine ethyl ester. (adapted from[27])

1.2.4 Metal ion imprinting

Metal ions can take part in imprinting either as a template or can directly be involved in the template-polymer interactions. With the latter binding is possible as metal ions are able to accept electrons into their “un filled orbitals of the outer coordination sphere” [2] from the heteroatoms of ligands. Therefore, the binding strength can range from weak bonds to strong bonds (which can behave covalently), depending on the metal, its oxidation state, and ligand characteristics [2, 22]. The first approach was reported in 1985 with the imprinting of amino acids [28].

1.3 Molecularly imprinted polymer syntheses

The synthesis of molecularly imprinted polymers is a chemically complex pursuit and demands a good understanding of chemical equilibrium, molecular recognition theory, thermodynamics and polymer chemistry in order to ensure a high level of molecular recognition [29-31]. The polymers should be rather rigid to preserve the structure of the cavity after splitting off the template. On the other hand, a high flexibility of the polymers should be present to facilitate a fast equilibrium between release and reuptake of the template in the cavity. These two properties are contradictory to each other, and a careful optimization became necessary. The challenge of designing and synthesizing a molecularly imprinted polymer can be a daunting prospect to the uninitiated practitioner, not least because of the sheer number of experimental variables involved, e.g. the nature and levels of template, functional monomer(s), cross-linker(s), solvent(s) and initiator, the method of initiation and the duration of polymerization. Moreover, optimization of the imprinted products is made more difficult due to the fact that there are many variables to consider, some or all of which can potentially impact upon the chemical, morphological and molecular recognition properties of the imprinted materials. Fortunately, in some instances it is possibly to rationally predict how changing any one such variable, e.g. the cross-link ratio, is likely to impact upon these properties [32-36].

1.3.1 Template

Generally, template molecules are target compounds in analytical processes. An ideal template molecule should satisfy the following three requirements. First, it should not contain groups involved in or preventing polymerization. Second, it should exhibit excellent chemical stability during the polymerization reaction. Finally, it should contain functional groups well adapted to assemble with functional monomers.

The imprinting of small, organic molecules (e.g., pharmaceuticals, pesticides, amino acids and peptides, nucleotide bases, steroids, and sugars) is now well established and considered almost routine. Optically active templates have been used in most cases during optimization. In these cases the accuracy of the structure of the imprint (the cavity with binding sites) could be measured by its ability for racemic resolution, which was tested either in a batch procedure or by using the polymeric materials as chromatographic supports.

One of the many attractive features of the molecular imprinting method is that it can be applied to a diverse range of analytes, however, not all templates are directly amenable to molecular imprinting processes. Most routine MIPs were synthesized using small organic molecules as template. Although specially adapted protocols have been proposed for larger organic compounds, e.g., proteins, cells, imprinting of much larger structures is still a challenge. The primary reason is the fact that larger templates are less rigid and thus do not facilitate creation of well-defined binding cavities during the imprinting process. Furthermore, the secondary and tertiary structure of large biomolecules such as proteins may be affected when exposed to the thermal or photolytic treatment involved in the synthesis of imprinted polymers. Rebinding is also more difficult, since large molecules such peptides and proteins do not readily penetrate the polymer network for reoccupation of binding pockets.

Table 1.1. Examples of various templates used in molecular imprinting.

Category of template molecule	*Specific examples*	*Reference*
Amino acids	Phenylalanine anilide	[37]
	Histidine	[38]
Antibiotics	Trimethoprim	[39]
	Penicillin	[40]
	Norfloxacin	[41]
Drugs	Propranolol	[42]
	Paracetamol	[43]
	Ibuprofen	[44]
Narcotics	Cocaine	[45]
Pesticides / herbicides	Carbaryl	[46]
	Linuron & isoproturon	[47]
	Cortisol	[48]
Steroids	Testosterone	[49]
	β-D-fructopyranose	[50]
Sugars	Methyl-α-D-glucopyranoside-6-acrylate	[51]

1.3.2 Functional monomers

Functional monomers are responsible for the binding interactions between the template and polymer matrix. It is clearly very important to match the functionality of the template with the functionality of the functional monomer in a complementary fashion in order to maximize complex formation. The functional monomer must also have a group that is capable of undergoing a polymerization reaction thus facilitating the formation of the growing polymer.

The role of the monomer is to provide functional groups which can form a complex with the template by covalent or non-covalent interactions. The strength of the interactions between template and monomer affects the affinity of MIPs [52, 53], and determines the accuracy and selectivity of recognition sites [54]. The stronger interaction provides the more stable complex and resulting in the higher binding capacity of the MIPs, and therefore, correct selection of the functional monomers is very important. Tedious trial-and-error tests are often required to select a suitable monomer. In order to perform rational design and convenient synthesis of MIPs, several strategies, such as spectroscopic measurement e.g., nuclear magnetic resonance [55, 56], uv-vis [57, 58], fourier-transform infrared spectroscopy [59], computer simulation [60], and isothermal titration calorimetry [61] have been employed to select optimal functional monomers capable of forming more stable complexes with templates. Research on how to choose and evaluate appropriate functional monomers has been reviewed recently [62]. Commonly used monomers for molecular imprinting include methacrylic acid (MAA), acrylic acid (AA), 2-or 4-vinylpyridine (2- or 4-VP), acrylamide, trifluoromethacrylic acid and 2-hydroxyethyl methacrylate (HEMA). Structures of several typical monomers are listed in Figure 1.7. MAA has been used as a ‘‘universal’’ functional monomer due to its unique characteristics, being capable to act as a hydrogen-bond donor and acceptor, and showing good suitability for ionic interactions [63].

Generally, the molar ratios between template and monomer in the synthesis process affect the affinity and imprinting efficiency of MIPs. Lower molar ratios induce less binding sites in polymers due to fewer template–monomer complexes, but over-high ones produce higher non-specific binding capacity, diminishing the binding selectivity. So, in order to gain high imprinting efficiency, the molar ratio of templates to monomers should be optimized.

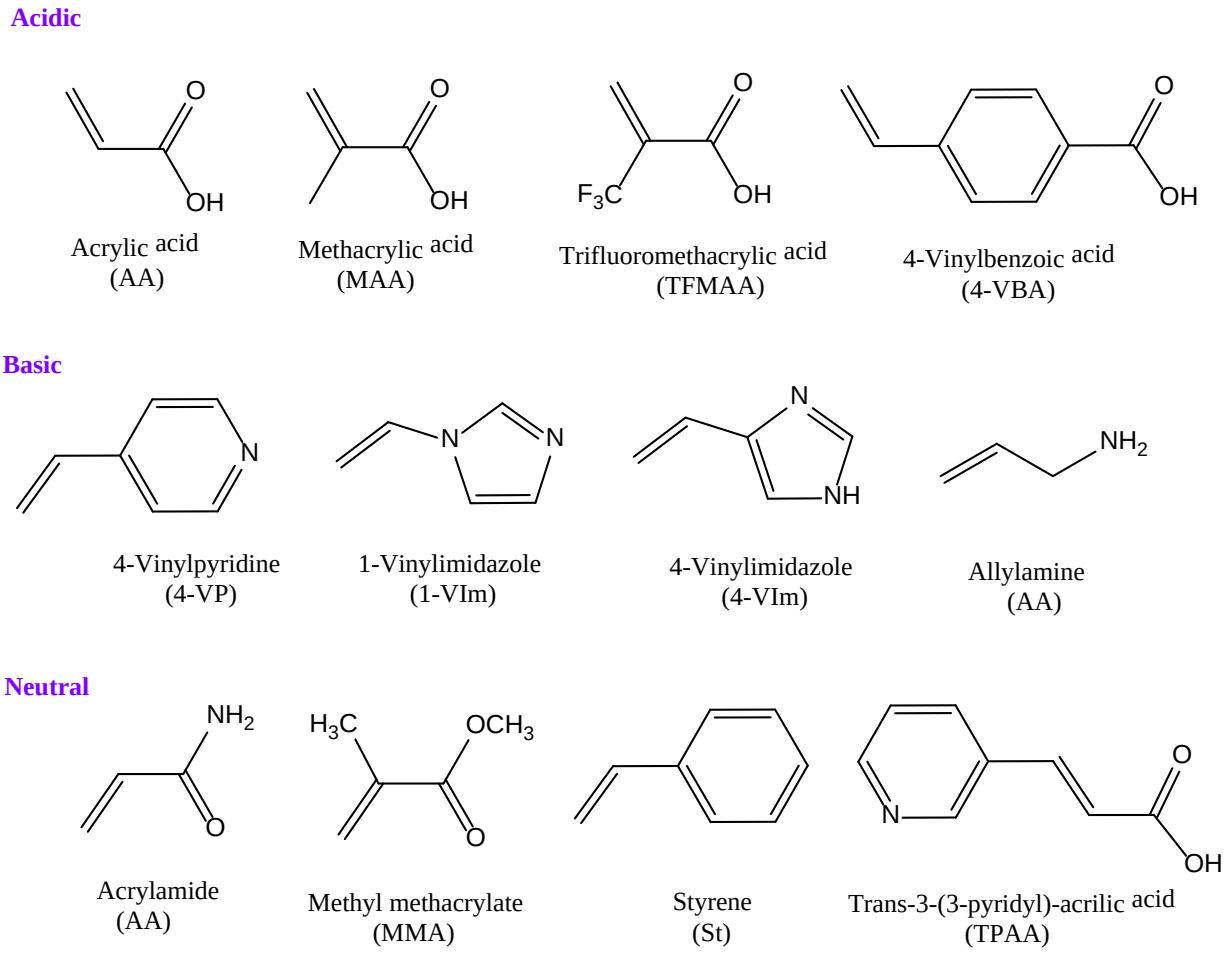

Figure 1.7. Structure of the most common monomers used for molecular imprinting.

1.3.3 Cross-linkers

For imprinted polymer synthesis, the cross-linker also fulfils important functions. The cross-linker is important in controlling the morphology of the polymer matrix, serves to stabilize the imprinted binding sites and imparts mechanical stability to the polymer matrix in order to retain its molecular recognition capability [24]. Different cross-linkers have been used (Figure 1.8). High cross-link ratios are generally used in order to access permanently porous (macroporous) materials with adequate mechanical stability. Ethylene glycol dimethacrylate (EGDMA) and trimethylolpropane trimethacrylate (TRIM) are the most commonly employed. Some authors found that cross-linker has a major impact on the physical characteristics of the polymers and much less effect on the specific interactions between the template and functional monomers [59, 64, 65]. TRIM as cross-linker gives polymers with more rigidity, structure order and effective binding sites than EGDMA. In the case of

polymerization obtained by precipitation method, it has been seen that optimizing the amount of cross-linker and reducing the concentration of the template, the polymer binding properties are improved and the level of non-specific interactions is decreased [66]. In another study it has been observed that the type of cross-linker strongly influences the final size and yield of MIP nanoparticles[67]. In fact, when divinylbenzene was used as the cross-linker, polydisperse MIP particles were obtained in low yield, whereas, trimethylolpropane trimethacrylate (TRIM) led to uniform nanoparticles in high yield (90%).

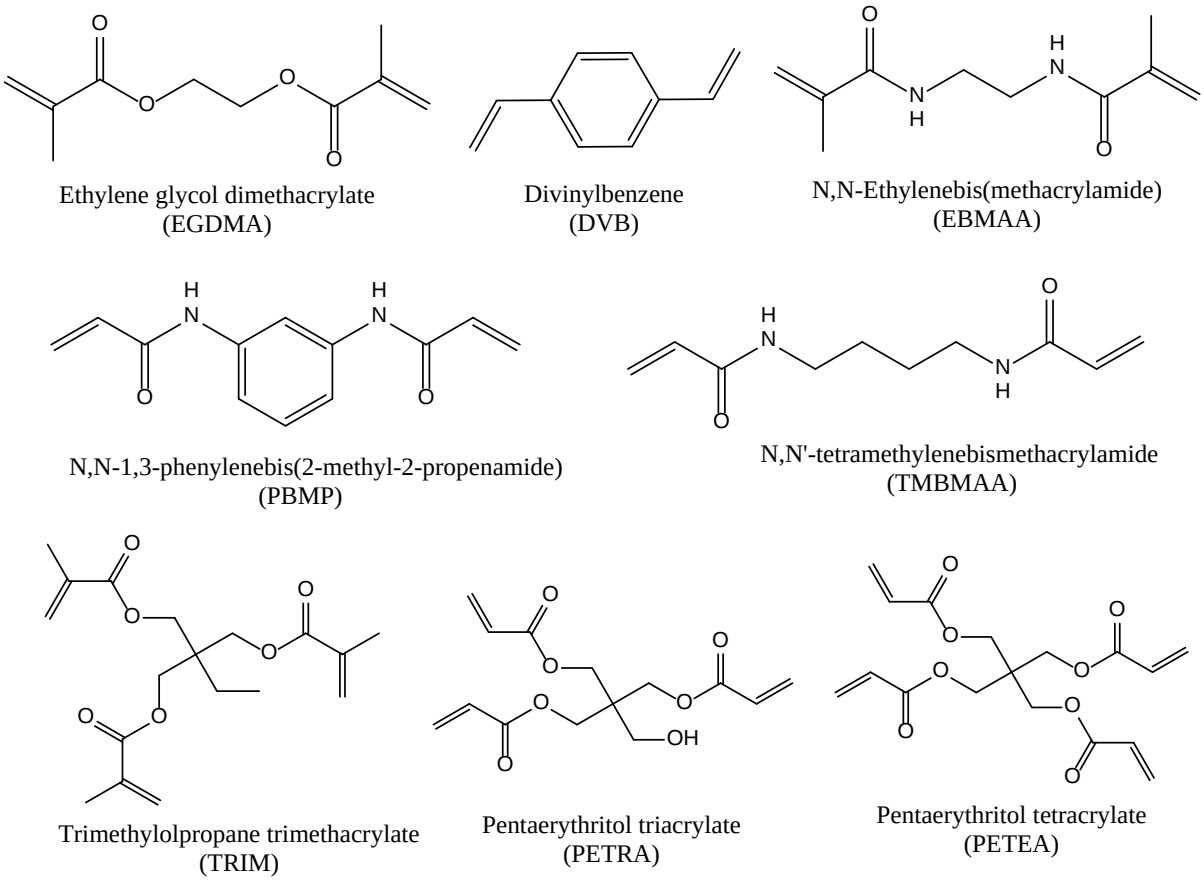

Figure 1.8. Structure of the most common cross-linkers used for molecular imprinting.

1.3.4 Solvents (porogens)

The synthesis of MIPs is conducted within an organic solvent which has the role of both solubilizing the pre-polymerization components and creating pores within the MIP structure necessary for access of targets to internal binding sites [29]. Formation of the pores and resultant pore size is dependent on solvent strength [68].

In the pre-polymerization mixture the monomers are completely soluble and early polymer growth continues in solution as a dispersion of highly cross-linked oligomers. The oligomers then grow and aggregate to form microspheres and larger clusters which, at a certain size, dependent on solvent strength, separate from the solvent. As the polymer dispersion precipitates, solvent rich domains are captured within the polymer structure, resulting in the formation of the pores. In a weakly solubilizing media, phase separation occurs early in polymerization and leads to the formation of larger pores sizes, whereas, in highly solubilizing media, phase separation occurs later and leads to the formation of smaller pore sizes [69]. Importantly, MIPs prepared in the absence of solvent lack porosity and have low selectivities [29].

The solvent can also have a significant effect on the stability of functional monomer interactions with the template in the pre-polymerization mixture. Highly polar solvents tend to destabilize polar non-covalent interactions, particularly protic solvents, which afford a high degree of disruption to hydrogen bond interactions [29]. On the other hand, highly polar and protic solvents can stabilize π-π stacking interactions between non-polar molecules, such as a chlorinated benzene template and an aromatic functional monomer, by solvophobic effects [70]. In addition, solvent polarization can stabilize molecular charges and dipoles of the functional monomer and template and result in stronger dipole interactions [71].

In the development of a MIP synthetic procedure, a compromise must be made between the stabilization of functional monomer interactions with the template and the solubility of the pre-polymerization mixture. These considerations usually result in the selection of a solvent from a small list of commonly used solvents consisting of chloroform ($CHCl_3$), acetonitrile (MeCN), dichloromethane (DCM), toluene and tetrahydrofuran (THF) [22].

1.3.5 Initiators

Many chemical initiators with different chemical properties can be used as the radical source in free radical polymerization (Figure 1.9). Normally they are used at low levels compared to the monomer, e.g. 1 wt. %, or 1 mol. % with respect to the total number of moles of polymerisable double bonds. The rate and mode of decomposition of an initiator to radicals can be triggered and controlled in a number of ways, including heat, light and by chemical/electrochemical means, depending upon its chemical nature. For example, the

azoinitiator azobisisobutyronitrile (AIBN) can be conveniently decomposed by photolysis (UV) or thermolysis to give stabilized, carbon-centred radicals capable of initiating the growth of a number of vinyl monomers. As an illustrative example of the use of AIBN, this initiator can polymerize methylmethacrylate under thermal or photochemical conditions to give poly (methyl methacrylate). Oxygen gas retards free radical polymerizations, thus in order to maximize the rates of monomer propagation, ensure good batch-to-batch reproducibility of polymerizations, removal of the dissolved oxygen from monomer solutions immediately prior to the polymerization is advisable. Removal of dissolved oxygen can be achieved simply by ultrasonication or by sparging of the monomer solution by an inert gas, e.g. nitrogen or argon.

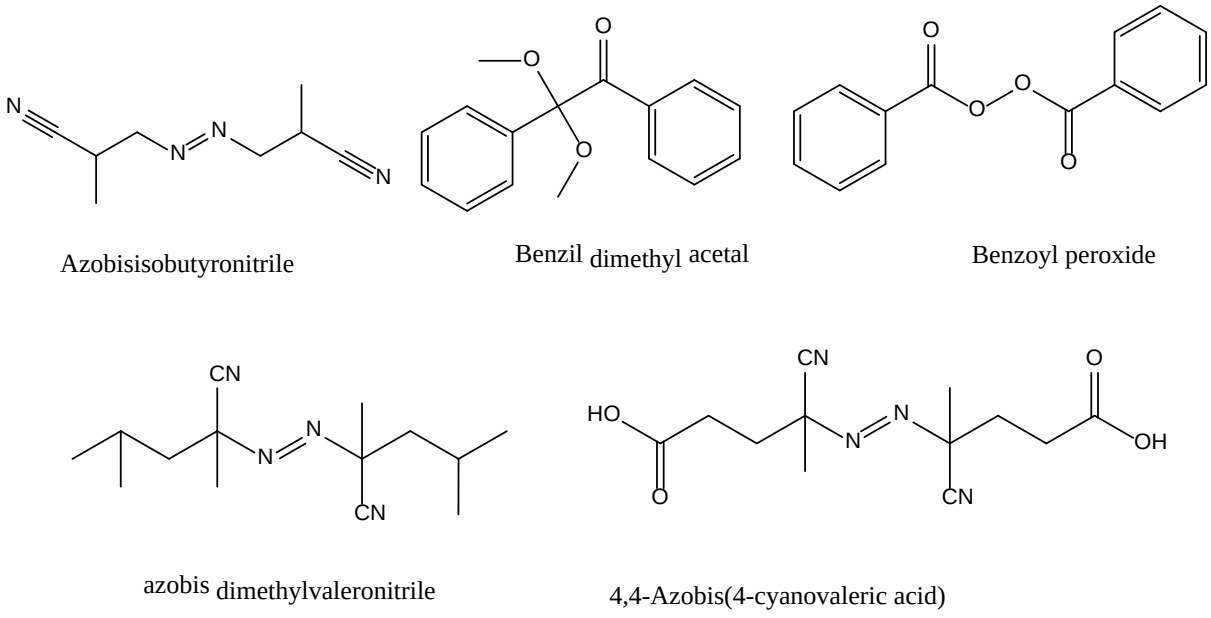

Figure 1.9. Chemical structure of common initiators used in molecular imprinting.

1.3.6 General polymerization procedures

The vast majority of monomers, especially liquid monomers, are normally supplied with polymerization inhibitor present to suppress on-shelf polymerization. Whilst it is certainly possible to polymerize monomer in the presence of inhibitor, especially when the levels of inhibitor are low and/or higher levels of polymerization initiator are present, to ensure good batch-to-batch reproducibility of experiments, both in house and inter-laboratory, it is probably advisable to remove the polymerization inhibitors from monomers, often in series

with a second purification step, e.g. distillation. Such purifications are often straight-forward to perform, with many rigorous literature procedures being readily available [72].

Oxygen gas retards free radical polymerizations, thus in order to maximize the rates of monomer propagation and to, once again, ensure good batch-to-batch reproducibility of polymerizations, removal of the dissolved oxygen from monomer solutions immediately prior to polymerization is advisable. Removal of dissolved oxygen can be achieved simply by ultrasonication or by sparging of the monomer solution by an inert gas, e.g. nitrogen or argon. If more rigorous degassing of monomer solutions is required, for whatever reason, then the method of freeze-pump-thaw comes into its own.

The majority of MIPs have been prepared via the free radial polymerization of vinyl monomers. Radical polymerization conditions are favored because they are mild, can utilize a large pool of commercially available monomers, and are compatible with most functional groups. This last attribute enables the use of monomers containing polar, aromatic, acidic, basic, and charged recognition groups. Polymerizations are carried out with 1 to 5% of a radical initiator such as 2,2-azobisisobutyronitrile (AIBN) or azo-bis-dimethylvaleronitrile (ABDV). Both thermal and UV-irradiation polymerization conditions have been used. The thermal irradiation conditions are more general and can be applied to a broader array of monomers, crosslinkers, and templates and yield more uniform polymers. UV-irradiation conditions can be carried out at lower temperatures, which are more favorable for the non-covalent imprinting conditions. MIPs have also been prepared using other polymerization methods. The largest and most successful of these are the imprinted sol- gels [73, 74]. MIPs have also been prepared using electropolymerization[75], condensation[76], step-growth[77], and metathesis polymerizations [78].

1.4 Living radical polymerization and MIPs

Radical polymerization is one of the most versatile chemical reactions as it allows for the conversion of a wide variety of vinyl monomers into polymeric materials. The extremely high reactivity of the radicals provides great versatility and tolerance of a wide variety of functional groups during polymerization allowing for the use of a broad spectrum of monomers and additives at various reaction conditions [79, 80]. Unfortunately, this high

reactivity also results in a large number of undesirable side reactions resulting in significant branching as well as a loss of control of the molecular weight and tacticity of the polymer[81, 82]. Living radical polymerization (LRP) promises better control over these parameters[83].

1.4.1 MIPs synthesis by free radical polymerization

Free radical polymerization is the most popular and general method to prepare MIPs due to its attractive properties, such as rapidity and simplicity in preparation, with no requirement for sophisticated or expensive instrumentation, and purity in the produced MIPs [79]. Vinyl based starting materials (monomers and cross-linkers) are used and the polymerization involves three principle steps; initiation to activate the monomers, propagation or growth of the active chain by sequential addition of monomers, and termination of active chain to form the final polymer chains. In practice, the initial step plays the most important role and can affect the overall success of the synthesis of MIPs as optical sensing receptor. External initiator is usually added to activate the polymerization process either by thermal or radiation process and the reactor is usually sealed under inert gas to avoid termination of the radical species. As a result, proper consideration must be given in ensuring a suitable reactor for such type of polymerization technique was available before MIPs can be produced. More advanced settings are required if the final formation of MIPs is to be in a given form such as thin layer, microbeads, nanorods, etc.

However, the monolithic polymer obtained by bulk polymerization has to be crushed, ground and sieved to an appropriate size, which is time-consuming and would reduce polymer yield (only 30–40% of polymer recovered as usable material). In addition, grinding operation results in irregular particles in shape and size, and some high affinity binding sites are destroyed and changed into low affinity sites. Bulk polymerization yields polymers with a heterogeneous binding site distribution which thus greatly confines the use of MIPs as chromatographic adsorbents [84].

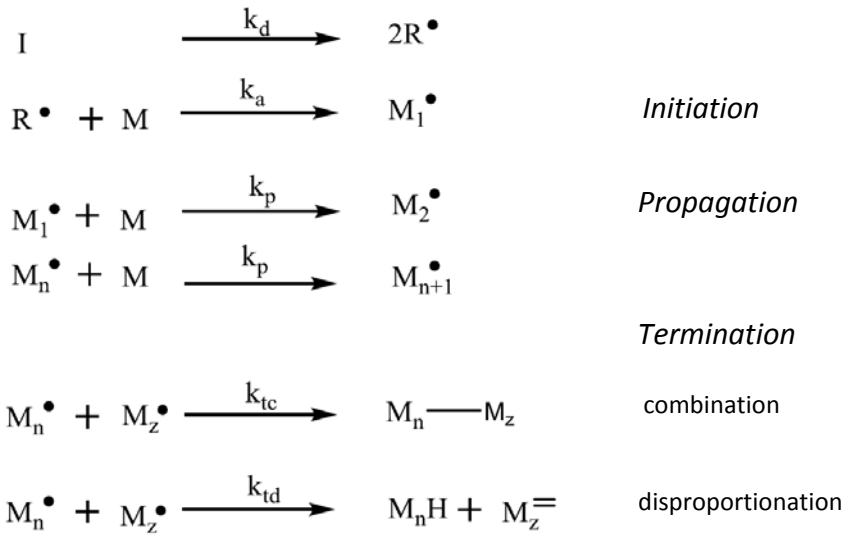

Figure 1.10. Schematic representation of free radical polymerization.

1.4.2 Limitation of free radical polymerization at MIPs

This method is the most popular since it is simple; nevertheless, crushing, grinding and sieving to obtain the appropriate particle sizes is tedious and time-consuming and often produces particles that are irregular in size and shape. In addition, some interaction sites are destroyed during grinding, reducing the MIP loading capacity and, since only a portion of the original polymer is used, this method suffers from high consumption of the template molecules [85]. Furthermore, another drawback to conventional FRP is the lack of control over chain propagation and termination because of the very high reactivity of the radicals. This results in the formation of polymer networks with heterogeneous structures with various imperfections, like primary and secondary cycles, and pendant double bonds [86]. The presence of heterogeneity within the network structures of imprinted polymers affects the quality of the binding sites formed within the networks and results in a broad distribution of binding sites with large proportions of low affinity sites and low overall capacity. Living/controlled radical polymerization (LRP) techniques offer the ability to create improved imprinted polymers with more homogeneous network structures and, as a result, better binding parameters. In addition, using LRP can lead to more control over network structures and a better understanding of their structure-property relationships; however, these

reactions are relatively new to the imprinting field and have not been used extensively in molecular imprinting.

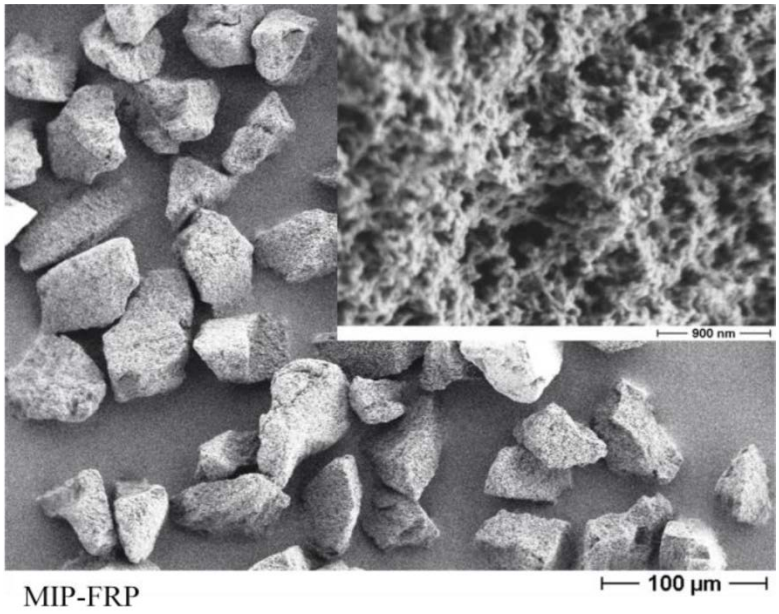

Figure 1.11. Irregularly shaped particles resulting from mechanical grinding of a "traditional" molecularly imprinted polymer (MIP-FRP).

1.4.3 MIPs synthesis by controlled radical polymerization

Living radical polymerization (LRP) offers the ability to control molecular weight, polydispersity, and tacticity while reducing microgel formation in polymers created via free-radical polymerization (FRP). The improved network architecture of polymers created via LRP has great potential, especially when considering imprinted networks which have traditionally been plagued by heterogeneity in network morphology and binding affinities. Using LRP can considerably improve template recognition and further delay template transport in imprinted polymers.

1.4.3.1 Iniferter polymerization

Otsu proposed a pseudo-living polymerization method based on the use of iniferters (standing for initiator-transfer agent-terminator) [87-89]. This first example of controlled radical polymerization (CRP) consists in the dissociation of dithiocarbamates into an initiating alkyl

radical and a second radical species that is stabilized and not capable of initiating a new polymer chain. When the energy supply to the reaction in the form of heat or UV irradiation ceases, the two radicals recombine and the chain growth stops. The system can later be re-initiated with the same or other monomers, thus providing some degree of living character.

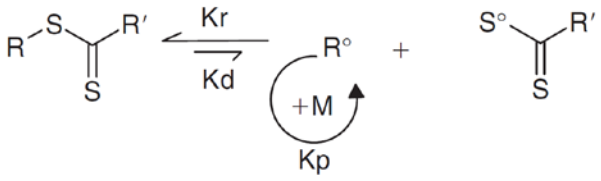

Figure 1.12. General mechanism of iniferter polymerization.

Considering iniferter-initiated polymerization, this allows for a control of the molecular weight that is not as good compared with the other CRP methods. This method was mainly used to achieve the synthesis of thin MIP films on supports by surface-initiation. In the context of MIPs, it has the advantage, though, of being compatible with the majority of functional monomers commonly used. Kobayashi and coworkers[90] were the first to use this CRP method for molecular imprinting. They reported photografting an MIP layer on a polyacrylonitrile membrane modified with a diethyldithiocarbamate iniferter.

Sellergren and coworkers [91] reported the L-phenylalanine anilide (L-PA) imprinted polymer via iniferter-modified supports. They used porous silica (DP ~ 100 nm) and gel-type or macroporous (12% nominal crosslinking density) Merrifield resins were modified with iniferter groups for grafting of crosslinked molecularly imprinted or non-imprinted polymer layers through iniferter polymerization. They explored that the nature of the support material is of crucial importance for successful grafting of molecularly imprinted polymer layers. Whereas templated sites appeared to be absent in composites prepared from polystyrene-based support materials, silica based grafts were more successful in this regard. Compared to the system based on immobilized azoinitiators, these systems exhibit the advantage that no or minimal propagation occurs in solution. This may open the way for continuous methods for the production of MIPs in beaded form. The living nature of the iniferter grafts may offer the additional possibility of consecutive grafting of multiple polymer layers [92].

1.4.3.2 Nitroxide mediated polymerization (NMP)

Nitroxide-mediated radical polymerization (NMP), also referred as stable free radical polymerization (SFRP), is one of the versatile methods for the controlled/living polymerizations. NMP is generally based on the use of nitroxyl radicals (nitroxides) or alkoxyamines. Solomon and Rizzardo [93, 94] and Moad and Rizzardo [95] first used alkoxyamines for the polymerization of various vinyl monomers. However, only low molecular weight polymers were obtained. Later Georges et al. [96] showed that high molecular weight polystyrene (Mn> 50,000) with low polydispersity (<1.5) could be prepared using benzoyl peroxide (BPO) and a nitroxyl radical such as 2,2,6,6-tetramethyl-1-piperidinyloxy (TEMPO).

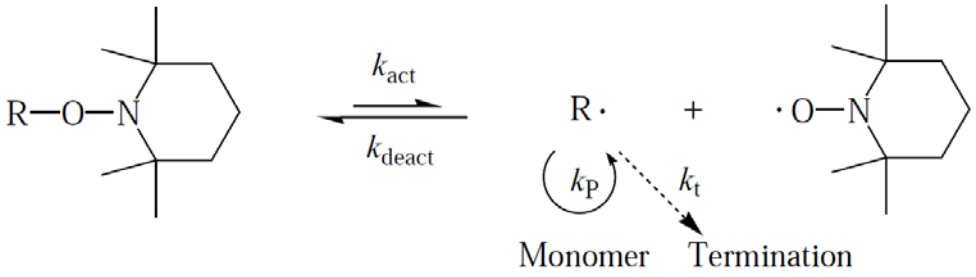

Figure 1.13. Mechanism of Nitroxide Mediated Polymerization (NMP).

Boonpangrak et al. [97] used sacrificial covalent imprinting and nitroxide-mediated LRP (NMP) to produce cholesterol imprinted polymers at a relatively high temperature of 125 ^{o}C with divinyl benzene as the crosslinker. They found that compared to MIPs prepared under the same condition using a traditional radical initiator, template cleavage from the covalently imprinted NMP polymer was much more efficient. The imprinted hydrolyzed polymer prepared by NMP also displayed an imprinting effect that was clearly superior to that obtained using traditional radical polymerization, particularly for the high affinity sites that were easily characterized by radioligand binding analysis.

Byrne and coworkers used non-covalent molecular imprinting based primarily on multiple hydrogen bonds to produce highly crosslinked polymer networks via UV FRP and iniferter controlled LRP reaction at 0 ^{o}C [98]. Imprinted polymers prepared using LRP demonstrated a 63% increase in binding capacities as compared to the corresponding polymers prepared via conventional FRP while retaining the average binding affinity and selectivity for the template molecule.

1.4.3.3 Atom transfer radical polymerization (ATRP)

Since its first discovery in 1995 [99-101], ATRP has drawn significant attention from both academic and industrial communities due to its versatility in the synthesis of polymers with predictable molecular weights, low dispersities and specific functionalities, the easy availability of many kinds of initiators and catalysts, and its general applicability for a wide range of monomers (such as (meth)acrylates, styrene and its derivatives, 2,4-vinylpyridine, acrylamides, and so on) [102, 103]. In a controlled ATRP system, a fast, dynamic equilibrium is established between the dormant species (e.g., alkyl halides) and active species (radicals), with transition metal complexes acting as reversible halogen atom transfer reagents (Figure 1.14), which keeps a very low radical concentration in the system and leads to negligible radical termination and controlled polymerization [104, 105].

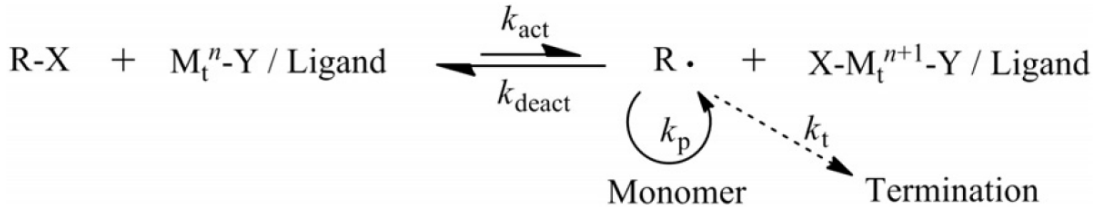

Figure 1.14. Mechanism of ATRP.

According to their different initiating species used, two kinds of ATRP processes are available, which are normal ATRP and reverse ATRP, respectively [106]. In the normal ATRP system, the initiating radicals stem from the reaction between an alkyl halide (or arenesulfonyl halide) and a transition metal complex in its lower oxidation state [e.g., Cu(I)/ligand]; while in the reverse ATRP system, a conventional radical initiator (e.g., AIBN) is used to generate primary radicals in the beginning of the polymerization, which are then deactivated by a transition metal complex in its higher oxidation state [e.g., Cu(II)/ligand]. In both systems, the equilibrium between the dormant species and active radicals can be quickly established soon after the polymerization starts.

The process can be applied to a wide range of monomers and at mild reaction, though it must be said that traces of oxygen can have a much more dramatic effect on the reaction rate than in a conventional radical polymerization. A further drawback, restricting industrial

application, is the presence of considerable amounts of metal in the product. Nonetheless, numerous well-defined complex polymer architectures have been prepared with ATRP [107].

With ATRP, the major limitation for this technique in the context of MIP synthesis is the small choice of monomers with suitable functional groups. Typical monomers used for molecular imprinting such as methacrylic acid and trifluoromethyl acrylic acid are incompatible, and with methacrylamide [108] and vinylpyridine [109], it is difficult to achieve high monomer conversion with the metal-ligand complex involved in ATRP. Template molecules also often carry functional groups that may inhibit the catalyst. Thus, the difficulty of obtaining high conversion in the presence of certain functional groups on monomer and template seems to make ATRP not the best choice for molecular imprinting.

Nevertheless, Wei et al. [110] describe the use of surface-confined ATRP to create imprinted polymer films with controlled thickness on a gold substrate, using 2-vinylpyridine as the functional monomer, ethylene glycol dimethacrylate as the cross-linker, and the fluorescent template didansyl-L-lysine. A linear increase in thickness was observed over time, and 15 nm-thick polymer films were obtained in 20 h at room temperature. When the adsorption properties of these films were studied using fluorescence measurements, an imprinting effect was observed, as the adsorption capacity and the association constant of the didansyl-L-lysine template on the MIP film were approximately two times higher than those measured with the non-imprinted control polymer film. In addition, another amino acid derivative, didansyl-L-cystine, adsorbed less well to the didansyl-L-lysine- MIP compared with the original template.

1.4.3.4 Reversible addition fragmentation chain transfer polymerization (RAFT)

The RAFT process was invented at the Commonwealth Scientific and Industrial Research Organization (CSIRO) in 1998 and became one of the most convenient and versatile techniques for preparing living polymers with low polydispersity and predictable molecular weights [111-113].

In recent years RAFT polymerization has emerged as a very attractive method for producing pseudo living free radical polymerizations [114, 115]. Its main potential lies in its versatility towards the types of monomers it can polymerize, including styrenic, (meth)acrylamides,

(meth)acrylates, acrylonitrile, vinyl acetates, vinyl formamide, vinyl chlorides as well as a range of other vinyl monomers [116]. Another advantage of the RAFT process is that it is carried out in the same conditions as a classic free radical polymerization except with the addition of a chain transfer agent (CTA) also referred to as a RAFT agent. As a result, RAFT polymerizations have been carried out in bulk, aqueous solutions, organic solutions, suspensions, emulsions, mini and micro emulsions, and ionic liquids and can be carried out at low temperatures [117, 118]. In addition to simple homopolymers, a large variety of macromolecular structures have been synthesized via RAFT including statistical, block, multiblock, gradient, and comb copolymers, telechelic (co)polymers, star, hyperbranched, and network (co)polymers [119, 120].

The RAFT process utilizes classic free radical initiators and monomers but also includes the presence of a CTA. These RAFT agents are most commonly dithioesters with the general structure shown in Figure 1.15.

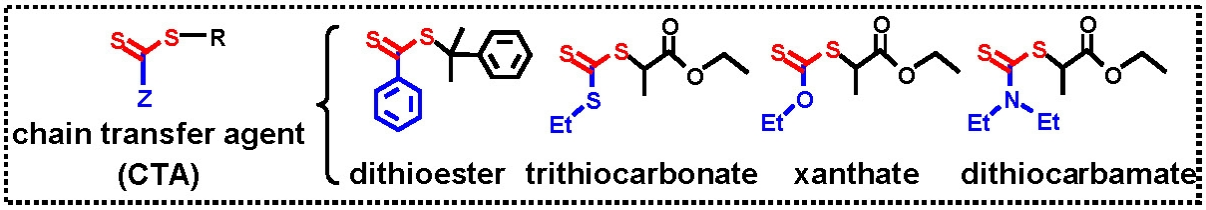

Figure 1.15. General form of RAFT chain transfer agents.

The Z group serves to activate or deactivate the reactivity of the C=S bond towards addition. The R group must form a stable free radical. A wide variety of RAFT agents bearing different Z and R groups have been synthesized and evaluated relative to their effectiveness in mediating the polymerization of vinyl monomers [121, 122]. Effective RAFT agents include: dithiobenzoates, dithioacetates, dithiocarbonates (xanthates), and trithiocarbonates. Some of the more versatile RAFT agents are 4-cyanopentanoic acid dithiobenzoate and carboxyl-terminated trithiocarbonate that were used in my experiments.

Upon completion of a RAFT polymerization the vast majority of chains will possess a thiocarbonylthio end-group, with the overall process able to be viewed as an insertion of monomer units between the S-R bond of the RAFT agent 1 (Figure 1.16) to give a polymer 2. The largely conserved RAFT end-group of 2, itself a macro-RAFT agent, facilitates the synthesis of block copolymers through the subsequent polymerization of a second monomer.

Additionally the thiocarbonylthio group provides a functional handle for a variety of post-polymerization modifications [123, 124].

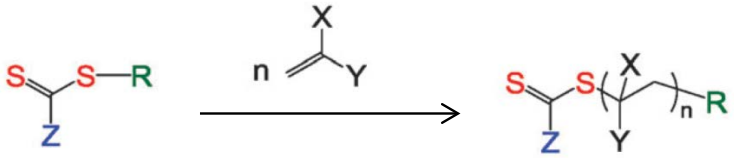

1 2

Figure 1.16. The overall outcome of the RAFT process.

The generally accepted mechanism of synthesis of homopolymer (macroRAFT agent) via the RAFT process is described in Figure 1.17. This process is highlighted by five distinct steps:

Initiation: involves in the release of free radicals from typical azo or peroxy initiators into the reaction system and the reaction of the initiator-derived radicals with monomers.

Chain transfer: the propagating polymeric chain adds to the reactive C=S bond of the chain transfer agent (CTA) to form intermediate radicals. These radicals can then fragment reversibly to produce a macroCTA and the re-initiating group R·.

Reinitiation: the released R· radical can reinitiate the polymerization by reacting with monomer and starting a new polymer chain which will propagate or react back on the macro-CTA. When the initial CTA is completely consumed, the polymerization system is controlled by the presence of macro-CTA.

Chain equilibrium: this step involves the exchange of active and dormant thiocarbonylthio capped chains. Each potential macroradical has equal probability of undergoing chain growth, promoting homogenous chain growth to yield a low PDI.

Termination: the polymerization is terminated via combination or disproportionation inherent to the free-radical polymerization processes. The majority of the polymer product (>90%) consists of polymeric chains with the reinitiating R group and thiocarbonyl thio groups at either end of the polymeric chain.

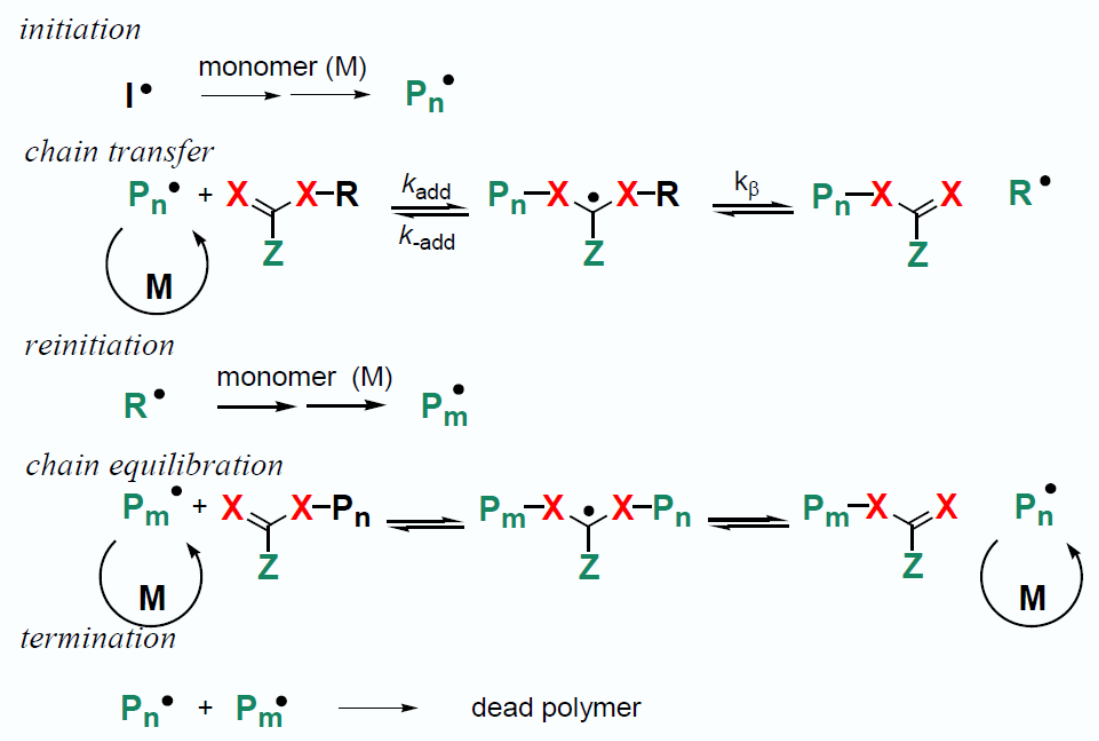

Figure 1.17. Mechanism of RAFT polymerization. (adapted from[125])

In conclusion, RAFT is arguably the most promising among the CRP methods to employ in MIP systems. Titirici and Sellergren [126] demonstrated the ability to successfully graft cross-linked l-phenylalanine anilide imprinted films onto mesoporous silica beads using RAFT polymerization. They reported that the use of RAFT polymerization offered better control of the grafting process resulting in lower solution polymerization, lower gelation, and a lack of particle agglomeration.

Xu et al. [127] combined RAFT and precipitation polymerization to create atrazine imprinted polymer microspheres for recovering atrazine from food matrices. They used MAA as the primary functional monomer for the atrazine template, EGDMA as the crosslinker and acetonitrile as the porogen. The results of equilibrium binding experiments showed that the RAFT MIP microspheres demonstrated 2.5 times higher template binding when compared to the corresponding FRP microspheres. Scatchard analysis revealed that template binding capacity and affinity were both nearly doubled simultaneously by using RAFT when compared to the corresponding FRP MIPs.

Recently, Yue et al. [128] reported the efficient synthesis of narrowly dispersed hydrophilic MIP nanoparticles with excellent specific molecular-recognition ability in real aqueous

solutions, including river water and biological samples. They used RAFT precipitation polymerization and provided for the first time narrowly dispersed highly cross-linked MIP nanoparticles with surface-grafted hydrophilic polymer brushes in a facile one-pot approach. The hydrophilic polymer brushes on the MIP nanoparticles not only significantly improved their surface hydrophilicity and led to their water compatibility, but they also acted as a protective layer to prevent proteins in the biological samples from accumulating on the nanoparticle surface and blocking the imprinting sites [129, 130] and thus enabled the MIP nanoparticles to function properly in such complex matrices.

1.4.4 Surface-initiated controlled radical polymerization and MIPs

Polymers grafted densely onto solid substrates (polymer brushes) have attracted much attention in the recent past as a novel method to modify surfaces owing to its potential applications in lithography, corrosion resistance, drug delivery, increased bio-compatibility of materials, biosensor, etc. [131, 132]. Different techniques have been used to generate polymer brushes for instance: conventional free radical polymerization, ring-opening metathesis polymerization, living anionic and cationic polymerization and controlled/living radical polymerization. To achieve a better control of molecular weight and molecular weight distribution and to synthesis block copolymer brushes, researchers have used controlled/living radical polymerization methods to make brushes. Numerous recent reports describe the use of living radical polymerization techniques to grow polymer chains from surfaces in a well-defined manner [130, 133, 134].

Thanks to the robustness and versatility of controlled radical polymerization (CRP), this surface-modification technique has been applied to many types of substrates [106, 132]. Spherical fine particles have been surface-modified via surface-initiated controlled radical polymerization (SI-CRP) in conjunction with various methods for initiator fixation, depending on the characteristics of the particle surfaces [133, 134].

The tethering of the polymer to the surface is generally performed either through physical adsorption or covalent attachment. Covalent attachment is often preferred due to the inherent resistance to degradation by temperature and solvents [131]. Covalent attachment of polymer brushes can be achieved by either *"grafting to"* or *"grafting from"* techniques (Figure 1.18). The "grafting to" technique employs a preformed polymer with a reactive endgroup to attach

the polymer chain onto the substrate (common reactive functional groups include thiols, silanes, amino or carboxylic groups). The “grafting to” technique usually involves low grafting densities due to steric repulsion between the already grafted chains and the incoming macromolecular units from solution that in turn preclude the access of new polymer chains to grafting sites on the surface. This effect is more pronounced when dealing with high molecular weight polymer chains. Conversely, in the “grafting from” strategy, polymer chains are straightforwardly synthesized from a substrate previously modified with polymerization initiators, the so-called “surface-initiated polymerization” in which polymerization occurs exclusively at the surface. Because the diffusion of monomer is not strongly hindered by the existing grafted polymer chains, this technique is more promising to achieve high graft densities [135].

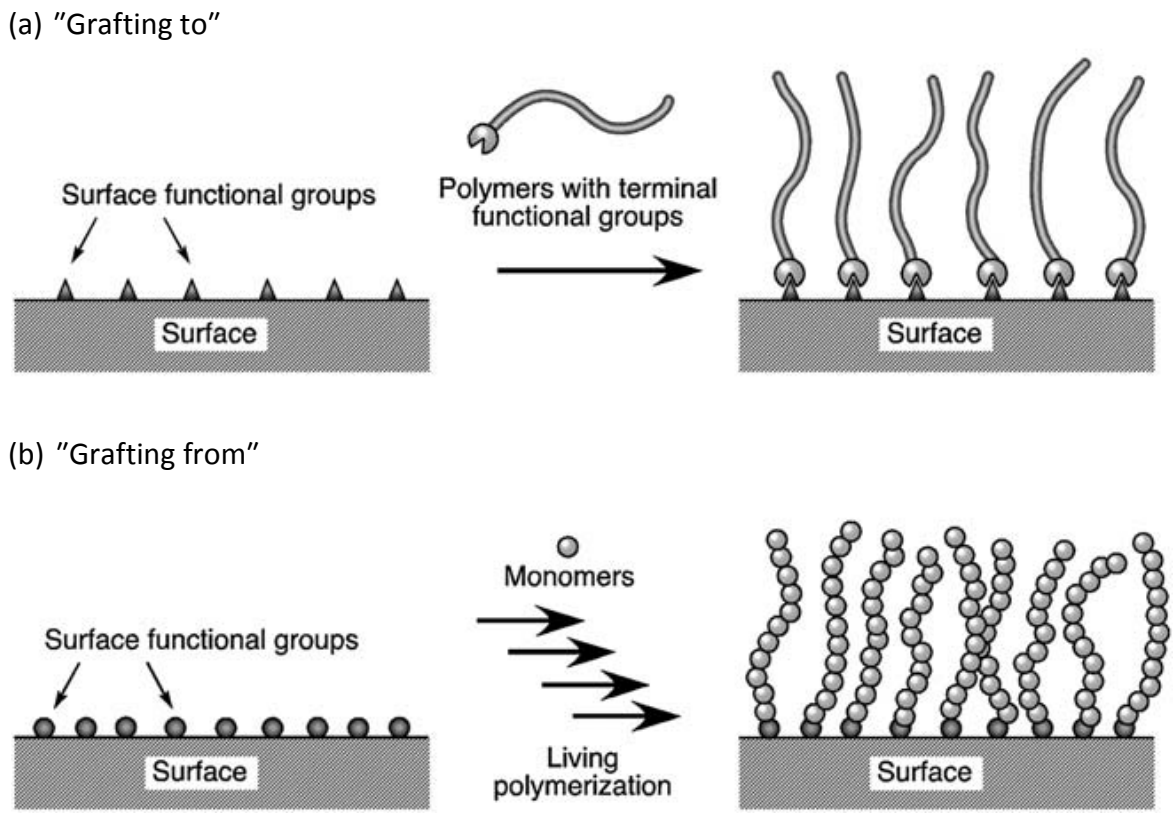

Figure 1.18. Schematic illustrations of (a) “grafting to” and (b) “grafting from” methodologies. (adapted from[136])

All known types of the surface-initiated controlled radical polymerization techniques have been utilized for preparing molecularly imprinted polymers onto different supports. The polymerization methods that have been employed are surface-initiated iniferter-mediated polymerization (SI-IMP), surface-initiated nitroxide mediated radical polymerization (SI-

NMP), surface-initiated atom transfer radical polymerization (SI-ATRP) and surface-initiated reversible addition fragmentation chain transfer polymerization (SI-RAFT). Many research papers have been published on the preparation of imprinted materials by surface-initiated controlled radical polymerization (Table1.2).

Table1.2. MIPs prepared by the surface-initiated controlled radical polymerization techniques.

Support	***Analyte***	***CRP method***	***Application***	***References***
Silica particles	Bovine milk	Iniferter	HPLC	[137]
Polystyrene beads	Glutathione	Iniferter	Separation	[138]
Silica particles	Sulfamethazine	Iniferter	HPLC	[139]
Silica particles	Thiabendazole	Iniferter	HPLC	[140]
Polystyrene beads	Lysozyme	Iniferter	Separation	[141]
Polystyrene beads, Silica particles	L/D- phenylalanine anilide	Iniferter	Chiral separation	[91, 92]
Flat surfaces	Theophylline	Iniferter	Separation	[142]
Carbon nanotubes	Theophylline	Iniferter	Biosensor	[143]
Silica particles	Lysozme	ATRP	Separation	[144]
Silica particles	protein	ATRP	separation	[145]
Silica particles	L-phenylalanine	ATRP	HPLC	[146]
Silica particles	Benzoic-acid	ATRP	Thermo-responsive LC	[147]
Graphite oxide	Propionamide	ATRP	separations	[148]
Silica particles	L-phenylalanine anilide	RAFT	separation	[126]
Silica particles	Dichlorophenoxyacetic acid	RAFT	separation	[149]
Fe_3O_4 NPs	Cholesterol	RAFT	separation	[150]
Silica particles	Theophylline	RAFT	SPE	[151]
Silica particles	2,4-dichlorophenol	RAFT	separation	[152]
Fe_3O_4 NPs	S-propranolol	RAFT	separation	[153]

1.4.4.1 MIPs via surface-initiated iniferter polymerization

The iniferter method for surface grafting of MIPs has been used for imprinting different templates and for different applications (e.g., solid-phase extraction (SPE) and chiral separation) [91, 92, 139, 140, 154]. As a kind of CRP, the iniferter technique has special advantages in making surface-modified materials. Polymerization in solution can be avoided by attaching the iniferter onto the support surface, because the active radicals remain bound to the surface whereas non-active radicals are in solution [92]. Meanwhile, block polymers with different properties can be grafted and the polymer layer thickness is more controllable. Using benzyl N,N-diethyldithiocarbamate as the iniferter, the polymerization can be initiated by UV irradiation, which is advantageous in MIP preparation because the template/monomer complexes are stable at low temperatures.

Yoshimi and colleagues grafted theophylline-imprinted MIP films onto cellulose membranes by photo-iniferter-induced living radical polymerization [142]. The results showed that the amount of the grafted MIP films could be easily controlled by tuning the UV irradiation time and the number of polymerization cycles. Moreover, they also showed obvious gate effect toward the template.

Sellergren and co-workers were the first to use iniferter-modified spherical silica/polymer particles for surface-grafting of MIP layers (Figure 1.19) [91]. The porous spherical silica particles and gel type or macroporous Merrifield resins were firstly modified with dithiocarbamate groups and subsequently used for the surface grafting of MIP layers by photo-iniferter-induced living radical polymerization. The MIP-grafted silica exhibited enantioselectivity for chromatographic separations. The additional possibility of consecutively grafting multiple MIP layers due to the living character of the iniferter polymerization was also demonstrated by the same group [92].

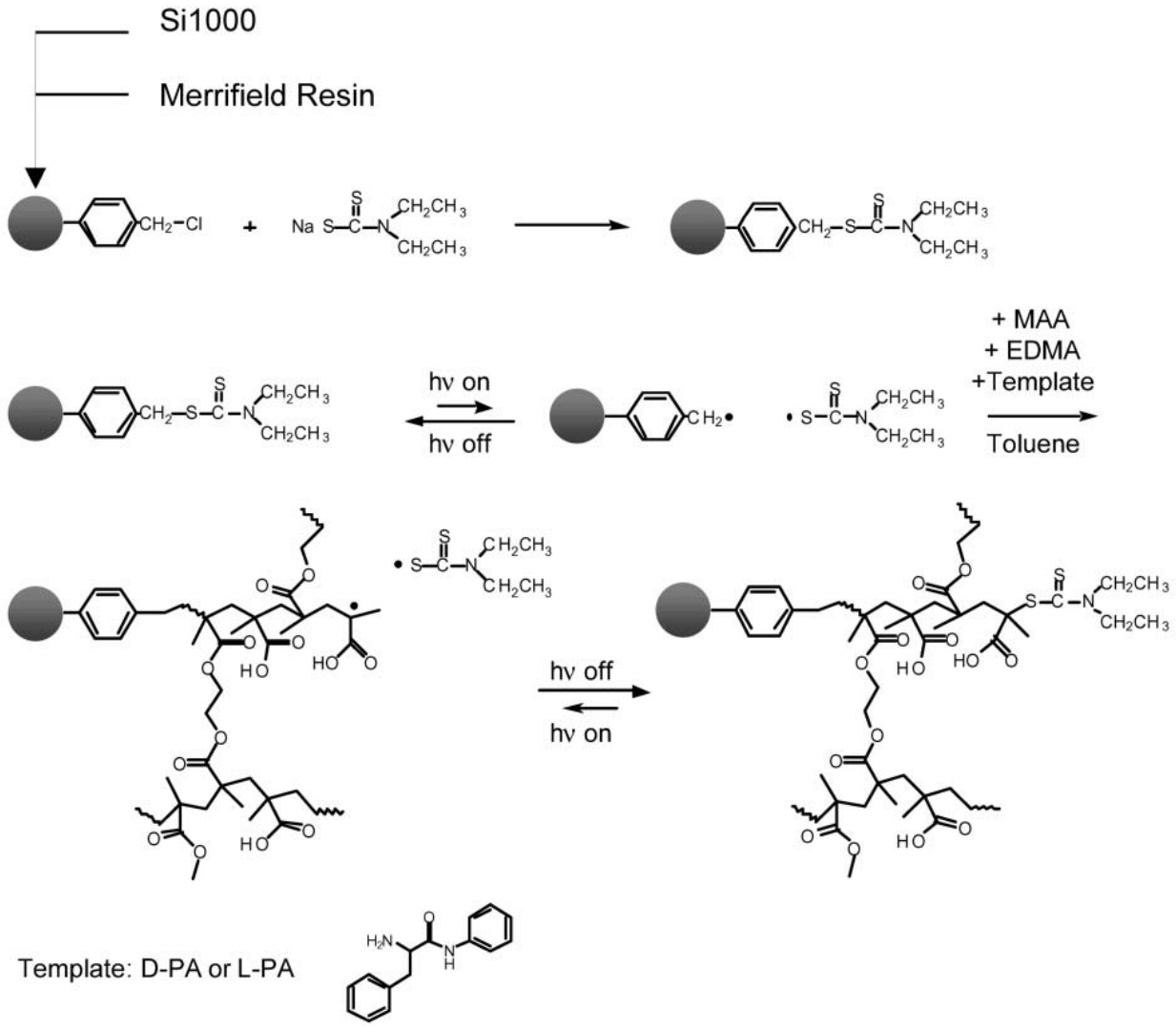

Figure 1.19. Surface-grafting of MIP layers on the spherical particles by photo-iniferter-induced living radical polymerization.(adapted from[91])

Dong et al. reported a novel restricted access-molecularly imprinted material with selectivity for sulfonamides by using surface-initiated iniferter method [137]. The material was prepared by grafting two layers with different functions on the silica support. The result has shown that this restricted access-MIP grafted silica not only has the selectivity for the template and its analog, but also has the ability of exclusion for bovine serum albumin (BSA). It indicated that the material possesses both properties of molecularly imprinted polymer and restricted access material.

Recently, Song et al. proposed a simple and effective approach to synthesize uniform surface imprinted polymer microspheres via surface-initiated iniferter polymerization [138]. They used polystyrene microspheres containing iniferter as support and glutathione as template

molecules. The synthesized glutathione surface imprinted polymer microspheres showed faster mass transfer and higher binding amounts rate toward template than non-imprinted polymer.

1.4.4.2 MIPs via surface-initiated atom transfer radical polymerization (SI-ATRP)

As mentioned above the ATRP technique has some limitation in the context of the MIP preparation. For instance the small choice of monomers with suitable functional groups and effect of the template molecule on ATRP catalyst makes it difficult to use as versatile method in the MIP technology [155]. However ATRP has also been used for the preparation of surface imprinted materials. Wang and coworkers described the synthesis of the MIP nanotube membrane using a porous anodic alumina oxide (AAO) membrane by surface-initiated atom transfer radical polymerization for the selective chemical separation [156]. The imprint molecule, functional monomer, and cross- linking agent used in this study were β-estradiol, 4-vinlpyridine (4-VP), and ethylene glycol dimethacrylate (EGDMA), respectively. The results showed that the MIP nanotube membranes had an 11 fold higher binding capacity and 13 fold better imprinting effect in comparison with traditionally formed bulk MIPs for the same template molecule.

Huang and Wirth used surface-initiated APRP to graft thin polymer films of polyacrylamide onto silica for protein separation [144]. Four proteins were separated in about 4 min on a polyacrylamide-modified silica, showing good efficiency. Much longer times were required for the same protein separation using dextranbonded or diol-modified silica. The higher separation efficiency of the column prepared via ATRP was attributed to the uniformly-coated films, which left sufficient pore volumes in the silica for size-exclusion chromatography (SEC). In addition, better peak symmetry for lysozyme was obtained compared with that on Zorbax GF-250. This indicates that the adsorption caused by the silanol groups was reduced, due to better surface coverage with the polymer.

Yoshikawa et al. by the use of surface-initiated atom transfer radical polymerization, grafted a low-polydispersity poly(2-hydroxyethyl methacrylate) (PHEMA) onto the inner surfaces of silica monoliths with mesopores of about 50 and 80 nm in mean size [145]. The interaction of

the polymer brushes with proteins was then studied. They found that concentrated pHEMA brushes were better at repelling proteins and provided long-term stability against biofouling.

Ihara and co-workers reported a new polymerizable N-octadecyl-L-phenylalaninederived self-assembling monomer and its polymerization from silica surface by ATRP to produce high-density organic phase for HPLC [146]. The new monomer was polymerized from initiator-grafted silica by surface-initiated ATRP in presence of CuBr/PMDETA catalyst. Polymer chains were grown from the silica surfaces to yield individual particles composed of a silica core and a well-defined, densely grafted outer polymer layer. The resulting composite was introduced as one potential application of the polymer-coated silica particles as high-density organic stationary phase for high-performance liquid chromatography.

Poly(N-isopropylacrylamide) is a well-known thermoresponsive polymer exhibiting a reversible temperature-response in aqueous medium. For developing thermoresponsive chromatographic matrices with a strong hydrophobicity, poly(N-isopropylacrylamide-co-n-butyl methacrylate) (poly(IPAAm-co-BMA)) brush grafted silica beads was prepared by Okano et al through a surface-initiated atom transfer radical polymerization (ATRP) with a CuCl/$CuCl_2$/Me6TREN catalytic system in 2-propanol at 25 °C for 16 h [147]. The results showed that retention times of the analytes increased with the increase in BMA composition ratio. Dehydration of grafted copolymer with large BMA composition was performed at low temperature. They indicated that the copolymer-brush-grafted surface prepared by ATRP was an effective tool for separating hydrophilic analytes at low temperature through modulating the strong hydrophobic interaction.

Recently, Ji and co-workers synthesized novel acrylamide (AA) molecularly imprinted polymer by atom transfer radical polymerization (ATRP) on graphite oxide (GO) particles. Propionamide (PAM) was used as a dummy template molecule, hydroxy ethyl acrylate (HEA) as a functional monomer, ethylene glycol dimethacrylate (EDMA) as a crosslinking agent, and acetonitrile as both solvent and dispersion medium [148]. The corresponding adsorption kinetic curves and adsorption isotherms showed that the AA adsorption reached equilibrium after 5 h, with large amounts of AA being adsorped in the first 100 min. The maximum AA adsorption capacity was 123.48 μmol/g according to Scatchard analysis, which indicated that the MIP possesses good AA adsorption capacity. This MIP-GO material was used to selectively determine AA in fried food samples.

More recently, Zhao and colleagues reported the novel macroporous core-shell molecularly imprinted polymers (MIP) for selective recognition of 2,4-dichlorophenoxyacetic acid (2,4-D) which were prepared by surface initiated atom transfer radical polymerization (SI-ATRP) [157]. By using one-step swelling and polymerization method, the monodispersed macroporous poly(glycidyl methacrylate) (PGMA) particles were synthesized and used as supporting matrix for preparing surface MIP particles (PGMA@MIP). Thanks to the inner and outer surface-located binding cavities and the macroporous structure, the PGMA@MIPs revealed desirable efficiency for template removal and mass transfer, and thus excellent accessibility and affinity toward template 2,4-D. They demonstrated that this novel macroporous core-shell imprinted material may become a powerful tool for rapid and efficient enrichment and separation of target compounds from the complicated samples.

1.4.4.3 MIPs via surface-initiated reversible addition fragmentation chain transfer polymerization (SI-RAFT)

Surface-initiated RAFT polymerization has been widely utilized as an approach to produce polymer brushes with precise structural and grafting density control. Two general routes to prepare surface-grafted polymer chains can be followed, that is (a) using a surface anchored radical initiator with free CTA in solution and (b) using a surface anchored CTA with an appropriate initiation method [158]. In both cases, the polymer chains are able to grow from the surface rather than diffuse to the surface against the concentration gradient of the existing grafted polymers. Thus compared to the grafting to approach surface initiated RAFT polymerization is more promising approach to construct dense and thick polymer layers on the surface of materials.

1.4.4.3.1 Grafting-from surface-anchored initiators

The immobilization of initiators on the material surfaces can be achieved by various techniques, including chemical reaction, plasma discharge and high-energy irradiation. The subsequent polymerization from these surface-anchored initiators in the presence of free CTA can generate surface-grafted polymer chains with uniform structure and adjustable length.

An early example of SI-RAFT polymerization was reported by Baum and Brittain, who prepared 30 nm-thick PMMA brushes as well as 11 nm-thick PS and poly(N,N-dimethylacrylamide) (PDMAM) brushes from azo-functionalized silicon wafers in the presence of the chain transfer agent (CTA) 2-phenylprop-2-yl dithiobenzoate and free initiator (2,2′-azoisobutyronitrile (AIBN)) (Figure 1.20) [159]. Addition of free initiator (e.g., AIBN) was shown to facilitate polymer brush growth not only because it acts as a scavenger for possible trace amounts of impurities in the polymerization mixture but also since it increases the amount of radicals in the system, which are necessary to avoid early termination by CTA capping, as the concentration of the surface initiators is particularly low.

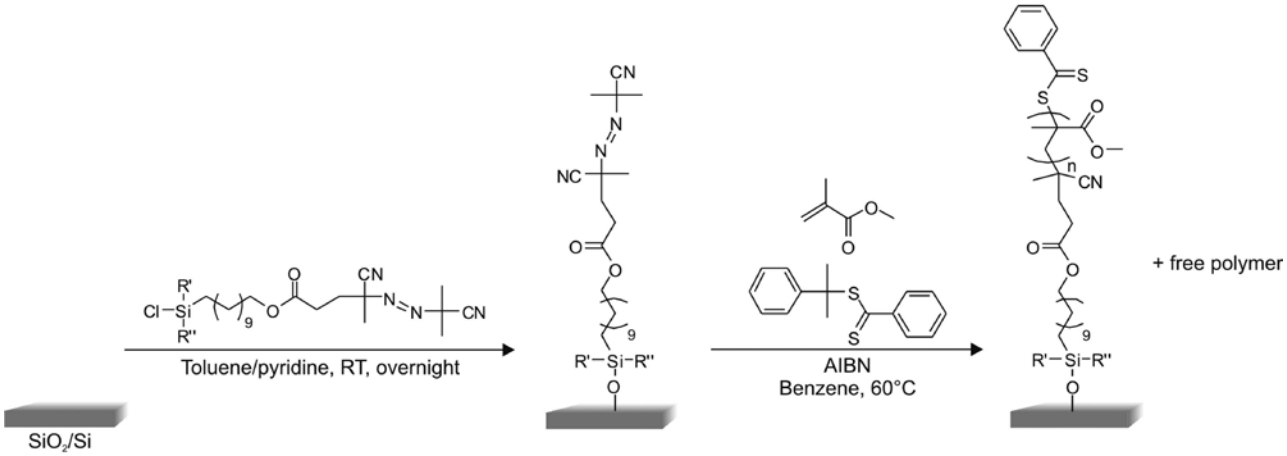

Figure 1.20. A general process of surface-initiated RAFT polymerizations from a surface-anchored azo initiator. (adapted from[159])

Titirici and Sellergren were first to introduce the surface grafted thin film MIP composite using RAFT polymerization from surface anchored azo initiator [126]. In the reaction, 2-phenylprop-2-yl-dithiobenzoate was used as the chain-transfer agent for imprinting L-phenylalanine anilide (Figure 1.21). The particles prepared via RAFT-mediated grafting appeared smooth with no agglomeration. The resulting materials could separate a racemate of phenylalanine anilide and some structural analogous within a few minutes. The materials exhibited superior mass transfer properties compared to the traditional imprinted bulk monoliths or materials prepared without the polymerization control through RAFT agents.

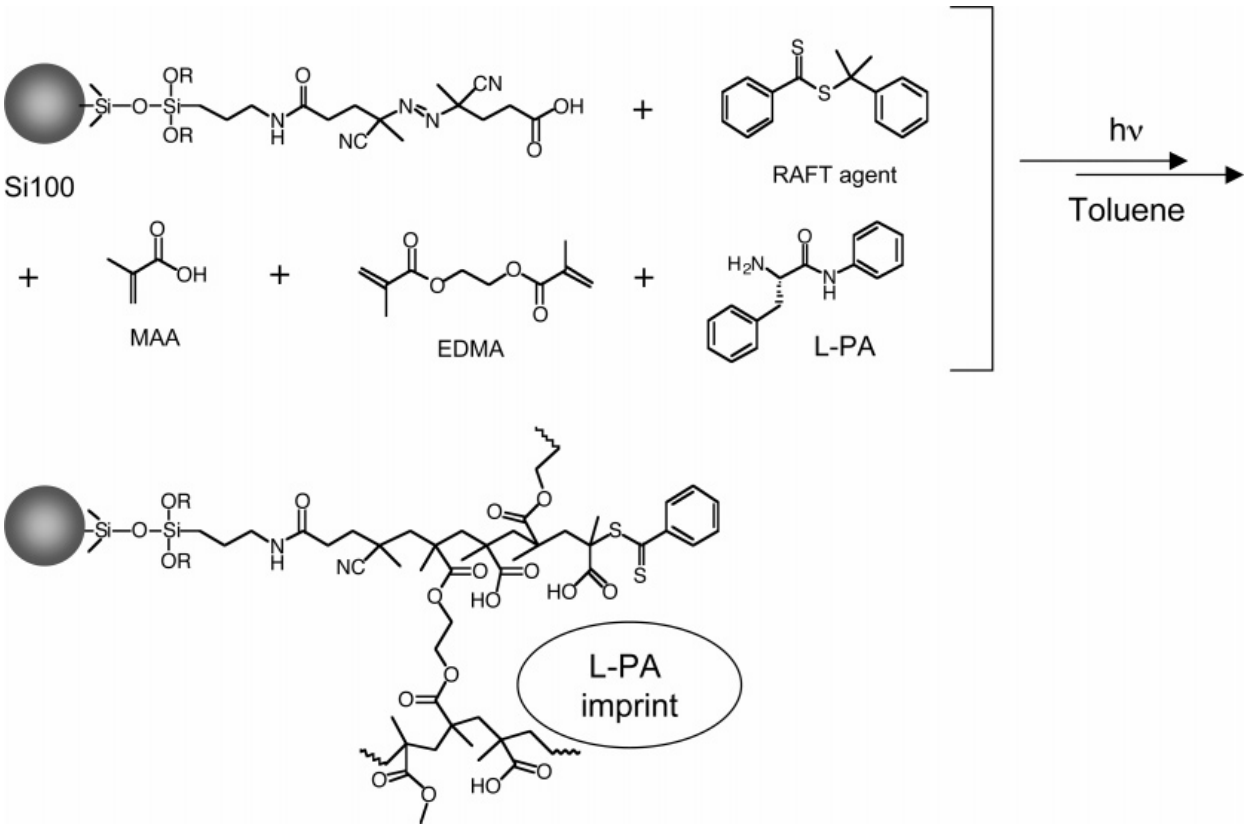

Figure 1.21. The grafting of L-phenylalanine anilide (L-PA) imprinted polymer films from porous silica supports controlled by addition of RAFT agent.(adapted from[126])

1.4.4.3.2 Grafting-from surface-anchored CTAs

An alternative way to modify the surface of materials via surface-initiated RAFT polymerization is grafting-from surface-anchored CTAs, which generally can be accomplished through either the R-group or Z-group approach (Figure 1.22). In the R-group approach, the RAFT agent is attached to the substrate surface via its leaving and reinitiating R group. The solid substrate acts as part of the leaving R group, and thus the propagating radicals are located on the terminal end of the surface-grafted polymer, which facilitates the growth of grafted polymer chains. This approach resembles a “grafting-from” approach. In the Z-group approach, the RAFT agent is attached to the surface via its stabilizing Z group. Because the RAFT agent is permanently attached to the surface, this approach resembles a “grafting-to” approach. The polymeric radicals always propagate in solution before they attach to the surface of substrate via the chain-transfer reactions with attached RAFT agents.

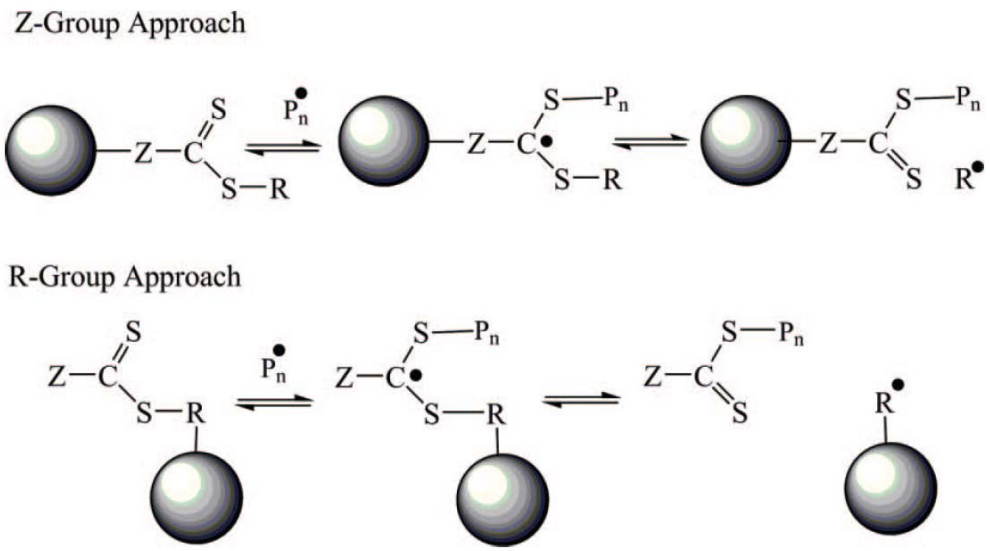

Figure 1.22. Two different approaches of surface attachment where RAFT agent attached to the surface via its Z or R group.(adapted from[160])

1.4.4.3.2.1 R-group approach

In order to attach the CTA to the inorganic surface via its R-group, several synthetic methodologies have been used. In the first known report using this approach, an ATRP macroinitiator grafted on silica particles was converted into a RAFT macroCTA by reaction with 1-phenylethyl dithiobenzoate in the presence of CuBr via an atom transfer addition[161].

Li and Benicewicz presented another approach, in which the addition of free CTA in solution was not necessary to control the polymerization. A CTA bearing a silane group was synthesized in four steps and immobilized onto silica surface by heating. Using careful conditions (low RAFT agent surface density, low initiator/CTA ratio and low monomer conversions), it was possible to limit chain termination by combination and a linear increase of number-average molecular weight (Mn) with conversion was observed. Nevertheless, polymerization retardation occurred, which was attributed to the local high CTA concentration on the surface [162]. Another very common strategy to attach the CTA to silica or silicon surfaces is the prior surface modification with hydroxyl or amine groups followed by esterification or amidation with a CTA bearing a carboxylic acid (in the presence of coupling agents) or an activated ester [163-165].

Some examples concerning the surface-initiated polymerization from metal surfaces using an anchored CTA via the R-group can be found in the literature. For instance, Skaff and Emrick synthesized a trithiocarbonate bearing a phosphine oxide ligand capable of binding to CdSe, which was then immobilized through ligand-exchange chemistry. Surface-initiated polymerization with different monomers was performed, yielding several (co)polymer-coated quantum dots [166]. Raula et al. modified the surface of Au NPs with 11-mercapto-1-undecanol and further reacted with a 4-cyanopentanoic acid dithiobenzoate. The so-formed anchored CTA was then used to produce polymer-grafted Au NPs by RAFT polymerization [167]. Certainly, the R-group approach stands as the most successful way to obtain thick polymer brushes with a narrow molecular weight distribution utilizing RAFT polymerization[135, 168].

1.4.4.3.2.2 Z-group approach

Alternatively, it is possible to attach the RAFT agent to the inorganic surface through its Z-group. However, this approach has been much less reported than the R-group one, which may be explained by the low grafting densities attained and the weakness of the bonds linking the inorganic surface to the polymer brushes. Since the polymer growth occurs strictly in solution, the chains must reach the inorganic surface to undergo reversible chain transfer reactions, being hindered by the already present chains. Besides, the thiocarbonylthio group is sensitive to hydrolysis, oxidation and nucleophilic attack and loss of grafted polymer chains can occur. Advantageously, this strategy enables the preparation of nanohybrids containing exclusively dormant chains.

This strategy was first employed by Perrier et al. for the synthesis of SiO_2 NPs grafted with poly(methyl acrylate) (PMA) [169] and has been since then mainly used for the modification of silica and silicon surfaces/NPs. In their pioneering work, activated silica NPs were reacted with 4-(chloromethyl)phenyltrimethoxysilane to introduce a chlorobenzyl group that further reacted with sodium methoxide and elemental sulfur, then with methyl-α-bromophenylacetate to lead the silica-supported CTA.

In order to covalently attach the CTA via its Z-group, the previous strategy has generally been used. That is, first the surface is modified with a chloro-containing group and further reacted with appropriate reactants to yield the Z-anchored CTA. For instance, Nguyen and

Vana synthesized silica immobilized cumyl dithiobenzoate to mediate the polymerization of styrene and methyl methacrylate (MMA) [170]. Wang et al. used a similar synthetic route to prepare a palygorskite-anchored benzyl dithiopropyltrimethoxysilane CTA [171] and Peng et al. modified Si(100) with a methoxycarbonylphenylmethyl dithiobenzoate to prepare polymer brushes via surface-initiated RAFT polymerization [172].

Both of the R-group and Z-group approach have been used to prepare the molecularly imprinted polymers. Lu et al. reported a general protocol for preparing surface-imprinted core-shell nanoparticles via surface RAFT polymerization using RAFT agent functionalized silica nanoparticles as the chain-transfer agent by copolymerization of 4-VP and EDMA in the presence of 2,4-dichlorophenoxyacetic acid (2,4-D) as template [149]. The resulting surface-imprinted core-shell nanoparticles bind the original template 2,4-D with an appreciable selectivity over structurally related compounds.

Wang and co-workers synthesized the theophylline imprinted composites using surface initiated RAFT polymerization from silica surface [151]. The authors observed that measured binding kinetics for theophylline to the MIP-Silica and MIPs prepared by conventional bulk polymerization demonstrated that MIP-Silica had improved mass-transfer properties. In addition, MIP-Silica was used as the sorbent in solid-phase extraction to determine theophylline in blood serum.

Unsal et al. used surface-controlled RAFT polymerization to prepare an ion-exchanger with polyanionic molecular brushes successfully [173]. The RAFT chain-transfer agent was covalently attached to monodispersive poly(dihydroxypropyl methacrylate-co-ethylene dimethacrylate) [poly(DHPM-co-EDMA)] particles. The 3-sulfopropyl methacrylate (SPM) was grafted from the surface of poly(DHPM-co-EDM) for protein separations.

Molecularly imprinted polymer for selective recognition and removal of chlorophenols from contaminated water prepared by RAFT silica mediated polymerization have been reported by Li et al. [152]. They used 2,4-dichlorophenol (2,4-DCP) as template, methacrylamide (MAAM)as functional monomer, divinylbenzene (DVB) as cross-linker in acetonitrile. The resulting silica-MIP showed outstanding affinity towards 2,4-DCP in aqueous solution. .

Gonzato et al. reported a general protocol to synthesize superparamagnetic molecularly imprinted polymer particles with a 7 nm MIP shell, using a RAFT-mediated approach [153]. S-propranolol imprinted composites were obtained by functionalizing amino-modified

nanoparticles with a trithiocarbonate agent and subsequently by polymerizing thin molecularly imprinted layers. The authors demonstrated that the resulting composites retain both a good imprinting effect and a superparamagnetic behavior using this reaction system.

Grafting techniques allow the graft a thin film of imprinted polymer on the substrates. Using this strategy, evenly distributed thin layers of MIPs with reduced mass-transfer resistance can be created. In addition, desirable formats [e.g., particles, tubes or microchips with different characteristics (size, porosity, pore volume, and surface area)] can be obtained. Many research papers have been published on the preparation of surface-imprinted materials by CRP (Table1.2).

1.5 Molecularly imprinted nanoparticles

Molecularly imprinted polymers have been mostly prepared by traditional bulk polymerization technique at the micro scale. Beside of some good applications of bulk material for chromatographic and SPE purposes, they still suffer from several drawbacks for instance tedious grind and sieving process, irregular shape and size, heterogeneous binding sites, possibility of template leakage and limit access to the binding sites. Molecularly imprinted nanoparticles are good candidate to address these drawbacks. MIP NPs have higher surface-to-volume ratios and greater total active surface areas per unit weight of polymer. Imprinted cavities are more easily accessible to the template, which improves binding kinetics and facilitates the template removal process, thus enhancing their overall performance [174-176].

Imprinted nanoparticles can be prepared by many techniques such as precipitation polymerization [13], solution polymerization [177], mini-emulsion polymerization [178], micro-emulsion polymerization [179], grafting approaches [175], sol-gel process [180], etc. MIP nanoparticles have already been used as enzyme mimics [181], drug delivery systems [182],antibody substitutes [183] catalysis[184], capillary electrochromatography [185], sensing application [186] and separation [187]. Molecular imprinting approach has also been extended to different types of nanomaterials, such as nanowires [188], nanotubes [189], nanofibers [190], nanofilms [191], nanogel [192], core-shell [193], quantum dots [194],

fullerene [195], dendrimers [196]. The most significant examples of these will be reviewed in the following sections.

1.5.1 Imprinted nanofibers, nanowires and nanotubes

To extend the range of possible application using the imprinting approach, a number of research groups have used other types of nanomaterials, such as nanowires, nanotubes and nanofibres in the context of MIP techniques.

The surface imprinting nanowires with highly selective recognition for a variety of template proteins, including albumin, hemoglobin, and cytochrome c were prepared by Li et al. [188]. They used alumina membranes as support material and a sol-gel template synthesis method to deposit silica nanotubes within the pores of the alumina membranes. They demonstrated that these imprinted nanowires have a good site accessibility toward the target protein molecules. Furthermore, the large surface area of the nanowires results in large protein molecule binding capacity of the imprinted nanowires.

Kan et al. reported an MIP composite containing multiwalled CNTs (MWNTs) for use as the selective layer in an electrochemical sensor [197]. The MIP was prepared with dopamine as the template and methacrylic acid and trimethylolpropane trimethacrylate as monomers. Vinyl groups introduced on MWNTs surface were found to be the key for the formation of the MWNTs-MIP composite, the thickness of the MIP layer being 15-20 nm (Figure 1.23). The authors demonstrated that MWNTs-MIPs not only possessed a rapid dynamic adsorption but also exhibited a higher selectivity toward dopamine compared to epinephrine.

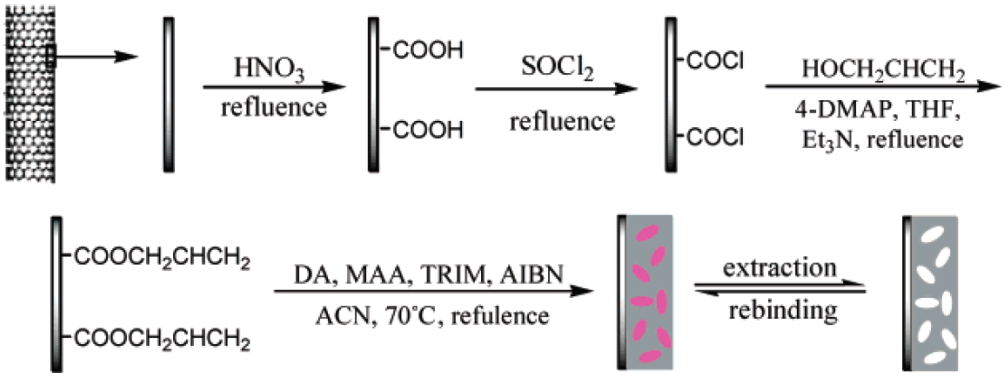

Figure 1.23. Synthesis route of multiwalled carbon nanotubes.(adapted from[197])

Chen and coworker synthesized a surface glycoprotein imprinting over magnetic Fe_3O_4@Au multifunctional nanofibers (NFs) [190]. The results showed that the magnetic multifunctional Fe_3O_4@Au NFs can not only direct the selective occurrence of imprinting polymerization, but also drive glycoprotein templates into the polymer through reversible covalent complex formation. The results also showed that the imprinted NFs reached saturated adsorption at 0.3 mg/mL within 90 min and exhibited significant specific recognition towards the template protein.

1.5.2 Imprinted nanofilms

Of the various imprinted nanomaterials, nanofilms with a thickness smaller than one micrometer are one of the most desirable forms of the feasible applications in chemosensors, and have thus attracted intense research interest in recent years [198, 199]. In addition to large surface-to-volume ratio and fast binding kinetics, the most remarkable advantage is that the molecularly imprinted nanofilms can be synthesized directly on the surfaces of electrochemical electrodes [200], quartz crystal microbalances (QCM) [201] and surface plasmon resonators (SPR) [202] for the detection of target analytes.

Ersöz et al. reported the combination of quartz crystal microbalance with MIP to prepare a sensor using the ability of glucose to chelate of copper (II) ion of methacrylamidohistidine (MAH) monomer to create ligand exchange (LE) assembled monolayer which is suitable for glucose determination [201]. The authors investigated the measurement of binding interaction of molecularly imprinted QCM sensor via ligand interaction, pH effect on frequency shift and recognition selectivity of glucose-imprinted polymer with respect to methyl-α-d-glucopyranoside and sucrose.

1.5.3 Imprinted microgel/nanogel

“Microgels” are defined as gel particles of any shape with an equivalent diameter of approximately 0.1 to 100 μm, whereas the diameter of “nanogels” is approximately 1 to 100 nm both exhibiting network structures that swell in a suitable solvent [203]. These materials may dissolve in solvents-just as linear polymers-however, preserving a nearly fixed conformation. They may swell and change their dimensions depending on the solvent and

environmental conditions. The precipitation polymerization method can be optimized to produce microgels/nanogels in the different size range. A characteristic of these materials is that they produce low-viscosity colloidal solutions after preparation in a suitable solvent that never reaches the point of precipitation. They are now increasingly being investigated as novel materials for applications in catalysis, drug delivery, sensing and medical diagnostics, etc. [192].

Recently, Pan et al. prepared thermo-responsive molecularly imprinted nanogels for specific recognition and controlled release of proteins (Figure 1.24) [192]. Polymerization carried out by using the aqueous precipitation polymerization with the aid of a surfactant, sodium dodecyl sulfate (SDS), lysozyme as the protein template and N-isopropylacrylamide as the major monomer. Simply by adjusting the SDS amount during polymerization, the size of nanogels could be finely controlled, ranging from a few hundred down to a few dozen nanometers. The authors demonstrated that compared to non-imprinted counterparts, the lysozyme-imprinted nanogels possessed higher rebinding capacity, more rapid rebinding kinetics, and much higher specificity toward lysozyme.

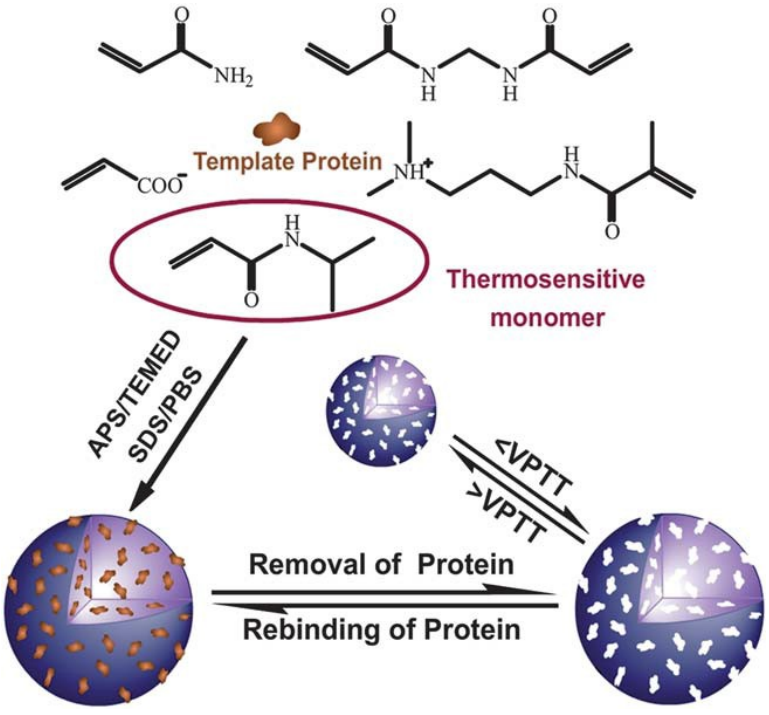

Figure 1.24. Schematic illustration of the preparation of thermo-responsive lysozyme- imprinted nanogels via aqueous precipitation polymerization and their shrinking/swelling behavior around the volume phase transition temperature (VPTT). (adapted from[192])

Haupt and co-workers reported the synthesis of soluble molecularly imprinted polymer nanogels as synthetic antibodies, with dimensions and molecular weights close to those of biological antibodies [204]. They used s-propranolol as template molecule, ethylene glycol dimethacrylate (EGDMA) as cross-linking, methacrylic acid (MAA) as functional monomer and a multi-initiator based on a G3-dendron and 8 iniferter moieties for the polymerization of MIP nanogels as synthetic antibody mimics. Nanogels were prepared by dilution method in 4 days at 30 ºC. They obtained monodisperse MIPs of a 17 nm, which is in the same size range as biological antibodies. The authors also observed a good imprinting effect despite the small particle size and the use of weak monomer-template interactions. In addition, they demonstrated the superiority of these nanogels compared with those initiated with the corresponding monoinitiator, in terms of target binding. Potentially, the living character of the iniferter polymerization allows for re-initiating the polymerization with different monomers, and thus for fine-tuning the surface properties of the particles.

1.5.4 Molecularly imprinted core-shell nanoparticles

Nowadays, core-shell structured nanoparticles have been raised great interests in the molecularly imprinting technology [5, 205, 206]. The main advantages of the core-shell approach are that the MIP layer can be very thin and uniform. Meanwhile, other functionalities such as magnetic and fluorescent properties can be conveniently built into the MIP as the core particle. Core-shell molecular imprinting of nanomaterials overcomes difficulties with template transfer and achieves higher binding capacities for macromolecular imprinting, which are more important to the imprinting of natural low-abundance proteins from cell extracts [207].

To date, many core-shell structured surface- imprinted MIP nanoparticles have been prepared using different methods such as emulsion polymerization [208], precipitation polymerization [209], grafting approaches [210], sol-gel process [211].

Molecular surface-imprinted polymers nanoparticles encapsulating magnetite modified with oleic acid, for recognition of salicylic acid were obtained by Zhu et al. with three-step miniemulsion polymerization [208].They demonstrated that the important factors for preparation of magnetic molecular imprinting polymers are polymerization process, solvents, miniemulsifying approaches, and co-stabilizer which had important role to obtain magnetic

molecular imprinting polymers (MMIPs) nanoparticles (NPs) with high saturation magnetization (Ms), regular morphology and good monodispersion. In addition, the high adsorption capacity and good selectivity for target molecule were displayed by the MMIPs NPs.

Clickable molecularly imprinted core-shell nanoparticles have been synthesized using a simple one-pot precipitation polymerization with sequential addition of monomers [209]. The authors described the synthesis of alkyne and azide coated MIP nanoparticles that can be used as molecular recognition building blocks. In addition, two well-established model templates, propranolol and 2,4-dichlorophenoxy acetic acid (2,4-D) were used to demonstrate the feasibility of this approach. The easily accessible clickable groups were provided a convenient means to conjugate different MIP nanoparticles into composite materials, which may be used to achieve simultaneous separation and detection of multiple analytes.

Zhou and co-workers reported a dendritic-grafting method introducing more functional groups to modify the SiO_2-coated magnetic nanoparticles (SiO_2-coated MNPs) for determination of estrogens in plasma samples (Figure 1.25) [212]. The magnetic MIPs (MMIPs) were obtained by using 17- ethyl estradiol (EE2) as a pseudo template, dendronized SiO_2-coated MNPs as the supporter, MAA as functional monomer and EGDMA as cross-linker agent. The resulting MMIPs showed high adsorption capacity, quick binding kinetics and good selectivity for trace estrogens and provided an effective tool for the monitoring of estrogens in food or environment.

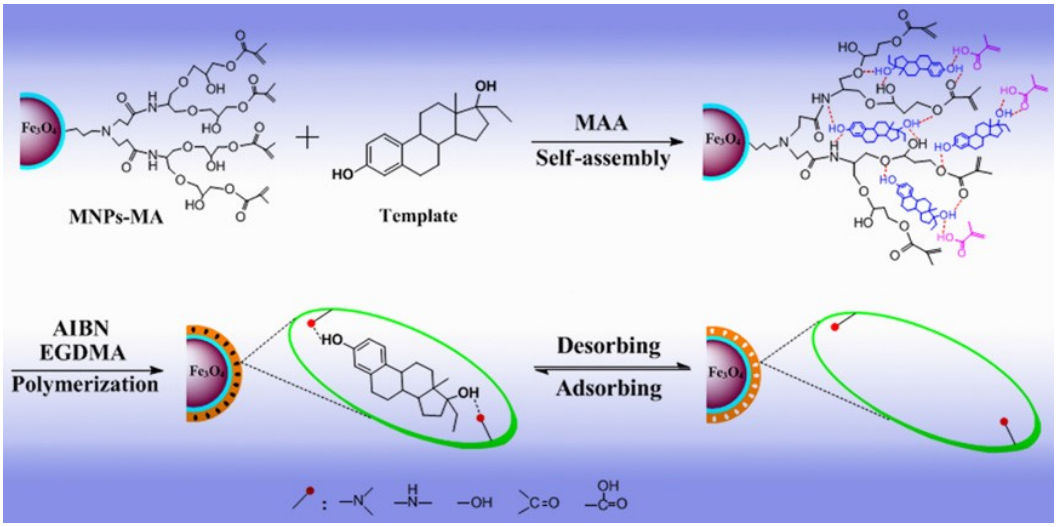

Figure 1.25. Schematic representation of the possible preparation process of magnetic MIPs. (adapted from[212])

Recently, Chen et al. proposed a strategy for imprinting of a protein on the surface of nanoparticles using a metal chelating monomer [210]. With lysozyme as a model protein template and Cu^{2+} chelating N-(4-vinyl)-benzyl iminodiacetic acid as the coordination monomer along with other monomers such as N-isopropylacrylamide, acrylamide and methylenebisacrylamide, protein imprinted polymer nanoshells were formed over vinyl-modified silica nanoparticles via surface polymerization in high-dilution monomer solution. The feed concentration of the crosslinking monomer was optimized toward achieving the best imprinting effect. The resultant core-shell imprinted particles showed greatly faster binding kinetics, elevated rebinding capacity and selectivity. More importantly, noticeably high binding affinity was achieved with an estimated dissociation constant of 4.1×10^{-8} M which is comparable to that of conventional antibodies.

Deng et al. prepared a nanoparticle-based metronidazole-imprinted polymer by combining a surface molecular imprinting technique with a sol-gel process [211]. Metronidazole was used as a template, 3-aminoprophyltriethoxysilane as the functional monomer, and tetraethyl orthosilicate as the cross-linker. The resulting magnetic molecularly imprinted polymer was used successfully for the determination of metronidazole by solid phase extraction coupled with spectrophotometric detection. The obtained material showed high adsorption capacity, good extraction performance and acceptable stability and repeatability.

1.6 Proteins and peptides imprinting

Obviously, proteins, and to a minor extent peptides, are an extremely important target class in life sciences. Synthetic polymer-based molecular receptors for peptides and proteins would open up a wide range of possibilities for new applications in biotechnology, diagnostics and chemistry, complementary to and extending beyond the scope of current antibody technology. Protein purification in one step, diagnostic tests in aggressive sample matrices and novel biosensors are some of the novel possibilities. Therapeutic MIPs in analogy to therapeutic antibodies may eventually have the largest commercial potential of all MIP applications [213]. Macromolecular targets like proteins pose additional difficulties, and classical imprinting approaches have mostly failed to deliver satisfactory results. Several reasons for this have been identified: proteins are in general not compatible with organic solvents and will quickly denature in prepolymerisation mixtures based on organic solvents

as porogens. Furthermore, mass transport of macromolecules may be prohibitively slow in a highly cross-linked polymer matrix. As a consequence, the protein templates may be difficult to remove from the binding pockets, thus reducing the surface sites available for rebinding [214]. Analogously, rebinding may be too slow for practical applications. Furthermore, the rigid structure of an MIP, lacking the segmental motions of conventional linear polymers, may effectively prevent proteins from entering the specific binding pockets, and unspecific adsorption at the polymer surface may be the predominant binding mode. Finally, the more availability of sufficient amounts of a highly purified protein target is not granted, and only few proteins are commercially available and low priced. The comparison of antibodies and MIPs has been shown in Table 1.3.

Table 1.3. Typical characteristics of antibodies and MIPs. (adapted from[215])

	Antibodies	*MIPs*
Affinity	$10^{-7} – 10^{-11}$ M	$10^{-3} – 10^{-10}$ M
Application	Physiological conditions	Organic or aqueous media
Capacity	~ 6 μmol.g^{-1}	~ 0.1 – 10 μmol.g^{-1}
Cost	£100's for μg quantities	£10's for g quantities
Production	Animal host, months	2 – 3 days
Reusability	Not usually	100's of times
Stability	Narrow temperature and pH range	Wide temperature and pH range
Storage time	Limited	Stable over period of years

There are a number of different strategies for creating polymeric receptors targeting peptides and proteins such as bulk, surface, and epitope imprinting. The following sections outline a number of the approaches used to create MIPs capable of recognizing biological macromolecules.

1.6.1 Bulk imprinting

Bulk imprinting, the standard technique which has been so successful for small molecular weight MIPs, is the most straightforward approach to macromolecular imprinting. The

advantages to this approach are that three-dimensional binding sites are formed for the entire protein and that there are a multitude of facile procedures already present in the literature. Polyacrylamides and their derivatives are among the most extensively used polymeric materials for bulk imprinting of proteins.

Molecularly imprinted polymers based on polyacrylamide hydrogels for the selective imprinting of bovine haemoglobin (BHb) have been developed by Hawkins et al [216]. For the first time, they explored in detail a variety of template removal strategies including varying ratios of sodium dodecylsulphate: acetic acid (SDS:AcOH) and also the use of a trypsin digest. The haemoglobin-imprinted composite exhibited specific selectivity to the template molecule over structurally similar proteins.

A simply hemoglobin (Hb) molecularly imprinted polymer (MIP) was prepared by Guo and co-workers using Hb as the imprinted molecule, acrylamide as the functional monomer and cross-linked chitosan beads as the supporting matrix [217]. The MIP was achieved by entrapment of the selective soft polyacrylamide gel in the pores of the cross-linked chitosan beads by letting acrylamide monomer and the protein diffuse into the pores of chitosan beads before starting the polymerization. The chitosan beads were freed from the surrounding polyacrylamide gel by washing. The resulting MIP showed higher adsorption capacity for Hb than the non-imprinted polymer with the same chemical composition, and the MIP also demonstrated selectivity for the imprinted molecule.

The template removal is a crucial step in protein imprinting, especially in the bulk approach, that is often not properly addressed. As a result, the alternative approaches of surface imprinting and epitope imprinting have attracted increasing interest.

1.6.2 Surface imprinting

A fundamental strategy of surface imprinting is to locate the imprinted sites at or close to the surface of the MIP, therefore enabling easy access to the target protein molecules. Thus, in comparison with bulk imprinting, the transfer of protein is much easier and the binding kinetic is less restricted although usually lower [218]. The selectivity can also decrease because only part of the protein is bound and recognized. Some elegant examples are discussed below.

The MIP nanoparticles themselves can be further applied as templates for surface imprinting. Dickert and co-workers have extended the concept of molecular imprinting by templating polymer with immunoglobulins and using these MIPs as stencils for designing actual plastic replicas of the initial antibody [219]. The created replicas had similar affinity profile as original antibodies.

A new and facile fabricating method for lysozyme molecularly imprinted polymer beads (lysozyme-MIP beads) in aqueous media was presented by Qin et al. [141]. Mesoporous chloromethylated polystyrene beads containing dithiocarbamate iniferter were used as supports for the grafting of lysozyme imprinted copolymers with acrylamide and N,N′-methylenebisacrylamide through surface initiated living-radical polymerization. The lysozyme-MIP column exhibited a pronounced imprinting effect and was capable of separating the template from competitive proteins, whereas the NIP column had no selective properties.

Chen et al. prepared silicon nanowires as the reinforcement material in protein molecular imprinting with dopamine as the monomer and bovine hemoglobin as the template molecule (Figure 1.26) [220]. The imprinted nanowires showed fast adsorption kinetics the equilibrium, significant selectivity and large binding capacity for the template protein.

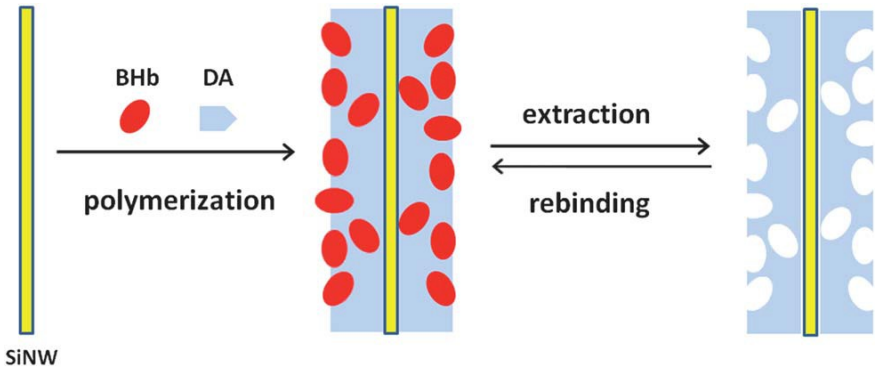

Figure 1.26. Schematic of preparation of MIP for bovine hemoglobin(BHb) recognition. (adapted from[220])

Surface imprinting results in the formation of specific cavities on the surface of the imprinted polymer. These cavities have particular shapes or steric effects that are complementary to parts or fragments of the protein template. However, because of the complexity and conformational flexibility of proteins, the interactions between the protein template and the functional monomer are not as specific and efficient as desired. As a result, protein surface-

imprinted polymers sometimes exhibit cross-reactivity, non-specific binding and low selectivity.

1.6.3 Epitope imprinting

In nature, antibody-antigen interactions depend on the recognition between the antibody and an antigenic site of the protein, the epitope. The epitope is a short amino-acid sequence complementary to binding site of antibody. In the field of molecular imprinting, Rachkov and co-workers applied this observation to develop a new concept for the synthesis of protein recognition polymers [221, 222]. Instead of the whole proteins, a short peptide sequence, often exposed at the protein surface, was used as a template for MIP preparation. Once the matrix has been polymerized the resultant imprinted material should be able to recognize and bind the whole protein.

The epitope approach has been successfully used to bind oxytocin by imprinting the Tyr-Pro-Leu-Gly amino acid sequence [221]. In this study, synthesis of the MIP was performed in an organic environment, but subsequent rebinding experiments were performed using chromatographic methods in both aqueous-rich and aqueous-poor mobile phases. In the aqueous-poor mobile phase, hydrogen bonds and ionic interactions are the dominating factor in creating selective recognition sites. In the aqueous-rich phase, ionic and hydrophobic interactions provide the dominant binding interaction.

Titirici and Sellergren reported hierarchical epitope imprinting for peptide recognition [223]. They used silica particles containing immobilised peptidic templates for the generation of hierarchically imprinted polymers. The pores of the silica mould were filled with a mixture of monomers/initiator and polymerised, followed by dissolution of the silica template. This method leaves behind imprinted polymers with binding sites located at the surface, which are capable of recognizing larger molecules with the same immobilised epitope.

Shea et al. chose C-terminal 9-mer peptides of target proteins as epitopes and prepared the peptide-imprinted polymers against the immobilized epitopes (Figure 1.27) [224]. The polymer films obtained had high selectivity for the target proteins including cytochrome c, alcohol dehydrogenase and albumin. A number of advantages therefore stem from using terminal peptide epitopes as the template, namely: the conformation of whole protein does

not need to be retained, allowing harsher solvent and temperature conditions to be used; selectivity in protein recognition can be controlled by the choice of epitope and its length; template removal is far more easily achieved than with whole protein and highly selective imprints can be obtained. On the other hand, a good knowledge of the protein structure is necessary, but there are a number of computational and database based methods available which can help. Another limitation is that custom synthesis may be required in order to prepare the templates which may be relatively costly and time-consuming.

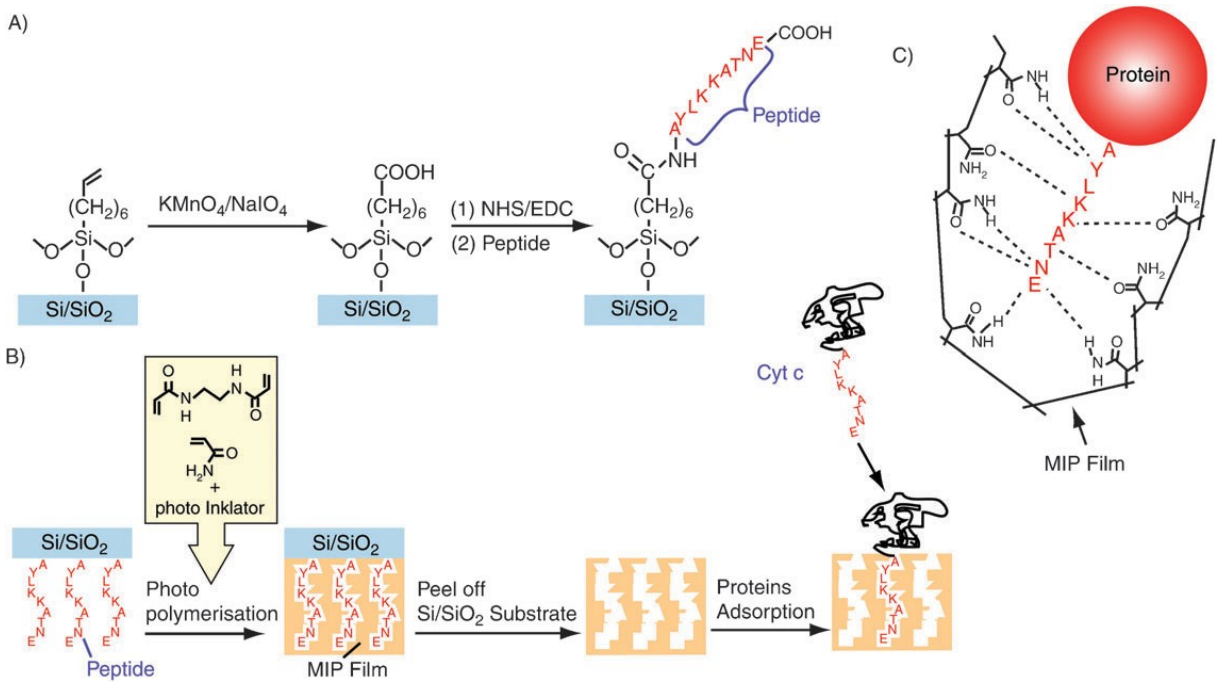

Figure 1.27. The surface-bound epitope approach employed by the group of Shea using C-terminal nonapeptides as templates for protein imprinting. (adapted from[224])

Sellergren and co-workers [225] developed an epitope-imprinting strategy that leads to a synthetic phosphotyrosine (pTyr)-selective imprinted polymer receptor. The resulting polymer displayed good binding affinities for the pTyr template, in the range of that observed for corresponding antibodies, and a clear preference for pTyr over phosphoserine (pSer). In further analogy to the antibodies, the imprinted polymer was capable of capturing short tyrosine phosphorylated peptides in the presence of an excess of their non-phosphorylated counterparts or peptides phosphorylated at serine.

Nevertheless, these data clearly show that such epitope-imprinting approaches are effective in providing sequence-specific recognition of proteins. Epitope imprinting could open a new way to prepare imprinted polymers for the recognition of various kinds of unknown or

unidentified proteins. This convenient technique may become essential for proteomics as a future technology in biotechnology and medicine.

It is worth to note that combination of nano-sized material and protein imprinting has been generated the powerful techniques in protein imprinting polymers [5, 226]. Lv et al. presented the newest developments concerned with use of nanomaterials, such as magnetic and silica nanoparticles, nanowires, carbon nanotubes, and quantum dots as supports enabling the preparation of protein-imprinted polymers via surface imprinting techniques [226]. The high molecular binding selectivity, fast binding kinetics, colloidal stability and in vivo applicability make MIP nanoparticles as one of the best chose for protein imprinting.

Chapter 2: Characterization Techniques

2.1 Thermogravimetric analysis (TGA)

Thermogravimetric analysis (TGA) was carried out using a TGAQ50 (TA instruments, Eschborn, Germany). The sample (~ 10-15 mg) was placed in a platinum pan, which is suspended in a sensitive balance together with the reference pan. The sample was then heated, in a furnace, with at a rate of 10 or 20°C/min, under N_2 atmosphere.

This analysis is a thermal method that involves the measurement of weight loss as a function of temperature or time. TGA can be used to quantify the mass change in a polymer associated with transitions or degradation processes [227].

The ligand and area density (D_s) of the immobilized ligand were calculated based on % weight loss of content versus the preceding step monitored by thermogravimetric analysis (Eq. 2-1 and Eq. 2-2) [228].

$$Ligand\ density\ (\mu mol/g) = \frac{\left[\left(\frac{\%W_{100-800}}{100-\%W_{100-800}}\right)\times 100 - \%W_{Silica}\right]}{Mw_L \times 100}\times 10^6 \qquad \text{Eq. 2-1}$$

$$Area\ density\ (\mu mol/m^2) = \frac{\left[\left(\frac{\%W_{100-800}}{100-\%W_{100-800}}\right)\times 100 - \%W_{Silica}\right]}{S \times Mw_L \times 100}\times 10^6 \qquad \text{Eq. 2-2}$$

Where

$\%W_{100\text{-}800}$ = % mass loss of modified silica between 100 ^{o}C and 800 ^{o}C

$\%W_{silica}$ = % mass loss of starting silica

M_w = molecular weight of coupled ligand

S = surface area of the silica support

The shell (film) thickness based on TGA mass loss was calculated according to Eq. 2-3:

$$d = \frac{D_{cs} - D_c}{2} \qquad \text{Eq. 2-3}$$

where D_{cs} and D_c are the average diameters of the core-shell and the core particles respectively. D_c was assumed equal to the number average particle size derived from DLS, whereas D_{cs} was obtained from the average volume of the core-shell particles (V_{cs}) according to Eq. 2-4:

$$D_{cs} = \sqrt[3]{\frac{6 \times V_{cs}}{\pi}} \qquad \text{Eq. 2-4}$$

where V_{cs} in turn is the sum of the core (V_c) and shell (V_s) volume (Eq. 2-5):

$$V_{cs} = V_c + V_s \qquad \text{Eq. 2-5}$$

V_c and V_s were in turn obtained from D_c and the total monomer volume (V_m) expressed in cc/g according to Eq. 2-6 and Eq. 2-7:

$$V_c = \frac{\pi \times D_c^3}{6} \qquad \text{Eq. 2-6}$$

$$V_s = \frac{10^{21} \times V_m}{N} \qquad \text{Eq. 2-7}$$

with N being equal to the number of particles calculated from D_c and the specific surface area of the core particles as Eq. 2-8:

$$N = \frac{10^{18} \times S_c}{\pi \times D_c^2} \qquad \text{Eq. 2-8}$$

The total monomer volume (V_m) from the mass loss (%) and average monomer density (ρ) was calculated as follows:

$$V_m = \frac{\%G}{\rho(100 - \%G)}$$ Eq. 2-9

where $\%G$ is the mass loss of the grafted polymer in % and average monomer density (ρ) assumed equal to one.

2.2 Scanning electron microscopy (SEM)

SEM was provided at the Department of Biochemical and Chemical Engineering, TU Dortmund. The SEM pictures were recorded on a Hitachi H-S4500 FEG in secondary electron mode with an acceleration voltage of 1 kV. The samples were deposited on holders with carbon foil. Scanning electron microscopy (SEM) gives information on the morphology and surface texture of the materials. Scanning electron microscopy is the most widely used technique to study the shape, size, morphology and porosity of polymers.

2.3 Transmission electron microscopy (TEM)

TEM pictures were used for the determination of the size, morphology and shell thickness of the core-shell nanoparticles. The TEM images were obtained using a energy filter transmission electron microscope (Philips CM200) provided by the Department of Biochemical and Chemical Engineering, TU Dortmund. The obtained particles (1 mg) were dispersed in isopropanol (SiNPs) or water (magNPs) and sonicated for 20 min, then a drop of the suspension was placed over a copper TEM grid.

2.4 Fourier transform infrared spectroscopy (FTIR)

This was performed using a TENSOR 27 Fourier transform infrared spectrometer (FTIR) from Bruker with a platinum ATR moiety. This instrument allows direct measurement of solids and solutions without any sample preparation.

2.5 Solution NMR

NMR spectra were recorded on a Bruker 500 spectrometer using $CDCl_3$ and DMSO as solvent.

2.6 Dynamic light scattering (DLS)

Particle sizes were measured with a Zetasizer Nano-ZS particle-size analyser from Malvern Instruments Ltd (UK). The obtained particles (2 mg) were dispersed in isopropanol (SiNPs) or water (magNPs) to a concentration ~ 10 μg mL^{-1} and sonicated for 20 min, then an aliquot of the dispersion of NPs (1 mL) was analysed by DLS at 25 °C.

2.7 Elemental analysis (EA)

Carbon, hydrogen, nitrogen and sulphur contents were performed using a Heraeus Elemental Analyzer CHN-O-Rapid (Elemental-Analysis system, GmbH). About 10 mg of dried sample was submitted for elemental analysis. This technique involves the catalytic combustion of the sample, with selective adsorption of the evolved gasses. The relative weight percentages of the elements (e.g. C, H, N and S) may thus be obtained.

From elemental microanalysis data, more precisely from the change in carbon and nitrogen contents in each step, we could estimate the amount of immobilized ligand on the silica surface. The ligand density of immobilized ligand was calculated based on the change in carbon (ΔC) or nitrogen (ΔN) content versus the preceding step [229], e.g. for ΔC:

$$Ligand\ density = \frac{m_C}{M_C} \times 10^3 \qquad \text{Eq. 2-10}$$

Where:

$$m_C = \frac{\%\Delta C}{100 - \frac{\%\Delta C \times M_W}{M_C}} \qquad \text{Eq. 2-11}$$

m_C = weight of carbon of the grafted ligand per gram of bare silica support

M_w = molecular weight of the coupled ligand,

M_C = weight of carbon per mole of coupled ligand,

The area density (*Ds*) of immobilized ligand was calculated based on the change in carbon (*⊿C*) content versus the preceding step, as follows:

$$D_s = \frac{m_C}{M_C \times S} \times 10^6 \qquad \text{Eq. 2-12}$$

where *S* is the surface area of the silica supports.

The coverage (*C*) was calculated as Eq. 2-13, assuming a maximum silanol group density of 8 μmol/m^2

$$C = 100 \times D/8 \qquad \text{Eq. 2-13}$$

The average distance d_L (nm) between the coupled ligands assuming a random ligand distribution was calculated as Eq. 2-14

$$d_L = \sqrt{\frac{10^{18}}{D \times 10^{-6} \times N}} \qquad \text{Eq. 2-14}$$

where *N* is the Avogadros number.

In addition, to calculate the grafting density of coupled ligand another equation has been reported which is in good agreement with aforementioned equations[228].

$$grafting\ density\ (\mu mol/m^2) = \frac{\%\Delta C}{[(1200N_C - \%\Delta C(M-1)) \times S]} \times 10^6 \qquad \text{Eq. 2-15}$$

Where $\%\Delta C$, N_C , *M* and *S* are the difference of carbon content after and before grafting, number of carbon atoms, the molecular weight of the grafted molecule and specific surface area(m^2/g) respectively.

The shell thickness based on elemental analysis was calculated as outlined in TGA thickness calculation but deriving the total monomer volume (V_m) from the carbon content (*%C*), average monomer density (ρ) assumed equal to one and grafting density (*%G*) as follows:

$$V_m = \frac{\%G}{\rho(100 - \%G)}$$ Eq. 2-16

where *%G* was calculated according to Eq. 2-17 from the nominal carbon content of the grafted polymer ($\%C_{pol}$) and the found carbon content (*%C*).

$$\%G = \frac{\%C}{\%C_{pol}} \times 100$$ Eq. 2-17

2.8 Nitrogen adsorption

Nitrogen adsorption measurements were performed on a Quantachrome Nova4000e (Quantachrome Corporation, Boynton Beach, FL) automatic adsorption instrument. Before measurements, the equivalent weight of 10 to 20 m^2 of sample were placed in a glass cell, and degassed under vacuum over night at 50 °C. The initial part of the resultant physisorption isotherm is attributed to monolayer-multilayer adsorption and in this region was applied the Brunauer-Emmett-Teller (BET) method to determine the surface area [230].

2.9 Binding experiments

2.9.1 Single point rebinding

Once a MIP has been synthesized, its specificity, binding capacity and selectivity towards the analyte are evaluated[231]. This can be done in chromatographic mode by using the MIP as a stationary phase in a chromatography set-up[232], or in a batch by equilibrium binding[233]. An imprinting factor, defined as the ratio of the amount bound to the MIP and the amount bound to the non-imprinted control polymer (NIP) is determined.

In a batch equilibrium experiments a small amount of polymer ($m_{polymer}$) is allowed to equilibrate for 24 h in a solution of the template or the target analyte. The supernatant solutions were analyzed using a Hewlett-Packard HP 1100 instrument (Agilent Technologies, Waldbronn, Germany) equipped with a UV-DAD detector, an autosampler and a commercially available column (Phenomenex Luna C-18, 150×4.6 mm).

The results of these experiments are expected to provide information on the nature of the imprinted sites. Both MIP and NIP were tested under the same conditions, the free concentration (C_{free}) of the analyte in the supernatants determined from the peak area and the amount bound, (q, μmol g^{-1}) was calculated according to Eq. 2-18:

$$q = \left(C_{initial} - C_{free}\right) \times \frac{V}{m} \qquad \text{Eq. 2-18}$$

where $C_{initial}$ and C_{free} (mmol L^{-1}) represent the initial and equilibrium concentration of analyte in solution, respectively. V (mL) is the volume of solution; and m (g) is the mass of the polymers.

2.9.2 Binding isotherm

Adsorption isotherms can yield important information concerning binding energies, modes of binding and site distributions in the interactions of small molecule ligands with receptors[234]. In the batch rebinding studies, a soluble ligand interacts with the binding sites in a solid adsorbent, i.e. the MIP or NIP. The adsorption isotherms are then simply plots of equilibrium concentration of bound ligand versus concentration of free ligand.

Non-linear fitting of theoretical isotherms to experimental data was performed using Sigmaplot 12.5, and best fits were evaluated with the Fisher test where a higher F value indicates a better fit [235]. The adsorption isotherm models evaluated were Langmuir (Eq. 2-19), Bi-Langmuir (Eq. 2-20) and Freundlich (Eq. 2-21) where q^* is the concentration in the stationary phase at equilibrium with concentration C, and C is the concentration in the mobile phase.

$$q^* = \frac{q_s b C}{1 + bC} \qquad \text{Eq. 2-19}$$

$$q^* = \frac{q_{s1} b_1 C}{1 + b_1 C} + \frac{q_{s2} b_2 C}{1 + b_2 C} \qquad \text{Eq. 2-20}$$

$$q^* = a C^m \qquad \text{Eq. 2-21}$$

The Langmuir models assume that one (Eq. 2-19) or two (Eq. 2-20) distinguishable classes of sites are present on the surface, each with saturation capacity q_s and association constant *b*. The dissociation constant K_d was calculated as the inverse of *b*. The Freundlich isotherm (Eq. 2-21), on the other hand, assumes sites with *a* Gaussian distribution of binding strengths. Here the width of the Gaussian distribution describes the degree of heterogeneity, through the index *m*. This parameter ranges from 1 (homogeneous samples) to 0 (heterogeneous samples). Moreover, with the use of *a* and *m* it is possible to characterize the affinity distribution of the polymer by calculating the average affinity constant, *K* (Eq. 2-22), and the average number of binding sites, *N* (Eq. 2-23), as described in [236].

$$K = \left(\frac{m}{m-1}\right)\left[(K_1^{1-m} - K_2^{1-m})/(K_1^{-m} - K_2^{-m})\right] \qquad \text{Eq. 2-22}$$

$$N = a(1 - m^2)(K_1^{-m} - K_2^{-m}) \qquad \text{Eq. 2-23}$$

$$K_1 = K_{min} = 1/C_{max} \qquad \text{Eq. 2-24}$$

$$K_2 = K_{max} = 1/C_{min} \qquad \text{Eq. 2-25}$$

For each model and each set of experimental data, the Fisher parameter was calculated according to Eq. 2-26[235]:

$$F_{calc.} = \frac{m-l}{m-1} \times \left[\sum_{i=1}^{m} (q_{exp,i} - \bar{q}_{exp,i})^2 \div \sum_{i=1}^{m} (q_{exp,i} - q_{\mathrm{t,i}})^2 \right] \qquad \text{Eq. 2-26}$$

where $q_{exp,i}$ are the experimental values of the solid- phase concentration of the adsorbate for a given system. $\bar{q}_{exp,i}$ is the mean value of the data, $q_{exp,i}$, for a given system, $q_{t,i}$ are the estimate of the solid phase concentration of the adsorbate by a given model, *l* is the number of adjusted parameters in the model, and m is the number of experimental data for a given system.

Chapter 3: MIP Core-Shell NPs for Chiral Recognition

3.1 Introduction

Molecularly imprinted polymer nanoparticles have been received much attention in recent years due to their significant properties such as higher surface-to-volume ratios, easy accessibility of imprinted cavities and more homogenous binding sites [5, 174]. They have many possible applications in separation science, enzyme mimics, sensor and drug delivery systems [181, 182].One of the most important type of the MIP nanoparticles is the core-shell structured MIP nanoparticles, which combine the excellent processability and multifunctional character of polymer matrices and inorganic particles. Various inorganic materials such as glass beads, gold, magnetite, carbon nanotubes and silica have been used to generate core-shell MIP nanoparticles [5]. Among them, silica particles are widely applied for the target core materials because of their optical transparency, biocompatibility, chemical and thermal resistance, mechanical stability and variable sizes, and low costs [237, 238].

To date, surface-initiated controlled radical polymerization (SI-CRP) from silica particles has been carried out using different approaches, including iniferter-mediated polymerization, nitroxide mediated radical polymerization(NMP), atom transfer radical polymerization (ATRP) and reversible addition fragmentation chain transfer polymerization (RAFT)[130, 238]. These techniques provide good ability to control molecular weight, polydispersity, thickness and functionality of grafting polymers. Among these techniques RAFT polymerization is a robust and versatile approach owing to its substantial properties such as compatibility to a wide range of monomers, adaptability with reaction conditions, absence of catalyst, ease of implementation and inexpensive relative to competitive technologies [114].

Surface-initiated reversible addition fragmentation chain transfer polymerization (SI-RAFT) has been used to prepare well-defined MIP composites [149, 151, 153]. Mostly the group of Sellergren is involved in making new formats of MIPs using surface initiated iniferter and/or RAFT polymerization techniques [91, 92, 126, 229, 239, 240]. The first of these consisted in the use of immobilized iniferters which allowed the synthesis of layer by layer grafting of different MIPs onto wide pore silica [92]. At the same time Rückert et al. reported the molecularly imprinted composite via iniferter-modified polystyrene- or silica-based supports

with a good recognition ability toward target template in the silica-based composites [91]. Titirici et al. investigated the effect of soluble RAFT agent at the grafting polymer from azo-initiator modified silica supports [126]. They demonstrated that the resulting polymers exhibit superior mass transfer properties compared to conventional bulk polymer and the polymer which prepared from azo-initiator modified surface in absence of soluble RAFT agent. More recently Mahadeo et al. reported the "grafting from" techniques via R-immobilized RAFT agent and iniferter-modified silica support to achieve more control on the film thickness and monomer conversion [229, 239, 240]. The authors used the living character of the iniferter and RAFT polymerization to produce layer by layer grafting of different MIPs onto wide pore silica. In addition, a novel class of porous materials generated after etching the disposable silica support [239, 240].

As far as we know, there are a few reports in the literature which describe the use of R-immobilized RAFT technique from silica core nanoparticels in MIPs context. In the current chapter, we used our previously well-established RAFT polymerization procedure to generate core-shell structured MIP nanoparticles for chiral discrimination. Silica nanoparticles with two different sizes ca 20 nm and ca 200 nm used as a support material. These cores modified by an aminosilane to introduce reactive amino groups for further coupling of a carboxylic acid containing RAFT agent. Before moving to graft cross-linked polymerization, the graft linear polymerization from RAFT modified silica nanoparticles was investigated. Afterwards the grafting of nano-shell molecularly imprinted polymers was carried out on RAFT-modified nano-silica support. The resulting beads were subsequently characterised by FTIR, TEM, DLS, TGA and elemental analysis. The polymers were tested for their affinity towards the template L-PA and its optical antipode D-PA in acetonitrile by reversed phase HPLC.

3.2 Results and Discussions

3.2.1 Silica nanoparticles

Herein, we used different silica core sizes as support martials to further modification. Colloidal silica MEK-ST (ca 20 nm) was obtained from Nissan Chemical as a 30 wt % dispersion in methylethylketone whereas silica nanoparticles (ca 100 nm, 200 nm, 330 nm)

were synthesised according to the Stöber procedure [241-244]. It involves the hydrolysis and condensation of tetraethoxysilane (TEOS) in the presence of water and with ammonia as a catalyst (pH 11.0-12.0) in alcohol (Figure 3.1). Several primary parameters including concentration of TEOS, ammonia, water, alcohol used as the solvent and reaction temperature have been reported that affect on the size and size distribution of silica particles[245]. By optimizing the quantity of the starting components the physical and chemical properties of NPs, such as NP size, porosity, monodispersity and colloidal stability can be tailored to suit different applications.

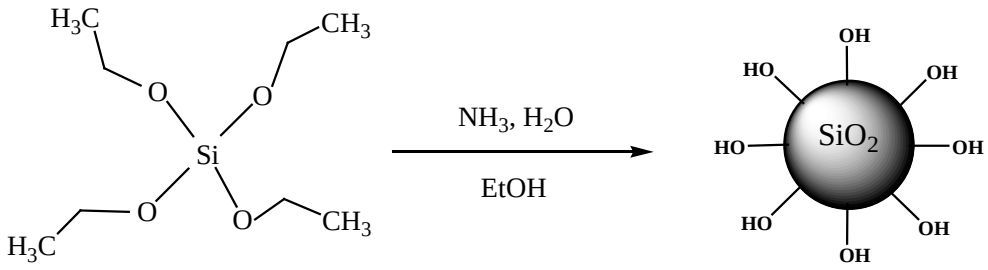

Figure 3.1. Schematic representation of the Stöber process.

The obtained particles were characterized by BET, DLS and TEM (Table 3.1). These nanoparticles SiNP1, SiNP2, SiNP3 and SiNP4 had particle sizes of ca 200 nm, ca 20 nm, ca 100 nm and ca 330 nm and a specific surface area 19 m^2/g, 182 m^2/g, 32 m^2/g and 11 m^2/g respectively. The TEM images showed that these nanoparticles had a nearly spherical shape and narrow particle size distribution (Figure 3.6).

Table 3.1. Properties of the silica bead supports

Support	Surface area(m^2/g)	Diameter $_{DLS}$ (nm)	Diameter $_{TEM}$ (nm)
SiNP1	19	211	200
SiNP2	182	25	20
SiNP3	32	123	100
SiNP4	11	364	330

3.2.2 Amino modified silica nanoparticles

The modification of silica nanoparticles can be achieved by using aminopropyltriethoxy silane (APTES) and aminopropyldimethylethoxysilane (APDMES) for two different sizes of

silica nanoparticles i.e. SiNP1 and SiNP2 respectively (Figure 3.2) [163, 246]. The silane coverage for a complete modification of the silica surface is expected to range from 3.5 to 4.0 μmol/m^2 [247]. Therefore, the amount of APTES was calculated according to the number of silanol groups on the silica surface (8 μmol/m^2) and the specific surface area for each silica sample. The reaction was performed under inert conditions and with an excess aminosilane, in order to obtain the maximum coverage of amino groups. The aminomodification of the colloidal silica nanoparticles with APDMES was performed using less amount of aminosilane according to the reported procedure by Li et al [163]. The reaction conditions and reagent stoichiometry had strong effect on the surface densities of the introduced ligands. The final products (SiNP1-NH_2 and SiNP2-NH_2) were characterized by FT-IR, TGA, TEM, DLS and elemental analysis. The surface densities of the introduced ligands were calculated from elemental analysis and TGA data.

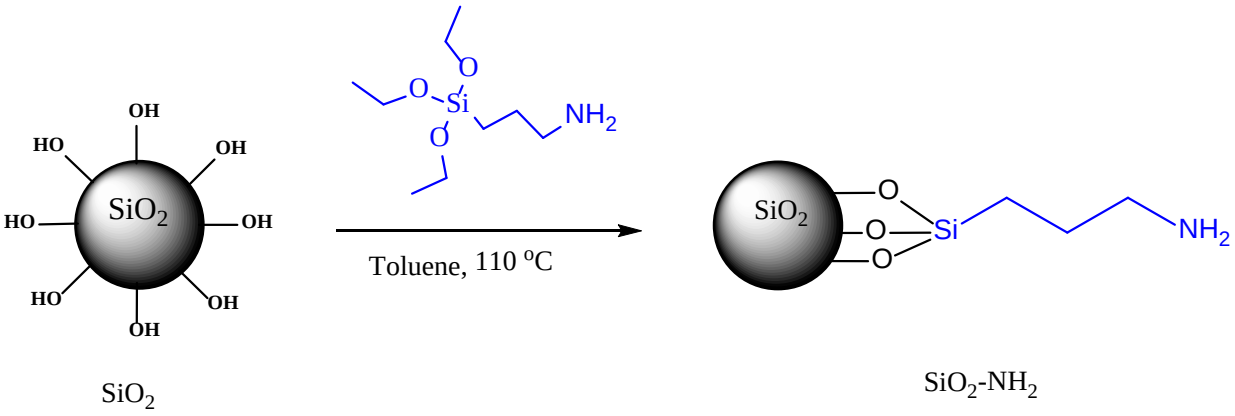

Figure 3.2. Amino modification of silica surface with APTES.

3.2.3 Immobilization of dithiobenzoate RAFT agent onto silica nanoparticles

The RAFT agent 4-cyanopentanoic acid dithiobenzoate (CPDB) was coupled to the aminofunctionalized silica cores via the R-group approach in accordance with our previous investigations (Figure 3.3) [229]. The carboxyl group of CPDB was first activated with ethyl chloroformate due to susceptibility of dithioesters to aminolysis even under mild conditions. The reactivity of the ethyl chloroformate activated ester bond is sufficiently high to selectively consume the amino groups in the presence of dithiobenzoate groups.

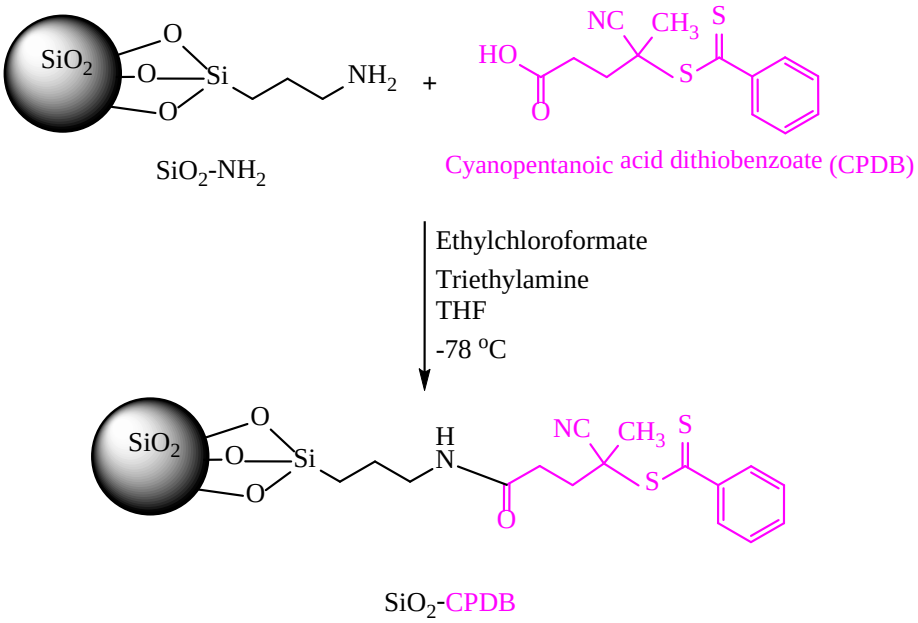

Figure 3.3. Immobilization of RAFT agent on silica surface.

After coupling the CPDB on silica surface a distinct pink color was apparent which associated with the dithioester. The color persisted through repeated washes with a THF/hexane solution, indicating that it was due to chain transfer agent covalently attached to the nanoparticle and not simply physically adsorbed. The colloidal stability of modified SiNP2 was evaluated in different solvents. Hence, whereas the bare and aminofunctionalized colloidal core particles SiNP2 and SiNP2-NH_2 formed stable dispersions in polar solvents (e.g. isopropanol, acetone, acetonitrile) the RAFT modified particles were partially aggregated nevertheless being well dispersible in alcohols such as isopropanol (Figure 3.4).

a) 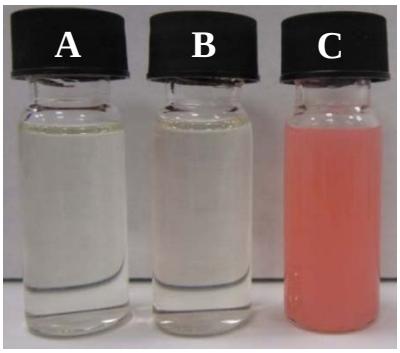

b) 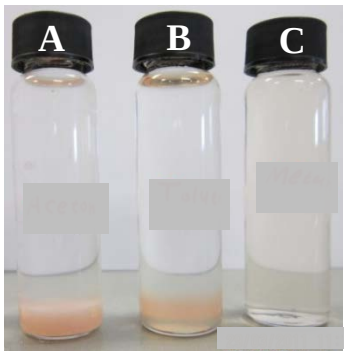

Figure 3.4. a) SiNP2 (A), SiNP2-NH_2 (B) and SiNP2-CPDB (C) dispersed in THF b) SiNP2-CPDB dispersed in acetone (A), toluene (B) and methanol (C).

3.2.4 Characterization of the resulting silica core nanoparticles

The products resulting from the previously described reactions were characterized using TEM, DLS, TGA, elemental microanalysis. In order to confirm successful immobilization step, the nanoparticles were characterized by elemental analysis and TGA. The percentage mass loss and percentage of carbon increased with each step respectively. The ligand and area density of coupled ligand were calculated by two methods. The obtained results are in good agreement (Table 3.2 and Table 3.3).

TGA analysis gives access to an estimated grafting density of coupled groups on silica surface by determining the differences of weight loss between pure and modified silica nanoparticles. TGA of the bare and modified silica nanoparticles are shown in Figure 3.5. TGA was performed between room temperature and 800 ^{o}C under N_2 atmosphere. For bare SiO_2, the weight loss up to 120 ^{o}C was related to physically combined water and unvolatilized solvent, while the weight loss from 120 to 800 ^{o}C was assigned to chemically combined water and silanol groups dehydroxylation on the silica nanoparticles [248]. This weight loss of modified supports can be attributed to the thermal decomposition of immobilised ligands on modified silica nanoparticles. The data are presented in Table 3.2.

Table 3.2. Characterisation of modified silica supports by TGA.

Support[a]	TGA (% mass loss)	Ligand density[b] (mmol/g)	Area density[b] (μmol/m^2)
SiNP1	6.78	-	-
SiNP1-NH_2	8.57	0.19	10.38
SiNP1-CPDB	9.78	0.08	4.56
SiNP2	2.73	-	-
SiNP2-NH_2	4.04	0.13	0.70
SiNP2-CPDB	6.01	0.09	0.49

a) The ligand immobilization was performed in two steps by consecutive coupling of 3-aminopropyltriethoxysilane (APTES) (SiNP1-NH_2) or 3-aminopropyldimethylethoxysilane (APDMES) (SiNP2-NH_2) and 4-cyanopentanoic acid dithiobenzoate (RAFT) on the indicated core beads as described in the experimental section. The SiNP1 displayed a number average particle size of 211 nm with a polydispersity index of 0.257 and a specific surface area of 19 m^2/g whereas the SiNP2 displayed an average particle size of 25 nm with a polydispersity of PDI=0.245 and a specific surface area of 182 m^2/g.

b) The ligand density and area density were calculated from the mass loss according to Eq. 2-1 and Eq. 2-2.

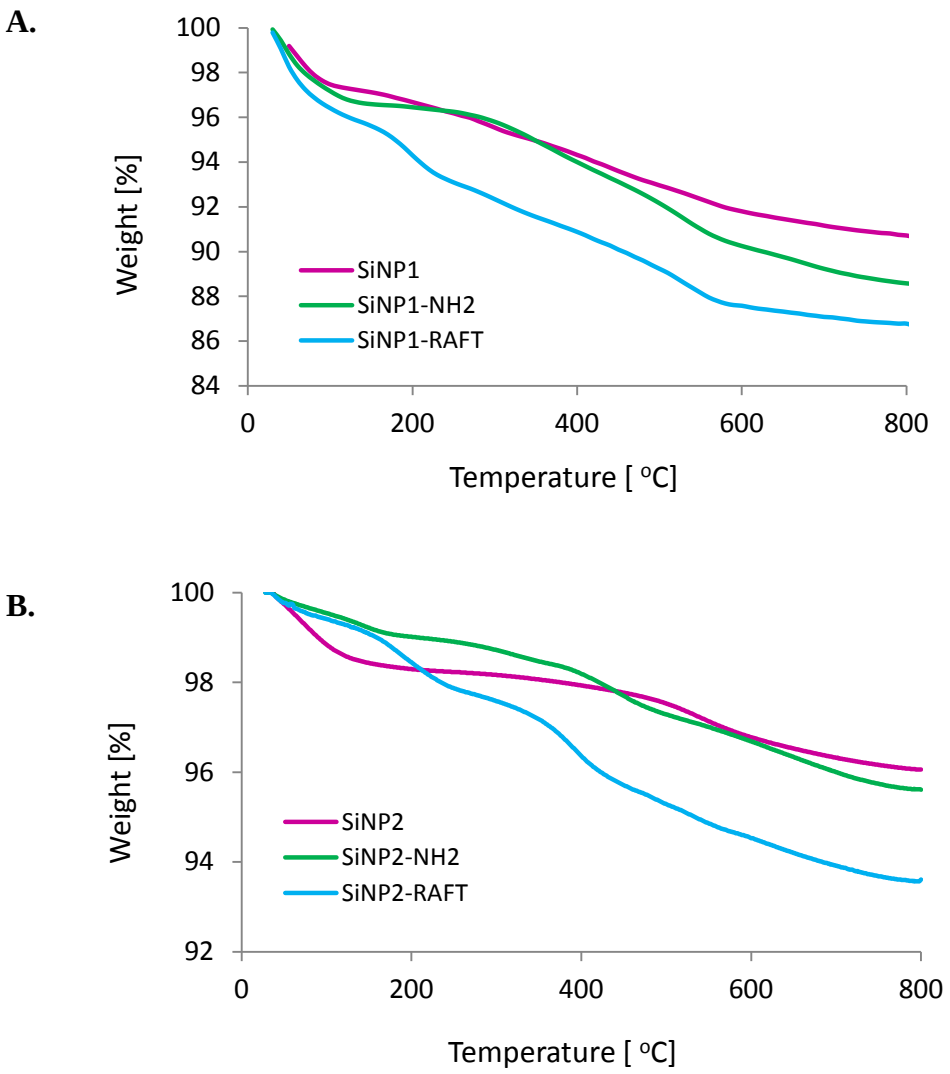

Figure 3.5. Thermal gravimetric analysis of SiNP1 (pink), SiNP1-NH_2 (green) and SiNP1-CPDB (blue) (A), SiNP2 (pink), SiNP2-NH_2 (green) and SiNP2-CPDB (blue) (B).

From elemental microanalysis data, more precisely from the change in carbon and nitrogen contents in each step, we could estimate the amount of immobilized ligand on the silica surface. The data are presented in Table 3.3. On the basis of the increase in carbon content, a maximum coverage of 49% coupled CPDB for SiNP1 support and 6% for SiNP2 was calculated. The distance between two ligands was 0.6 nm for SiNP1 support and 1.9 nm for SiNP2 which is likely higher than the first step (Table 3.3). This indicates that the coupling reaction was successfully formed.

Table 3.3. Results from the characterisation of modified silica beads by elemental analysis.

Modified support[a]	%C	%N	%S	Ligand density[b] (mmol/g)	Area density[b] (μmol/m^2)	Coverage[c] (%)	Distance[d] (nm)
SiNP1-NH_2	1.19	0.43	-	0.20	10.72	134	0.4
SiNP1-CPDB	2.34	0.38	0.49	0.075	3.96	49	0.6
SiNP2-NH_2	2.10	0.81	-	0.36	2.01	25	0.9
SiNP2-CPDB	3.33	0.69	0.56	0.081	0.44	6	1.9

a) The ligand immobilization was performed in two steps by consecutive coupling of 3-aminopropyltriethoxysilane (APTES) (SiNP1-NH_2) or 3-aminopropyldimethylethoxysilane (APDMES) (SiNP2-NH_2) and 4-cyanopentanoic acid dithiobenzoate (RAFT) on the indicated core beads as described in the experimental section.

b) The ligand density and area density were calculated on the basis of the increase in carbon content, as described in Eq. 2-10 and Eq. 2-12.

c) The coverage (C) was calculated according to Eq. 2-13, assuming a maximum silanol group density of 8 μmol/m^2.

d) The average distance d_L (nm) between the coupled ligands assuming a random ligand distribution was calculated according to Eq. 2-14.

The yield of coupling in each step was calculated based on results obtained from elemental analysis. From Table 3.3 can be observed that the final densities of the functional groups after modifying the silica with the corresponding silanes ranged between 0.20 mmol/g for SiNP1-NH_2 and 0.36 mmol/g for SiNP2-NH_2. The final densities of immobilized RAFT agent were in the range of 0.075 mmol/g for SiNP1-CPDB and 0.081 mmol/g for SiNP2-CPDB.

The morphology of the particles was characterized with TEM. As shown in Figure 3.6 and Figure 3.7, the particles exhibited spherical structures with a diameter about 200 nm and 20 nm for SiNP1-CPDB and SiNP2-CPDB respectively.

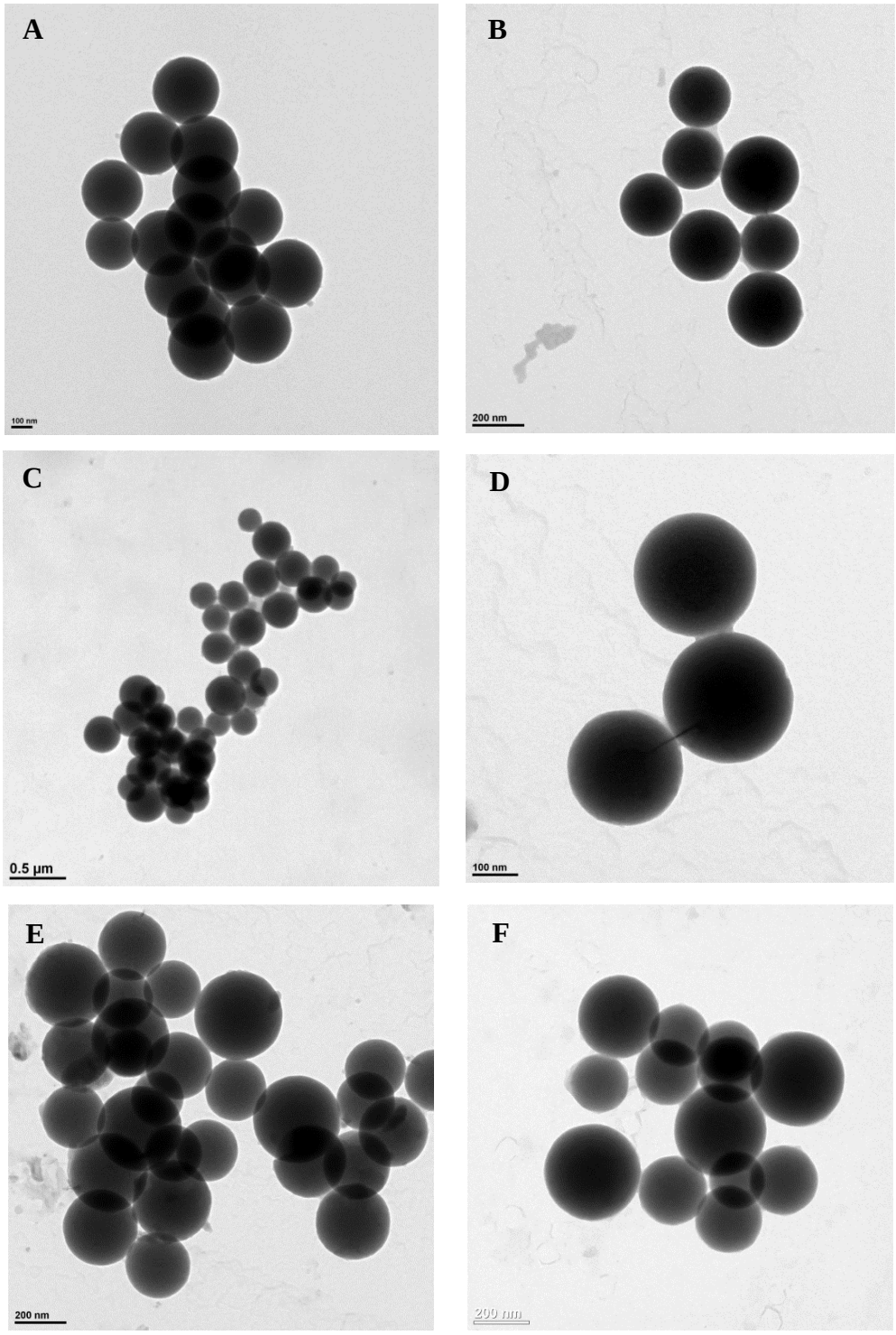

Figure 3.6. TEM images of SiNP1 (A, B), SiNP1-NH_2 (C, D), and SiNP1-CPDB (E, F). The scale bar is 100 nm in the case of (A, D); 500 nm for (C) and 200 nm for (B, E, F).

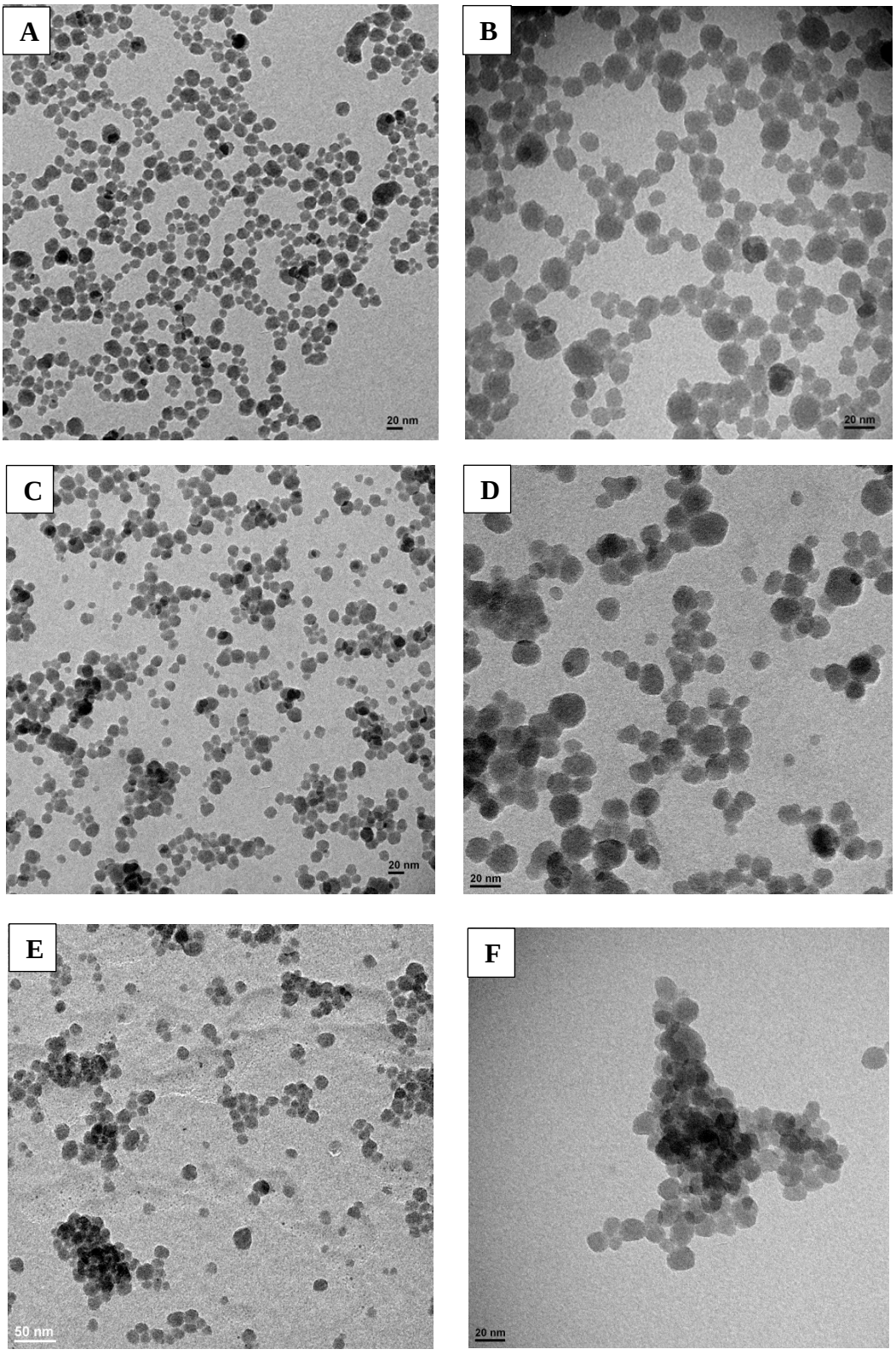

Figure 3.7. TEM images of SiNP2 (A,B), SiNP2-NH_2 (C,D), and SiNP2-CPDB (E,F). The scale bar is 20 nm in the case of (A), (B), (C), (D), (F); and 50 nm for (E).

The particle sizes were further measured with DLS, which showed an average particle size with a relatively narrow distribution of tow samples (Figure 3.8 and Figure 3.9).The number average particle size and polydispersity of resultant nanoparticles are presented in Table 3.4. Compared with the data obtained by TEM, the slight increase in diameter in DLS was observed due to aggregation of modified particles.

Table 3.4. Number average particle size and polydispersity from DLS of nanoparticles used in the study.

Particle [a]	Diameter (nm)	Polydispersity
SiNP1	211	0.257
SiNP1-NH_2	243	0.245
SiNP1-CPDB	331	0.352
SiNP2	25	0.245
SiNP2-NH_2	31	0.183
SiNP2-CPDB	65	0.341

a) The dispersing solvent was isopropanol.

A.

		Size (d.nm):	% Intensity:	St Dev (d.nm):
Z-Average (d.nm): 211.0	Peak 1:	260.4	100.0	90.79
PdI: 0.257	Peak 2:	0.000	0.0	0.000
Intercept: 0.949	Peak 3:	0.000	0.0	0.000
Result quality : Good				

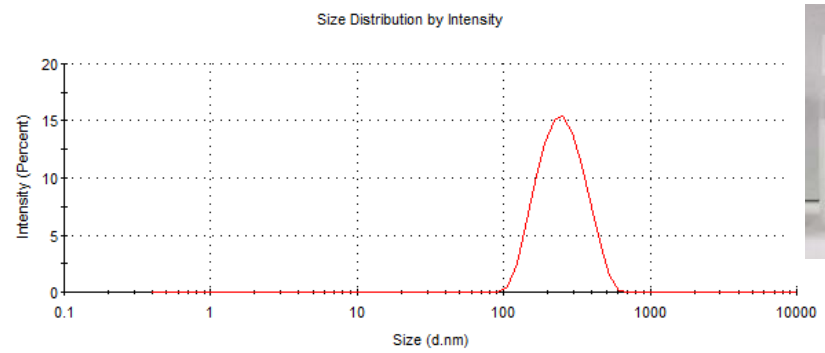

B.

		Size (d.nm):	% Intensity:	St Dev (d.nm):
Z-Average (d.nm): 243.0	Peak 1:	266.3	96.0	124.0
PdI: 0.245	Peak 2:	4901	4.0	674.4
Intercept: 0.319	Peak 3:	0.000	0.0	0.000
Result quality : Refer to quality report				

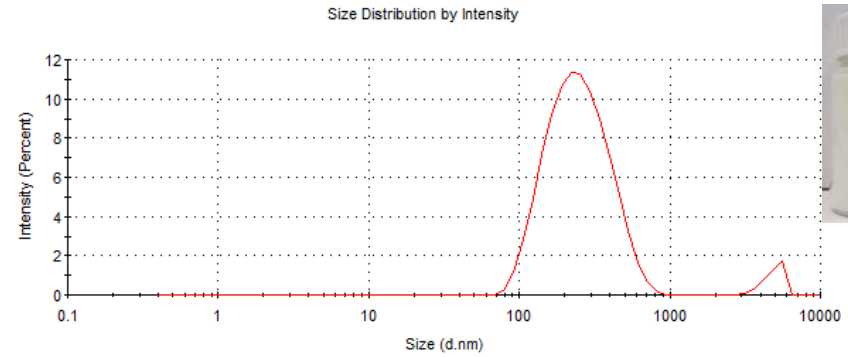

C.

		Size (d.nm):	% Intensity:	St Dev (d.nm):
Z-Average (d.nm): 331.0	Peak 1:	277.8	97.1	80.16
PdI: 0.352	Peak 2:	5443	2.9	274.1
Intercept: 0.508	Peak 3:	0.000	0.0	0.000
Result quality : Refer to quality report				

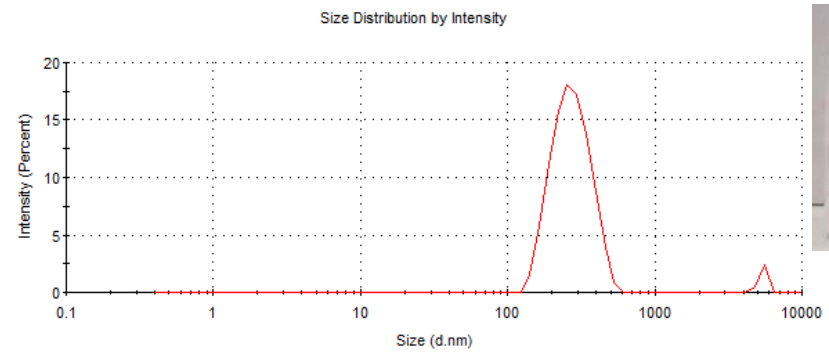

Figure 3.8. DLS analysis of SiNP1 (A), SiNP1-NH_2 (B) and SiNP1-CPDB (C).

A.

		Size (d.nm):	% Intensity:	St Dev (d.nm):
Z-Average (d.nm): 25.10	Peak 1:	33.98	100.0	18.67
PdI: 0.245	Peak 2:	0.000	0.0	0.000
Intercept: 0.900	Peak 3:	0.000	0.0	0.000
Result quality : Good				

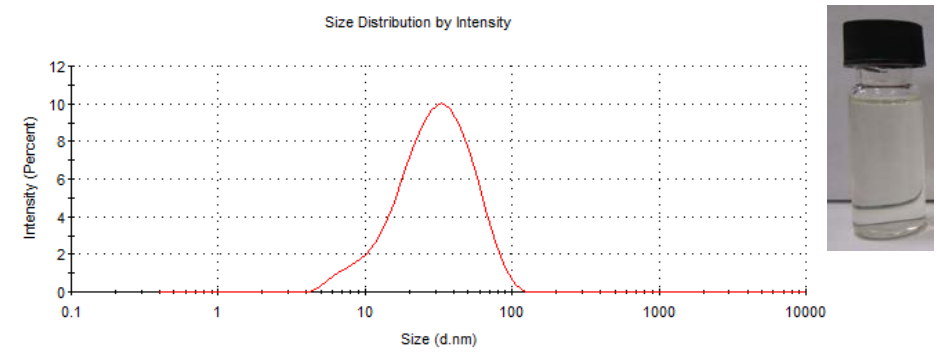

B.

		Size (d.nm):	% Intensity:	St Dev (d.nm):
Z-Average (d.nm): 31.91	Peak 1:	37.36	98.3	16.94
PdI: 0.183	Peak 2:	4171	1.7	1016
Intercept: 0.957	Peak 3:	0.000	0.0	0.000
Result quality : Good				

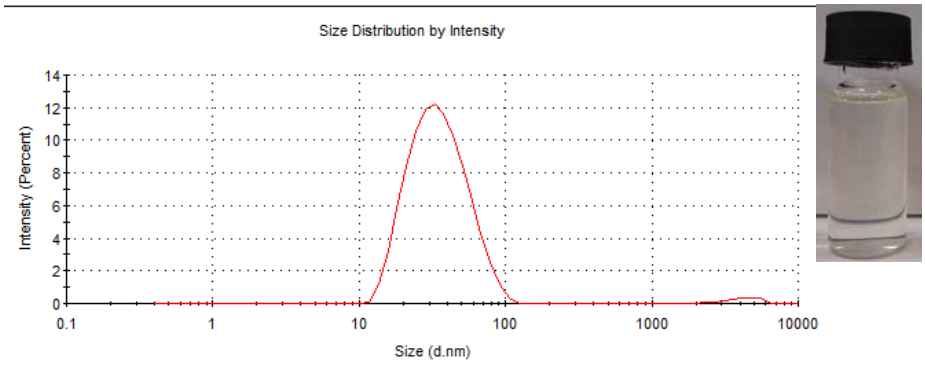

C.

		Size (d.nm):	% Intensity:	St Dev (d.nm):
Z-Average (d.nm): 65.53	Peak 1:	63.22	92.9	24.28
PdI: 0.341	Peak 2:	5202	4.0	474.5
Intercept: 0.867	Peak 3:	506.5	3.1	125.0
Result quality : Good				

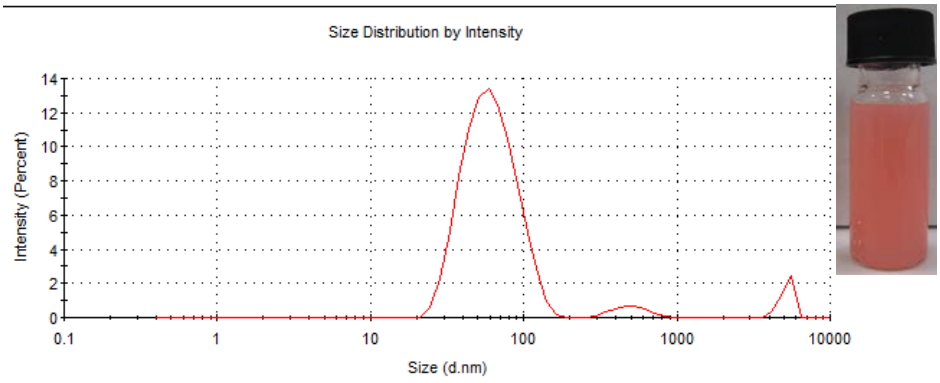

Figure 3.9. DLS analysis of SiNP2 (A), SiNP2-NH_2 (B) and SiNP2-CPDB (C).

3.2.5 Synthesis of trithiocarbonate RAFT agent

The appropriate choice of RAFT agent is important to the success of RAFT polymerizations. This holds true whether polymerizations are conducted in aqueous or nonaqueous media. Indeed, some general guidelines regarding appropriate choice of RAFT agent for a given monomer/monomer family can be found in two recent reviews[114, 249]. Trithiocarbonates are versatile RAFT agents and have previously been shown to facilitate the polymerization of acrylamide in aqueous media [250]. These RAFT agents are readily synthesized, cause less retardation and are more hydrolytically stable than dithiobenzoates [251]. We have chosen the trithiocarbonate RAFT agent as a chain transfer agent to polymerize acrylamide monomers in aqueous media (Figure 3.10). This RAFT agent was synthesized by reacting of carbon disulfide, chloroform, acetone and sodium hydroxide in the presence of a phase transfer catalyst (PTC) [252].

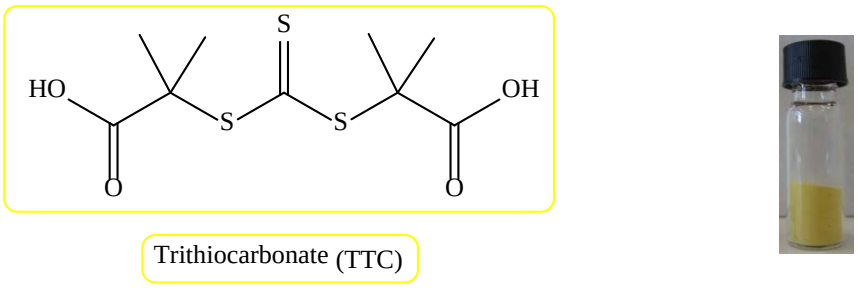

Figure 3.10. Chemical structure of trithiocarbonate RAFT agent used to create MIPs.

3.2.6 Immobilization of trithiocarbonate RAFT agent onto silica nanoparticles

The RAFT agent S,S′-Bis(α,α′-dimethyl-α″-acetic acid)- trithiocarbonate (TTC) was coupled to the aminofunctionalized silica core in accordance with our previous investigations (Figure 3.11) [229].The colloidal silica nanoparticles with 25 nm core size were first modified by using 3-aminopropyldimethylethoxysilane (APDMES) to introduce amino groups on silica support. The subsequent step was the coupling of trithiocarbonate RAFT agent in presence of ethylchloroformate and triethylamine under N_2 protection at -78 ^{o}C. After coupling the TTC on silica surface a distinct yellow color was apparent which associated with the trithiocarbonate. The color persisted through repeated washes with a THF/hexane solution, indicating that it was due to chain transfer agent covalently attached to

the nanoparticle and not simply physically adsorbed. The final products (SiNP-NH_2 and SiNP-RAFT) were characterized by FT-IR, TGA, TEM, DLS and elemental analysis. The surface densities of the introduced ligands were calculated from elemental analysis and TGA data.

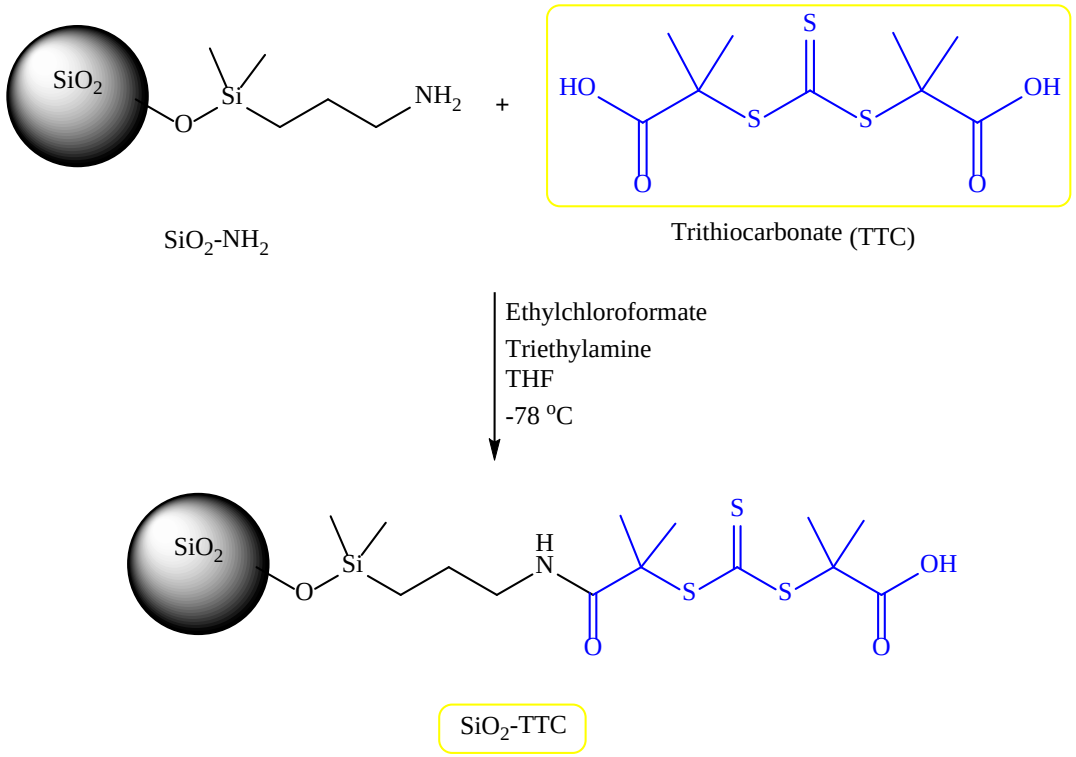

Figure 3.11. Immobilization of RAFT agent on silica surface.

3.2.7 Characterization of surface-modified silica nanoparticles

The products resulting from the previously described reactions were characterized using TEM, TGA, elemental microanalysis. In order to confirm successful immobilization step, the nanoparticles were characterized by elemental analysis and TGA. The percentage mass loss and percentage of carbon increased with each step respectively. The ligand density and area density of coupled ligand were calculated by two methods. The obtained results are presented in (Table 3.5 and Table 3.6). TGA analysis gives access to an estimated grafting density of coupled groups on silica surface by determining the differences of weight loss between pure and modified silica nanoparticles. TGA of the bare and modified silica nanoparticles are shown in Figure 3.12. TGA was performed between room temperature and 800 ^{o}C under N_2 atmosphere. This weight loss of modified supports can be attributed to the thermal

decomposition of immobilized ligands on modified silica nanoparticles. The data are presented in Table 3.5.

Table 3.5. Characterisation of modified silica supports by TGA.

Support[a]	TGA (% mass loss)	Ligand density[b] (mmol/g)	Area density[b] (μmol/m^2)
SiNP-NH_2	3.81	0.104	0.57
SiNP-TTC	5.71	0.085	0.49

a) The ligand immobilization was performed in two steps by consecutive coupling of 3-aminopropyldimethylethoxysilane (APDMES) (SiNP-NH_2) and S,S′-Bis(α,α′-dimethyl-α′′-acetic acid)-trithiocarbonate (TTC) on the indicated core beads as described in the experimental section. The SiNP displayed an average particle size of 25 nm with a polydispersity of PDI= 0.245 and a specific surface area of 182 m^2/g.
b) The ligand density and area density were calculated from the mass loss according to Eq. 2-1 and Eq. 2-2.

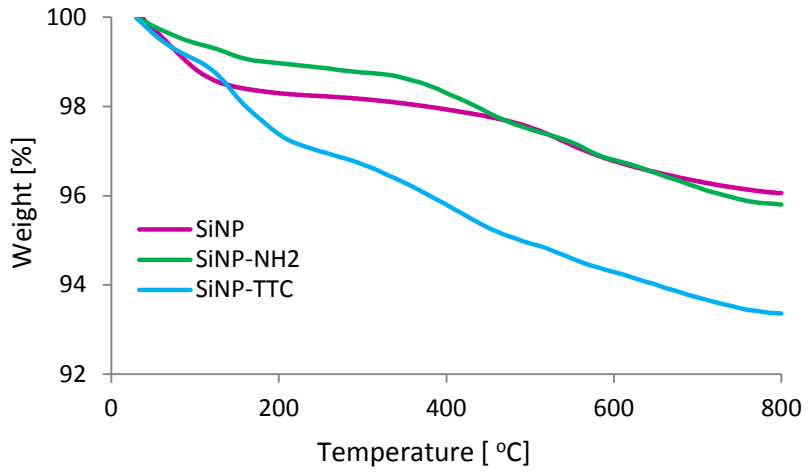

Figure 3.12. Thermal gravimetric analysis of SiNP (pink), SiNP-NH_2 (green) and SiNP-TTC (blue).

From elemental microanalysis data, more precisely from the change in carbon and nitrogen contents in each step, we could estimate the amount of immobilized ligand on the silica surface. The data are presented in Table 3.6. On the basis of the increase in carbon content, a maximum coverage of 23% coupled amino groups and 8% coupled trithiocarbonate groups was calculated. The distance between two ligands was 0.9 nm for SiNP-NH_2 support and 1.7 nm for SiNP-TTC which is likely higher than the first step (Table 3.6). This indicates that the coupling reaction was successfully formed.

Table 3.6. Results from the characterisation of modified silica beads by elemental analysis.

Modified support[a]	%C	%N	%S	Ligand density[b] (mmol/g)	Area density[b] (μmol/m^2)	Coverage[c] (%)	Distance[d] (nm)
SiNP-NH_2	1.96	0.74	-	0.34	1.87	23	0.9
SiNP-TTC	3.12	0.58	0.82	0.11	0.61	8	1.7

a) The ligand immobilization was performed in two steps by consecutive coupling of 3- aminopropyldimethylethoxysilane (APDMES) (SiNP-NH_2) and S,S′-Bis(α,α′-dimethyl-α′′-acetic acid)-trithiocarbonate (TTC) on the indicated core beads as described in the experimental section.

b) The ligand density and area density were calculated on the basis of the increase in carbon content, as described in Eq. 2-10 and Eq. 2-12.

c) The coverage (C) was calculated according to Eq. 2-13, assuming a maximum silanol group density of 8 μmol/m^2.

d) The average distance d_L (nm) between the coupled ligands assuming a random ligand distribution was calculated according to Eq. 2-14.

The yield of coupling in each step was calculated based on results obtained from elemental analysis. From Table 3.6 can be observed that the final density of the functional groups after modifying the silica with the corresponding silane was 0.34 mmol/g. The final density of immobilized trithiocarbonate RAFT agent was in the range of 0.11 mmol/g.

The morphology of the particles was characterized with TEM. As shown in Figure 3.13, the particles exhibited spherical structures with some aggregation and a diameter about 20-25 nm.

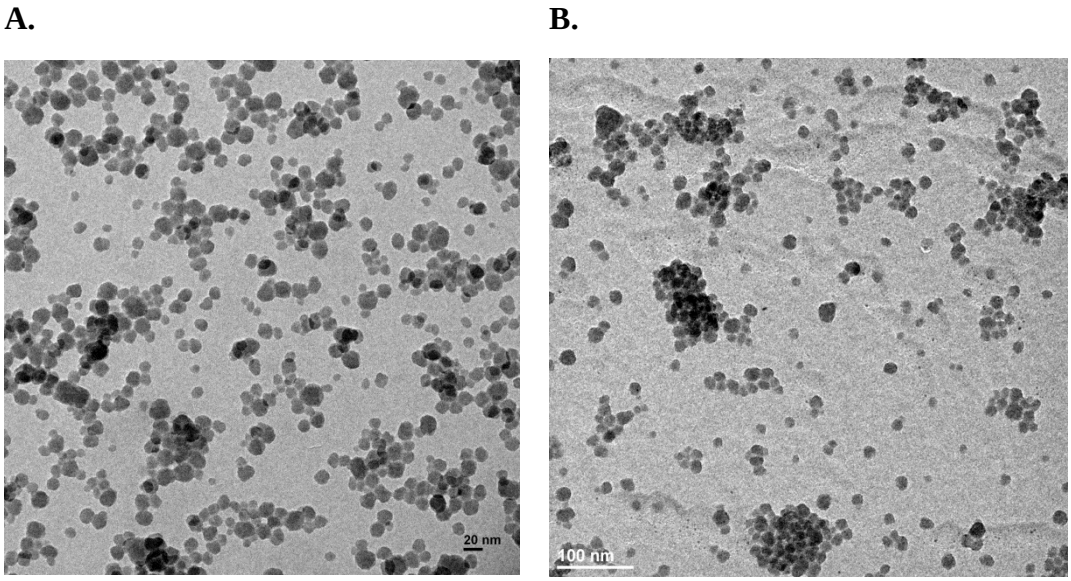

Figure 3.13. TEM images of SiNP-NH_2 (A), SiNP-TTC (B). The scale bar is 20 nm in the case of (A) and 100 nm for (B).

3.2.8 Optimization for the grafted linear polymers from silica support

In the early studies and before moving to graft cross-linked polymerization, the graft linear polymerization from RAFT-modified silica nanoparticles was investigated (Figure 3.14). Due to solubility of ungrafted linear polymers, separation of these polymers from grafted polymers were much easier than insoluble crosslinked free polymers. This property cause to obtain the pure grafted linear polymers by repeated centrifugation-redispersion procedure. RAFT-modified silica nanoparticles were used to investigate the kinetics of MMA and styrene surface graft polymerization by Benicewicz and co-workers [162, 163, 253]. They demonstrated that the cleaved PMMA and PSt had a number-average molecular weight of 37900 g/mol, 8500 g/mol and a PDI of 1.07 and 1.10, respectively. For MAAM surface graft polymerization, we expected to achieve a number-average molecular weight of 72000 g/mol, and a PDI of 1.05 [250]. Based on these studies, methyl methacrylate (MMA), styrene (St) and methacrylamide (MAAM) were grafted from silica substrate and characterized by TGA, TEM and elemental analysis.

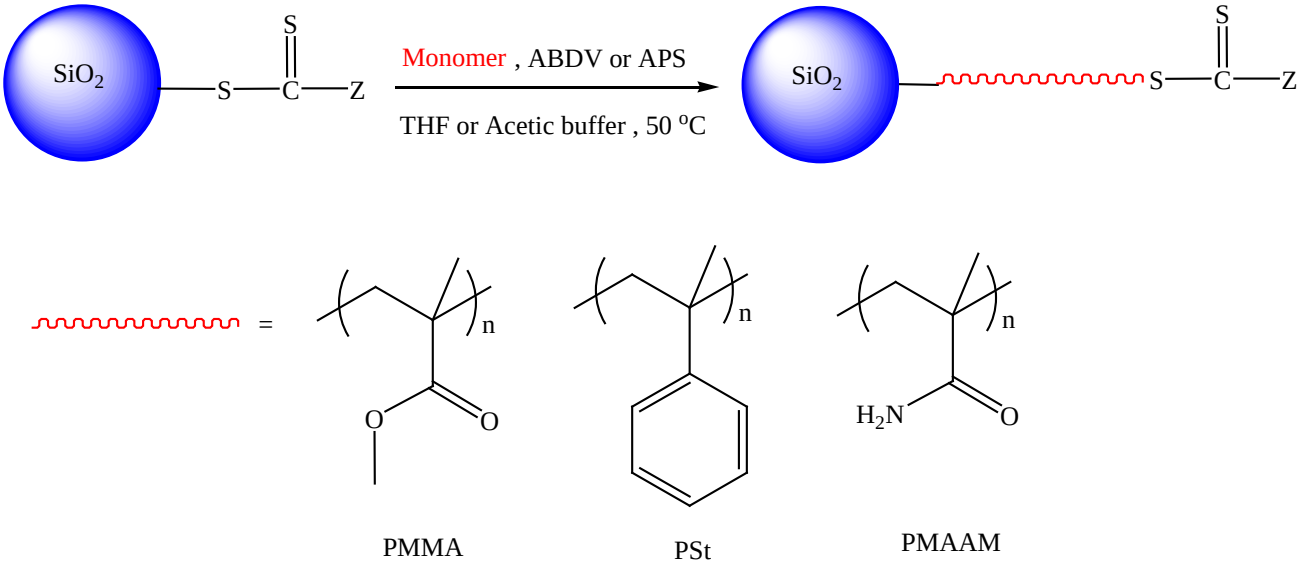

Figure 3.14. Schematic representation of graft polymerization from RAFT-modified silica nanoparticles.

3.2.8.1 Methyl methacrylate graft polymerization from RAFT-modified silica nanoparticles (SiO_2-g-PMMA)

The graft polymerization of methyl methacrylate (MMA) from the RAFT-modified silica nanoparticles was carried out in the presence of ABDV as a conventional radical initiator. The polymerization was carried out at a mild temperature, 50 °C, in THF. Two different sizes of core silica nanoparticles i.e. 100 nm and 200 nm were used as solid support. The effect of polymerization time and the molar ratios of ABDV/RAFT on the graft polymerization were investigated. The pure PMMA-grafted silica particles were obtained by repeated centrifugation-redispersion procedure in the THF solution. TGA, TEM, SEM and elemental analysis were used to characterize the PMMA-grafted silica nanoparticles (Table 3.7). The results showed that high conversion efficiency can be achieved via increasing the polymerization time and the molar ratios of ABDV/RAFT [163, 254].

3.2.8.2 Styrene graft polymerization from RAFT-modified silica nanoparticles (SiO_2-g-PSt)

Surface-initiated RAFT polymerization onto SiNP was performed employing styrene (St) as monomer in the presence of ABDV as a conventional radical initiator. Polymerization was

conducted in THF at 50 ^{o}C. After polymerization, the polystyrene grafted SiNP were extensively purified by repeating the cycle of centrifugation and redispersion in THF to remove the free polymers from the particles. The resulting polymers were characterized by TGA, TEM, SEM and elemental analysis (Table 3.7). The results revealed that in surface-initiated RAFT polymerization mediated via dithiobenzoate as a chain transfer group, the conversion efficiency of polystyrene chains was low even at longer polymerization times. This might be attributed to unavoidable steric hindrance during graft polymerization [163, 254].

3.2.8.3 Methacrylamide graft polymerization from RAFT-modified silica nanoparticles (SiO_2-g-PMAAM)

The graft polymerization of methacrylamide (MAAM) from the RAFT-modified silica nanoparticles was carried out in the presence of ammonium persulfate (APS) as a radical initiator in acetic buffer solution (pH5, 10mM). The trithiocarbonate-modified silica nanoparticles were used for methacrylamide graft polymerization in aqueous media (See 3.2.6). Trithiocarbonate RAFT agents are readily synthesized, cause less retardation and are more hydrolytically stable than dithiobenzoates [251]. Acidic buffer (pH5) was used as polymerization media to avoid loss of trithiocarbonate end groups via a combination of aminolysis and hydrolysis[250, 255]. After polymerization, the PMAAM-grafted SiNP were extensively purified by repeating the cycle of centrifugation and redispersion in water to remove the free polymers from the particles. The resulting polymers were dried at 40 ^{o}C under vacuum and characterized by TGA, TEM, SEM and elemental analysis (Table 3.7).

3.2.9 Characterization of grafted linear polymers

After polymerization, the beads were subsequently characterized by TGA, TEM, SEM, and elemental analysis. Elemental analysis and TGA were used to confirm the successful grafting of polymers on silica cores. By using the TGA mass loss data the gravimetric conversion of grafted polymers on silica cores were calculated. The results revealed that the conversion efficiency of polymer chains was increased by using long polymerization time. The results are listed in Table 3.7.

The SEM and TEM images of the polymer grafted silica NPs are shown in Figure 3.16 and Figure 3.17. Both images demonstrated the highly uniform spherical morphology with the size of about 100 nm and 200 nm. In the comparison of TEM images before and after polymerization, a shell structure can be seen on the silica particles after polymerization with a uniform thickness of the shells which are signed via arrow in Figure 3.16 and Figure 3.17. The results obtained from these techniques confirmed that grafting occurred from the surface of the silica support. The soluble ungrafted free polymer in the wash fractions was precipitated in n-hexane and then subjected to TGA analyses. The gravimetric yield of the ungrafted free polymer after drying is shown in Table 3.8.

Table 3.7. Results from the characterization of grafted linear polymers.

Polymer name [a]	Solvent	Time (h)	RAFT/ Initiator	%C	%N	%S	Mass loss [b] (%)	Conv.[c] (%)
SiO_2-g-PMMA-1[d]	THF	15	1/1	7.36	0.63	0.49	18	16
SiO_2-g-PMMA-2[d]	THF	18	1/1	8.25	0.69	0.51	26.7	38
SiO_2-g-PMMA-3[e]	THF	20	1/1	8.91	0.67	0.47	19.2	22
SiO_2-g-PMMA-4[e]	THF	20	5/1	7.89	0.61	0.47	17	16.5
SiO_2-g-PSt-1[d]	THF	40	1/1	6.54	0.57	0.51	13.6	3.1
SiO_2-g-PSt-2[d]	THF	40	2/1	6.43	0.62	0.48	13.5	3
SiO_2-g-PSt-3[d]	THF	72	1/1	7.88	0.59	0.49	15.1	4.6
SiO_2-g-PSt-4[d]	THF	72	2/1	7.41	0.60	0.56	15	4.4
SiO_2-g-PMAAM-1[e]	buffer	16	2/1	6.12	1.49	0.41	9	16
SiO_2-g-PMAAM-2[e]	buffer	16	4/1	5.93	1.37	0.39	7	9.5
SiO_2-g-PMAAM-3[e]	buffer	24	1/1	6.85	1.68	0.40	13	31
SiO_2-g-PMAAM-4[e]	buffer	24	2/1	6.14	1.54	0.42	9.6	19

a) See experimental section for details.

b) Mass loss by thermal gravimetric analysis (TGA).

c) Gravimetric conversion: Conversion= mass loss (TGA)/mass of monomer feed.

d) Silica core size is 100 nm.

e) Silica core size is 200 nm.

Table 3.8. Amount of ungrafted free polymers in the wash fractions.

Polymer name [a]	Solvent	Time (h)	RAFT/ Initiator	Weight (mg)	Gravimetric yield [b] (%)
PMMA-1	THF	15	1/1	250	53
PMMA-2	THF	18	1/1	210	45
PMMA-3	THF	20	1/1	231	49
PMMA-4	THF	20	5/1	195	41
PSt-1	THF	40	1/1	520	57
PSt-2	THF	40	2/1	490	54
PSt-3	THF	72	1/1	593	65
PSt-4	THF	72	2/1	549	60
PMAAM-1	buffer	16	2/1	170	53
PMAAM-2	buffer	16	4/1	142	44
PMAAM-3	buffer	24	1/1	161	50
PMAAM-4	buffer	24	2/1	144	45

a) Ungrafted free polymer in the wash fractions.

b) Gravimetric yield= gravimetric mass of ungrafted polymer /mass of monomer feed.

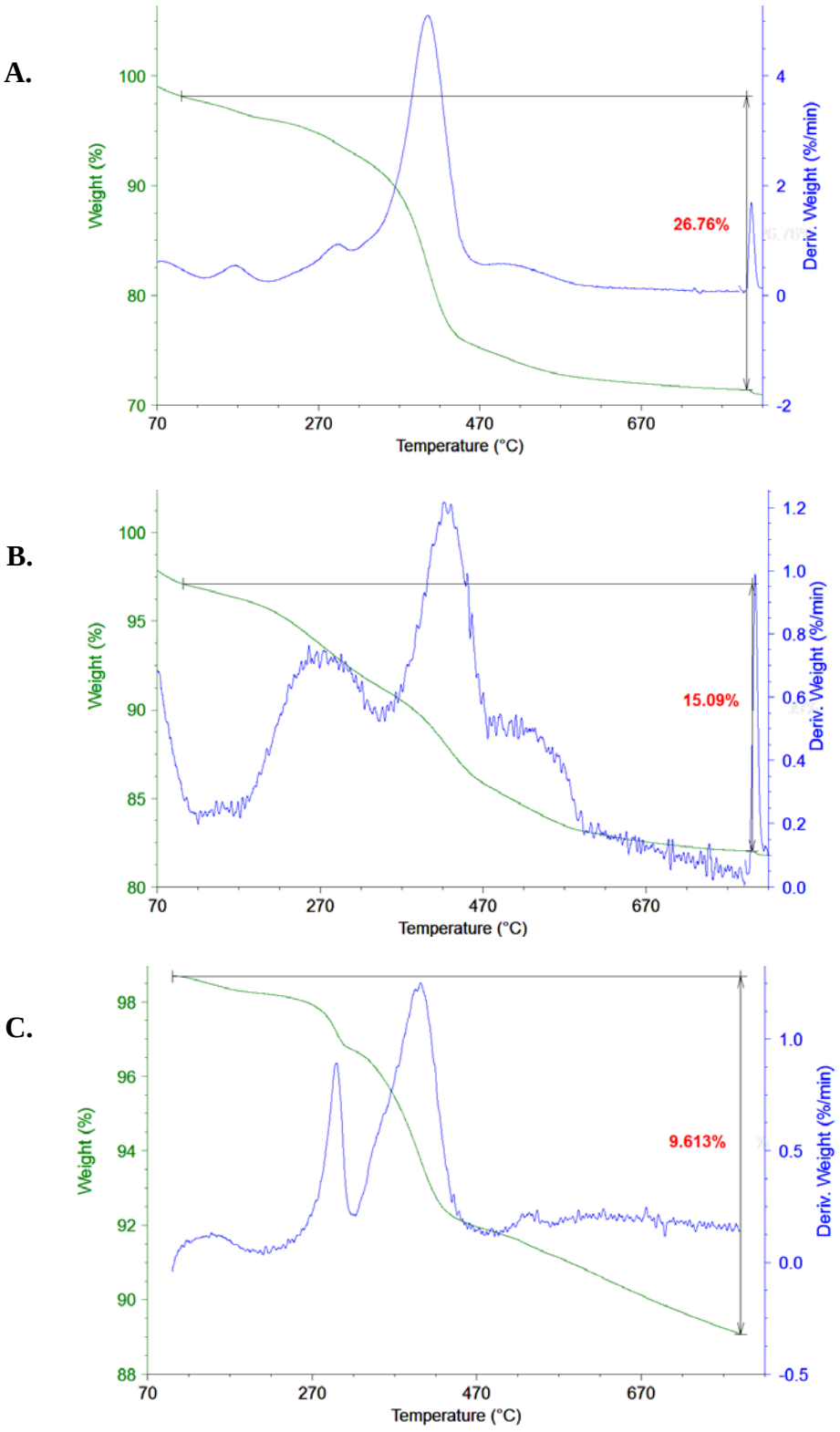

Figure 3.15. Thermal gravimetric analysis of SiO_2-g-PMMA-2 (A), SiO_2-g-PSt-3 SiO_2-g-PMAAM-4 (C).

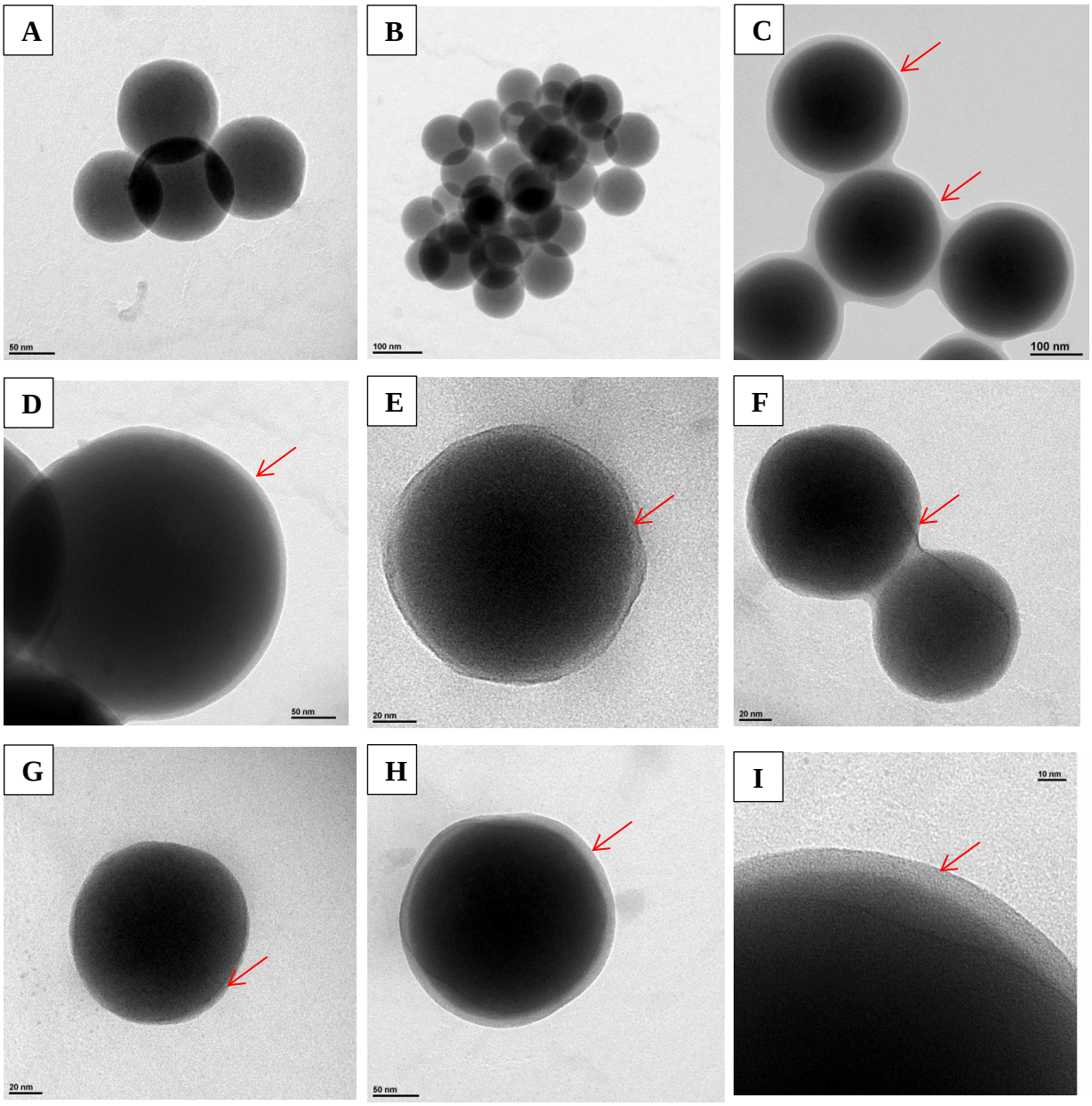

Figure 3.16. TEM images of bare silica NPs (A, B); SiO_2-g-PMMA (C, D, E); SiO_2-g-PSt (F, G); SiO_2-g-PMAAM (H, I). The polymer shells are indicated by arrows. The scale bar is 50 nm in the case of (A, D, H) 100 nm for (B, C) 20 nm for(E, F, G) and 10 nm for (I).

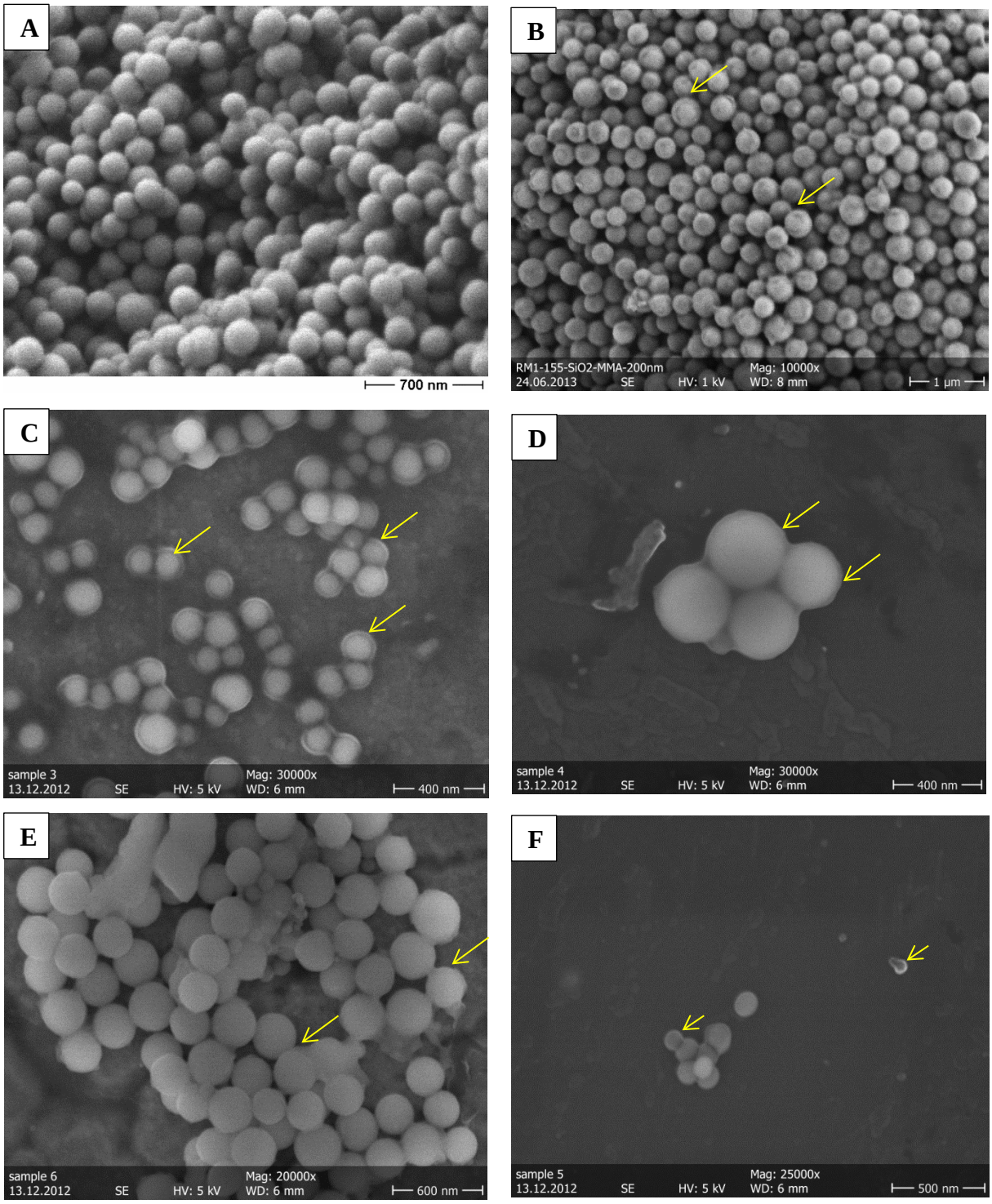

Figure 3.17. SEM images of bare silica NPs (A); SiO_2-g-MMA (B, C, D); SiO_2-g-MAAM(E); SiO_2-g-PSt (F). The polymer shells are indicated by arrows.

3.2.10 Grafting of molecularly imprinted polymer shells via RAFT-modified silica core nanoparticles

The “grafting from” technique for producing L-phenylalanine anilide (L-PA) imprinted core-shell nanoparticles was investigated using our previously reported procedure [229, 239]. Imprinted copolymers of methacrylic acid (MAA) and ethyleneglycol dimethacrylate (EDMA) were then grafted from the supports as shown in Figure 3.18, that is, in a 1:5 molar ratio of MAA to EDMA in presence of 5 mol % of Lphenylalanine anilide (L-PA) as chiral template and toluene as solvent. Grafting requires an external source of primary radicals which was here provided by a soluble initiator, added in substoichiometric amounts with respect to the RAFT agent [239].

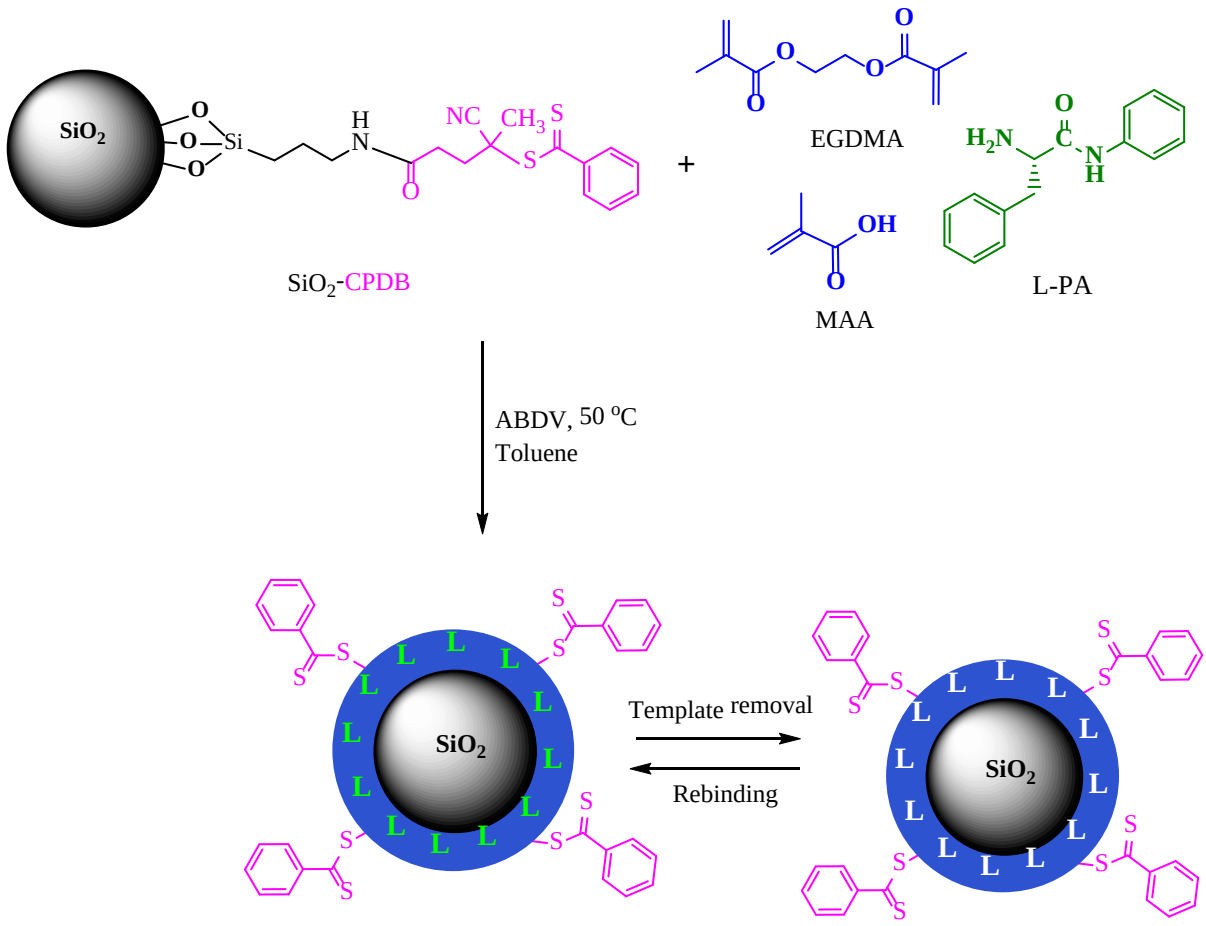

Figure 3.18. Procedure used to synthesise silica core-MIP shell nanoparticles.

In preparing the grafting polymer, a molar ratio CPDB/ABDV = 4 and CPDB/ABDV= 3 were used for SiNP1-MIP&NIP and SiNP2-MIP&NIP, respectively. The relatively low ABDV/CPDB ratio helped to reduce the amount of free polymer derived from the initiator, and yet maintain a moderate polymerization rate [163]. The quantity of monomer relative to the silica supports were adjusted to result in shells/films with approximately 16 nm (SiNP1) or 4 nm (SiNP2) thick shells. After polymerization the beads were isolated by centrifugation and subjected to repetitive washing-centrifugation cycles in order to remove any leachables (e.g. template, oligomers, unreacted monomers). Five cycles were sufficient for exhaustive template removal as concluded by HPLC analysis of the washing fractions. After drying at 40 ^{o}C under vacuum, the light pink MIP particles were obtained, suggesting the presence of dithioester groups there. The light pink NIP particles with surface-immobilized dithioester groups were then prepared and purified under the identical conditions except that the template was omitted. The procedure is shown in Table 3.9.

Table 3.9. Procedure for the preparation of core-shell L-PA imprinted nanoparticles.

Polymer name[a]	Template	L-PA (µmol)	Si-RAFT (mg)	MAA (µmol)	EGDMA (µmol)	Toluene (mL)	RAFT/ ABDV
SiNP1-MIP[b]	L-PA	17	400	135	676	15	4/1
SiNP1-NIP[b]	-	-	400	135	676	15	4/1
SiNP2-MIP[c]	L-PA	50	400	404	2020	15	3/1
SiNP2-NIP[c]	-	-	400	404	2020	15	3/1

a) See experimental section for details.

b) Silica core size is 200 nm.

c) Silica core size is 20 nm.

3.2.11 Characterization of grafted imprinted polymer shells

After polymerization, the beads were subsequently characterized by FTIR, TEM, DLS, TGA and elemental analysis. Figure 3.19 displays the TGA and DTG curves of grafted polymers. It can be observed from TGA curves that the weight loss of SiNP1-MIP, SiNP1-NIP, SiNP2-MIP and SiNP2-NIP between 100 ^{o}C and 800 ^{o}C is 30%, 29%, 50%, 50%, respectively. By

using the TGA mass loss data the gravimetric conversion and shell thickness (nm) of grafted polymers on silica cores were calculated. The apparent shell thickness was 18 nm for SiNP1-MIP&NIP and 4 nm for SiNP2-MIP&NIP.

Elemental analysis was used to confirm the successful grafting of polymers on silica cores. From elemental microanalysis data, more precisely from the change in carbon and nitrogen contents in each step, we could estimate the amount of grafted polymer on the silica surface. The data are presented in Table 3.10. On the basis of the increase in carbon content the apparent shell thickness was calculated. The obtained shell thickness was 19 nm and 18 nm for SiNP1-MIP&NIP and 2.7 nm for SiNP2-MIP&NIP.

In Table 3.10 the apparent thickness, calculated from the TGA mass loss data and elemental analysis, have been compared with the nominal thickness, estimated assuming the grafted shell to consist of monomers forming a liquid film covering the core surface. The somewhat lower measured thickness compared to the nominal values agrees with our previous report [239] and can be attributed to solution chain growth, nevertheless resulting in an acceptable conversion of monomer to shell polymer.

Table 3.10. Results from the characterization of imprinted and nonimprinted core shell beads.

Polymer name [a]	%C	%N	%S	Mass loss [b] (%)	Conv.[c] (%)	d_{nom}[d] (nm)	d_{EA}[e] (nm)	d_{TGA}[f] (nm)
SiNP1-MIP	18.20	0.30	0.82	30	87	16	19	18
SiNP1-NIP	17.23	0.29	0.64	29	84	16	18	18
SiNP2-MIP	22.86	0.35	0.90	50	94	4.1	2.7	4.0
SiNP2-NIP	22.53	0.33	0.78	50	93	4.1	2.7	4.0

a) See experimental section for details.

b) Mass loss by thermal gravimetric analysis (TGA).

c) Gravimetric conversion: Conversion=mass loss (TGA)/mass of monomer feed.

d) The shell thickness (nm) was calculated according to Eq. 2-3.

e) The shell thickness (nm) was calculated according to Eq. 2-3, Eq. 2-16 and Eq. 2-17.

f) The shell thickness (nm) was calculated according to Eq. 2-3 and Eq. 2-9.

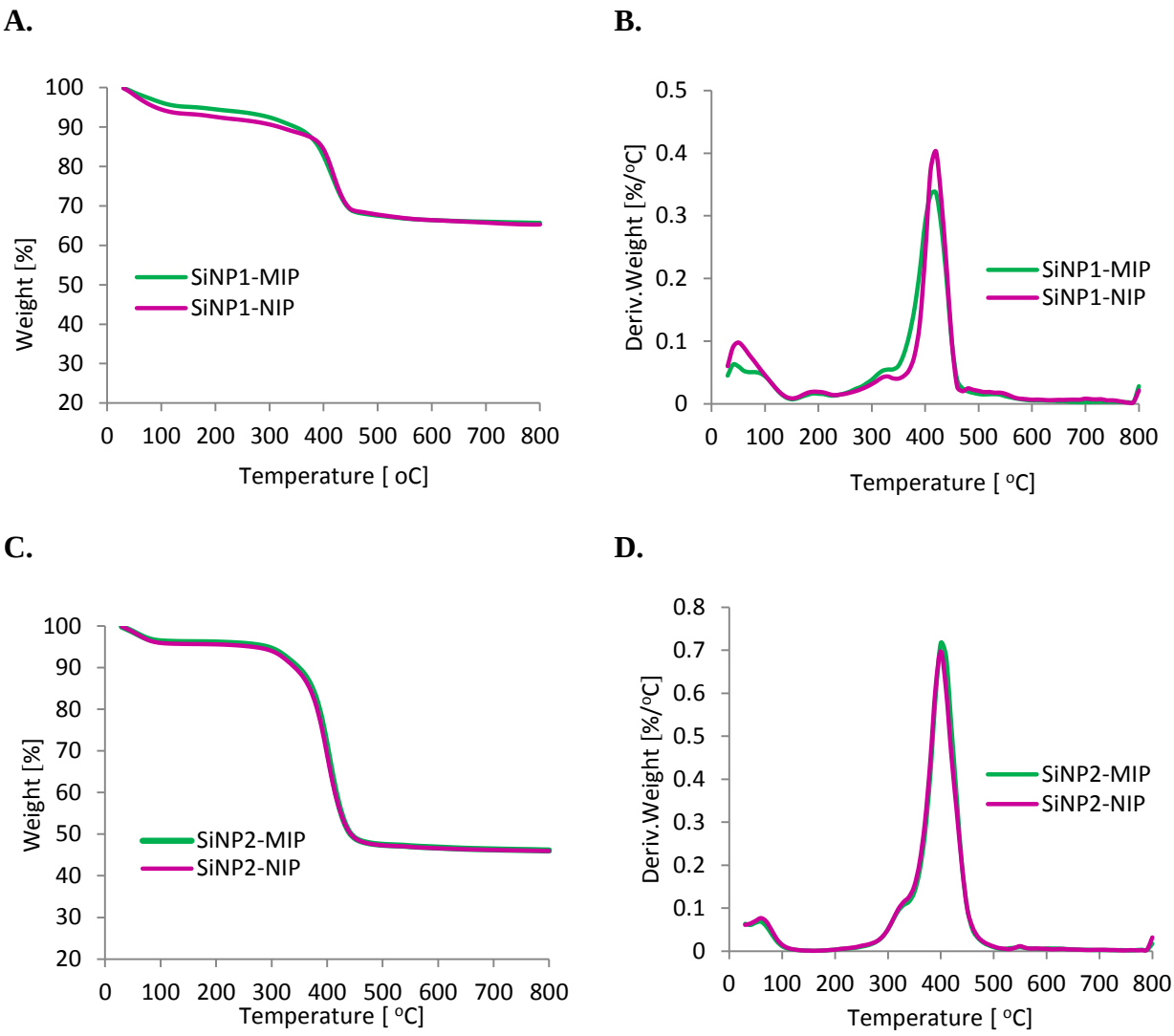

Figure 3.19. Thermal gravimetric analysis of the L-PA imprinted and nonimprinted core shell nanoparticles; TGA of SiNP1-MIP and SiNP1-NIP (A), DTG of SiNP1-MIP and SiNP1-NIP (B), TGA of SiNP2-MIP and SiNP2-NIP (C), DTG of SiNP2-MIP and SiNP2-NIP (D).

The TEM images of the L-PA imprinted and nonimprinted core-shell nanoparticles SiNP1-MIP&NIP and SiNP2-MIP&NIP are shown in Figure 3.20. An inorganic silica core appears darker than the grafted organic polymer shell due to the difference in density. Comparison of TEM images of grafted polymer silica nanoparticles with images of bare silica particles and RAFT modified silica support confirmed a successful grafting of the polymer shell on the silica particles. The average particle size as estimated by TEM measurements of these grafted silica core shell particles was found to be in the range of 190–220 nm and 20-25 nm with a

shell thickness of 15–20 nm and 3-5 nm for SiNP1-MIP&NIP and SiNP2-MIP&NIP, respectively.

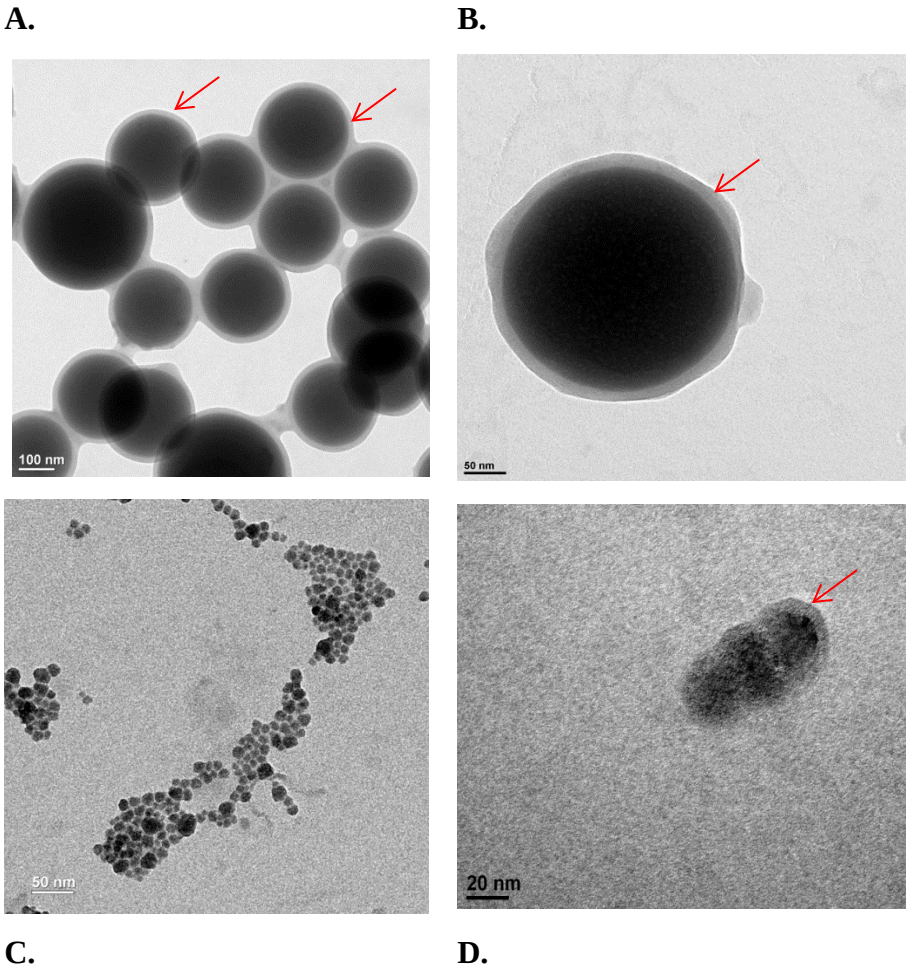

Figure 3.20. TEM images of the L-PA imprinted and nonimprinted core-shell nanoparticles SiNP1-MIP and SiNP1-NIP (A, B), SiNP2-MIP and SiNP2-NIP (C, D). The polymer shells are indicated by arrows. The scale bar is 100 nm in the case of (A) 50 nm for (B) and (C) and 20 nm for (D).

The particle sizes measured by DLS were slightly bigger than the sizes obtained from TEM due to the aggregation of the particles (Figure 3.21). The TEM images further revealed separate or smaller aggregates of polydisperse particles.

The FTIR spectra of the core-shell beads shown in Figure 3.22 display two characteristic bands i.e. the carbonyl stretching of the polymer matrix at ca 1740 cm^{-1} and the siloxane vibration of silica core at ca 1120 cm^{-1}.

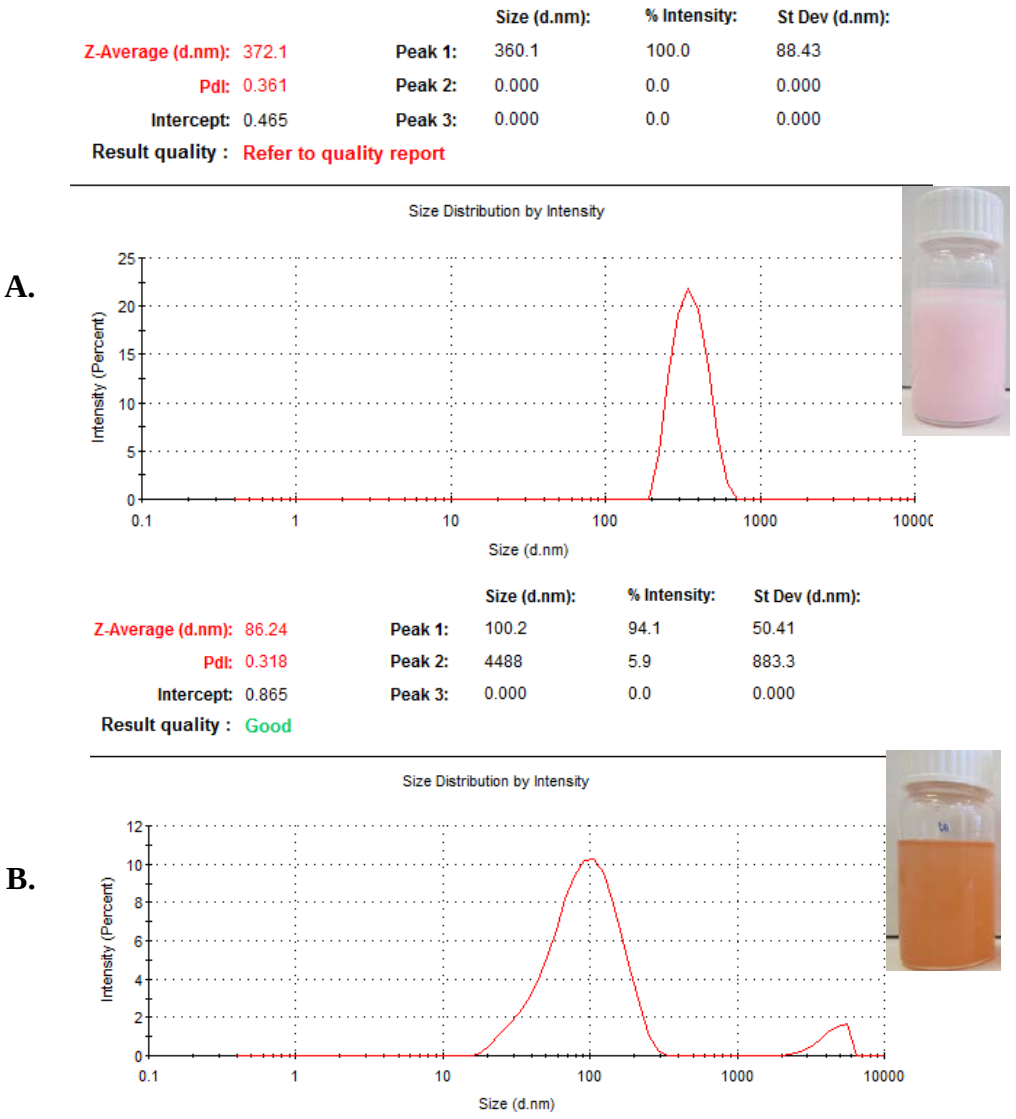

Figure 3.21. DLS analysis of the L-PA imprinted core-shell nanoparticles SiNP1-MIP (A) and SiNP2-MIP (B).

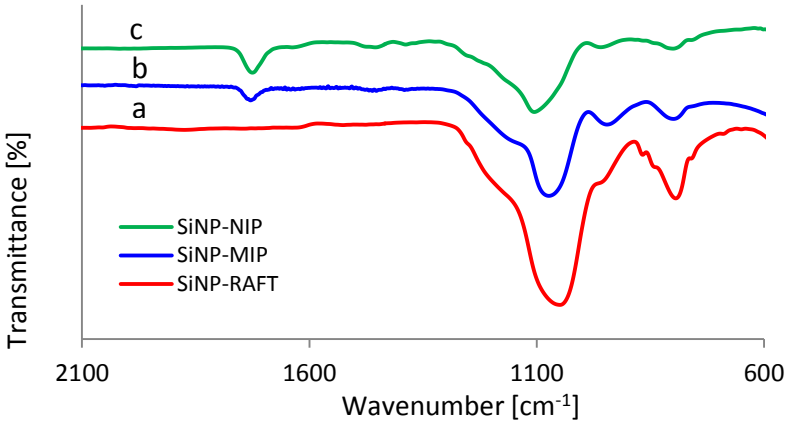

Figure 3.22. FTIR spectra of SiNP-RAFT(a) SiNP-MIP(b), SiNP-NIP(c). Curves were shifted for clarity.

3.2.12 Binding isotherms of the imprinted polymers

In order to evaluate the binding properties, the particles were subsequently tested for their affinity towards the template L-PA and its optical antipode D-PA in acetonitrile. After incubating the particles with solutions of L-PA or D-PA of known concentrations the free concentration of the solutes were determined by reversed phase HPLC. Binding curves were then constructed by plotting the specific amount of bound solute against the free concentration of solute.

As shown in Figure 3.23, the amount of template peptide bound to the MIPNPs at equilibrium, increased with increasing initial concentration of the template. The core-shell particles display a distinct saturation behavior with a clear preference for the templated L-form. In fact, the binding curve for the D-form coincides with the binding curve for the nonimprinted particles indicating the presence of highly discriminative imprinted sites. Judging from the sigmoidal and more shallow shape of the curve obtained for the particles produced using the larger cores (NP-MIP1) compared with the colloidal size particles (NP-MIP2) both the quality and accessibility of the templated sites appears to increase with decreasing particle size. This can be understood in terms of shell thickness and particle surface area to volume ratio. The large core particles exhibit ca 4 times thicker shells compared to the colloidal sized particles but only ca two thirds of the grafting density of the latter. Therefore, the different total uptake of LPA of NP-MIP1 and NP-MIP2 can in part be attributed to the fact that the larger particles contain less binding sites per unit weight. Another factor accounting for the difference is the ca 10x lower surface area (ca $19 m^2/g$) of the large particles compared to the colloidal sized particles (ca $182 m^2/g$). This dramatically impedes site access probably leaving a portion of the sites buried and nonaccessible. This problem is even more pronounced for the mesoporous composite material where access is hindered to polymer grafted in the narrower pores of the composite[239].

The binding isotherms were subsequently fitted to mono-Langmuir (Eq. 2-19), bi-Langmuir (Eq. 2-20), and Freundlich (Eq. 2-21) isotherm model. The resulting parameters are given in Table 3.11 to Table 3.13. For each model and each set of experimental data, the Fisher parameter was calculated according to Eq. 2-26. The fisher values in Figure 3.24 reflect which of the model provides the best fit to a particular isotherm, a higher number indicating a better fit. The affinity constant (K) and total number of binding sites (N) were calculated

according to Eq. 2-22 and Eq. 2-23. Based on Freundlich binding parameters (Table 3.13), the total number of binding sites (N) and binding capacity (a) of NP-MIP2 towards L-PA (N_{LPA}= 21.06 (μmol/g), a_{LPA}= 25.09±2.9 μmol/g $(mol^{-1})^{m}$), were higher than that for NP-MIP2 towards D-PA (N_{DPA}= 10.55 (μmol/g), a_{DPA}=13.5±0.32 μmol/g $(mol^{-1})^{m}$). The heterogeneous index (m) of imprinted polymers network was high and indicated more homogenous network formation (m=1). This result agrees with effect of controlled radical polymerization in the formation of more homogeneous and uniform crosslinked networks [153, 256]. All these together indicated the successful creation of high affinity binding sites on the surface of imprinted nanoparticles for L-PA discrimination.

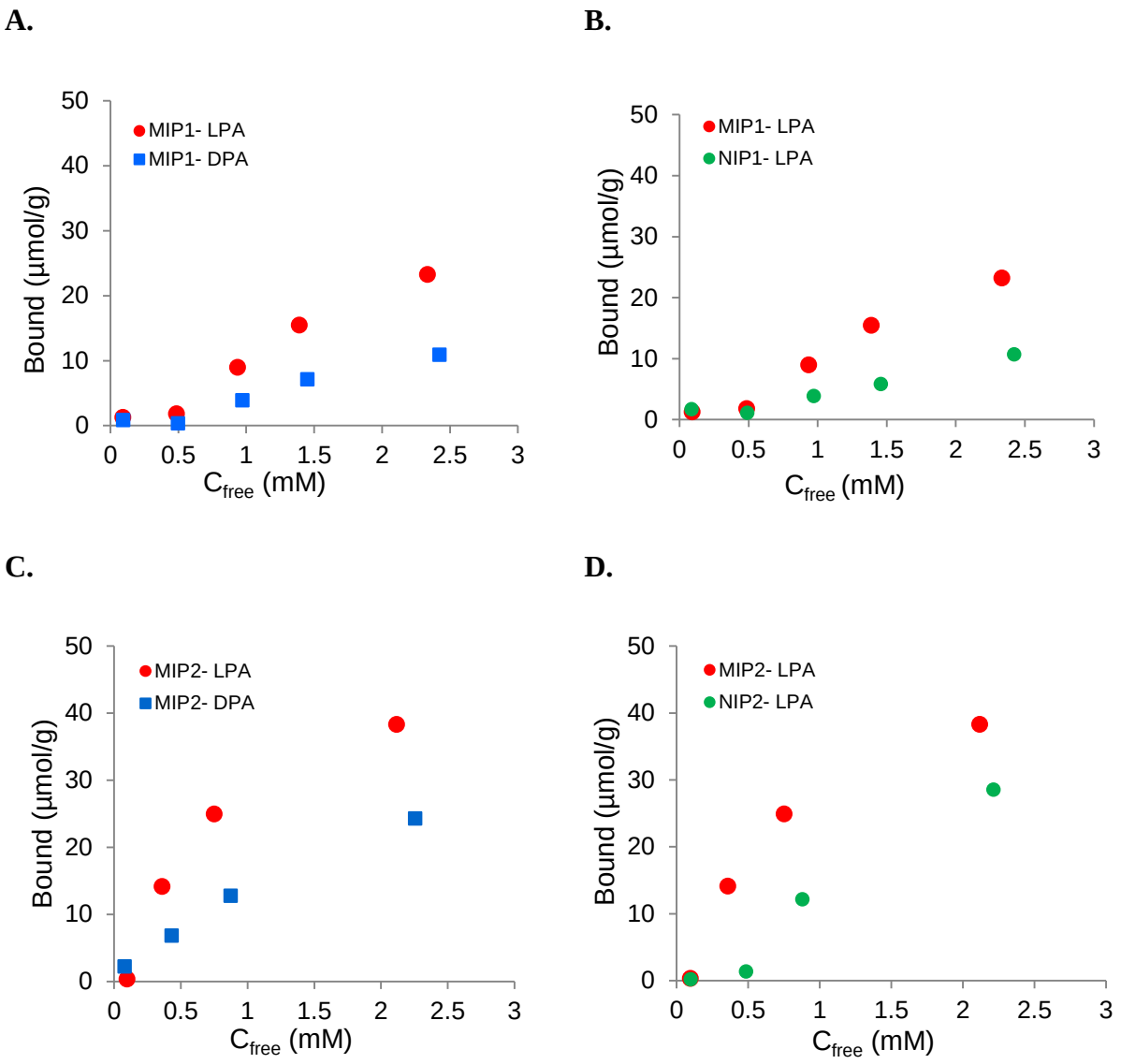

Figure 3.23. Equilibrium binding isotherms of L-PA (circles) and D-PA (squares) on imprinted and nonimprinted core-shell particles in acetonitrile. A) L-PA imprinted SiNP1-MIP, B) L-PA imprinted SiNP1-MIP (red circles) and SiNP1-NIP (green circles), C) L-PA imprinted SiNP2-MIP, D) L-PA imprinted SiNP2-MIP (red circles) and SiNP2-NIP (green circles).

Table 3.11. Mono-Langmuir isotherm fitting parameters obtained by nonlinear regression of data shown in Figure 3.23.

Polymer name		k_d (mM)	q_s (μmol/g)	r^2	***F***- value
NP-MIP1	LPA	4.44×10^{7} ± inf	4.45×10^{8} ± inf	0.9519	39
	DPA	1.58×10^{8} ± inf	6.97×10^{8} ± inf	0.9303	26
NP-NIP1	LPA	2.16×10^{8} ± inf	9.10×10^{8} ± inf	0.9747	76
NP-MIP2	LPA	1.20± 0.53	61.01± 13.23	0.9743	75
	DPA	3.04±0.60	57.07± 7.28	0.9975	809
NP-NIP2	LPA	1.37×10^{8} ± inf	1.72×10^{9} ± inf	0.9516	39

Table 3.12. Bi-Langmuir Isotherm fitting parameters obtained by nonlinear regression of data shown in Figure 3.23.

Polymer name		k_d1 (mM)	q_s1 (μmol/g)	k_d2 (mM)	q_s2 (μmol/g)	r^2	***F***- value
NP-MIP1	LPA	1.01×10^{7}	5.15×10^{7}	1.02×10^{7}	5.00×10^{7}	0.9519	14
	DPA	1.69×10^{7}	3.75×10^{7}	1.64×10^{7}	3.60×10^{7}	0.9303	ND
NP-NIP1	LPA	2.14×10^{7}	4.54×10^{7}	2.08×10^{7}	4.34×10^{7}	0.9747	15
NP-MIP2	LPA	1.20 ±inf	27.76 ±inf	1.20 ±inf	33.24 ±inf	0.9743	28
	DPA	3.99 ±inf	65.12±inf	2.47×10^{-12}	0.82 ±inf	0.9993	ND
NP-NIP2	LPA	1.66×10^{7}	1.06×10^{8}	1.70×10^{7}	1.06×10^{8}	0.9516	10

ND= not determined

Table 3.13. Freundlich isotherms fitting parameters obtained by nonlinear regression of data shown in Figure 3.23.

Polymer name		Affinity constant, K (mM^{-1})	Total number of binding sites , N ($\mu mol\ g^{-1}$)	Heterogen-eity parameter, m	Binding capacity, a ($\mu mol/g\ (mol^{-1})^m$)	Regression coefficient, r^2	F-value
NP-MIP1	LPA	ND	ND	1.11±0.21	9.35±1.44	0.9792	46
	DPA	ND	ND	1.20±0.26	3.86±0.79	0.9500	38
NP-NIP1	LPA	ND	ND	1.20±0.08	3.68±0.23	0.9945	363
NP-MIP2	LPA	13.13	21.06	0.61±0.15	25.09±2.9	0.9364	29
	DPA	22.15	10.55	0.72±0.03	13.5±0.32	0.9981	1036
NP-NIP2	LPA	ND	ND	1.20±0.27	11.1±2.34	0.9649	55

ND= not determined (negative value)

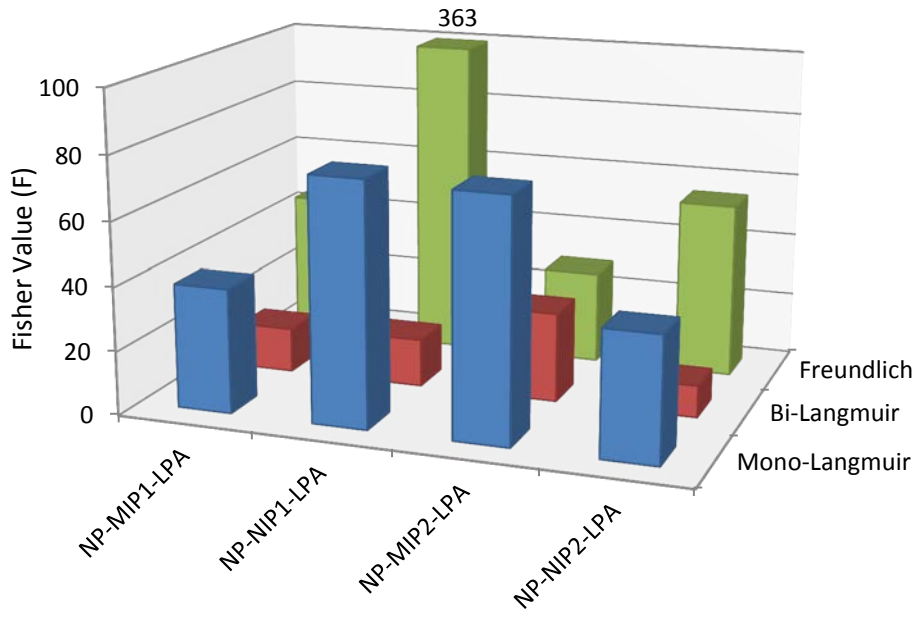

Figure 3.24. Fisher values obtained by fitting the L/D-PA binding curves in Figure 3.23 to mono-Langmuir, bi-Langmuir and Freundlich isotherm models (see Table 3.11 to Table 3.13).

3.3 Conclusions

A versatile and effective method was developed to prepare silica surface-imprinted nanoparticles with a uniform core-shell structure and controllable layer thickness by introducing RAFT groups to the surface of silica beads followed by copolymerization with functional monomers. According to the binding-isotherm results, the MIPNPs exhibited a much-higher binding affinity for the template molecule than the NIPNPs. In addition, MIPNPs were able to discriminate the template L-PA and its optical antipode D-PA.

The results of our research demonstrated that the size of the core particles has an important role in binding properties of core shell particles. Comparison of the particles produced using the larger cores and the smaller core size revealed that the core-shell particles with smaller core size display higher binding affinity than larger one. This can be attributed to high specific surface area and grafting density of the colloidal size particles (NP-MIP2).

3.4 Experimental

3.4.1 Synthesis of monodisperse SiO_2 nanoparticles

Monodisperse SiO_2 nanoparticles 330 nm, 200 nm and 100 nm in diameter were prepared by using a slightly modified Stöber process [241-244]. In a typical synthesis operation, two solutions with equal volumes were rapidly mixed to give a total volume of ~250 mL: one solution contained ethanol (113.61 mL) and TEOS (11.39 mL), while the other contained ethanol (40.99 mL), water (76.50 mL), and ammonium hydroxide (25 wt % in water, 7.56 mL). The reaction mixture generally turns turbid white as SiO_2 particles formed after ~10 min. The reaction was allowed to continue for 6 h at room temperature, with moderate stirring, for full completion (yield 3.5g). Afterwards, they were collected by centrifugation (5000 rpm, 10 min) and washed by repeating redispersion in pure ethanol at least three times. The obtained nanoparticles were then dispersed and stored in 50 mL of toluene.

Table 3.14. Reaction conditions for the preparation of silica NPs of various sizes.

Silica core	Size (nm)	Surface area (m^2/g)	Ethanol (mL)	TEOS (mL)	Water (mL)	NH_4OH, 25%w (mL)	Yield (g)
SiNP2 [a]	20	182	-	-	-	-	-
SiNP3	100	32	158	11.39	76.5	3.77	3.1
SiNP1	200	19	155	11.39	76.5	7.56	3.5
SiNP4	330	11	230	13.8	33	22.4	3.9

a) Colloidal silica nanoparticles are commercial available and purchased from Nissan chemical company.

3.4.2 Synthesis of amino modified silica nanoparticles

The synthesis of SiNP1-NH_2 was carried out according to the method reported in the literature [175, 246]. A suspension (7.00 g, 100 mL) of silica nanoparticles (SiNP1) in toluene was added to a three-necked round-bottom flask with stirring for 15 min under N_2. According to the theoretical number of silanol groups on the silica surface (8 μmol/m^2) an excess amount of (3-aminopropyl) triethoxysilane (1.26 g, 5.71 mmol) was added to the mixture and refluxed at 130 °C under N_2 protection overnight, thereafter cooled to room temperature and was then precipitated into a large amount of hexanes (500 mL). The particles were recovered by centrifugation at 5000 rpm for 10 min and redispersed in 40 mL of acetone followed by reprecipitation in 300 mL of hexanes. The aminofunctionalized particles were dispersed directly into 70 mL of THF for subsequent coupling of the RAFT agent.

Amino modified colloidal silica nanoparticles (SiNP2-NH_2) were synthesized following a method previously reported [163]. A suspension (25 mL) of colloidal silica nanoparticles (7.5 g, SiNP2) in methyl ethyl ketone was added to a three-necked round-bottom flask together with 3- aminopropyldimethylethoxysilane (0.62 g, 3.7 mmol) and dried THF (40 mL). The reaction mixture was heated at 85 °C under N_2 protection overnight. Thereafter the mixture was cooled to room temperature and was then precipitated into a large amount of hexanes (500 mL). The particles (SiNP2-NH_2) were recovered by centrifugation at 3000 rpm for 15 min and redispersed in acetone (40 mL) followed by reprecipitation in hexanes (300 mL).

The aminofunctionalized particles were dispersed directly into THF (70 mL) for subsequent coupling of the RAFT agent.

Table 3.15. Reaction conditions for the amino modification of silica NPs of various sizes.

Modified support	Size (nm)	SiO_2 (g)	APDMES (mmol)	APTES (mmol)	THF (mL)	Toluene (mL)
SiNP2-NH_2	20	7.5	3.7	-	40	-
SiNP3-NH_2	100	5.8	-	7.42	-	100
SiNP1-NH_2	200	7.0	-	5.71	-	100

* The whole reactions were refluxed overnight under N_2 protection.

3.4.3 Synthesis of dithiobenzoate modified silica core particles

A slightly modified version of the procedure reported by Li et al. was followed [163]. In a three-necked round bottom flask (250 mL), equipped with an overhead stirrer, 4-cyanopentanoic acid dithiobenzoate (0.385 g, 1.38 mmol), ethylchloroformate (132 μL, 1.38 mmol) and triethylamine (TEA) (192 μL, 1.38 mmol) were dissolved in THF (50 mL). The solution was purged with N_2 and cooled in an ethanol-liquid nitrogen bath for 40 minutes at -70 ºC. After that, 7.00 g (70 mL) of amino modified silica (1.38 mmol of amino groups) were added at -10 ºC and the reaction was allowed to proceed overnight. After that, the particles were precipitated in hexane (500 mL) and collected by centrifugation (5000 rpm, 10 min). Then, they were redispersed in acetone (80 mL), precipitated again in 300 mL of hexane, centrifugated at 5000 rpm during 10 min. The obtained nanoparticles (SiNP1-CPDB) were dried under vacuum at room temperature (6.5 g, 93% yield).

In order to prepare the RAFT-modified colloidal silica NPs the same method was followed. In a three-necked round bottom flask (250 mL), equipped with an overhead stirrer, CPDB (0.74 g, 2.65 mmol), ethylchloroformate (254 μL, 2.65 mmol) and triethylamine (TEA) (370 μL, 2.65 mmol) were dissolved in dry THF (50 mL) under nitrogen in a three-necked round bottom flask. The solution was purged with N_2 and cooled in an ethanol-liquid nitrogen bath at -78 ºC. After stirring for 40 min the temperature was adjusted to -10 °C and a suspension of amino functionalized silica core particles (7.18 g; 2.65 mmol of amino groups) in THF

(65 mL) was added and the reaction allowed to proceed overnight. Thereafter the particles were precipitated in hexane (500 mL) and collected by centrifugation (3500 rpm, 15 min). They were subsequently redispersed in acetone (80 mL), precipitated again in 300 mL of hexane, centrifugated at 3500 rpm during 15 min, and redispersed in 100 mL THF. The resulting nanoparticles (SiNP2-CPDB) were dried under vacuum at room temperature (6.8 g, 91% yield).

Table 3.16. Reaction conditions for the RAFT modification of silica NPs of various sizes.

Modified support	Size (nm)	SiO_2-NH_2 (g)	CPDB (mmol)	$ClCOOC_2H_5$ (mmol)	TEA (mmol)	THF (mL)
SiNP2-CPDB	20	7.18	2.65	2.65	2.65	120
SiNP3-CPDB	100	6.0	1.15	1.15	1.15	120
SiNP1-CPDB	200	7.0	1.38	1.38	1.38	120

3.4.4 Synthesis of S,S′-Bis(α,α′-dimethyl-α″-acetic acid)- trithiocarbonate

The trithiocarbonate RAFT agent was synthesized following a previously described procedure [252, 257]. Carbon disulfide (21.73 mL, 0.36 mol), chloroform (72.49 mL, 0.90 mol), acetone (66.12 mL, 0.90 mol), and tetrabutylammonium hydrogen sulfate (2.41 g, 7.10 mmol) were mixed with 120 mL of toluene in a 2 L three-necked round-bottom flask equipped with a mechanical stirrer and an addition funnel under nitrogen. Sodium hydroxide (50%) (201.6 g, 2.52 mol) was added dropwise over 90 min in order to keep the temperature below 25 °C. The reaction was stirred overnight. 900 ml water was added to the mixture, the layers were separated. The organic layer was discarded and the aqueous layer was acidified with 120 mL concentrated HCl (caution! gas, mercaptan odor) to precipitate the product as yellow solid. 50 ml toluene was added to stir with the mixture. Filtered and rinsed the solid with toluene to collect 13.83 grams of product after drying in the air to constant weight (21.75 % yield).

H NMR (DMSO-d6, ppm from TMS): 1.59 (s, 12H), 12.91 (s, 2H). C-13 NMR (DMSO-d6): 25.76, 57.25, 176.26, 220.50

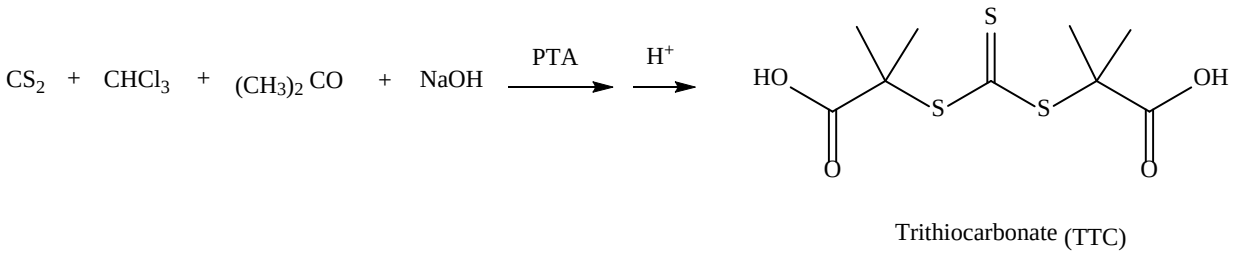

Figure 3.25. Synthesis of carboxyl-terminated trithiocarbonate RAFT agent.

3.4.5 Synthesis of trithiocarbonate modified silica core particles

A slightly modified version of the procedure reported by Li et al. was followed [163]. A suspension (30 mL) of colloidal silica nanoparticles (9 g, SiNP2) in methyl ethyl ketone was added to a three-necked round-bottom flask together with 3-aminopropyldi methyl-ethoxysilane (0.81g, 5.02 mmol) and dried THF (50 mL). The reaction mixture was heated at 85 °C under N_2 protection overnight. Thereafter the mixture was cooled to room temperature and was then precipitated into a large amount of hexanes (500 mL). The particles (SiNP-NH_2) were recovered by centrifugation at 3000 rpm for 15 min and redispersed in acetone (50 mL) followed by reprecipitation in hexanes (300 mL). The aminofunctionalized particles were dispersed directly into THF (70 mL) for subsequent coupling of the RAFT agent. In a three-necked round bottom flask (250 mL), equipped with an overhead stirrer, TTC (0.25 g, 0.94 mmol), ethylchloroformate (89 μL, 0.94 mmol) and triethylamine (TEA) (130 μL, 0.94 mmol) were dissolved in dry THF (50 mL) under nitrogen in a three-necked round bottom flask. The solution was purged with N_2 and cooled in an ethanol-liquid nitrogen bath at -78 ºC. After stirring for 40 min the temperature was adjusted to -10 °C and a suspension of amino functionalized silica core particles (9 g, 0.94 mmol of amino groups) in THF (70 mL) was added and the reaction allowed to proceed overnight. Thereafter the particles were precipitated in hexane (500 mL) and collected by centrifugation (3500 rpm, 15 min). They were subsequently redispersed in acetone (80 mL), precipitated again in 300 mL of hexane, centrifugated at 3500 rpm during 15 min, and redispersed in 100 mL THF. The resulting nanoparticles (SiNP-TTC) were dried under vacuum at room temperature (8.1 g, 90% yield).

3.4.6 Preparation of methyl methacrylate grafted polymer from RAFT-modified silica nanoparticles

RAFT agent anchored silica nanoparticles(100 mg, 10.4 μmol) , methyl methacrylate (0.50mL, 4690 μmol) and THF (5 mL) were added into a 20 mL glass tube, followed by sonication for 10 min. The prepolymerization mixture was purged of oxygen by either bubbling with N_2 for 15 min or by three successive freeze-pump-thaw cycles. The polymerization was carried out at 50 ^oC for a prescribed time. The pure PMMA-grafted silica particles were obtained by repeated centrifugation-redispersion procedure in the THF solution. The upper clean liquid was collected, and the fresh THF (10 ml) was added into the residue. This procedure was repeated three times until no polymer was in THF. The resulting polymers were dried at 40 ^oC in a vacuum oven for 12 h.

Table 3.17. Polymerization procedure for the methyl methacrylate graft polymerization.

Polymer name	Si-RAFT (mg)	MMA (μmol)	RAFT (μmol)	ABDV (μmol)	THF (mL)	Time (h)
SiO_2-g-PMMA-1[a]	100	4690	10.4	10.4	5	15
SiO_2-g-PMMA-2[a]	100	4690	10.4	10.4	5	18
SiO_2-g-PMMA-3[b]	100	4690	8.2	8.2	5	20
SiO_2-g-PMMA-4[b]	100	4690	8.2	1.6	5	20

a) Silica core size is 100 nm.

b) Silica core size is 200 nm.

3.4.7 Preparation of styrene grafted polymer from RAFT-modified silica nanoparticles

RAFT agent anchored silica nanoparticles (100 mg, 10.4 μmol) , styrene (1 mL, 8720 μmol) and THF (5 mL) were added into a 20 mL glass tube, followed by sonication for 10 min. The prepolymerization mixture was purged of oxygen by either bubbling with N_2 for 15 min or by three successive freeze-pump-thaw cycles. The polymerization was carried out at 50 ^oC for a prescribed time. The pure PSt-grafted silica particles were obtained by repeated

centrifugation-redispersion procedure in the THF solution. The upper clean liquid was collected, and the fresh THF (10 ml) was added into the residue. This procedure was repeated three times until no polymer was in THF. The resulting polymers were dried at 40 ^{o}C in a vacuum oven for 12 h.

Table 3.18. Polymerization procedure for the styrene graft polymerization.

Polymer name	Si-RAFT (mg)	Styrene (μmol)	RAFT (μmol)	ABDV (μmol)	THF (mL)	Time (h)
SiO_2-g-PSt-1	100	8720	10.4	10.4	5	40
SiO_2-g-PSt-2	100	8720	10.4	5.2	5	40
SiO_2-g-PSt-3	100	8720	10.4	10.4	5	72
SiO_2-g-PSt-4	100	8720	10.4	5.2	5	72

* Silica core size is 100 nm.

3.4.8 Preparation of methacrylamide grafted polymer from RAFT-modified silica nanoparticles

RAFT agent anchored silica nanoparticles (200 mg, 14 μmol) , methacrylamide (320 mg, 3760 μmol) and acetic buffer (5 mL, pH5, 10mM) were added into a 20 mL glass tube, followed by sonication for 10 min. The prepolymerization mixture was purged of oxygen by either bubbling with N_2 for 15 min or by three successive freeze-pump-thaw cycles. The polymerization was carried out at 50 ^{o}C for a prescribed time. The pure PMAAM-grafted silica particles were obtained by repeated centrifugation-redispersion procedure in the water solution. The upper clean liquid was collected, and the fresh water (10 ml) was added into the residue. This procedure was repeated three times until no polymer was in water. The resulting polymers were dried at 40 ^{o}C in a vacuum oven for 12 h.

Table 3.19. Polymerization procedure for the methacrylamide graft polymerization.

Polymer name	Si-TTC (mg)	MAAM (μmol)	TTC (μmol)	APS (μmol)	Buffer (mL)	Time (h)
SiO_2-g-PMAAM-1	200	3760	14	7	5	16
SiO_2-g-PMAAM-2	200	3760	14	3.5	5	16
SiO_2-g-PMAAM-3	200	3760	14	14	5	24
SiO_2-g-PMAAM-4	200	3760	14	7	5	24

* Silica core size is 200 nm.

3.4.9 Synthesis of core-shell MIPs using a soluble L-PA

RAFT modified core particles (SiNP1: 400mg corresponding to 32 μmol RAFT groups) were suspended in a prepolymerization mixture containing L-PA (4.1 mg, 17 μmol), MAA (11.5 μL, 135 μmol) and EGDMA (127 μL, 676 μmol) dissolved in 15 mL of dry toluene. Nonimprinted particles were produced identically but leaving out L-PA (SiNP1-NIP). The prepolymerization mixture was purged of oxygen by either bubbling with N_2 for 15 min or by three successive freeze-pump-thaw cycles where after the initiator ABDV (2.01 mg, 8.1 μmol) was added. This corresponds to a molar ratio of RAFT/initiator of 4. Polymerization was initiated at 50°C and allowed to proceed for 22 h. Template removal was then carried out by incubating the particles four times with MeOH 80%, Formic acid 15%, 5% H_2O (15 mL) leaving the suspension to incubate 1 h followed by centrifugation at 5000 rpm. The final step washing was carried out with pure methanol (15 ml) for 30 min. Thereafter the particles were dried under vacuum at 40 ºC resulting in 491 mg (90%) of SiNP1-MIP and 482 mg (88%) of SiNP1-NIP. All the supernatants were collected and analyzed by reverse phase HPLC for the presence of template.

In order to prepare the L-PA imprinted polymers by using the colloidal silica NPs the same method was followed. RAFT modified core particles (SiNP2: 400mg corresponding to 33 μmol RAFT groups) were suspended in a prepolymerization mixture containing L-PA (12 mg, 50 μmol), MAA (34 μL, 404 μmol) and EGDMA (381 μL, 2020 μmol) dissolved in 15 mL of dry toluene. Nonimprinted particles were produced identically but omitting L-PA

(SiNP2-NIP). The prepolymerization mixture was purged of oxygen by either bubbling with N_2 for 15 min or by three successive freeze-pump-thaw cycles where after the initiator ABDV (2.75 mg, 11.0 μmol) was added. This corresponds to a molar ratio of RAFT/initiator of 3. Polymerization was initiated at 50 °C and allowed to proceed for 22 h. Template removal was then carried out by incubating the particles four times with MeOH 80%, Formic acid 15%, 5% H_2O (15 mL) leaving the suspension to incubate 1 h followed by centrifugation at 5000 rpm. The final step washing was carried out with pure methanol (15 ml) for 30 min. Thereafter the particles were dried under vacuum at 40 ºC resulting in 730 mg (87%) of SiNP2-MIP and 750 mg (89%) of SiNP2-NIP. All the supernatants were collected and analyzed by reverse phase HPLC for the presence of template.

Table 3.20. Polymerization procedure for the preparation of L-PA imprinted core-shell NPs.

Polymer name	Si-RAFT (mg)	L-PA (μmol)	MAA (μmol)	EGDMA (μmol)	RAFT (μmol)	ABDV (μmol)	Toluene (mL)
SiNP1-MIP [a]	400	17	135	676	32	8	15
SiNP1-NIP [a]	400	-	135	676	32	8	15
SiNP2-MIP [b]	400	50	404	2020	33	11	15
SiNP2-NIP [b]	400	-	404	2020	33	11	15

a) Silica core size is 200 nm.

b) Silica core size is 20 nm.

3.4.10 Template synthesis

The templates L- and D-phenylalanine anilide (L-PA and D-PA) were synthesized following a previously described procedure [258, 259]. The synthesis consists of two different steps: synthesis of BOC-L/D-phenylalanine anilide followed by deprotection.

3.4.10.1 Synthesis of BOC-L/D-phenylalanine anilide

BOC-L-phenylalanine anilide was prepared by condensation of *BOC*-L-phenylalanine and aniline in DMF using DCC and HOBt as condensation agents. 0.05 mol (4.5 mL) of freshly distilled aniline were added under stirring to a solution of 0.06 mol (15.7 g) *BOC*-L/D-Phe-OH, 0.06 mol (8.1 g) HOBt and 0.08 mol (16.5 g) DCC in 200 mL dry DMF. After stirring for a few hours, the mixture was filtered, the filtrate dried over $MgSO_4$ and filtered. The filtrate was then reduced to dryness under reduced pressure. The solid residue was dissolved in DCM and washed with 300 mL each of 1M $NaHCO_3$, 0.5 M HCl and water. The product obtained after evaporation of DCM was recrystallised from ethanol.

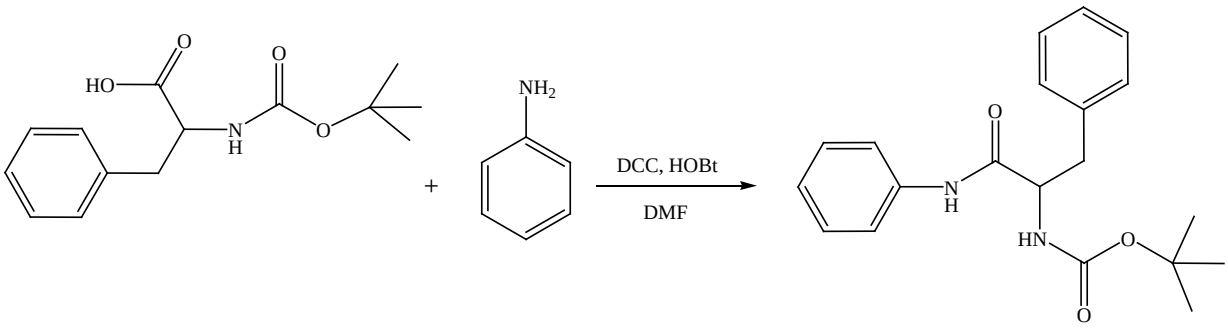

Figure 3.26. Synthesis of BOC-L /D phenylalanine aniline.

3.4.10.2 Synthesis of L/D-phenylalanine anylide

BOC-protecting group was removed by treatment with trifluoroacetic acid. To a solution of 0.03 mol *BOC*-L/D-phenylalanine anilide in 30 mL DCM were added 30 mL TFA under cooling with an ice/salt mixture. The mixture was stirred for 2 h and reduced to dryness under reduced pressure. The solid residue was dissolved in 100 mL toluene and the same amount of

1M HCl was added. After stirring for a short time, the phases were separated and the toluene phase was washed again with 1M HCl. The combined aqueous phases were basified with 5M NaOH and extracted with DCM. After drying over $MgSO_4$, filtration and evaporation of the solvent, the residue is recrystallised from tert butylmethyl ether.

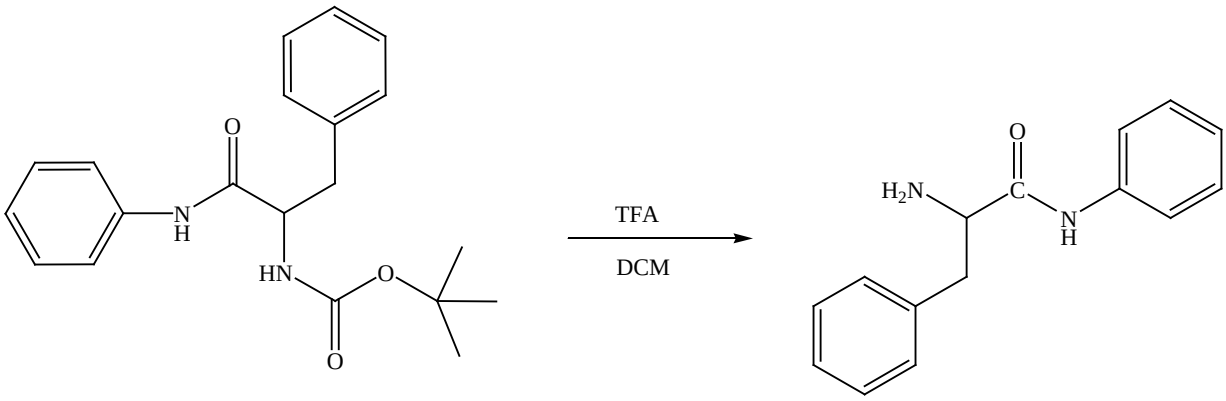

Figure 3.27. Synthesis of L /D- phenylalanine anilide.

Elemental Analysis: %C= 75.06; %H= 6.71; %N=11.6

^{1}H-NMR ($CDCl_3$): δ=1.4 (s, 2H, -NH_2), δ=2.76 (m, 1H, -CH_2^{β}), δ=3.3 (m, 1H, -CH_2^{β}), δ=3.7 (m, 1H, -CH) δ=7.05 (m, 2H, m- NH-C_6H_5); δ=7.3 (m, 5H, -C_6H_5), δ= 7.5(m, 3H, o- and p- in NHC_6H_5), δ=9.37(s, 1H, NH)

3.4.11 Batch binding tests of NPs for their affinity for L-PA and D-PA.

Dry template free polymer (10 mg) was weighed into 10 separate HPLC vials followed by addition of solutions (1.0 mL) of D- or L-PA (0.1-2.5 mM) in acetonitrile (the test was downscaled for samples available in limited quantities). The vials were sealed and their contents allowed to equilibrate overnight at room temperature with gentle shaking. After 15 h incubation at room temperature the supernatants were sampled (30 μL) and the aliquots diluted in 270 μL water and transferred to HPLC vials for measurement of unbound solute concentration by reversed phase HPLC. The HPLC system consisted of an Agilent HPLC 1100 series instrument (Agilent) equipped with a UV-DAD detector and an autosampler. The

column was a reversed phase (C18) column (Phenomenex Luna C-18, 150 × 4.6 mm), the mobile phase: MeOH/H_2O: 62/38 (0.2% TFA), flow rate: 1.0 mL/min, the injection volume was 10 μL and the detection performed by UV absorbance at 265 nm. The resulting peak areas were used to calculate the amount of bound analyte on the polymer (in μmol/g of polymer). The binding results are averages of two independent experiments.

Chapter 4: Solid-Phase Synthesis of MIP Core-Shell NPs using Magnetic Template

4.1 Introduction

MIPs are perceived to have several shortcomings such as heterogeneous binding site, template occlusion, template recovery and upscaling for commercial exploitation. Several approaches such as thermodynamically controlled polymerizations [98, 229], thermal curing or annealing [260] and immobilized templates on sacrificial support [261, 262] have been proposed to address these problems. An elegant approach in this context is surface imprinting of nanoparticles by solid phase synthesis [263-265]. The nanoparticles are here synthesized in presence of template modified solid supports whereby growing particles adhere to the support surface. Post-synthesis, the particles can be affinity purified in situ leading to high affinity receptors in template free form.

A solid-phase synthesis approach to prepare molecularly imprinted nanoparticles (MIP-NPs) towards trypsin has been described by Ambrosini et al [265]. The inhibitor of trypsin, p-aminobenzamidine, was attached to the glass beads. After addition of trypsin to form the PAB-trypsin complex, polymerization was conducted around the immobilized enzyme. N-isopropylacrylamide (NIPAM) was used as the major component in the polymer recipe in order to obtain thermoresponsive MIP-NPs. The MIP-NPs are released by a simple temperature change, resulting in template-free MIP-NPs that exhibit high specificity and selectivity for trypsin.

Recently Poma et al. reported a reusable solid-phase template approach for the synthesis of MIP nanoparticles and their precise manufacture using a prototype automated UV photochemical reactor [263]. In this approach the immobilized template have been used more than 30 times without loss of performance.

A limitation with the examples demonstrated thus far is related to the low specific surface area of the solid support beads. This translates into low particle yields (< 1 mg/g support beads) and a need for large reactors which essentially limits the technique to serial synthesis protocols [266].

As a part of this thesis a novel scalable process to produce surface imprinted nanoparticles in high yield and in template free form was developed (see MSc thesis of Melanie Berghaus) [267]. This is based on the use of nanosized magnetic placeholder templates (Figure 4.1) in a process tolerating high template concentrations. The increased product yield should make this method ideal for both small-scale parallel synthesis and large-scale synthesis by established polymerization techniques. In this chapter we demonstrate the feasibility of the concept focusing on an extensively studied model system combined with RAFT mediated polymerization [239] from nanosized silica cores (Figure 4.8).

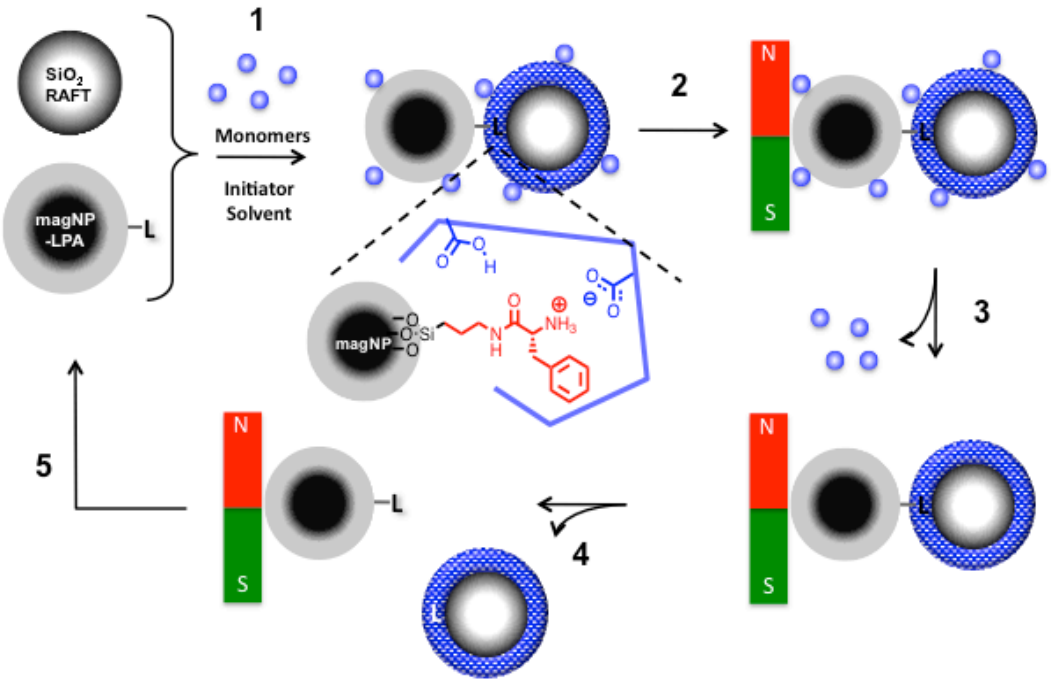

Figure 4.1. Principle of using magnetic templates for synthesis, affinity enrichment and purification of surface imprinted core-shell nanoparticles. (1) Polymerization of monomers in presence of the binary particle suspension, (2) Separating the magnetic template and polymers adhering to the template from the crude reaction mixture. (3) Washing off loosely bound unreacted monomers and oligomers, (4) Gradually releasing the polymer adhering to the magnetic template by physical or chemical means thereby enriching high affinity MIP particles. (5) Reuse of the magnetic template repeating steps 1-4 [268] .

4.2 Results and Discussions

4.2.1 Synthesis of magnetic core-silica shell nanoparticles (magNP@SiO_2)

Before the beginning of this study, Fe_3O_4 modified nanoparticles have been prepared in our group [267, 268]. The Fe_3O_4 nanoparticles were prepared by the coprecipitation method [268, 269]. The growth of silica shells on Fe_3O_4 nanoparticles was developed by a sol-gel process using tetraethyl orthosilicate (TEOS)[270]. The formation of a silica coating on the surfaces of iron oxide nanoparticles could provide a good biocompatible, non-toxic coating and easily modified with various groups for bioconjugation purposes[271]. The method used to prepare magNP@SiO_2 is shown in Figure 4.2. The size and shape of magNP@SiO_2 were examined by transmission electron microscopy (TEM). The TEM images revealed that the diameter of the resultant particles was in the range of 10-15 nm. FT-IR spectra of magNP and magNP@SiO_2 are shown in Figure 4.3. In comparison with the curve of pure magNP, the characteristic peaks of the Si-O-Si group at approximately 1100 cm^{-1} indicated the formation of silica shells on the surface of magNP.

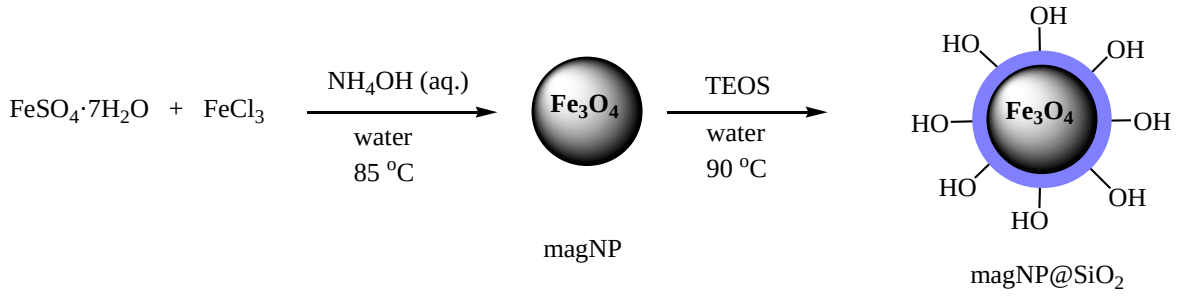

Figure 4.2. Schematic illustration of the synthesis of magnetic core-silica shell nanoparticles.

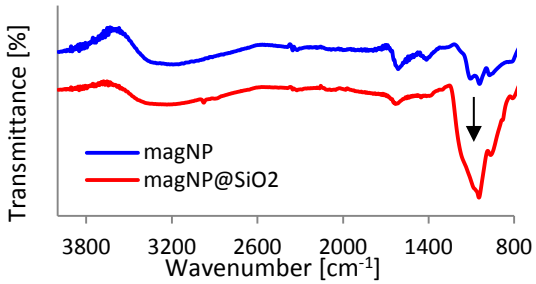

Figure 4.3. FTIR spectra of magNP (blue line), magNP@SiO_2 (red line). The Fe-O-Fe band of the core is accompanied by the Si-O-Si band at ca 1100 cm^{-1} in the IR-spectra of the magnetite particles after the application of the silica shell.

4.2.2 Aminofunctionalization of magnetic silica nanoparticles (magNP-NH_2)

The surface hydroxyl groups of magNP@SiO_2 were reacted with methoxy groups of 3-aminopropyltrimethoxylsilane to introduce amine groups on the surface of magNP@SiO_2. The synthesis rote is shown in Figure 4.4. The presence of free amine groups on the particles was confirmed by the ninhydrine test (Ruhemann's purple).

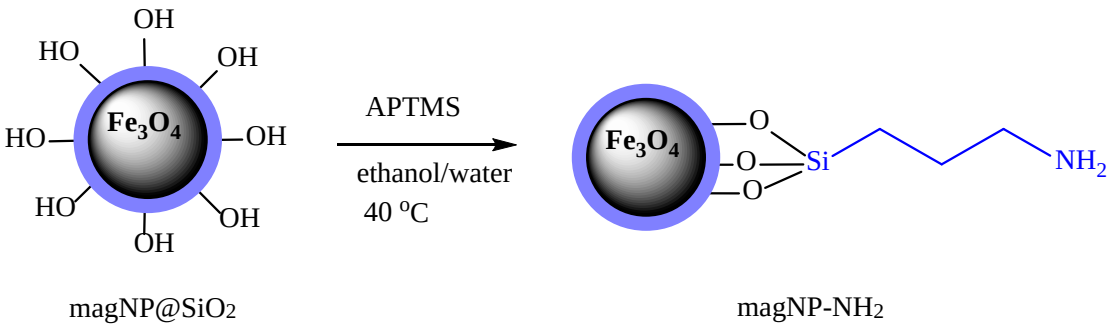

Figure 4.4. Aminomodification of magnetic-silica core-shell nanoparticles.

4.2.3 Immobilization of L-phenylalanine on magNP-NH_2 (magNP-L-Phe)

The aminomodified magnetic silica nanoparticles (magNP-NH_2) were used as core particles to immobilize the protected L-phenylalanine template on the surface of magnetic nanoparticles. First the protected template was converted to active ester by reacting with N-hydroxysuccinimide. Then the activated ester form template was reacted with amino groups of magNP to furnish the immobilized template on the surface of magNP (magNP-Fmoc-L-Phe). Fmoc deprotection was achieved by treating the particles in 20% piperidine in DMF. The resulting fulvene-piperidine adduct was quantified by measuring the absorption of the supernatants at 301 nm. This measurement was used to estimate the loading of L-Phe on the magnetic particles. The schematic synthesis route of template immobilization is shown in Figure 4.5. From elemental microanalysis data, coverage and distance amount of immobilized template on the surface of magNP were calculated. Results are demonstrated in Table 4.1.

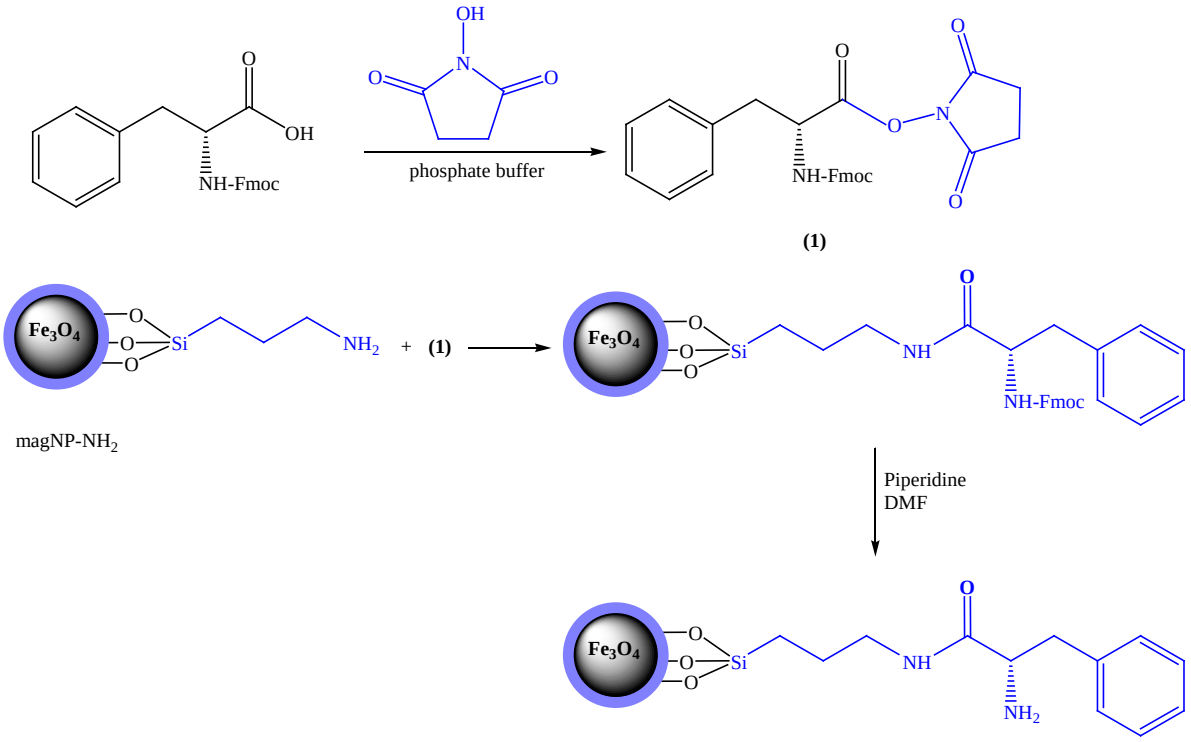

Figure 4.5. Synthesis route of template immobilization on the surface of magNP-NH_2.

Table 4.1. Results from the characterisation of modified silica beads by elemental analysis.

Modified support[a]	%C	%N	%S	Ligand[b] density (mmol/g)	Area density[b] (μmol/m^2)	Coverage[c] (%)	Distance[d] (nm)
magNP-L-Phe	0.86	0.25	-	0.0016	0.014	0.2	11

a) The ligand immobilization was performed in two steps by consecutive coupling of 3-aminopropyltrim ethoxysilane (APTMS) and L-Phe on the indicated core beads as described in the experimental section. The magnetic core-shell particles displayed an average particle size of 220 nm with a polydispersity of PDI= 0.245 and a specific surface area of 110 m^2/g.

b) The ligand density and area density were estimated from the release of fulvene-piperidine adduct upon deprotection of immobilized Fmoc-Phe.

c) The coverage (C) was calculated according to Eq. 2-13, assuming a maximum silanol group density of 8 μmol/m^2.

d) The average distance d_L (nm) between the coupled ligands assuming a random ligand distribution was calculated according to Eq. 2-14.

FTIR spectra of aminofunctionalized magNP@SiO_2 prior to and after coupling of Fmoc-L-Phe are shown in Figure 4.6. In comparison with the curve of aminofunctionalized magNP@SiO_2, the characteristic peaks of the amide groups indicated the immobilization of Fmoc-L-Phe on the surface of magNP@SiO_2.

The TEM images of modified magnetite nanoparticles are shown in Figure 4.7. These images displayed spherical shape before and after template coupling with more aggregates after template immobilization.

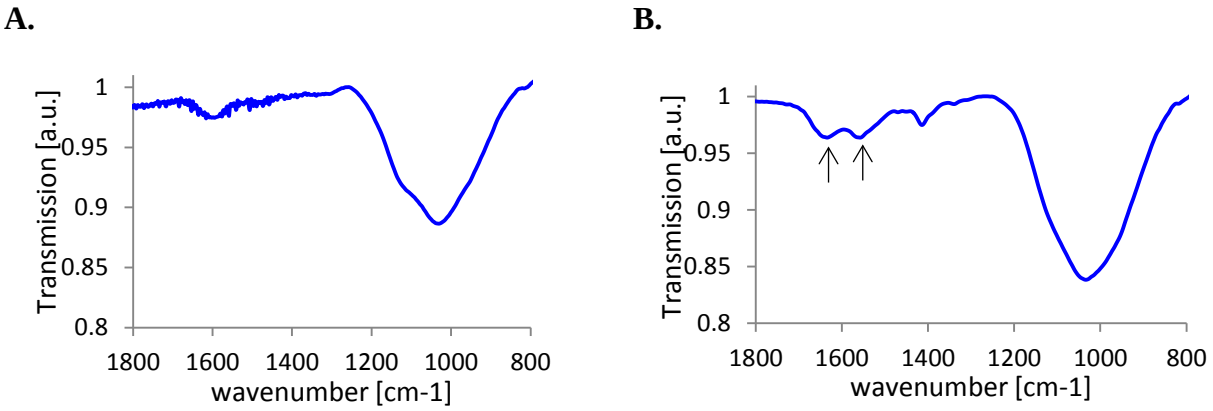

Figure 4.6. FTIR spectra of of aminofunctionalized magNP@SiO_2 prior to (A) and after (B) coupling of Fmoc-L-Phe. In (B) the amide I and II bands have been indicated by arrows.

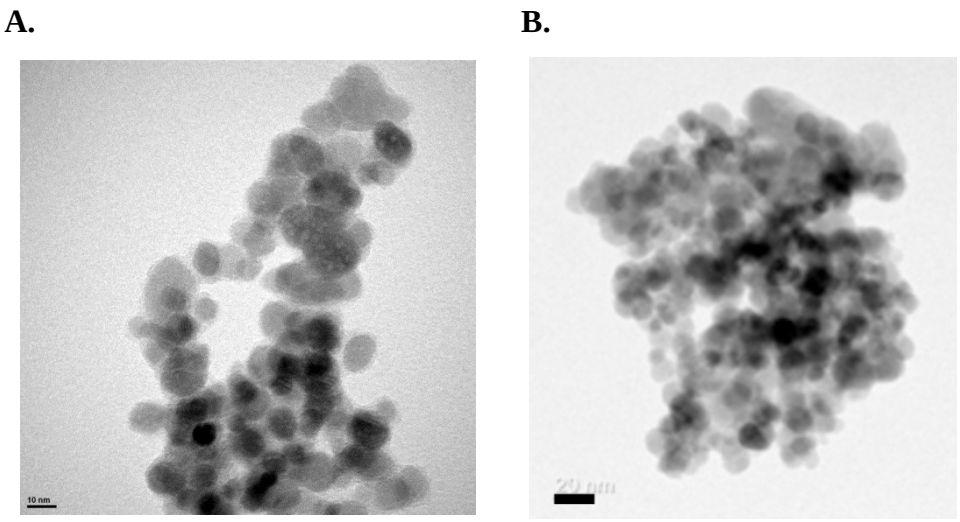

Figure 4.7. TEM images of magNP@SiO_2 (A) and magNP-L-Phe (B).The scale bar is 10 nm in the case of (A) and 20 nm for (B).

4.2.4 Grafting imprinted polymer nanoshell onto surface of RAFT-modified silica nanoparticles

Based on the developed procedure in previous chapter (See in section 3.2.10), the grafting imprinted core-shell nanoparticles were prepared using RAFT modified silica support and magnetic template. The approach to synthesize magNP-L-Phe imprinted nanoparticles is outlined in Figure 4.8. To achieve grafting imprinted polymer, methacrylic acid (MAA), ethyleneglycol dimethacrylate (EGDMA), magNP-L-Phe, toluene and ABDV were used as functional monomer, crosslinker, template, porogen and initiator, respectively.

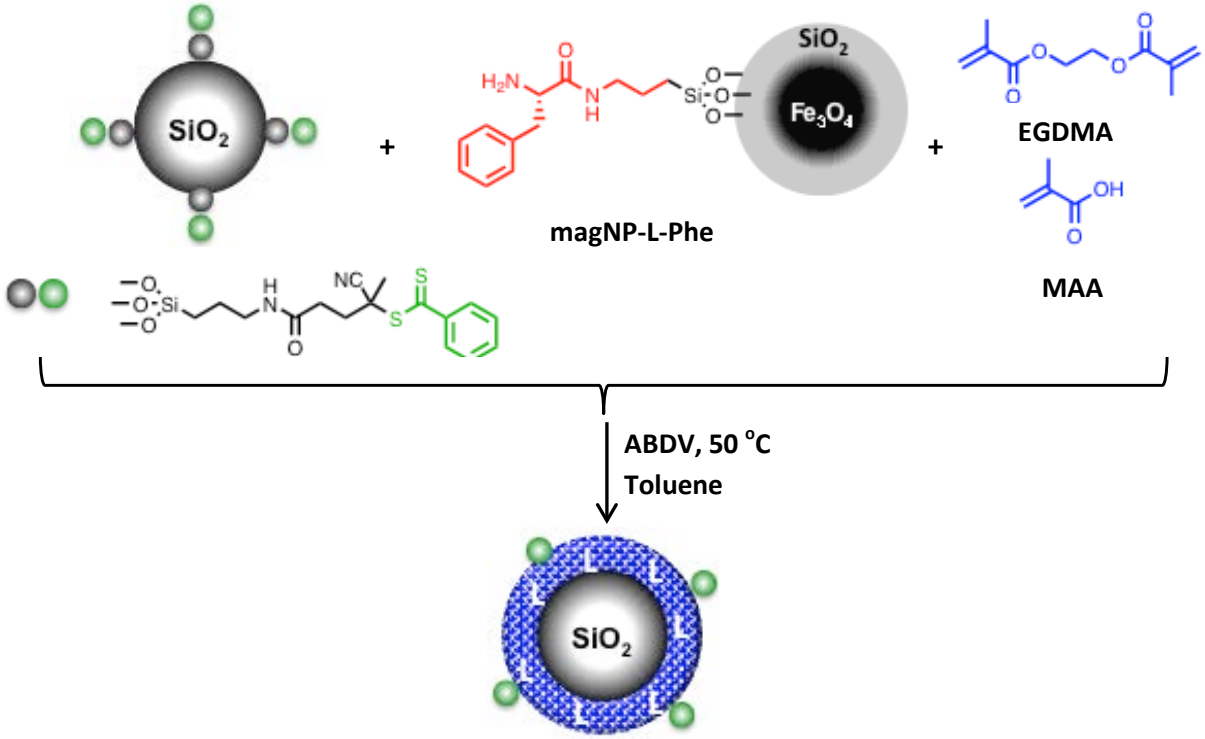

Figure 4.8. Procedure used to synthesize silica core-MIP shell nanoparticles using magnetic template.

In preparing the grafting polymer, a molar ratio EDMA/MAA= 5 and CPDB/ABDV = 3 were used. The relatively low ABDV/CPDB ratio helped to reduce the amount of free polymer derived from the initiator, and yet maintain a moderate polymerization rate [163]. The quantity of monomer relative to the silica support was adjusted to result in shell/film with approximately 4 nm thick shell. After polymerization the beads were isolated by an external magnetic field, and subjected to repetitive washing cycles in order to remove any leachables (e.g. template, oligomers, unreacted monomers). The magnetic fraction was washed by elution of the strongly bound particles by acidified methanol. After drying at 40 ^{o}C under

vacuum, the light pink MIP particles were obtained, suggesting the presence of dithioester groups there. Ca 17 mg particles (SiNP-MIP) were recovered in the elution fraction corresponding to an overall gravimetric yield of ca 9% assuming quantitative conversion of monomer to core-shell polymer. The procedure is shown in Table 4.2.

Table 4.2. Procedure for the preparation of core-shell L-PA imprinted nanoparticles.

Polymer name [a]	Template	Template mass (mg)	L-Phe (µmol)	Si-RAFT (mg)	MAA (µmol)	EGDMA (µmol)	Toluene (mL)	RAFT/ ABDV
SiNP-MIP	magNP-L-Phe	50	0.49	100	101	505	3	3/1

a) See experimental section for details.

4.2.5 Polymer characterization

After polymerization, the beads were subsequently characterised by FTIR, TEM, DLS, TGA and elemental analysis. Analysis of the different particle fractions by TGA (Figure 4.9) showed an increasing mass loss in the order magNP-L-Phe/SiNP-MIP after washing (37%), magNP-L-Phe/SiNP-MIP prior to washing (40%) and released SiNP-MIP (43%). This order is expected assuming the aggregates to consist of silica core/polymer shell particles loosely and strongly adhered to magnetic FeO/SiO_2 particles. By using the TGA mass loss data the gravimetric conversion and shell thickness (nm) of grafted polymer on silica core were calculated. The apparent shell thickness was 3.2 nm.

Elemental analysis was used to confirm the successful grafting of polymer on silica core. From elemental microanalysis data, more precisely from the change in carbon and nitrogen contents in each step, we could estimate the amount of grafted polymer on the silica surface. The data are presented in Table 4.3. On the basis of the increase in carbon content the apparent shell thickness was calculated. The obtained shell thickness was 2.4 nm.

In Table 4.3 the apparent thickness, calculated from the TGA mass loss data and elemental analysis, have been compared with the nominal thickness, estimated assuming the grafted shell to consist of monomers forming a liquid film covering the core surface. The somewhat lower measured thickness compared to the nominal values agrees with our previous report

[239] and can be attributed to solution chain growth, nevertheless resulting in an acceptable conversion of monomer to shell polymer.

Table 4.3. Results from the characterisation of imprinted core-shell beads.

Polymer name [a]	%C	%N	%S	Mass loss [b] (%)	Conv.[c] (%)	d_{nom}[d] (nm)	d_{EA}[e] (nm)	d_{TGA}[f] (nm)
SiNP-MIP	20.50	0.32	0.43	43	82	4.1	2.4	3.2

a) See experimental section for details.

b) Mass loss by thermal gravimetric analysis (TGA).

c) Gravimetric conversion: Conversion=mass loss (TGA)/mass of monomer feed.

d) The shell thickness (nm) was calculated according to Eq. 2-3.

e) The shell thickness (nm) was calculated according to Eq. 2-3, Eq. 2-16 and Eq. 2-17.

f) The shell thickness (nm) was calculated according to Eq. 2-3 and Eq. 2-9.

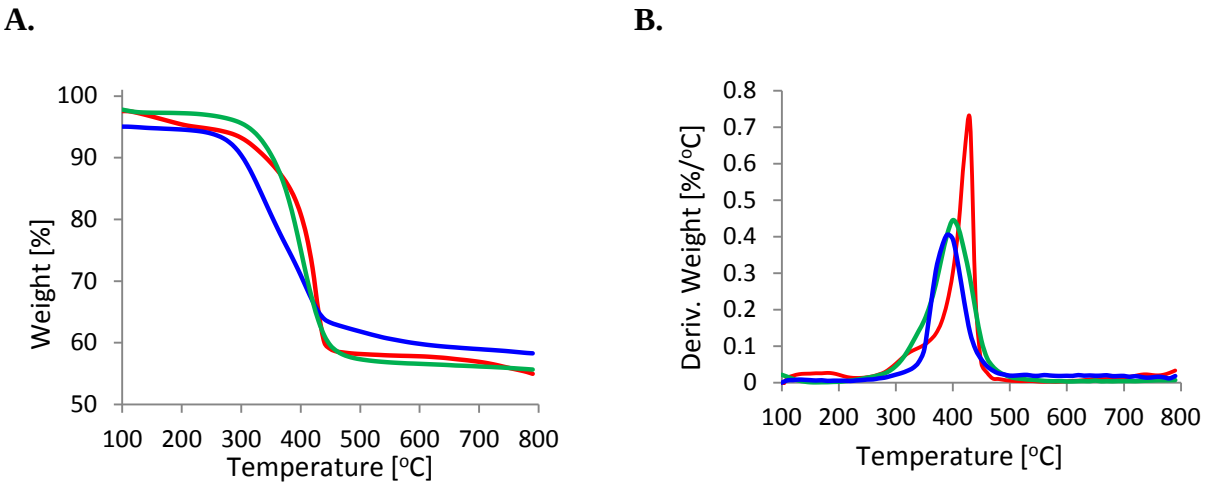

Figure 4.9. Thermal gravimetric analysis of the L-Phe imprinted core-shell nanoparticles using magnetic template; TGA (A), DTG (B); crude magNP-L-Phe/SiNP-MIP prior to washing (red), magNP-L-Phe/SiNP-MIP after washing (blue) and released SiNP-MIP (green).

The TEM and SEM images of the mag-L-Phe imprinted core-shell nanoparticles are shown in Figure 4.10. An inorganic silica core appears darker than the grafted organic polymer shell due to the difference in density. Comparison of TEM images of grafted polymer silica nanoparticles with images of bare silica particles and RAFT modified silica support confirmed a successful grafting of the polymer shell on the silica particles. The average

particle size as estimated by TEM measurements of these grafted silica core-shell particles was found to be in the range of 20-25 nm with a shell thickness of 2-4 nm .

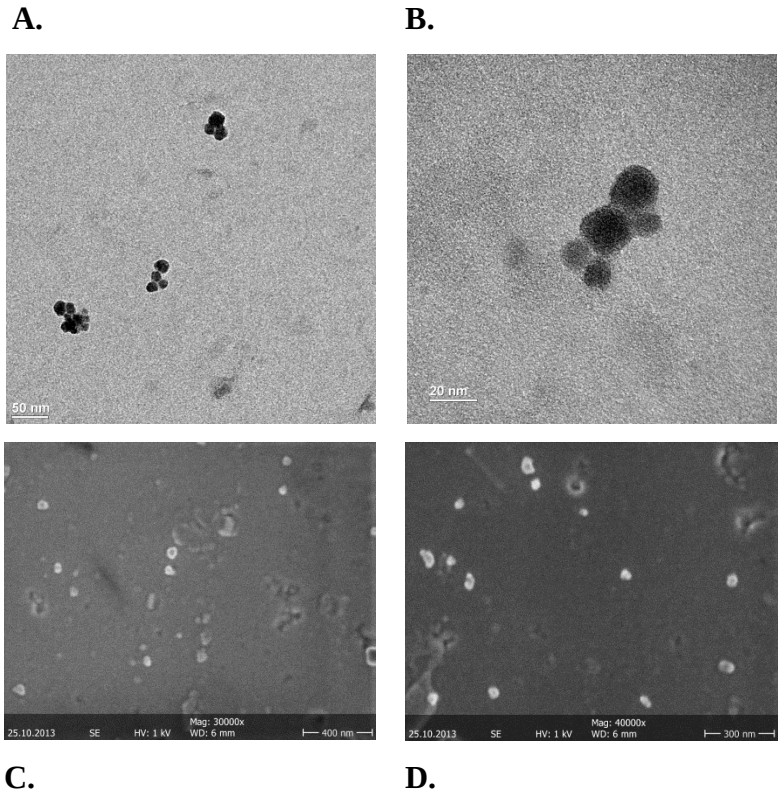

Figure 4.10. TEM (A, B) and SEM (C, D) images of the L-Phe imprinted core-shell nanoparticles using magnetic template. The scale bar is 50 nm in the case of (A) 20 nm for (B) 400 nm in the case of (C) and 300 nm for (D).

The FTIR spectra of the core-shell beads shown in Figure 4.11 display two characteristic bands i.e. the carbonyl stretching of the polymer matrix at ca 1740 cm^{-1} and the siloxane vibration of silica core at ca 1120 cm^{-1}.

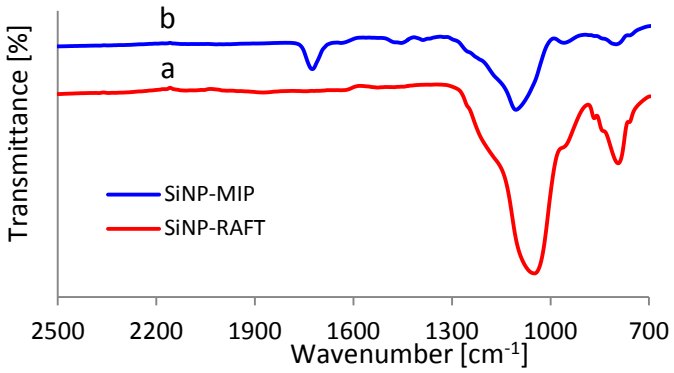

Figure 4.11. FTIR spectra of SiNP-RAFT(a) and SiNP-MIP (b).

The DLS data demonstrated a Z-average size of 45 nm and a polydispersity of 0.255.The particles size measured by DLS was slightly bigger than the size obtained from TEM due to the aggregation of the particles (Figure 4.12). The TEM images further revealed separate or smaller aggregates of polydisperse particles.

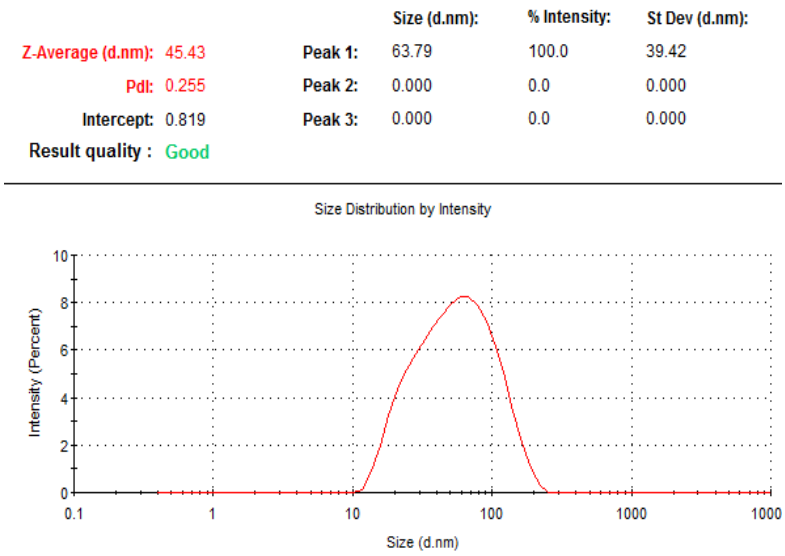

Figure 4.12. DLS results of the magnetic L-Phe imprinted nanoparticles.

4.2.6 Binding isotherms of the imprinted polymers

In order to evaluate the binding properties, the particles were subsequently tested for their affinity towards the template L-PA and its optical antipode D-PA in acetonitrile. After incubating the particles with solutions of L-PA or D-PA of known concentrations the free

concentration of the solutes were determined by reversed phase HPLC. Binding curves were then constructed by plotting the specific amount of bound solute against the free concentration of solute.

As shown in Figure 4.13, the amount of template peptide bound to the MIPNPs at equilibrium, increased with increasing initial concentration of the template. Interestingly the material prepared using the magnetic placeholder template showed somewhat steeper binding curves and higher uptake of L-PA compared to SiNP-MIP2 (See Figure 3.23). Hence the immobilized ligand seems rather effective in generating imprinted sites complementary to L-PA. The enantioselectivity and affinity appears particularly striking given that the particles were generated using ca 10 times less template compared to the conventional procedure. The here reported method profit from the high surface to volume ratio of template decorated magnetic nanoparticles potentially allowing a much higher product yield of affinity enriched imprinted particles. In addition, the use of immobilized templates and RAFT mediated surface initiated polymerization should lead to more accessible and uniform binding sites.

The isotherms were subsequently fitted to mono-Langmuir, bi-Langmuir and Freundlich isotherm models. The resulting isotherm parameters are shown in Table 4.4, Table 4.5 and Table 4.6. The Fisher values in Figure 4.14 reflect which of the models provides the best fit to a particular isotherm, a higher number indicating a better fit. According to the Fisher value, the experimental binding isotherm was best fitted to the Freundlich isotherm model. Compared with D-PA, the imprinted polymer for L-PA revealed high total number of binding sites (N= 34.10 μmol/g) and binding capacity (a= 37.84 ±1.89μmol/g $(mol^{-1})^{m}$). All these together indicated the presence of high affinity binding sites on the surface of imprinted nanoparticles.

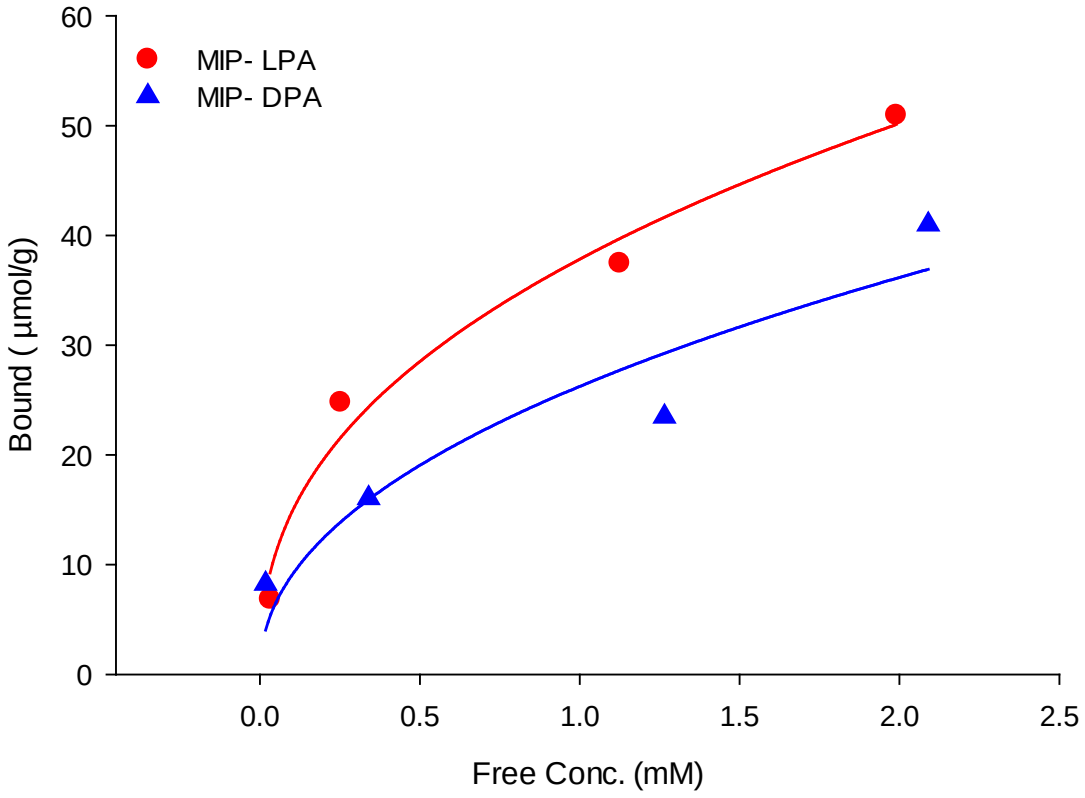

Figure 4.13. Equilibrium binding isotherms of L-PA (circles) and D-PA (triangle) on imprinted core-shell particles in acetonitrile. The MIPs were synthesized using the magnetic template.

Table 4.4. Mono-Langmuir isotherm fitting parameters obtained by nonlinear regression of data shown in Figure 4.13.

Polymer name		k_d (mM)	q_s (µmol/g)	r^2	***F***- value
SiNP-MIP	LPA	0.33 ±0.16	55.04 ±7.38	0.9576	45
	DPA	1.47 ±2.28	64.16 ±49.08	0.7928	7.6

Table 4.5. Bi-Langmuir isotherm fitting parameters obtained by nonlinear regression of data shown in Figure 4.13.

Polymer name		k_d1 (mM)	q_s1 (µmol/g)	k_d2 (mM)	q_s2 (µmol/g)	r^2	***F*-value**
SiNP-MIP	LPA	0.085 ±inf	27.37 ±inf	1.49×10^{9}	1.79×10^{10}	0.9949	ND
	DPA	0.003 ±inf	9.42 ±inf	3.44×10^{9}	4.87×10^{10}	0.9622	ND

ND= not determined

Table 4.6. Freundlich isotherms fitting parameters obtained by nonlinear regression of data shown in Figure 4.13.

Polymer name		Affinity constant, ***K***(mM^{-1})	Total number of binding sites ,***N*** ($\mu mol\ g^{-1}$)	Heterogen-eity parameter, ***m***	Binding capacity, ***a*** (µmol/g $(mol^{-1})^{m}$)	Regression coefficient, r^2	***F*-value**
SiNP-MIP	LPA	20.49	34.10	0.41± 0.06	37.84 ±1.89	0.9794	95
	DPA	39.60	25.84	0.46± 0.17	26.25±3.47	0.8845	15

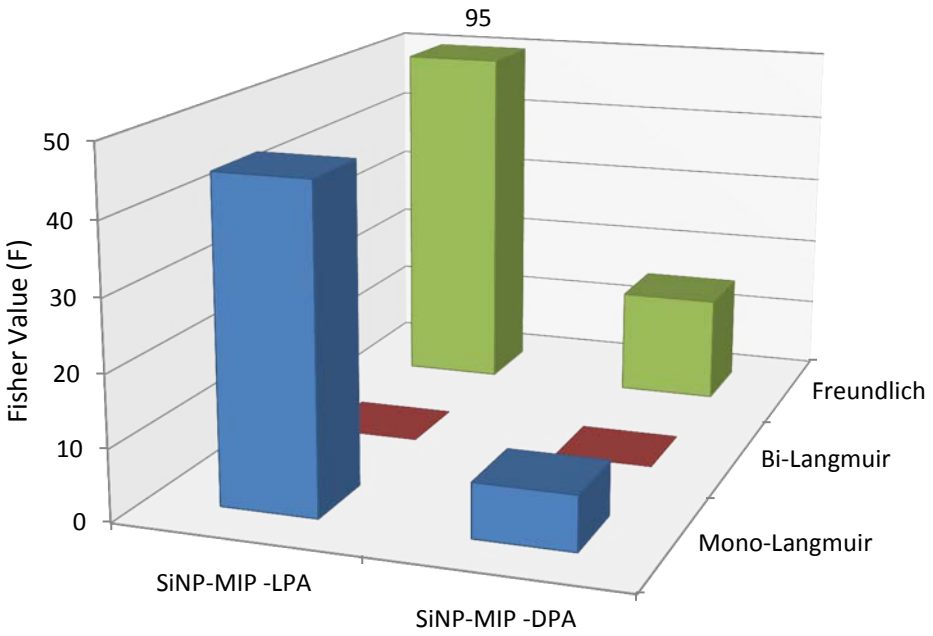

Figure 4.14. Fisher values obtained by fitting the L/D-PA binding curves in Figure 4.13 to mono-Langmuir, bi-Langmuir and Freundlich isotherm models (see Table 4.4 to Table 4.6).

4.3 Conclusions

Core-shell MIP NPs were produced using a new approach which relies on immobilization of the template on a magnetic solid support. Combination of surface initiated RAFT polymerization and solid phase synthesis offers significant advantages when compared to traditional approaches which rely on free template in solution, such as receptors in template free form, template reusability and high affinity binding site.

The results of our research demonstrated that the MIP NPs prepared via this method has high accessible binding site and good discrimination towards the template L-PA and its optical antipode D-PA. These aspects in addition to the fact that polymerization take place in homogenous media hold great promise with respect to method scalability and parallel synthesis. We are currently exploiting these possibilities while applying the concept to other model systems including those of biological significance. The results of this chapter have been submitted for publication [272].

4.4 Experimental

4.4.1 Synthesis of magnetic core nanoparticles (magNP)

A slightly modified version of the procedure reported by Ma et al. was followed [269]. $FeSO_4 \cdot 7H_2O$ (6 g) and anhydrous $FeCl_3$ (7 g) were dissolved in water (200 mL) under N_2 with vigorous stirring at 85 °C. An aqueous solution of 25% ammonia (15 mL) was then quickly added leading to a change of color from orange to black due to the precipitation of the magnetite nanoparticles. The solution was stirred for 30 min at elevated temperature and then allowed to cool down to room temperature. Afterwards, the magnetic particles were collected using a magnet and washed with 3 x 50 mL water and in a final step with 50 mL 0.2 M NaCl solution. The particles were finally dried at 80 °C under vacuum leading to 11 g of dry magNP.

4.4.2 Silica coating on the surface of magnetic nanoparticles (magNP@SiO_2)

Following the procedure reported by Taylor et al. [270], dry magNP (2 g) was dispersed in 50 mL water by sonication. The particles were collected by a magnet and subsequently dispersed in a 10% (v/v) aqueous solution of TEOS (230 mL). After addition of glycerol (200 mL) the pH was adjusted to 4.6 with glacial acetic acid. The dispersion was then heated to 90 °C under N_2 atmosphere and stirred using an overhead stirrer for 2 hours. After washing with water (3x200 mL) and ethanol (3x100 mL), the particles were dried in a vacuum oven at 40 °C leading to 2 g of dry magNP@SiO_2.

4.4.3 Aminofunctionalization of magnetic silica nanoparticles (magNP-NH_2)

magNP@SiO_2 (1 g) was dispersed in a solution (30 mL) of ethanol/water (1/1, v/v) by sonication for 30 min. 3-aminopropyltrimethoxysilane (APTMS) (4 mL) was added to the dispersion under N_2 atmosphere and the dispersion stirred at 40 °C overnight. The dispersion was thereafter cooled to room temperature and the particles collected with a magnet and washed with ethanol, and three times with deionized water. Finally, the particles were dried under vacuum at 60 °C leading to 1 g of dry magNP-NH_2. The presence of free amine groups on the particles was confirmed by the ninhydrine test (Ruhemann's purple).

4.4.4 Immobilization of L-phenylalanine on magNP-NH_2 (magNP-L-Phe)

Fmoc-Phe-OH (1.9 mg) was converted to the active ester by dissolving it in 10 mL phosphate buffer (50mM, pH7.5) followed by addition of N-(3-dimethylaminopropyl)-N′-ethylcarbodiimide (EDC) (5 mM) and N-hydroxysuccinimide (10 mM). The reaction was allowed to proceed for 15 min followed by addition of 500 mg of magNP-NH_2. The dispersion was sonicated for 10 min and was thereafter incubated over night at room temperature. Fmoc deprotection was achieved by treating the particles in 20% piperidine in DMF (5 x 5 mL). The resulting fulvene-piperidine adduct was quantified by measuring the absorption of the supernatants at 301 nm. This measurement was used to estimate the loading

of L-Phe on the magnetic particles. In parallel, fluorescence of the supernatants was measured using an excitation wavelength of 300 nm and detecting the emission at 400 nm.

4.4.5 Synthesis of core-shell MIPs using magNP-L-Phe as template (SiNP-MIP)

A suspension of RAFT-modified core particles (SiNP-RAFT: 100 mg), MAA (8.6 µL), EDMA (95 µL) in 3 mL of dry toluene was added to magNP-L-Phe (50 mg), previously dispersed in toluene by sonication. The prepolymerization mixture was purged of oxygen by either bubbling with N_2 for 15 min or by three successive freeze-pump-thaw cycles where after the initiator ABDV (0.93 mg) was added. This corresponds to a ratio of RAFT/initiator of 3. Polymerization was initiated at 50 °C and allowed to proceed for 22 h. After polymerization the particles were collected by magnet and washed by intermittent magnetic separation with toluene (3 mL) followed by five times with MeOH 80%, Formic acid 15%, 5% H_2O (3 mL). Each elution step was accompanied by sonication of the suspension for 15 min. The supernatants containing the free SiNP-MIP2 were collected and pooled followed by isolation of the particles by centrifugation. In order to clean them from small traces of remaining magNP-L-Phe, they were washed by intermittent magnetic separation with 1) 1M HCl (3 mL) overnight resulting in a color change from brownish to pink; 2) three times with water (3 mL) until pH was neutral and 3) MeCN (3 mL) and thereafter dried under vacuum at 40 °C. This resulted 17 mg of dry particles (ca 9 % gravimetric yield).

4.4.6 Batch binding tests of NPs for their affinity for L-PA and D-PA.

Dry template free polymer (2 mg) was weighed into 10 separate HPLC vials followed by addition of solutions (0.2 mL) of D-PA or L-PA (0.1-2.5 mM) in acetonitrile (the test was downscaled for samples available in limited quantities). The vials were sealed and their contents allowed to equilibrate overnight at room temperature with gentle shaking. After 15 h incubation at room temperature the supernatants were sampled (30 µL) and the aliquots diluted in 270 µL water and transferred to HPLC vials for measurement of unbound solute concentration by reversed phase HPLC. The HPLC system consisted of an Agilent HPLC 1100 series instrument (Agilent) equipped with a UV-DAD detector and an autosampler. The

column was a reversed phase (C18) column (Phenomenex Luna C-18, 150 × 4.6 mm), the mobile phase: MeOH/H_2O: 62/38 (0.2% TFA), flow rate: 1.0 mL/min, the injection volume was 10 μL and the detection performed by UV absorbance at 265 nm. The resulting peak areas were used to calculate the amount of bound analyte on the polymer (in μmol/g of polymer). The binding results are averages of two independent experiments.

Chapter 5: Epitope Imprinted Core-Shell Nanoparticles Targeting β-Amyloid

5.1 Introduction

Alzheimer's disease (AD) is the most common cause of late life dementia in humans and the fourth leading cause of death in the developed world. It is believed that cerebral deposition of amyloid plaques is central to the disease process. Thus, microscopically, AD is characterised by marked degeneration of the neurons and their synapses and by the presence of large numbers of senile plaques and neurofibrillary tangles in the cerebral neocortex and hippocampus. The plaques are made up of Amyloid deposits mainly comprising aggregates of a 39-42 residue peptide called β-amyloid (Aβ).

In this work we have investigated the epitope imprinted core-shell nanoparticles via surface initiated RAFT polymerization for β-amyloid template. Epitope imprinted nanoparticles (NPs) were prepared by grafting of poly-(ethyl ammonium methacrylate -co- diarylurea -co-divinylbenzene) in presence of a β-amyloid template from a RAFT modified 200 nm and 20 nm sized silica cores. After the removal of the template by intensive wash, the resultants MIPs were characterized by FTIR, TEM, TGA and elemental analysis. The polymers were examined by equilibrium rebinding for their affinity towards the β-amyloid template by reversed phase HPLC.

5.1.1 Choice of the amyloid peptide epitopes

The C-terminal part of Aβ peptides, in general, has been suggested to be involved in the dimerization and aggregation of Aβ[273] and one fragment, in particular, has been considered to be the major pathogenic form in Alzheimer's disease, the 42 amino acid sequence ($A\beta_{1-42}$):

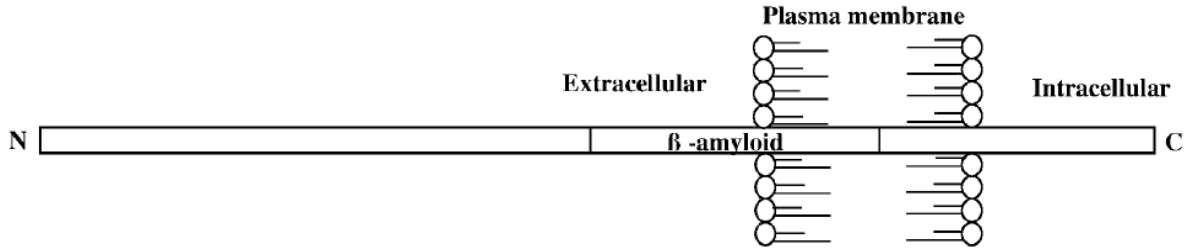

***Aβ$_{1-42}$*:**

H-Asp-Ala-Glu-Phe-Arg-His-Asp-Ser-Gly-Tyr-Glu-Val-His-His-Gln-Lys-Leu-Val-Phe-Phe-Ala-Glu-Asp-Val-Gly-Ser-Asn-Lys-Gly-Ala-Ile-Ile-Gly-Leu-Met-Val-Gly-Gly-Val-Val-Ile-Ala-OH

Figure 5.1. Schematic representation of the amyloid precursor protein (APP) and the location of the Aβ peptide(up) and the 42 amino acid sequence of Aβ$_{1-42}$ (down).

In order to prepare MIPs for discrimination of the C-termini of Aβ$_{1-42}$, we selected the corresponding C-terminal hexapeptide sequences (marked in green) as templates.

5.2 Results and Discussions

5.2.1 Template synthesis

In contrast to previously published examples involving hydrophilic peptide sequences as templates, the imprinting of the hydrophobic and strongly self-aggregating amyloid peptides have posed new challenges. The C-terminal sequence Aβ$_{37-42}$ exhibit notoriously poor solubility in a variety of solvents, and they precipitate in water to form fibers of aggregated peptide in a stable antiparallel β-sheet conformation [274]. Poor solubility was also confirmed for the acetylated templates, and only a few solvents [e.g., dimethyl sulfoxide (DMSO), N,N-dimethylformamide (DMF), formic acid] were capable of dissolving the peptides at sufficiently high concentrations for molecular imprinting. DMSO was therefore chosen as the base solvent in the preparation of the first set of MIPs. Transforming of template into its tetrabutylammonium salt (AcGGVVIA^{-} TBA^{+}) enhanced the solubility significantly, and polymerization could then be performed in less competitive solvents, including up to 65% acetonitrile. This was used to prepare a second set of MIPs.

The hexapeptide template, H-Gly-Gly-Val-Val-Ile-Ala-OH ($A\beta_{37\text{-}42}$), was acetylated on the N-terminal and transformed to the TBA salt of the acetylated peptide and used as a template for the epitope imprinting. From the different methods tested for the acetylation the best results were obtained by dissolving the peptide, $A\beta_{37\text{-}42}$ in a minimum amount of DMSO followed by addition of NH_4HCO_3 (50 mM) and acetic anhydride in MeOH. The reaction was monitored by a ninhydrin test, as described in the experimental section and the reaction time determined by a negative ninhydrin test, i.e. trace amounts of free amino groups. The purity of the final compound was determined by RP-HPLC which was in the range of 95-98%. The TBA salt of the acetylated peptide was prepared by addition of 1 eq. of tetrabutyl-ammonium hydroxide in methanol and used directly after drying.

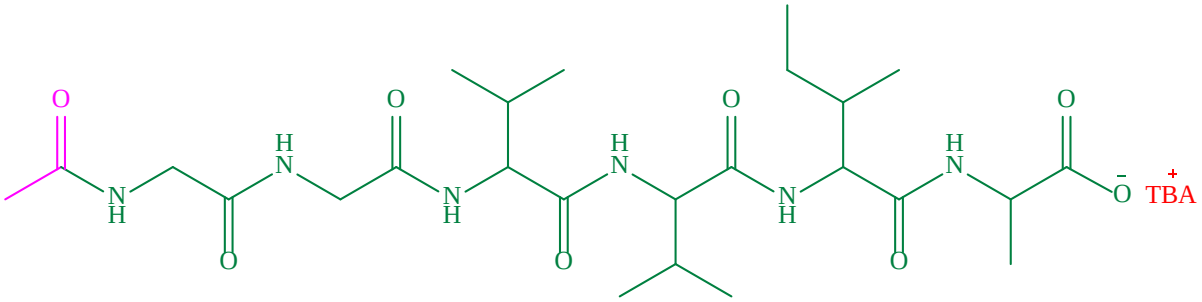

Figure 5.2. Chemical structure of the template used for the synthesis of the imprinted polymers (Ac-Gly-Gly-Val-Val-Ile-Ala-O^- TBA^+, Ac-$A\beta_{37\text{-}42}$-TBA).

5.2.2 Grafting of beta-amyloid imprinted polymers from RAFT-modified silica nanoparticles

The β-amyloid imprinted polymers were produced based on the previously developed procedure in our group [275]. The grafting polymer from RAFT-modified silica support were conducted by using diarylurea as comonomer, ethyl ammonium methacrylate as a functional monomer, divinylbenzene as a crosslinker, in presence of Ac-$A\beta_{37\text{-}42}$-TBA as a template in organic media (Figure 5.3). In order to improve the template solubility, polymerization was performed in less competitive solvents, including up to 65% acetonitrile and 35% DMSO. The 1,3-diarylurea was used as host monomer which is capable of forming a twofold hydrogen bond to the template oxyanion [276].The previously combinatorial method in our group revealed that the polymer prepared using the hydrophobic cross-linker divinylbenzene (DVB) displayed the highest template binding among the cross-linkers tested [275].

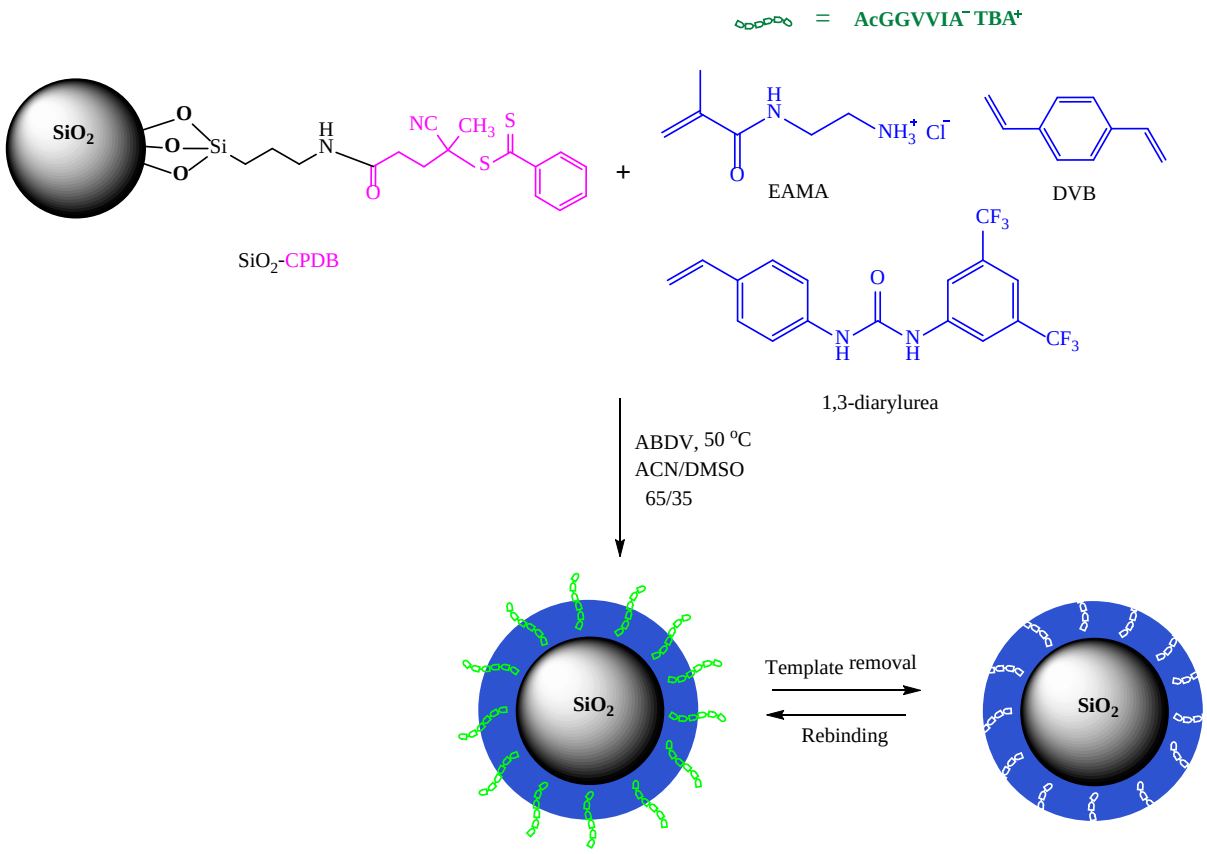

Figure 5.3. Procedure for preparing beta-amyloid imprinted polymers from RAFT-modified silica nanoparticles for binding of the C-terminus of $A\beta_{33\text{-}42}$.

The polymerization was carried out at 50 °C for 40 h. The ratio among template, comonomer, functional monomer and crosslinker was 0.04: 0.04: 4: 20, respectively. In preparing the grafting polymers, a molar ratio RAFT/ABDV = 4 and RAFT/ABDV= 3 were used. The quantity of monomer relative to the silica supports were adjusted to result in shells/films with approximately 30 nm (SiNP-MIP-1) or 4 nm (SiNP-MIP-2, 3, 4) thick shells. After polymerization the beads were isolated by centrifugation and subjected to repetitive washing-centrifugation cycles in order to remove any leachables (e.g. template, oligomers, unreacted monomers). Five cycles were sufficient for exhaustive template removal as concluded by HPLC analysis of the washing fractions. After drying at 40 °C under vacuum, the light pink MIP particles were obtained. The light pink NIP particles with surface-immobilized dithiobenzoate groups were then prepared and purified under the identical conditions except that the template was omitted. The procedure is shown in Table 5.1.

Table 5.1. Procedure for the preparation of core-shell beta-amyloid imprinted nanoparticles.

Polymer name [a]	Template: Ac-Aβ_{37-42}-TBA (μmol)	SiNP-RAFT (mg)	Urea (μmol)	EAMA (μmol)	DVB (μmol)	ACN/ DMSO (mL)	RAFT/ ABDV
SiNP-MIP-1[b]	5.11	700	5.11	511	2556	15	3/1
SiNP-NIP-1[b]	-	700	5.11	511	2556	15	3/1
SiNP-MIP-2[c]	5.31	400	5.31	531	2653	15	3/1
SiNP-NIP-2[c]	-	400	5.31	531	2653	15	3/1
SiNP-MIP-3[c]	3.98	300	3.98	398	1990	7	4/1
SiNP-NIP-3[c]	-	300	3.98	398	1990	7	4/1
SiNP-MIP-4[d]	3.98	300	3.98	398	1990	7	4/1
SiNP-NIP-4[d]	-	300	3.98	398	1990	7	4/1

a) See experimental section for details.

b) Silica core size is 200 nm and the particles were modified by dithiobenzoate RAFT agent.

c) Silica core size is 20 nm and the particles were modified by dithiobenzoate RAFT agent.

d) Silica core size is 20 nm and the particles were modified by trithiocarbonate RAFT agent.

5.2.3 Polymer characterization

After polymerization, the beads were subsequently characterized by TGA, TEM, and elemental analysis. Elemental analysis and TGA were used to confirm the successful grafting of polymers on silica cores. Figure 5.4 displays the TGA and DTG curves of grafted polymers. It can be observed from TGA curves the weight loss of the resulting polymers between 100 ^{o}C and 800 ^{o}C which are listed in Table 5.2. By using the TGA results the gravimetric conversion and shell thickness (nm) of grafted polymers on silica cores were calculated. The results demonstrated that the conversion efficiency of polymer chains was increased by using the less amount of solvent for polymerization.

From elemental microanalysis data, more precisely from the change in carbon and nitrogen contents in each step, we could estimate the amount of grafted polymer on the silica surface.

The data are presented in Table 5.2. On the basis of the increase in carbon content the apparent shell thickness was calculated. In Table 5.2 the apparent thickness, calculated from the TGA mass loss data and elemental analysis, have been compared with the nominal thickness, estimated assuming the grafted shell to consist of monomers forming a liquid film covering the core surface. The somewhat lower measured thickness compared to the nominal values agrees with our previous report [239] and can be attributed to solution chain growth, nevertheless resulting in an acceptable conversion of monomer to shell polymer.

The TEM images of the polymer grafted silica NPs are shown in Figure 5.5. The images demonstrated the highly uniform spherical morphology with the size of about 200-220 nm and 20-25 nm. In the comparison of TEM images before and after polymerization, a shell structure can be seen on the silica particles after polymerization in with a uniform thickness of the shells which are signed via arrow in Figure 5.5. The results obtained from these techniques confirmed that grafting successfully occurred from the surface of the silica support.

Table 5.2. Results from the characterisation of imprinted and nonimprinted core-shell beads.

Polymer name [a]	%C	%N	%S	Mass loss [b] (%)	Conv.[c] (%)	d_{nom}[d] (nm)	d_{EA}[e] (nm)	d_{TGA}[f] (nm)
SiNP-MIP-1[g]	18.50	0.47	0.54	24.9	36	30	23.6	18.5
SiNP-NIP-1[g]	18.38	0.42	0.75	25.3	37	30	23.4	18.8
SiNP-MIP-2[h]	19.36	0.56	0.68	21	41	4.31	2.2	1.3
SiNP-NIP-2[h]	21.42	0.58	0.66	23	47	4.31	2.5	1.5
SiNP-MIP-3[h]	24.15	0.62	0.69	23	61	4.31	2.9	1.5
SiNP-NIP-3[h]	22.76	0.59	0.67	21.5	54	4.31	2.7	1.4
SiNP-MIP-4[i]	23.89	0.61	0.56	22.2	61	4.31	2.9	1.4
SiNP-NIP-4[i]	25.93	0.68	0.59	25.4	75	4.31	3.2	1.6

a) See experimental section for details.

b) Mass loss by thermal gravimetric analysis (TGA).

c) Gravimetric conversion: Conversion=mass loss (TGA)/mass of monomer feed.

d) The shell thickness (nm) was calculated according to Eq. 2-3.

e) The shell thickness (nm) was calculated according to Eq. 2-3, Eq. 2-16 and Eq. 2-17

f) The shell thickness (nm) was calculated according to Eq. 2-3 and Eq. 2-9.

g) Silica core size is 200 nm and the particles were modified by dithiobenzoate RAFT agent.

h) Silica core size is 20 nm and the particles were modified by dithiobenzoate RAFT agent.

i) Silica core size is 20 nm and the particles were modified by trithiocarbonate RAFT agent.

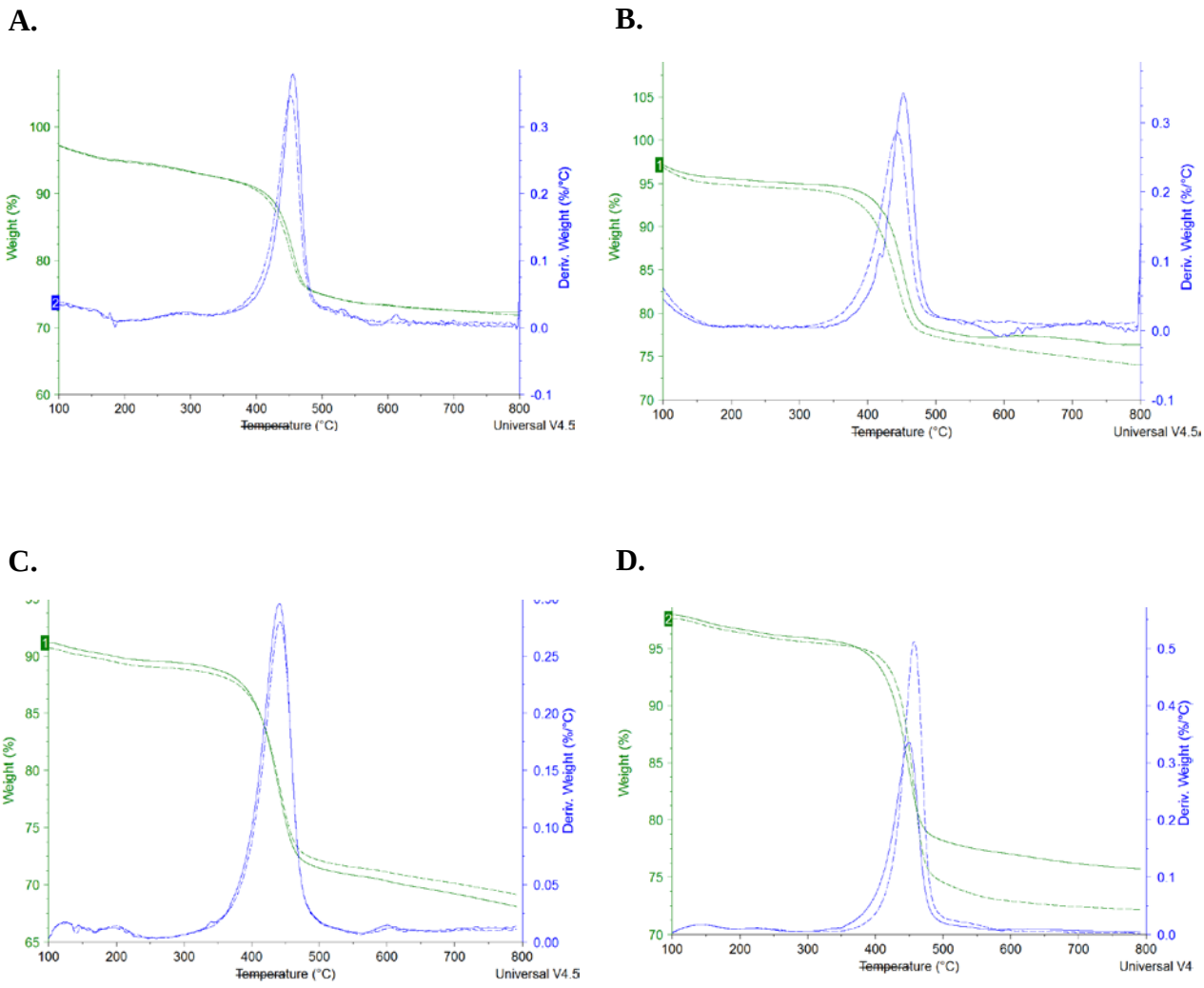

Figure 5.4. Thermal gravimetric analysis of the beta-amyloid imprinted and nonimprinted core-shell nanoparticles; TGA and DTG of SiNP-MIP-1 and SiNP-NIP-1 (A), TGA and DTG of SiNP-MIP-2 and SiNP-NIP-2 (B), TGA and DTG of SiNP-MIP-3 and SiNP-NIP-3 (C), TGA and DTG of SiNP-MIP-4 and SiNP-NIP-4 (D).

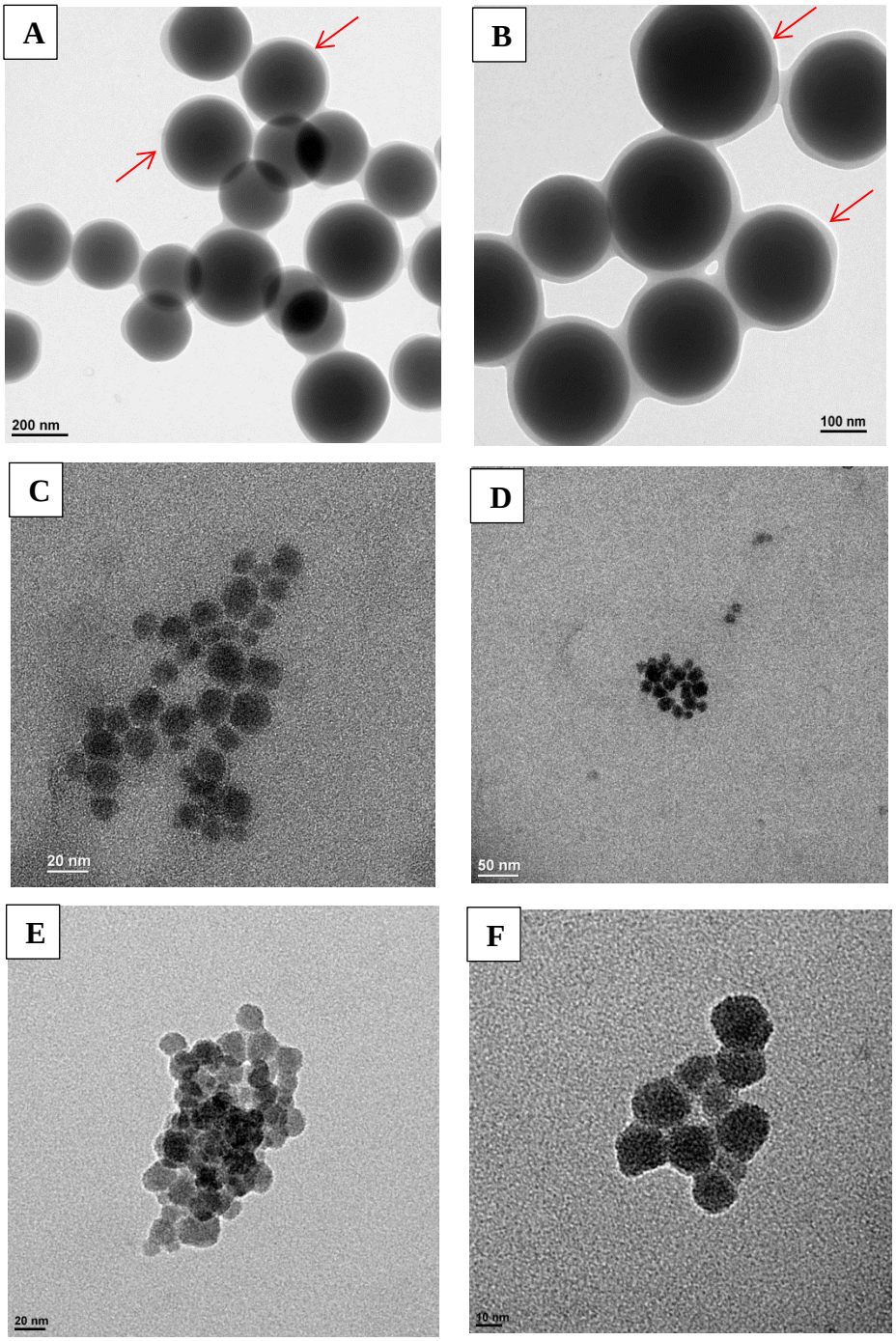

Figure 5.5. TEM images of SiNP-MIP-1 and SiNP-NIP-1 (A, B); SiNP-MIP-2 and SiNP-NIP-2 (C, D); SiNP-MIP-3 and SiNP-NIP-3 (E, F). The polymer shells are indicated by arrows. The scale bar is 200 nm in the case of (A) 100 nm for (B) 20 nm for(C, E) 50 nm for (D) and 10 nm for (F).

5.2.4 Binding isotherms

The polymers were freed from the template by washing in methanol and acidified methanol and then subjected to a template-rebinding experiment. The recovery of first three washing fraction was 11.68 %, 13.83 %, 18.14 % and 15.47 % for SiNP-MIP-1, SiNP-MIP-2, SiNP-MIP-3 and SiNP-MIP-4, respectively and the washing continued until the template could not be detected in the washing solution by RP-HPLC. The low recovery percentage can be attributed to the lower detected peak area for template in washing solution (MeOH) than the standard stock solution (GuHCl). The template $A\beta_{33-42}$ was added in free and nonacetylated form. The batch rebinding experiments were conducted in 4 M GuHCl using a range of Ab_{33-42} concentrations from 0.005 mM to 0.2 mM. The binding isotherms recorded in 4 M GuHCl are informative in regard to the affinity of those sites under denaturing conditions. After incubating the particles with solutions of $A\beta_{33-42}$ of known concentrations the free concentration of the solutes were determined by reversed phase HPLC. As can be seen obviously from binding isotherms (Figure 5.6), the resulting polymers which prepared in diluted condition (SiNP-MIP-1, 2 and SiNP-NIP-1, 2) revealed same adsorption capacity at the both imprinted and nonimprinted polymers. This behavior can be attributed to low concentration of template in diluted prepolymerization mixture which cause the week interaction among the functional monomers and template. In contrast, at the both resulting polymers which generated in concentrated condition the imprinted particles displayed slightly more adsorption capacity than the nonimprinted particles in high range of template concentrations. In addition, GuHCl was used as rebinding media and the peptide should be in a wide range of different denatured states, not in the native state. Therefore, the different denatured states might be caused the low binding capacity.

The notoriously poor solubility of $A\beta_{33-42}$ in aqueous media posed a considerable problem for the rebinding tests. The results of calibration plot therefore reflected this problem and there were some points at each calibration curve which caused to obtain low coefficient of correlation for a linear regression of all data points. Furthermore, in order to separate polymer nanoparticles from free $A\beta_{33-42}$ the particles were subjected to centrifugation. After this process and in spite of using low speed rotation, some $A\beta_{33-42}$ was precipitated from supernatant. Consequently, the somewhat lower differences at adsorption capacity of the imprinted and nonimprinted particles could be attributed to poor solubility of beta amyloid in aqueous media.

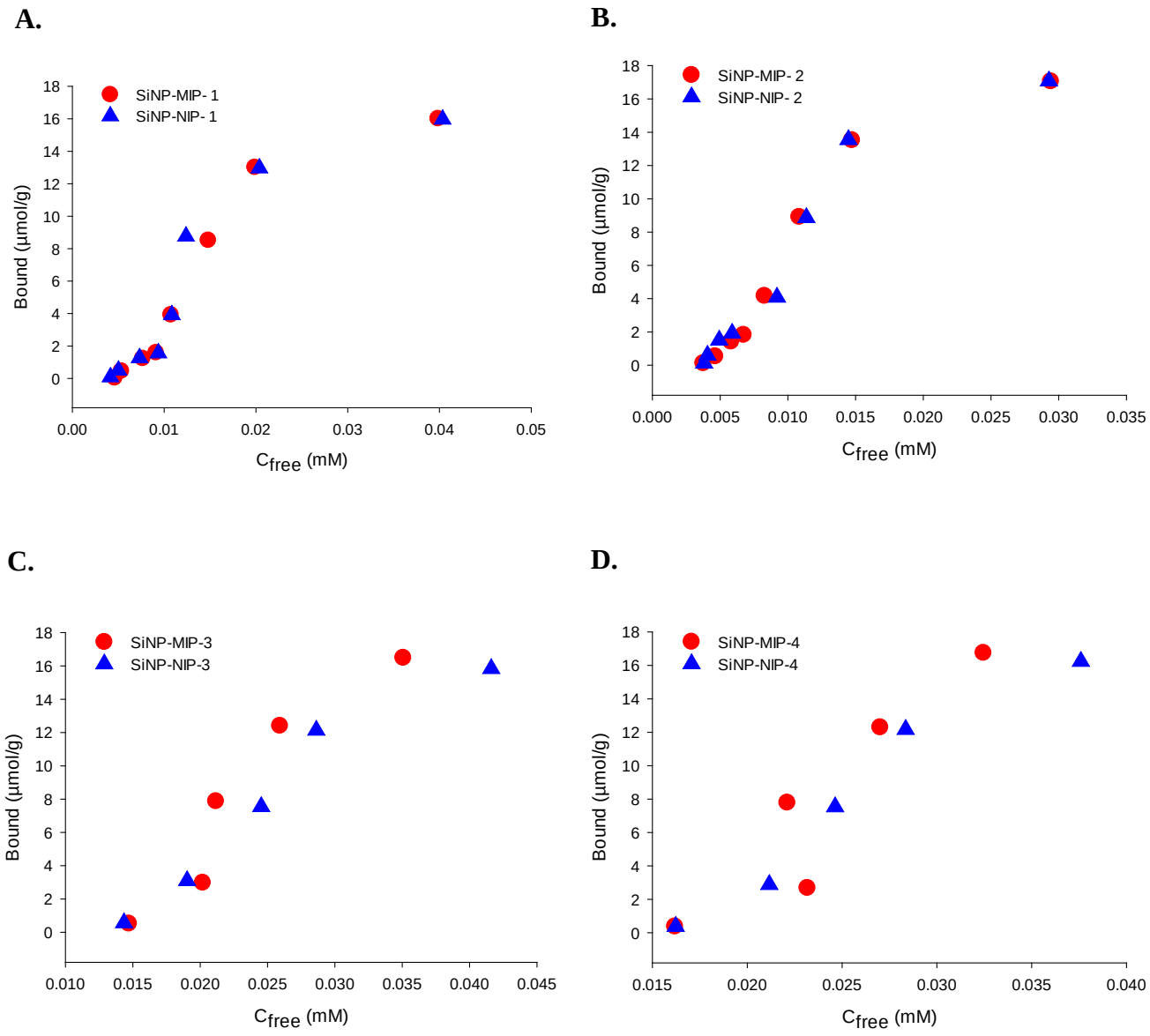

Figure 5.6. Equilibrium binding isotherms of Ab_{33-42} on imprinted (circles) and nonimprinted (triangles) core-shell particles in GuHCl (4M)/ACN: 90/10 (v/v). A) SiNP-MIP-1(red circles) and SiNP-NIP-1(blue triangles), B) SiNP-MIP-2(red circles) and SiNP-NIP-2(blue triangles), C) SiNP-MIP-3 (red circles) and SiNP-NIP-3 (blue triangles), D) SiNP-MIP-4 (red circles) and SiNP-NIP-4 (blue triangles).

5.3 Conclusions

Synthetic receptors for beta amyloid peptides have been prepared by epitope imprinted core-shell nanoparticles. Two silica nanoparticles with core diameters of 200 nm and 20 nm were modified via dithiobenzoate and trithiocarbonate RAFT agent and used as solid supports. The final MIPs were designed using TBA salt of the acetylated $A\beta_{37-42}$ as a template for the recognition of $A\beta_{33-42}$. The batch rebinding results demonstrated that the resulting polymers which prepared in diluted condition showed same adsorption capacity at the both imprinted and nonimprinted polymers. In contrast, at the both resulting polymers which generated in concentrated condition the imprinted particles displayed slightly more adsorption capacity than the nonimprinted particles in high range of template concentrations. This behavior can be attributed to low concentration of template in diluted prepolymerization mixture which cause the week interaction among the functional monomers and template. The poor solubility of $A\beta_{33-42}$ in aqueous media caused a considerable problem for the rebinding tests. For this reason more investigations need to address this problem and get more optimistic results.

5.4 Experimental

5.4.1 Acetylation of $A\beta_{37-42}$

The peptide, H-GGVVIA-OH (100 mg) was dissolved in the minimum amount of DMSO by adding aliquots of 100 µl. After the addition of NH_4HCO_3 (50 mM), 1.2 equivalents of acetic anhydride in MeOH were added drop-wise and the mixture stirred for 12 h. The reaction was monitored by adding a drop of the supernatant to 100 µl of ninhydrin in solution (0.1% in ethanol) and heating the mixture at 100 °C for 10 min. A positive test (solution turning purple) is obtained for free amino groups of the peptide in solution. The product was dried under vacuum at 50 °C for 24 h. In order to remove the remaining salts, the product was washed with small fractions of cold water, lyophilized and characterized by RP-HPLC (column: Phenomenex Luna C-18, 125×4.6 mm, mobile phase: water/MeOH (65/35) + 0.1%

TFA, flow rate: 1 ml/min, inj. vol.: 100 µl, tr(H-GGVVIA-OH)= 6.25 min tr(Ac-GGVVIA-OH)= 14.94 min, purity 95%) .

5.4.2 Tetrabutylammonium salt preparation of acetylated $A\beta_{37-42}$

The acetylated hexapeptide, Ac-$A\beta_{37-42}$, was mixed with a solution of tetrabutylammonium hydroxide in MeOH (1M), in an equimolar ratio and allowed to react for 4 h stirring at room temperature. The salt was dried under vacuum and used straightforward without any further characterization.

5.4.3 Preparation of beta-amyloid imprinted polymers from RAFT-modified silica nanoparticles

RAFT modified core particles (SiNP: 700mg corresponding to 65.1 µmol RAFT groups) were suspended in a prepolymerization mixture containing Ac-$A\beta_{37-42}$-TBA (4.1 mg, 5.11 µmol), Urea (1.91 mg, 5.11 µmol), EAMA (84.2 mg, 511 µmol) and DVB (362 µL, 2556 µmol) dissolved in 15 mL ACN/DMSO(65/35). Nonimprinted particles were produced identically but leaving out Ac-$A\beta_{37-42}$-TBA. The prepolymerization mixture was purged of oxygen by either bubbling with N_2 for 15 min or by three successive freeze-pump-thaw cycles where after the initiator ABDV (5.4 mg, 21.7 µmol) was added. This corresponds to a molar ratio of RAFT/initiator of 3. Polymerization was initiated at 50 °C and allowed to proceed for 40 h. Template removal was then carried out by incubating the particles two times with MeOH (15 mL), two times with MeOH/HCl (0.1M)(90/10, v/v) (15 mL) leaving the suspension to incubate 2 h followed by centrifugation at 5000 rpm. The final step washing was carried out with pure methanol (15 ml) for 1 h. Thereafter the particles were dried under vacuum at 40 ºC resulting in 850 mg (76%) of SiNP-MIP-1, 820 mg (73%) of SiNP-NIP-1, 650 mg (78%) of SiNP-MIP-2, 640 mg (76%) of SiNP-NIP-2, 520 mg (83%) of SiNP-MIP-3, 500 mg (80%) of SiNP-NIP-3, 490 mg (78%) of SiNP-MIP-4 and 480 mg (76%) of SiNP-NIP-4. All the supernatants were collected and analyzed by reverse phase HPLC for the presence of template. The recovery of first three washing fraction was 11.68 %, 13.83 %, 18.14 % and 15.47 % for SiNP-MIP-1, SiNP-MIP-2, SiNP-MIP-3 and SiNP-MIP-4, respectively and the washing continued until the template could not be detected in the

washing solution by RP-HPLC. The low recovery percentage can be attributed to the lower detected peak area for template in washing solution (MeOH) than the standard stock solution (GuHCl).

Table 5.3. Polymerization procedure for the beta-amyloid imprinted polymers.

Polymer name	Si-RAFT (mg)	Urea (mg)	EAMA (mg)	DVB (μL)	RAFT (μmol)	ABDV (μmol)	ACN/ DMSO (mL)	Time (h)
SiNP-MIP-1[a]	700	1.91	84.2	362	65.1	21.7	15	40
SiNP-NIP-1[a]	700	1.91	84.2	362	65.1	21.7	15	40
SiNP-MIP-2[b]	400	1.98	87.4	376	33.2	11	15	40
SiNP-NIP-2[b]	400	1.98	87.4	376	33.2	11	15	40
SiNP-MIP-3[b]	300	1.49	65.5	282	33.8	8.45	7	40
SiNP-NIP-3[b]	300	1.49	65.5	282	33.8	8.45	7	40
SiNP-MIP-4[c]	300	1.49	65.5	282	25.2	6.3	7	40
SiNP-NIP-4[c]	300	1.49	65.5	282	25.2	6.3	7	40

a) Silica core size is 200 nm and the particles were modified by dithiobenzoate RAFT agent.

b) Silica core size is 20 nm and the particles were modified by dithiobenzoate RAFT agent.

c) Silica core size is 20 nm and the particles were modified by trithiocarbonate RAFT agent.

* Ac-$A\beta_{37\text{-}42}$-TBA used as a template with the equivalent of urea monomer.

** The solvent mixture ratio of ACN/DMSO is 65/35(v/v).

5.4.4 Batch rebinding

Standard stock solution of $A\beta_{33-42}$ was prepared in GuHCl(4M)/DMSO(80/20). First, $A\beta_{33-42}$ was dissolved in DMSO and then diluted by GuHCl (4 M). Dry template free polymer (90 mg) was dispersed in 1.6 mL ACN and 0.2 mL isopropanol with sonication. The resulting polymers were hydrophobic and using organic solvent was necessary to mix them with GuHCl buffer. Then, 200 µL (10 mg) of dispersed polymer was added into separate Eppendorf tubes by addition of solutions (1.0 mL) of different concentration of $A\beta_{33-42}$ (0.005 mM to 0.2 mM) in GuHCl(4 M) (the test was downscaled for samples available in limited quantities). This sample preparation was separately done for MIPNPs and NIPNPs. The vials were sealed and their contents allowed to equilibrate overnight at room temperature with gentle shaking. After 22 h incubation at room temperature the supernatants were sampled (300 µL) and transferred to HPLC vials for measurement of unbound solute concentration by reversed phase HPLC. The HPLC system consisted of an Agilent HPLC 1200 series instrument (Agilent) equipped with a UV-DAD detector and an autosampler. The column was a reversed phase (C18) column (Phenomenex Luna C-18, 150 × 4.6 mm), the mobile phase: water/MeOH(80/20)(0.1% TFA)(70%) and water/MeOH(20/80) (0.1% TFA) (30%), (gradient elution) flow rate : 1.0 mL/min, the injection volume was 100 µL and the detection performed by UV absorbance at 205 nm. The resulting peak areas were used to calculate the amount of bound analyte on the polymer (in µmol/g of polymer). The binding results are averages of two independent experiments.

Chapter 6: Nano-Sized Core-Shell Particles by Grafting of Thin Films Imprinted with a Hydrophilic Peptide from Nonporous Silica Cores

6.1 Introduction

In this work we have combined the nano-sized surface imprinting with epitope approach in aqueous media in order to recognize a hydrophilic decapeptide epitope template (T10) corresponding to the solvent exposed C-terminus of the human immunoglobulin G (IgG) heavy chain. Epitope imprinted core-shell nanoparticles (NPs) were prepared by grafting of poly-(methacrylicacid-co-methacrylamide-co-ethylbisacrylamide) and/or poly-(bisphosphonic acid-co-methacrylamide-co-ethylbisacrylamide) in presence of a decapeptide template from a RAFT modified 20 nm sized silica core. After the removal of the template by intensive wash, the resultant MIPs were characterised by FTIR, TEM, TGA and elemental analysis. The polymers were examined by equilibrium rebinding for their affinity towards the template T10 in aqueous media by reversed phase HPLC.

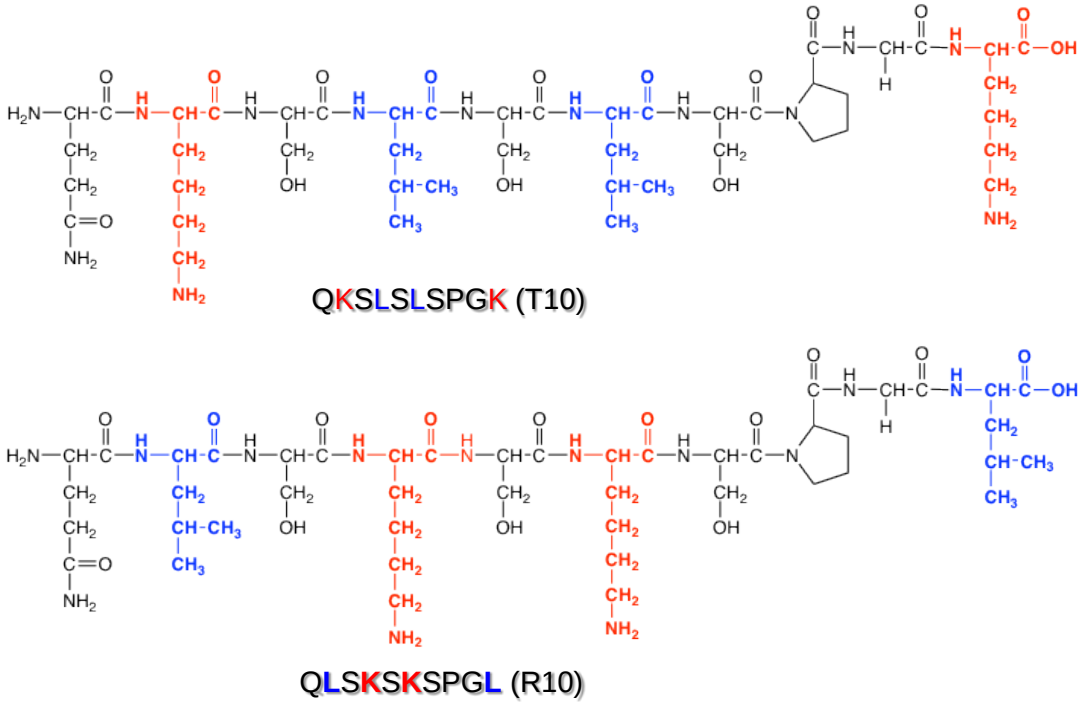

Figure 6.1. Structure of the selected C-terminal epitope decapeptide (T10) and its reference decapeptide (R10).

6.1.1 Selection of the functional and crosslinking monomers

From the aspect of molecular recognition in molecular imprinting, there are many parameters which can influence the properties of produced polymers. In supermolecular chemistry strong and selective recognition could be obtained by applying the concept of multivalency[277]. Considering the complexity of a protein/peptide, it is quite important to find the optimum monomer composition which can interact effectively with the functionalities on the protein surface, since the strength of the interactions will affect the affinity and thus the capacity, selectivity and sensitivity [278]. Furthermore, due to the solubility properties and sensitive structural nature of proteins and peptides, imprinting can generally be performed in aqueous environment, which limits the choice of monomers.

Methacrylic acid (MAA) is a common functional monomer in peptide imprinting which has already successfully been used for imprinting peptides in our group [275]. The carboxylic group in methacrylic acid capable to provide a hydrogen bond and proton donor as well as a hydrogen bond acceptor [1]. In addition it has been demonstrated that MAA has a strong tendency to form hydrogen-bonded dimers. The ability of MAA to form dimers might be one reason to its extraordinary success and versatility as an MIP functional monomer[279].

With considering the type of amino acids on the template, we examined anionic bisphosphonic monomer as another functional monomer which is specific for different amino acid residues on the template with different binding mechanisms and binding strength. This functional monomer can bind to lysines and arginines, and has been successfully developed into an effective lysozyme binder in aqueous buffer[280]. Methacrylamide (MAAM) was selected as a backbone monomer. MAAM is highly water soluble and has widely been used in peptide imprinted polymer [13]. Moreover, NH_2-group of methacrylamide can form strong hydrogen bonds with peptides in polar solvents. N,N′-ethylenebisacrylamide (EBA) was used as a hydrophilic cross-linker to create T10 epitope imprinted polymer in aqueous media. Structure of functional monomers and cross-linker are shown in Figure 6.2.

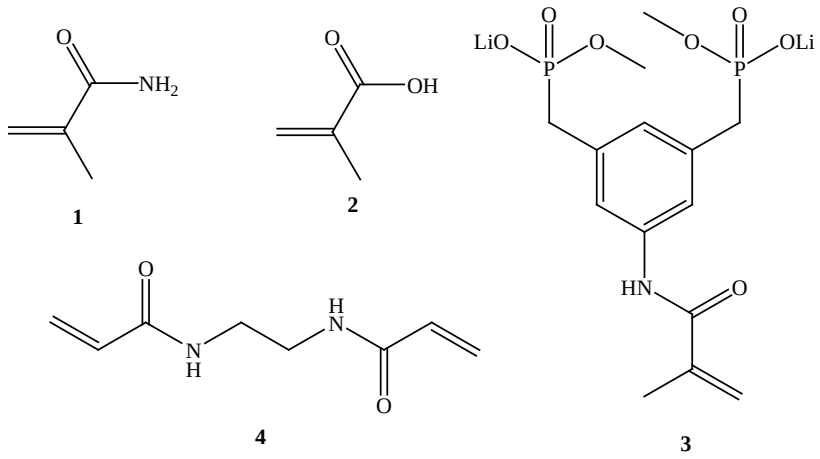

Figure 6.2. Functional monomers and cross-linker used to create decapeptide MIPs, (1): Methacrylamide (MAAM), (2): Methacrylic acid (MAA), (3): 5-(methacryloylamido)-m-xylylene bisphosphonic acid dimethylester dilithium salt, (4): N,N′-ethylenebisacrylamide (EBA).

6.2 Results and Discussions

6.2.1 Grafting of T10 and R10 imprinted polymers from dithiobenzoate-modified silica nanoparticles

The epitope imprinted polymers were prepared from dithioester modified silica nanoparticles as the solid support, T10 and R10 as the template, methacrylic acid (MAA) as a functional monomer, methacrylamide (MAAM) as a comonomer, N,N′-ethylenebisacrylamide (EBA) as a cross-linker, THF as porogen and ABDV as an initiator. The polymerization was carried out at 50 ^{o}C for 16 h. The ratio among template, functional monomer, comonomer and crosslinker was 2: 10: 100: 100, respectively. In preparing the grafting polymer, a molar ratio CPDB/ABDV = 1 was used. The quantity of monomer relative to the silica supports were adjusted to result in shells/films with approximately 3 nm thick shells. After polymerization the beads were isolated by centrifugation and subjected to repetitive washing-centrifugation cycles in order to remove any leachables (e.g. template, oligomers, unreacted monomers). After drying at 40 ^{o}C under vacuum, the light pink MIP particles were obtained. The NIP particles with surface-immobilized dithioester groups were then prepared and purified under the identical conditions except that the template was omitted. The procedure is shown in Table 6.1.

Table 6.1. Procedure for the preparation of T10 and R10 imprinted core-shell nanoparticles.

Polymer name[a]	Template	SiNP-CPDB (mg)	MAA (µmol)	MAAM (µmol)	EBA (µmol)	THF (mL)	Buffer (mL)	CPDB/ ABDV
SiNP-MIP-A	T10	180	49.83	498.23	498.25	20	1	1
SiNP-NIP-A	-	180	49.83	498.23	498.25	20	1	1
SiNP-MIP-B	R10	180	49.83	498.23	498.25	20	1	1
SiNP-NIP-B	-	180	49.83	498.23	498.25	20	1	1

a) See experimental section for details.

* Silica core size is 20 nm and the particles were modified by dithiobenzoate RAFT agent.

6.2.2 Polymer characterization

After polymerization, the beads were subsequently characterised by TGA, TEM, and elemental analysis. The TGA curves of grafted polymers are shown in Figure 6.3. By using the TGA results the gravimetric conversion and shell thickness (nm) of grafted polymers on silica cores were calculated. The TGA weight loss of ca. 38%, 37%, 35% and 36% for the SiNP-MIP-A, SiNP-NIP-A, SiNP-MIP-B and SiNP-NIP-B in the interval 100-800 °C indicates a shell thickness of ca 2.45 nm, 2.54 nm, 2.70 nm and 2.63 nm assuming that the monomers are quantitatively incorporated into the shell.

Elemental analysis was used to confirm the successful grafting of polymers on silica cores. From elemental microanalysis data, more precisely from the change in carbon and nitrogen contents in each step, we could estimate the amount of grafted polymer on the silica surface. The data are presented in Table 6.2. On the basis of the increase in carbon content the apparent shell thickness was calculated. The obtained shell thickness was 3.73 nm and 3.93 nm for SiNP-MIP-A, SiNP-NIP-A and 3.66 nm and 3.59 nm for SiNP-MIP-B, SiNP-NIP-B. In Table 6.2 the apparent thickness, calculated from the TGA mass loss data and elemental analysis, have been compared with the nominal thickness, estimated assuming the grafted shell to consist of monomers forming a liquid film covering the core surface.

The TEM images of the resulting core-shell nanoparticles are shown in Figure 6.4 which agglomerated after solvent evaporation. Comparison of TEM images of grafted polymer silica nanoparticles with images of bare silica particles and RAFT modified silica support confirmed a successful grafting of the polymer shell on the silica particles.

Table 6.2. Results from the characterisation of R10 and T10 imprinted and nonimprinted core-shell beads.

Polymer name [a]	%C	%N	%S	Mass loss [b] (%)	Conv.[c] (%)	d_{nom}[d] (nm)	d_{EA}[e] (nm)	d_{TGA}[f] (nm)
SiNP-MIP-A	25.88	5.83	0.37	38	90	3.14	3.73	2.70
SiNP-NIP-A	26.73	5.76	0.34	37	88	3.14	3.93	2.63
SiNP-MIP-B	24.79	5.38	0.38	35	83	3.14	3.66	2.45
SiNP-NIP-B	24.51	5.47	0.36	36	85	3.14	3.59	2.54

a) See experimental section for details.

b) Mass loss by thermal gravimetric analysis (TGA).

c) Gravimetric conversion: Conversion=mass loss (TGA)/mass of monomer feed.

d) The shell thickness (nm) was calculated according to Eq. 2-3.

e) The shell thickness (nm) was calculated according to Eq. 2-3, Eq. 2-16 and Eq. 2-17

f) The shell thickness (nm) was calculated according to Eq. 2-3 and Eq. 2-9.

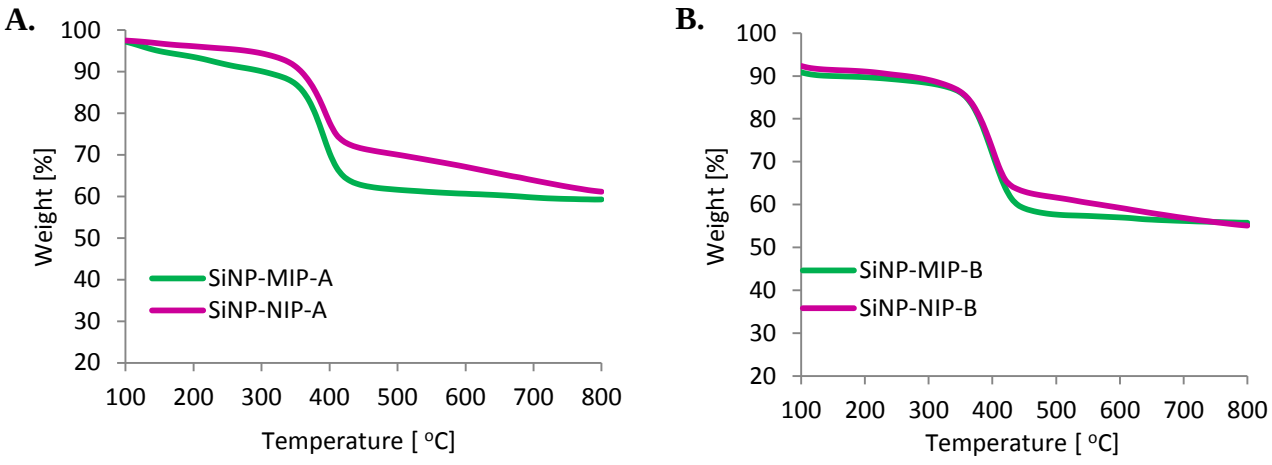

Figure 6.3. Thermal gravimetric analysis of the T10 and R10 imprinted and nonimprinted core-shell nanoparticles; TGA of SiNP-MIP-A and SiNP-NIP-A (A), TGA of SiNP-MIP-B and SiNP-NIP-B (B).

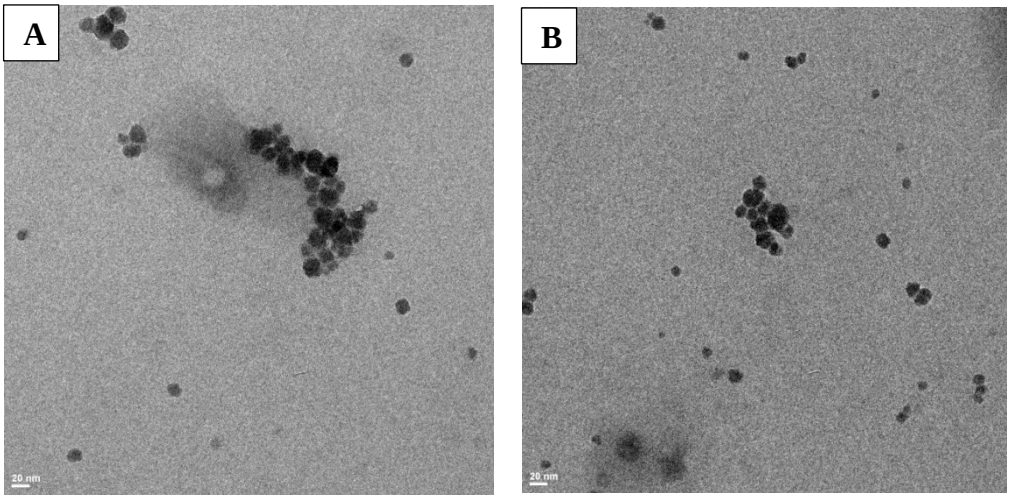

Figure 6.4. TEM images of the T10 and R10 imprinted and nonimprinted core-shell nanoparticles SiNP-MIP-A and SiNP-NIP-A (A), SiNP-MIP-B and SiNP-NIP-B (B). The scale bar is 20 nm.

6.2.3 The reductive aminolysis of grafting polymers

In order to analyze the functional properties of the NPs, the dithioester of the terminal RAFT groups were first converted to thiols by using aminolysis reaction. This conversion was carried out using butylamine as aminolysis reagent in THF for 3 h under N_2 protection (Figure 6.5). To avoid the oxidative coupling of the thiol end groups, a small amount of antioxidant in the form of aqueous sodium ($Na_2S_2O_4$) was added [281]. By addition of aqueous sodium bisulfite the formation of disulfides which result from oxidative coupling of thiols could be effectively suppressed.Successful aminolysis was confirmed by disappearance of the pink color and the UV absorption band at 302 nm characteristic for the dithioester RAFT group (Figure 6.6).

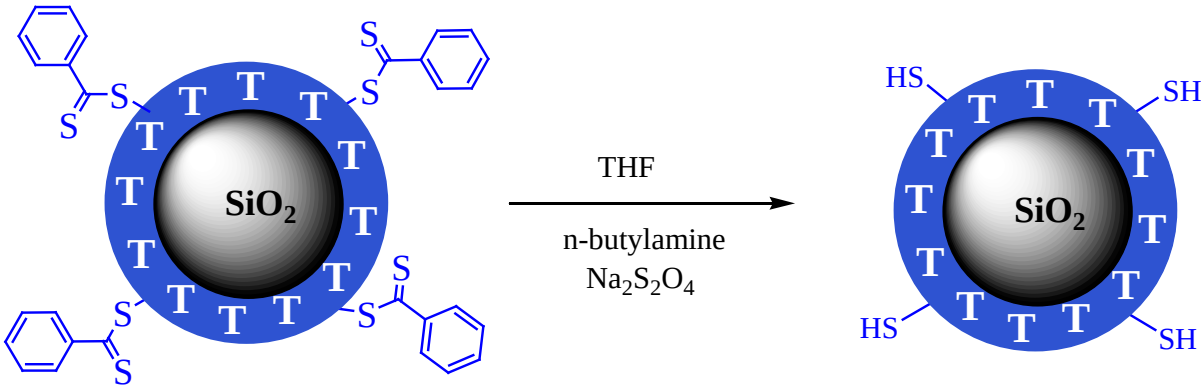

Figure 6.5. Aminolysis of grafting polymers.

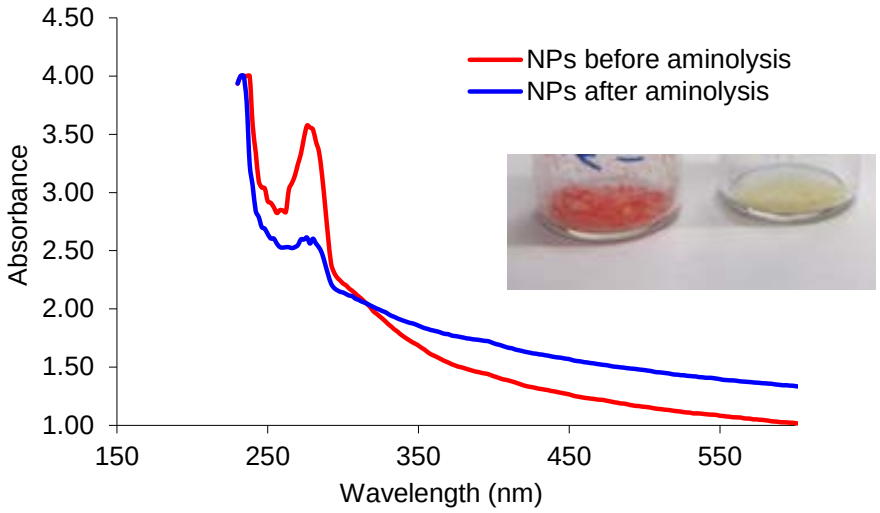

Figure 6.6. UV spectra of RAFT modified particles prior to (red trace) and after (blue trace) aminolysis. The inset shows the particle appearance prior to (left vial) and after (right vial) aminolysis.

6.2.4 Binding study via BCA assay

Assays based on bicinchoninic acid (BCA) are widely used in the quantification of proteins. Thereby, proteins or peptides reduce Cu^{2+} ions (green) to Cu^{1+} (biuret reaction), which form an intense purple complex with BCA [282]. The complex has an absorption maximum at 562 nm. In the binding experiments, imprinted or non-imprinted polymers (10 mg) were mixed with 1 mL of phosphate buffer (50mM, pH 7.4) containing T10 template and/or IgG concentrations range from 0.075 to 1.2 mg mL^{-1}. The mixtures were incubated for 24 h at 19 ^{o}C by gentle shaking. Afterwards the mixtures were centrifuged and the concentration was determined by BCA assay. Both aminolysed and non-aminolysed particles were characterized by this method. The results demonstrated that BCA assay was not good method for binding study of colloidal imprinted and non-imprinted nanoparticles due to the interaction of dithioester and thiol groups with BCA regent. After incubation of particles with template and protein, the particles were separated from supernatant to determine the free concentration of the template or protein. As can be seen in Figure 6.7 despite the ultra-centrifugation some colloidal particles were remained in supernatant which made an error at binding study.

A.

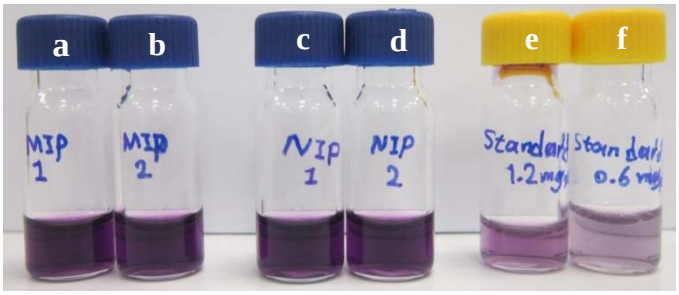

B.

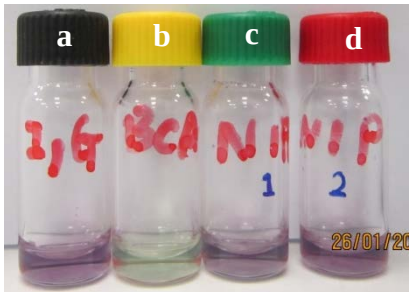

Figure 6.7. Photograph of BCA protein and peptide assay. Solution of supernatant of imprinted and non-imprinted polymers with BCA reagent(a-d), solution of T10 with BCA reagent(e,f) (A); solution of BCA reagent and IgG(a), BCA reagent(b), solution of non-aminolysed and aminolysed particles with BCA reagent(c,d) (B).

6.2.5 Grafting of T10 imprinted polymer onto silica nanoparticles via RAFT polymerization in organic media

The epitope imprinted core-shell nanoparticles in organic media were prepared by using methacrylic acid (MAA), methacrylamide (MAAM), N,N′-ethylenebisacrylamide (EBA), decapeptide (T10), THF, acetic buffer solution (pH5, 10 mM), ABDV as the functional monomer, comonomer, crosslinker, template, porogen, co-porogen and initiator respectively. Due to insolubility of template (T10) and poor solubility of ethylenebisacrylamide (EBA) in THF, the acetic buffer solution (pH5, 10 mM) was added to prepolymerization mixture to solubilize T10 and EBA in organic media. The polymerization was carried out at 50 ^{o}C for 15 h. The ratio among template, functional monomer, comonomer and crosslinker was 2: 10: 100: 100, respectively. In preparing the grafting polymer, a molar ratio TTC/ABDV = 3 was used. The relatively low ABDV/TTC ratio helped to reduce the amount of free polymer derived from the initiator, and yet maintain a moderate polymerization rate [163]. The quantity of monomer relative to the silica supports were adjusted to result in shells/films with

approximately 4 nm thick shells. After polymerization the beads were isolated by centrifugation and subjected to repetitive washing-centrifugation cycles in order to remove any leachables (e.g. template, oligomers, unreacted monomers). Five cycles were sufficient for exhaustive template removal as concluded by HPLC analysis of the washing fractions. The recovery of first three washing fractions was 76.45% and the washing continued until the template could not be detected in the washing solution by RP-HPLC. After drying at 40 ^{o}C under vacuum, the light yellow MIP particles were obtained. The light yellow NIP particles with surface-immobilized trithiocarbonate groups were then prepared and purified under the identical conditions except that the template was omitted. The procedure is shown in Table 6.3.

Table 6.3. Procedure for the preparation of core-shell T10 imprinted nanoparticles in organic media.

Polymer name[a]	T10 (µmol)	SiNP-TTC (mg)	MAA (µmol)	MAAM (µmol)	EBA (µmol)	THF (mL)	Buffer (mL)	TTC/ ABDV
SiNP-MIP1	26.00	300	124.52	1245.20	1245.20	10	1	3/1
SiNP-NIP1	-	300	124.52	1245.20	1245.20	10	1	3/1

a) See experimental section for details.

* Silica core size is 20 nm and the particles were modified by trithiocarbonate RAFT agent.

6.2.6 Grafting of T10 imprinted polymer onto silica nanoparticles via aqueous RAFT polymerization

The “grafting from” technique for producing epitope imprinted core- shell nanoparticles in aqueous solution was investigated. To find polymers which could afford high selectivity, functional monomer combinations were applied and two different polymers were grafted on silica support. In first protocol, methacrylic acid (MAA), methacrylamide (MAAM), N,N′-ethylenebisacrylamide (EBA), decapeptide (T10), acetic buffer solution (pH5, 10mM), ammonium persulfate (APS) were used as the functional monomer, comonomer, crosslinker, template, porogen and initiator respectively. In second protocol instead of methacrylic acid (MAA), 5-(methacryloylamido)-m-xylylene bisphosphonic acid dimethylester dilithium (BPA) was applied as functional monomer. The polymerization was carried out at 50 ^{o}C for

23 h. The ratio among template, functional monomer, comonomer and crosslinker for the first and second polymers was 2: 10: 100: 100 and 2: 4: 100: 100, respectively. In preparing the grafting polymer in water, acidic buffers (pH 5) was used to avoid loss of trithiocarbonate end groups via a combination of aminolysis and hydrolysis [250, 255]. If the chemical structure of trithiocarbonate compounds cannot be preserved throughout the reaction, polymerization is either inhibited or carried out without control. The aminolysis reaction can be avoided by working in slight acidic conditions in which almost all of the amines are protonated and so the nucleophilic attack on the trithiocarbonate is prevented.

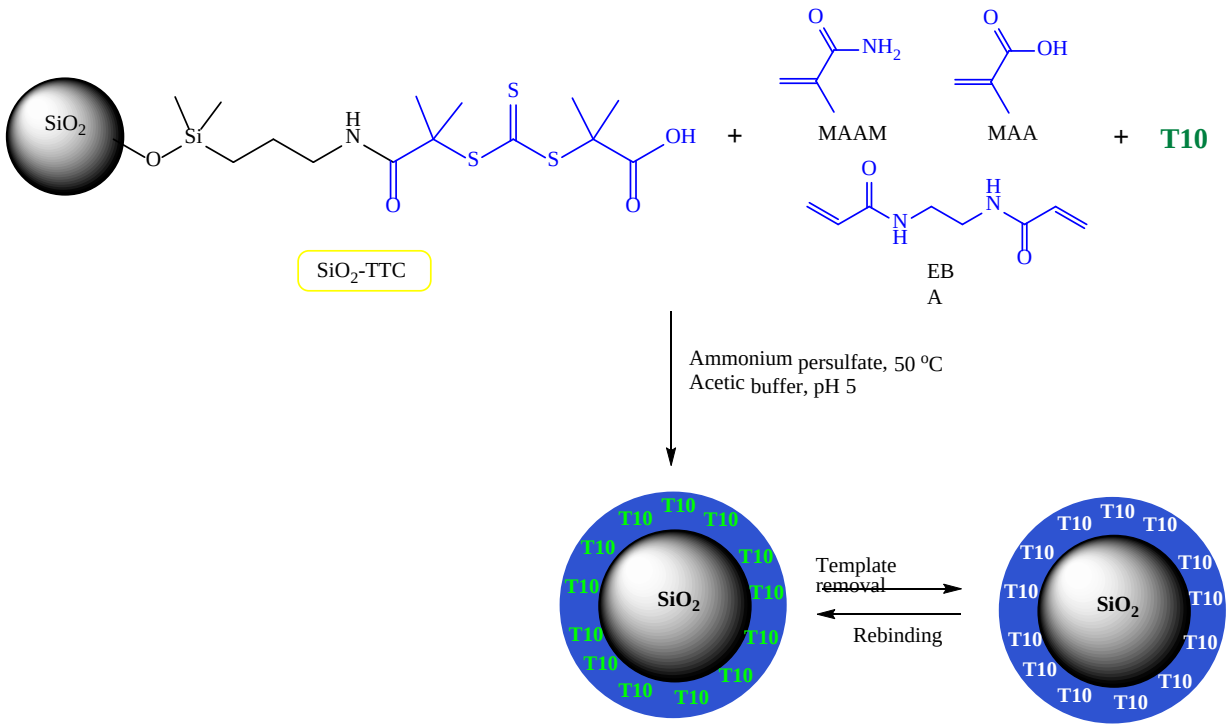

Figure 6.8. Procedure used to synthesis silica core-MIP shell nanoparticles for decapeptide in aqueous media.

In preparing the grafting polymer, a molar ratio TTC/APS = 2 was used. The relatively low APS/TTC ratio helped to reduce the amount of free polymer derived from the initiator, and yet maintain a moderate polymerization rate [163]. The quantity of monomer relative to the silica supports were adjusted to result in shells/films with approximately 4 nm thick shells. After polymerization the beads were isolated by centrifugation and subjected to repetitive washing-centrifugation cycles in order to remove any leachables (e.g. template, oligomers, unreacted monomers). Five cycles were sufficient for exhaustive template removal as concluded by HPLC analysis of the washing fractions. The recovery of first three washing fractions was 54.98 % for SiNP-MIP2 and 49.03 % for SiNP-MIP3 and the washing

continued until the template could not be detected in the washing solution by RP-HPLC. After drying at 40 ^{o}C under vacuum, the light yellow MIP particles were obtained, suggesting the presence of trithiocarbonate groups there. The light yellow NIP particles with surface-immobilized trithiocarbonate groups were then prepared and purified under the identical conditions except that the template was omitted. The procedure is shown in Table 6.4.

Table 6.4. Procedure for the preparation of core-shell T10 imprinted nanoparticles in aqueous media.

Polymer name[a]	T10 (µmol)	SiNP-TTC (mg)	MAA (µmol)	BPA (µmol)	MAAM (µmol)	EBA (µmol)	Buffer (mL)	TTC/ APS
SiNP-MIP2	16.60	200	83.01	-	830.13	830.13	5	2/1
SiNP-NIP2	-	200	83.01	-	830.13	830.13	5	2/1
SiNP-MIP3	16.17	200	-	32.35	808.66	808.66	5	2/1
SiNP-NIP3	-	200	-	32.35	808.66	808.66	5	2/1

a) See experimental section for details.

* Silica core size is 20 nm and the particles were modified by trithiocarbonate RAFT agent.

Table 6.5. Amount of the resultant template from the T10 MIPs in the different wash fractions.

Polymer name	Wash 1 (mg)	Wash 2 (mg)	Wash 3 (mg)	Wash 4 (mg)	Template removal (%)
SiNP-MIP1	19.05	0.38	0.518	-	76.45
SiNP-MIP2	7.84	1.27	-	-	54.98
SiNP-MIP3	7.51	0.62	-	-	49.03

* Washing solution is NaCl (0.5M) at stage 1, 2 and MeOH (0.1% TFA) at stage 3 and 4.

** The template was detected in the washing solution by RP-HPLC.

6.2.7 Polymer characterization

After polymerization, the beads were subsequently characterised by TGA, TEM, FTIR and elemental analysis. Figure 6.9 displays the TGA and DTG curves of grafted polymers. It can be observed from TGA curves that the weight loss of SiNP-MIP1, SiNP-NIP1, SiNP-MIP2, SiNP-NIP2, SiNP-MIP3 and SiNP-NIP3 between 100 ^{o}C and 800 ^{o}C is 44%, 41%, 36%, 34%, 39%, 38%, respectively. By using the TGA results the gravimetric conversion and shell thickness (nm) of grafted polymers on silica cores were calculated. The apparent shell thickness was 3.34 nm and 3.03 nm for SiNP-MIP1, SiNP-NIP1 and 2.54 nm and 2.36 nm for SiNP-MIP2, SiNP-NIP2 and 2.83 nm and 2.73 nm for SiNP-MIP3, SiNP-NIP3.

Elemental analysis was used to confirm the successful grafting of polymers on silica cores. From elemental microanalysis data, more precisely from the change in carbon and nitrogen contents in each step, we could estimate the amount of grafted polymer on the silica surface. The data are presented in Table 6.6. On the basis of the increase in carbon content the apparent shell thickness was calculated. The obtained shell thickness was 3.89 nm and 3.52 nm for SiNP-MIP1, SiNP-NIP1 and 3.05 nm and 2.96 nm for SiNP-MIP2, SiNP-NIP2 and 3.37 nm and 3.27 nm for SiNP-MIP3, SiNP-NIP3.

In Table 6.6 the apparent thickness, calculated from the TGA mass loss data and elemental analysis, have been compared with the nominal thickness, estimated assuming the grafted shell to consist of monomers forming a liquid film covering the core surface. The somewhat lower measured thickness compared to the nominal values agrees with our previous report [239] and can be attributed to solution chain growth, nevertheless resulting in an acceptable conversion of monomer to shell polymer.

Table 6.6. Results from the characterisation of T10 imprinted and nonimprinted core-shell beads.

Polymer name [a]	%C	%N	%S	Mass loss [b] (%)	Conv.[c] (%)	d_{nom}[d] (nm)	d_{EA}[e] (nm)	d_{TGA}[f] (nm)
SiNP-MIP1	25.83	4.39	0.81	44	85	4.31	3.89	3.34
SiNP-NIP1	24.17	4.17	0.79	41	79	4.31	3.52	3.03
SiNP-MIP2	21.87	3.25	0.73	36	70	4.31	3.05	2.54
SiNP-NIP2	21.36	3.41	0.70	34	66	4.31	2.96	2.36
SiNP-MIP3	23.45	4.12	0.65	39	75	4.31	3.37	2.83
SiNP-NIP3	22.96	4.07	0.61	38	73	4.31	3.27	2.73

a) See experimental section for details.

b) Mass loss by thermal gravimetric analysis (TGA).

c) Gravimetric conversion: Conversion=mass loss (TGA)/mass of monomer feed.

d) The shell thickness (nm) was calculated according to Eq. 2-3.

e) The shell thickness (nm) was calculated according to Eq. 2-3, Eq. 2-16 and Eq. 2-17

f) The shell thickness (nm) was calculated according to Eq. 2-3 and Eq. 2-9.

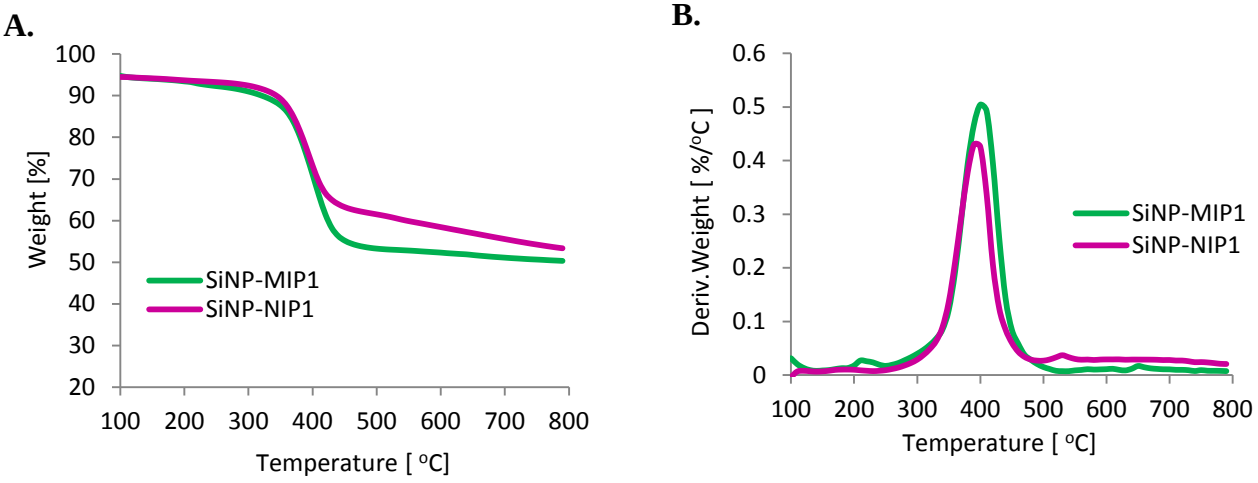

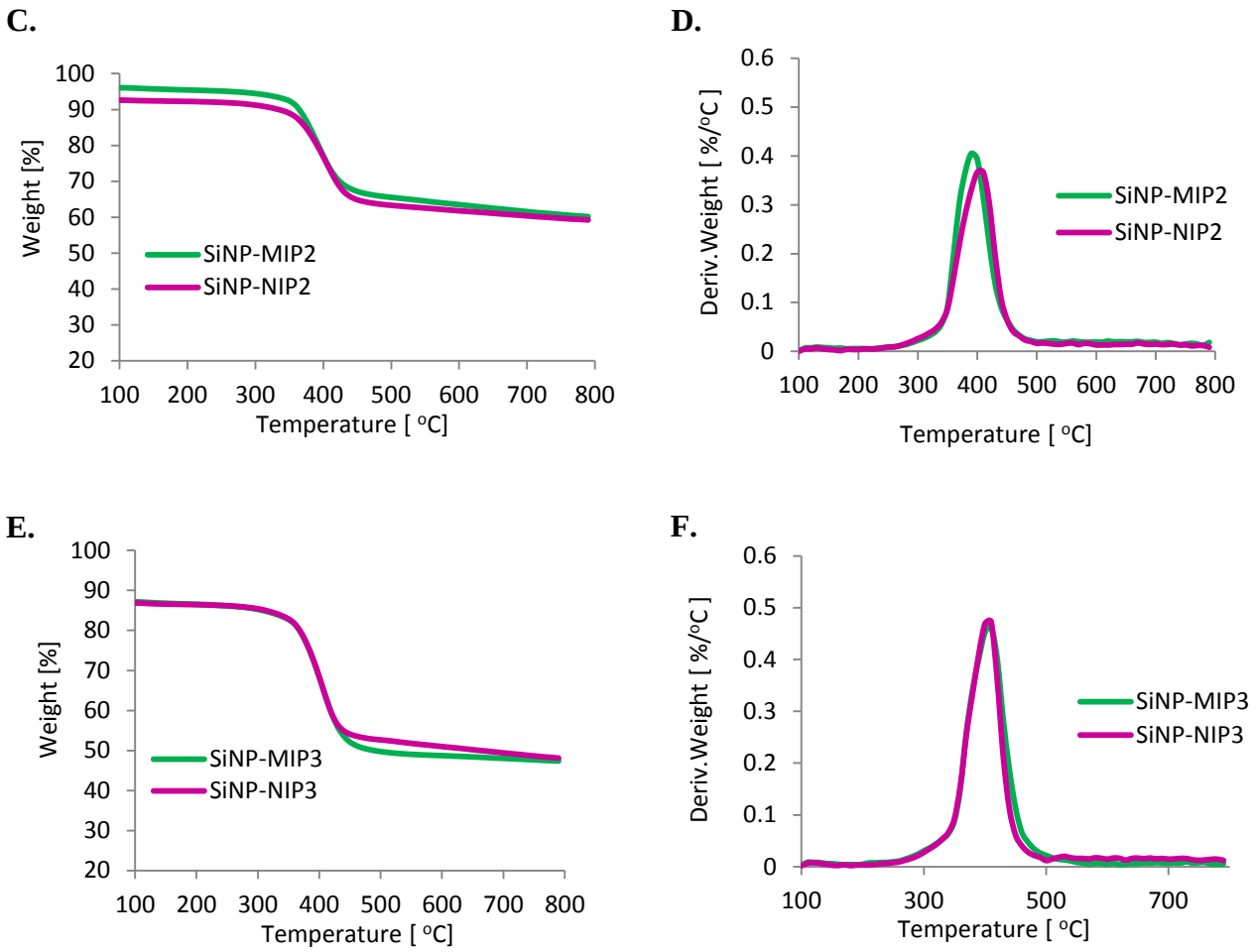

Figure 6.9. Thermal gravimetric analysis of the T10 imprinted and nonimprinted core-shell nanoparticles; TGA of SiNP-MIP1 and SiNP-NIP1 (A), DTG of SiNP-MIP1 and SiNP-NIP1(B), TGA of SiNP-MIP2 and SiNP-NIP2 (C), DTG of SiNP-MIP2 and SiNP-NIP2 (D), TGA of SiNP-MIP3 and SiNP-NIP3 (E), DTG of SiNP-MIP3 and SiNP-NIP3 (F).

TEM was used to characterize the morphology of the polymer grafted silica nanoparticles. Thin layers of polymer grafted silica nanoparticles were prepared by casting a drop of dilute suspension of grafted nanoparticles in isopropanol onto a copper grid and evaporating the solvent. The TEM images of the T10 imprinted and nonimprinted core-shell nanoparticles are shown in Figure 6.10 which agglomerated after solvent evaporation. An inorganic silica core appears darker than the grafted organic polymer shell due to the difference in density. Comparison of TEM images of grafted polymer silica nanoparticles with images of bare silica particles and RAFT modified silica support confirmed a successful grafting of the polymer shell on the silica particles. The average particle size as estimated by TEM

measurements of these grafted silica core-shell particles was found to be in the range of 20-25 nm with a shell thickness of 3-4 nm for the resultant nanoparticles.

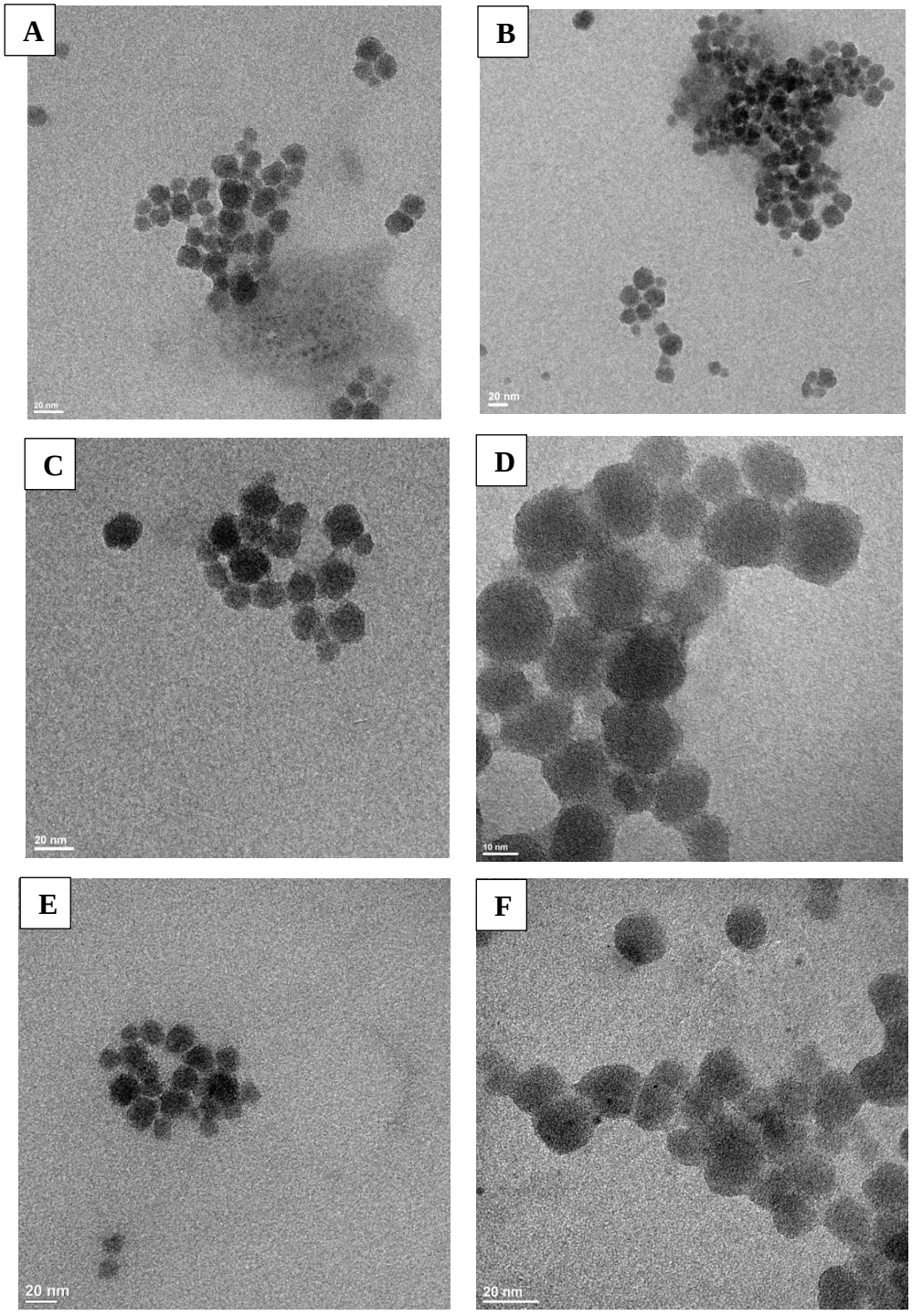

Figure 6.10. TEM images of the T10 imprinted and nonimprinted core-shell nanoparticles SiNP-MIP1 (A), SiNP-NIP1 (B), SiNP-MIP2 (C), SiNP-NIP2 (D), SiNP-MIP3 (E) and SiNP-NIP3 (F). The scale bar is 20 nm in the case of (A), (B), (C), (E), (F) and 10 nm for (D).

The FTIR spectra of the core-shell beads shown in Figure 6.11 display two characteristic bands i.e. the carbonyl stretching of the polymer matrix at ca 1740 cm^{-1} and the siloxane vibration of silica core at ca 1120 cm^{-1}.

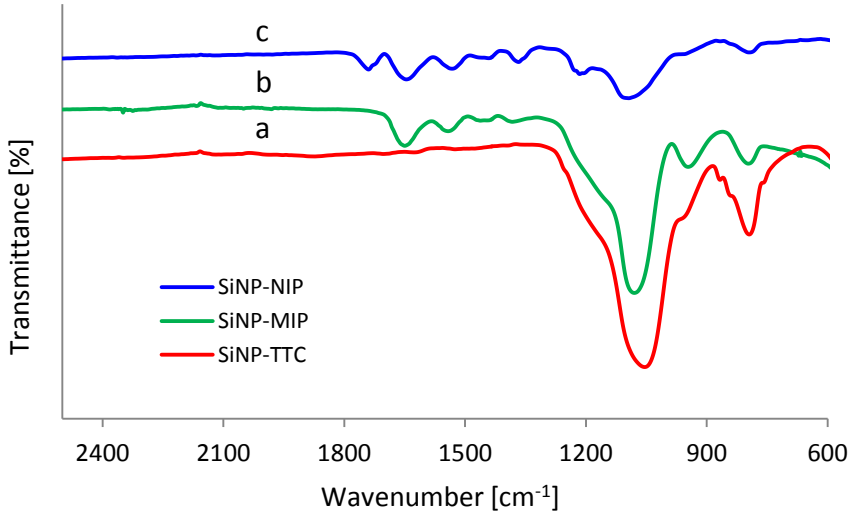

Figure 6.11. FTIR spectra of SiNP-TTC (a), SiNP-MIP (b), SiNP-NIP (c).

6.2.8 Binding isotherms

The adsorption capacity is an important factor in the evaluation of the selective recognition and the special binding of the molecular imprinting technique. The adsorption isotherm of imprinted and nonimprinted polymers was plotted by the batch rebinding experiments which were conducted in HEPES buffer (pH7.0, 10 mM) using a range of T10 concentrations from 0.075 to 1.2 mg mL^{-1}. For non-covalent imprinting, molecular recognition is attributed not only to the binding sites that complement molecules in shape and size, but also to the binding media including pH, ionic strength and type of solvent and so on. Based on it, HEPES buffer with 10 mM concentration at pH7.0 was selected for the evaluation of T10 adsorption amount. After incubating the particles with solutions of T10 of known concentrations the free concentrations of the solutes were determined by reversed phase HPLC.

As shown in Figure 6.12, the amount of template peptide bound to the MIPNPs at equilibrium, increased with increasing initial concentration of the template. The core-shell particles display a distinct saturation behavior with a clear preference for the decapeptide template. The maximum adsorption capacities of SiNP-MIP1, SiNP-NIP1 which prepared in

organic media were 60.98 mg g^{-1} and 61.80 mg g^{-1} at 1.2 mg mL^{-1}. The maximum adsorption capacities for polymers prepared in aqueous media i.e. SiNP-MIP2, SiNP-NIP2, SiNP-MIP3 and SiNP-MIP3 at 1.2 mg mL^{-1} were 23.88 mg g^{-1}, 16.69 mg g^{-1}, 26.28 mg g^{-1} and 23.15 mg g^{-1}, respectively. As can be seen obviously from binding isotherms, the resulting polymers which prepared in organic media (SiNP-MIP1 and SiNP-NIP1) revealed same adsorption capacity at the both imprinted and nonimprinted polymers. This behavior can be attributed to creating of nonspecific binding sites in organic media. In contrast, for both polymers prepared in aqueous media the imprinted particles displayed more adsorption capacity than the nonimprinted particles in all range of template concentrations.

The binding isotherms were subsequently fitted to mono-Langmuir (Eq. 2-19), bi-Langmuir (Eq. 2-20), and Freundlich (Eq. 2-21) isotherm models. The resulting parameters are given in Table 6.7 to Table 6.9. For each model and each set of experimental data, the Fisher parameter was calculated according to Eq. 2-26. The fisher values in Figure 6.13 reflect which of the model provides the best fit to a particular isotherm, a higher number indicating a better fit. The affinity constant (*K*) and total number of binding sites (*N*) were calculated according to Eq. 2-22 and Eq. 2-23. According to mono-Langmuir and bi-Langmuir binding parameters, all imprinted polymers showed higher adsorption capacity than corresponding nonimprinted polymers (Table 6.7 and Table 6.8). The difference of adsorption capacity between imprinted and nonimprinted polymers prepared via MAA as functional monomer was much higher than of MIP and NIP prepared using BPA as functional monomer. Based on Freundlich binding parameters (Table 6.9), the total number of binding sites (*N*) and binding capacity (*a*) of SiNP-MIP2 (*N*= 15.76 (mg/g), *a*= 25.34±1.42 mg/g $(g^{-1})^m$) and SiNP-MIP3 (*N*= 16.98 (mg/g), *a*= 27.90±1.20 mg/g $(g^{-1})^m$), were higher than that for SiNP-NIP2 (*N*= 10.71 (mg/g), *a*= 17.24±0.98 mg/g $(g^{-1})^m$) and SiNP-NIP3 (*N*= 14.85 (mg/g), *a*= 24.16±0.90 mg/g $(g^{-1})^m$).

These results, together with the rather similar physical formats of the MIP and NIP particles clearly reveals the successful generation of selective binding sites in the obtained MIP particles and thus the successful molecular imprinting process. Furthermore, by comparison of two preparation protocols can be seen that the obtained polymer via MAA as functional monomer had better performance than once prepared using BPA as functional monomer. This could be attributed to dimer structure of MAA in polymerization mixture and a stable cyclic hydrogen bonding among MAA and acid or amide groups of template [1, 279].

A.

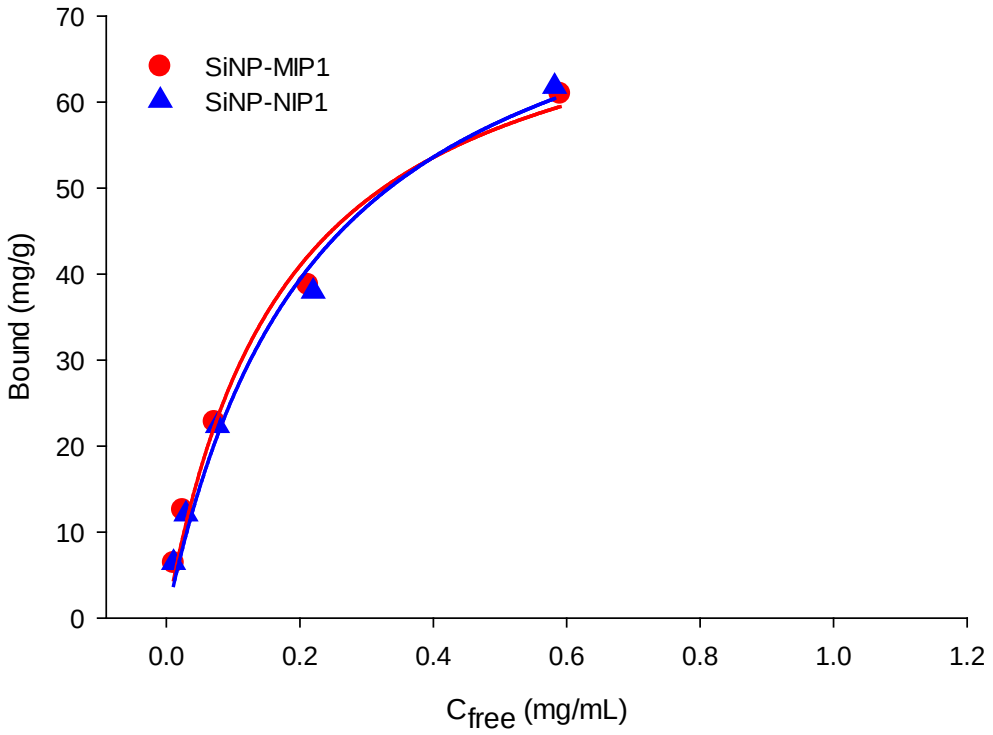
SiNP-MIP1
SiNP-NIP1
Bound (mg/g)
0
10
20
30
40
50
60
70
0.0
0.2
0.4
0.6
0.8
1.0
1.2
C free (mg/mL)

B.

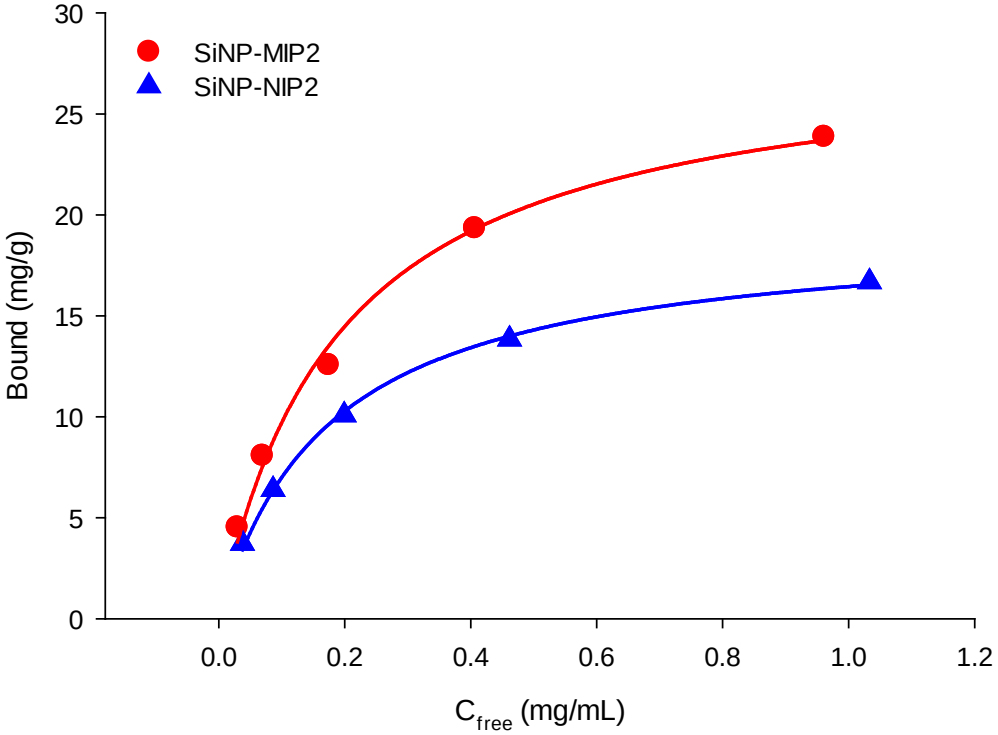
SiNP-MIP2
SiNP-NIP2
Bound (mg/g)
0
5
10
15
20
25
30
0.0
0.2
0.4
0.6
0.8
1.0
1.2
C free (mg/mL)

C.

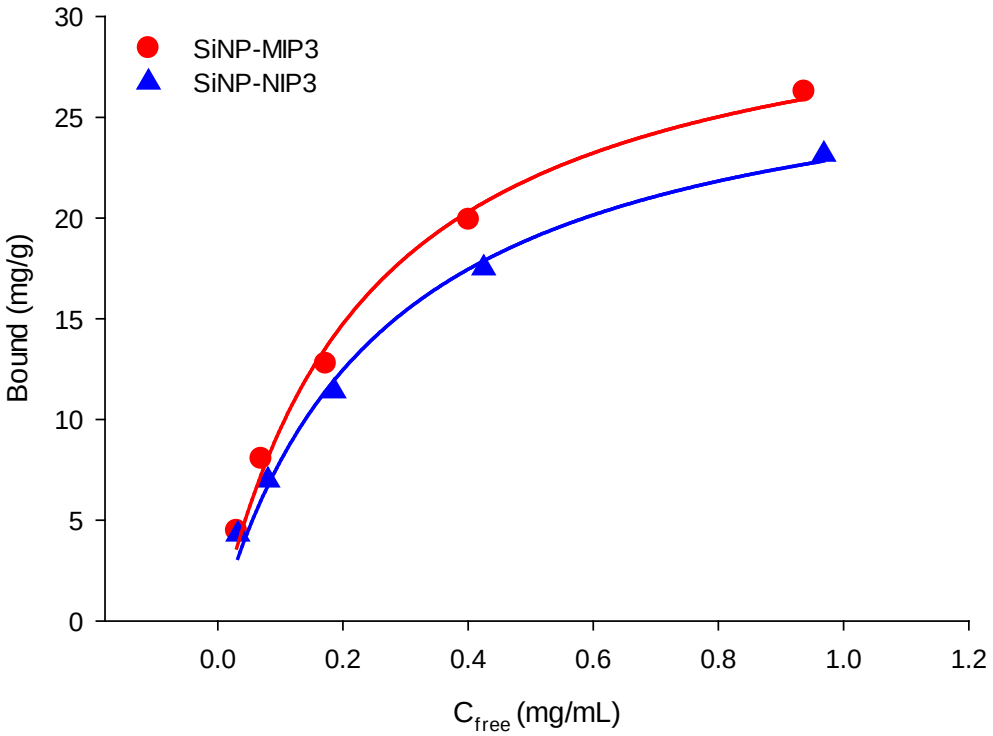

Figure 6.12. Equilibrium binding isotherms of T10 on imprinted (circles) and nonimprinted (triangles) core-shell particles in buffer. A) SiNP-MIP1(red circles) and SiNP-NIP1(blue triangles), B) SiNP-MIP2(red circles) and SiNP-NIP2(blue triangles), C) SiNP-MIP3 (red circles) and SiNP-NIP3 (blue triangles).

Table 6.7. Mono-Langmuir isotherm fitting parameters obtained by nonlinear regression of data shown in Figure 6.12.

Polymer name		k_d (mg/mL)	q_s (mg/g)	r^2	***F***- value
SiNP-MIP2	T10	0.192±0.025	28.44±1.29	0.9931	430
SiNP-NIP2	T10	0.176± 0.010	19.35±0.36	0.9984	1875
SiNP-MIP3	T10	0.24±0.034	32.59± 1.75	0.9927	409
SiNP-NIP3	T10	0.26±0.040	29.14± 1.72	0.9915	350

Table 6.8. Bi-Langmuir isotherm fitting parameters obtained by nonlinear regression of data shown in Figure 6.12.

Polymer name		k_d1 (mg/mL)	q_s1 (mg/g)	k_d2 (mg/mL)	q_s2 (mg/g)	r^2	***F*-value**
SiNP-MIP2	T10	0.010± 0.081	2.63±7.64	0.281±0.187	27.69± 5.60	0.9978	151
SiNP-NIP2	T10	0.022±0.014	1.93±0.85	0.235± 0.016	18.15±0.75	1.000	3284
SiNP-MIP3	T10	0.023± 0.055	4.40±6.13	0.426± 0.221	32.07±3.73	0.9992	420
SiNP-NIP3	T10	2.66×10^{-13}	2.06±0.83	0.405± 0.044	29.97± 0.53	0.9999	3363

Table 6.9. Freundlich isotherms fitting parameters obtained by nonlinear regression of data shown in Figure 6.12.

Polymer name		Affinity constant, $\boldsymbol{K}$ $(mg/mL)^{-1}$	Total number of binding sites , $\boldsymbol{N}$ (mg/g)	Heterogen-eity parameter, $\boldsymbol{m}$	Binding capacity, $\boldsymbol{a}$ (mg/g $(g^{-1})^m$)	Regression coefficient, $\boldsymbol{r^2}$	***F*-value**
SiNP-MIP2	T10	31.09	15.76	0.41± 0.04	25.34± 1.42	0.9731	108
SiNP-NIP2	T10	22.63	10.71	0.38± 0.04	17.24± 0.98	0.9659	85
SiNP-MIP3	T10	35.83	16.98	0.45± 0.04	27.90± 1.20	0.9857	206
SiNP-NIP3	T10	34.10	14.85	0.46± 0.03	24.16± 0.90	0.9884	256

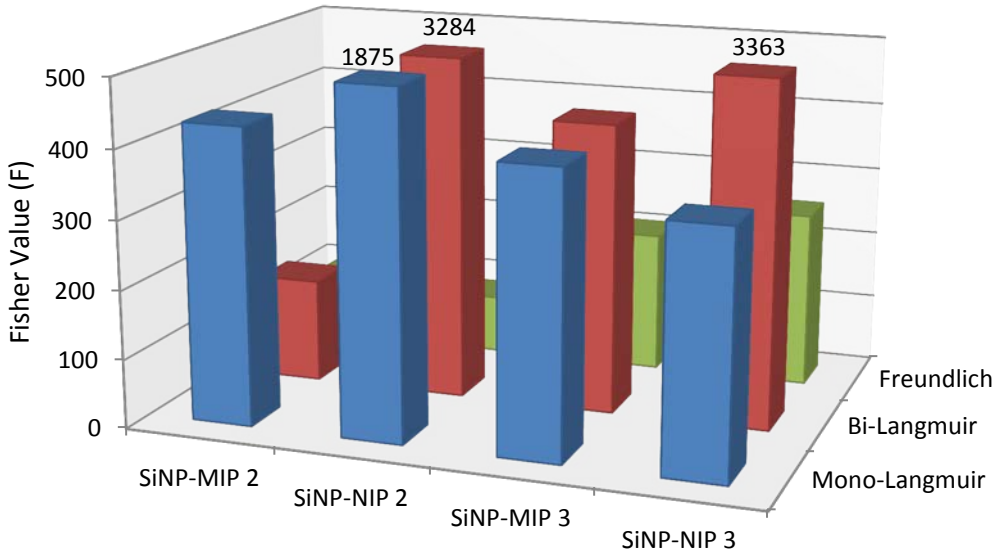

Figure 6.13. Fisher values obtained by fitting the T10 binding curves in Figure 6.12 to mono-Langmuir, bi-Langmuir and Freundlich isotherm models (see Table 6.7 to Table 6.9).

6.3 Conclusions

The epitope imprinted polymer anchored on the surface of silica nanoparticles have been developed with exposed peptide fragments from the C-terminus on the heavy chain of IgG as templates in aqueous and organic media. For polymers prepared in organic media, the resulting imprinted and nonimprinted particles revealed a similar adsorption capacity towards T10 template. When the synthesis was performed in aqueous media, the imprinted particles displayed a higher adsorption capacity than the nonimprinted particles. Compared to polymer grafted using the bisphosphonic acid monomer, polymer obtained via methacrylic acid as functional monomer showed better imprinting performance. In future work, the resultant polymer will be used for the recognition of IgG as target protein.

Our results provide a new potential for peptides and protein imprinting in aqueous media using SI-RAFT technique and it might also be transferred to epitopes of other proteins. We believe that such synthetic MIP nanoparticles are highly promising alternatives to biological receptors with great potential in many analytical applications and other areas.

6.4 Experimental

6.4.1 Aminolysis of the dithioester end groups in the RAFT polymers

In order to analyze the surface assembly of the particles in solution, they were subjected to aminolysis by butylamine to give free thiol groups on the surface [281]. SiNP-MIP-A and SiNP-NIP-B (50 mg, corresponding to ca 4 μmol RAFT groups) were dissolved in THF (1 mL) containing 20 μL of aqueous $Na_2S_2O_4$. The reaction mixture was purged of oxygen by either bubbling with N_2 for 10 min or by three successive freeze-pumpthaw cycles. Butylamine (40 μL, 0.4 mmol) was then added, and the reaction was stirred for 3 h under N_2. Upon the addition of butylamine, an immediate color change from pink to yellow was observed. The resulting product was then washed with THF (2x) and methanol (1x) and was then collected by centrifugation and dried under vacuum at 40 ^oC (42 mg, 84 % mass yield).

6.4.2 BCA protein assay

This assay is based on the reduction of Cu^{2+} to Cu^{+} by protein in an alkaline medium (biuret reaction). For protein quantification, a general procedure is as following: 25 μL of the standard or unknown sample was pipetted in a microplate well and 200 μL of the working reagent (50:1 reagent A:B; A includes sodium bicinchoninate. B includes cupric sulfate) was added to each well. Then the plate was covered and agitated at room temperature for 30 min thereafter the UV absorbance at 562 nm was measured.

6.4.3 Synthesis of 5-(methacryloylamido)-m-xylylene bisphosphonic acid dimethylester dilithium salt

Monomer was prepared in the group of Prof. Dr. Thomas Schrader in Universität Duisburg-Essen; and converted to the dilithium salt form as follows [85]:

5-(Methacryloylamido)-m-xylylene bisphosphonic acid tetramethylester (591mg, 1.46 mmol) was dissolved in 35 mL of absolute acetonitrile under nitrogen. A solution of lithium bromide (283 mg; 3.26 mmol) in 9 mL of acetonitrile was added and the reaction mixture was refluxed for 8 hours under nitrogen. During this period the product precipitates from the

reaction mixture. The solvent was decanted and the white solid was washed three times with acetonitrile. A white solid was obtained after being dried in vacuum (Yield: 576 mg, 96 %).

^{1}H-NMR (D_2O): δ (ppm) = 1.99 (s, 3H, H-7); 3.01 (d, 4H, H-2); 3.51 (d, 6H, H-1); 5.54 (s, 1H, H-6); 5.79 (s, 1H, H-6); 7.00-7.04 (m, 1H, H-3); 7.18-7.21 (m, 2H, H-4).

^{13}C-NMR (D_2O): δ (ppm) = 18.1, 33.7, 52.0-52.2 (m), 121.6-122.0 (m), 128.3-128.6 (m), 135.9-136.2 (m), 136.9-137.1 (m), 140.1, 171.3.

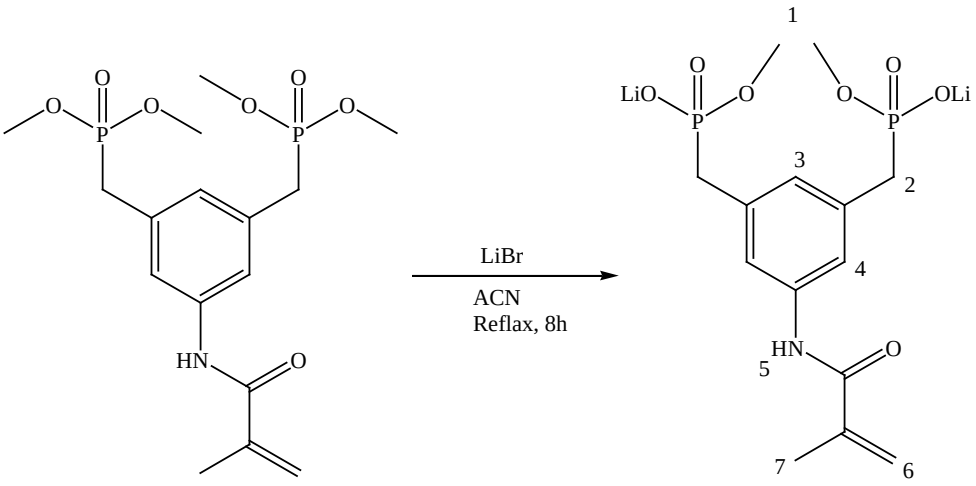

Figure 6.14. Synthesis of 5-(methacryloylamido)-m-xylylene bisphosphonic acid dimethylester dilithium salt.

6.4.4 Synthesis of PEG-TTC macro chain transfer agent

A slightly modified version of the procedure reported by Zhong et al. was followed [283]. In a 50 mL round-bottom flask equipped with a magnetic stir bar, S,S'-Bis(a,a'-dimethyl-a"-acetic acid)-trithiocarbonate (TTC) (0.10 g, 0.37 mmol) was stirred to dissolve in 20 mL of anhydrous dichloromethane (DCM).The mixture of 1-Ethyl-3-(3-dimethylaminopropyl) carbodiimide hydrochloride(EDC)(0.072g, 0.37mmol) in 4 mL DCM and N,N-diisopropylethylamine (EDIPA)(0.048 g, 0.37 mmol) was then added drop-wise, and the reaction was stirred at room temperature for 20 min. Then 0.142 g (0.188 mmol) of methoxypolyethylene glycol amine (PEG-NH_2, 750) was added and allowed to react for 32 h at room temperature. The solution was precipitated in cold diethyl ether. The product was collected by centrifuge, and dried in the vacuum oven overnight at room temperature (yield: 0.138 g, 73%).

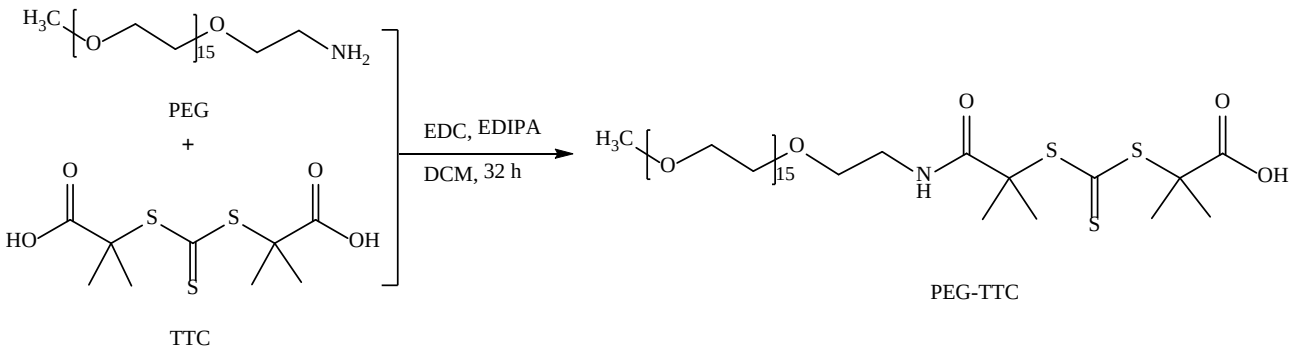

Figure 6.15. Synthesis of PEG-TTC macro chain transfer agent.

6.4.5 Preparation of T10 imprinted core-shell MIPs in organic media

TTC modified core particles (SiNP: 300 mg corresponding to 25.41 μmol RAFT groups) were suspended in a prepolymerization mixture containing T10 (26 mg, 24.90 μmol), MAA (10.56 μL, 124.52 μmol), MAAM (105.97 mg, 1245.20 μmol) and EBA (209.44 mg, 1245.20 μmol) dissolved in 10 mL THF and 1 mL of acetic buffer solutions (pH5, 10mM). Nonimprinted particles were produced identically but leaving out T10 (SiNP-NIP1). The polymerization mixture was subjected to three freeze-thaw cycles under nitrogen where after the initiator ABDV (2.10 mg, 8.47 μmol) was added. This corresponds to a molar ratio of TTC/initiator of 3. Polymerization was initiated at 50 °C and allowed to proceed for 15 h. Template removal was then carried out by incubating the particles two times with NaCl (0.5M, 15 mL), two times with MeOH (0.1% TFA, 15 mL) leaving the suspension to incubate 2 h followed by centrifugation at 5000 rpm. The final step washing was carried out with pure methanol (15 ml) for 30 min. Thereafter the particles were dried under vacuum at 40 ºC resulting in 590 mg (94%) of SiNP-MIP1 and 575 mg (92%) of SiNP-NIP1. All the supernatants were collected and analyzed by reverse phase HPLC for the presence of template.

6.4.6 Preparation of T10 imprinted core-shell MIPs using MAA in aqueous media

TTC modified core particles (SiNP: 200 mg corresponding to 17 μmol RAFT groups) were suspended in a prepolymerization mixture containing T10 (17.34 mg, 16.60 μmol), MAA (7.04 μL, 83.01 μmol), MAAM (70.64 mg, 830.13 μmol) and EBA (139.63 mg, 830.13 μmol) dissolved in 5 mL of acetic buffer solutions (pH5, 10mM). Nonimprinted particles were produced identically but leaving out T10 (SiNP-NIP2). The polymerization mixture was subjected to three freeze-thaw cycles under nitrogen where after the initiator APS (1.90 mg, 8.47 μmol) was added. This corresponds to a molar ratio of TTC/initiator of 2. Polymerization was initiated at 50°C and allowed to proceed for 23 h. Template removal was then carried out by incubating the particles two times with NaCl (0.5 M, 15 mL), two times with MeOH (0.1% TFA, 15 mL) leaving the suspension to incubate 2 h followed by centrifugation at 5000 rpm. The final step washing was carried out with pure methanol (15 ml) for 30 min. Thereafter the particles were dried under vacuum at 40 ºC resulting in 360 mg (86%) of SiNP-MIP2 and 340 mg (81%) of SiNP-NIP2. All the supernatants were collected and analyzed by reverse phase HPLC for the presence of template.

6.4.7 Preparation of T10 imprinted core-shell MIPs using BPA in aqueous media

TTC modified core particles (SiNP: 200 mg corresponding to 17 μmol RAFT groups) were suspended in a prepolymerization mixture containing T10 (16.88 mg, 16.17 μmol), BPA (12.59 mg, 32.35 μmol), MAAM (68.82 mg, 808.66 μmol) and EBA (136.02 mg, 808.66 μmol) dissolved in 5 mL of acetic buffer solutions (pH5, 10mM). Nonimprinted particles were produced identically but leaving out T10 (SiNP-NIP3). The polymerization mixture was subjected to three freeze-thaw cycles under nitrogen where after the initiator APS (1.90 mg, 8.47 μmol) was added. This corresponds to a molar ratio of TTC/initiator of 2. Polymerization was initiated at 50 °C and allowed to proceed for 23 h. Template removal was then carried out by incubating the particles two times with NaCl (0.5M, 15 mL), two times with MeOH (0.1% TFA, 15 mL) leaving the suspension to incubate 2 h followed by centrifugation at 5000 rpm. The final step washing was carried out with pure methanol (15 ml) for 30 min. Thereafter the particles were dried under vacuum at 40 ºC resulting in

350 mg (84%) of SiNP-MIP3 and 335 mg (80%) of SiNP-NIP3. All the supernatants were collected and analyzed by reverse phase HPLC for the presence of template.

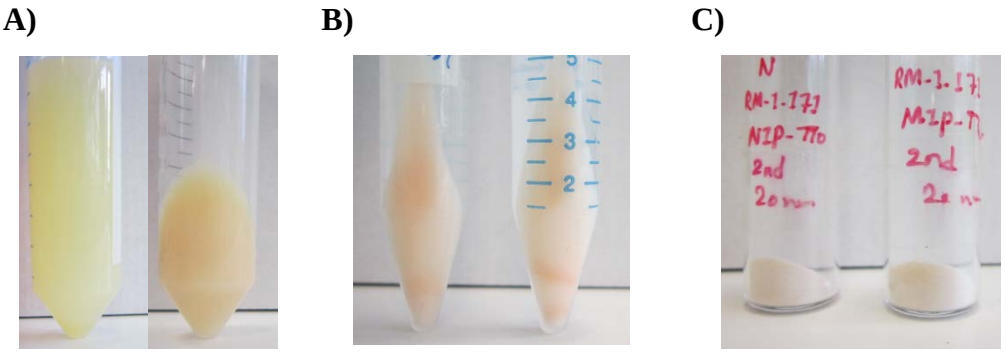

Figure 6.16. Picture of TTC modified silica, imprinted and nonimprinted particles; A) SiNP-TTC, B) SiNP-MIP and NIP (before drying), C) SiNP-MIP and NIP (after drying).

6.4.8 Binding experiments

Dry template free polymer (70 mg) was dispersed in 2.8 mL HEPES buffer (pH7, 10 mM) with sonication. Then, 400 µL (10 mg) of dispersed polymer was added into 5 separate Eppendorf tubes by addition of solutions (1.0 mL) of different concentration of T10 (0.075-1.2 mg mL^{-1}) in HEPES buffer (pH7, 10 mM) (the test was downscaled for samples available in limited quantities). This sample preparation was separately done for MIPNPs and NIPNPs. The vials were sealed and their contents allowed to equilibrate overnight at room temperature with gentle shaking. After 15 h incubation at room temperature the supernatants were sampled (420 µL) and the aliquots diluted in 80 µL HEPES buffer and transferred to HPLC vials for measurement of unbound solute concentration by reversed phase HPLC. The HPLC system consisted of an Agilent HPLC 1200 series instrument (Agilent) equipped with a UV-DAD detector and an autosampler. The column was a reversed phase (C18) column (Phenomenex Luna C-18, 150 × 4.6 mm), the mobile phase: water (0.1% TFA)(88%) and ACN (0.1% TFA) (12%), (gradient elution) flow rate : 1.0 mL/min, the injection volume was 20 µL and the detection performed by UV absorbance at 220 nm. The resulting peak areas were used to calculate the amount of bound analyte on the polymer (in mg/g of polymer). The binding results are averages of two independent experiments.

Conclusions and Perspectives

Imprinted NPs can be produced by a) precipitation polymerization, b) two phase mini-emulsion polymerization, by c) pregel interrupted polymerization or by d) grafting to or e) from either a soluble or nonsoluble core. In the context of imprinting, the grafting from approach e) by controlled radical polymerization (CRP) is particularly attractive overcoming key limitations of the other approaches (a and d: excessive dilution and need for extensive compositional optimization, b: template effects on emulsification and c: nonstoichiometric monomer incorporation). Grafting of imprinted films by CRP, in particular by an R-immobilized RAFT agent, has furthermore proven effective in enhancing the polymer binding site accessibility and hence binding capacity for the imprinted target. This was therefore the method of choice in our investigation.

In spite of the aforementioned drawbacks, these polymerization techniques have successfully been used for targeting different templates. Multifunctional polymer-based NPs with selective protein affinity were prepared by using precipitation polymerization [284]. More recently, high selective imprinted nanoparticle polymers by a mini-emulsion polymerization technique have been reported for controlled release and analysis of risperidone in human plasma samples [285]. MIP nanogels of protein dimensions with good binding affinity and specificity were prepared by using pregel interrupted polymerization [204].

In our investigation, surface-initiated RAFT polymerization has been used to prepare molecularly imprinted core-shell nanoparticles towards different templates in organic and aqueous media. Silica nanoparticles with different sizes ca 20 nm, ca 100 nm and ca 200 nm were used as a support material. Due to versatility and adaptability of RAFT polymerization with different monomers and conditions, RAFT is arguably the most promising among the CRP methods to employ in MIP systems.

In the early studies and before moving to graft cross-linked polymerization, the graft linear polymerization from RAFT modified silica nanoparticles was investigated. Afterwards the grafting of L-PA imprinted polymers was carried out on RAFT-modified silica support. In order to prepare imprinted core-shell MIPs via this method there were several difficulties in finding the right balance between all parameters (i.e. solid support content, RAFT/initiator ratio, monomer concentration, amount of solvent, etc). After plenty of attempts, the

polymerization procedure was successfully optimized and the first promising core-shell NPs were generated in our group.

In the first part of the work, well-established RAFT polymerization procedure was used to generate core-shell structured MIP nanoparticles for chiral discrimination. According to the binding-isotherm results, the MIPNPs exhibited a much-higher binding affinity for the template molecule than the NIPNPs. In addition, MIPNPs were able to discriminate the template L-PA and its optical antipode D-PA. The results of our research demonstrated that the size of the core particles has an important role in binding properties of core-shell particles. Comparison of the particles produced using the larger cores and the smaller core size revealed that the core-shell particles with smaller core size displayed a higher binding affinity than those with larger cores. This can be attributed to high specific surface area and grafting density of the colloidal size particles.

Based on the successful MIP generation in the first part, solid-phase synthesis of MIP core-shell NPs using magnetic template was investigated in the second part of the work. The final aim of this study was to develop a novel scalable process to produce surface imprinted nanoparticles in high yield and in template free form. Combination of surface initiated RAFT polymerization and solid phase synthesis offers significant advantages when compared to traditional approaches which rely on free template in solution, such as receptors in template free form, template reusability and high affinity binding sites. The results demonstrated that the MIPNPs prepared via this method have high accessible binding site and good discrimination towards the template L-PA and its optical antipode D-PA. These aspects in addition to the fact that polymerization take place in homogenous media hold great promise with respect to method scalability and parallel synthesis.

In the third part of the work, the epitope imprinted core-shell nanoparticles via surface initiated RAFT polymerization for β-amyloid template were developed. The silica nanoparticles with different sizes were modified via dithiobenzoate and trithiocarbonate RAFT agent and used as solid supports. The final MIPs were designed using TBA salt of the acetylated $A\beta_{37-42}$ as a template for the recognition of $A\beta_{33-42}$. The batch rebinding results demonstrated that the resulting polymers which prepared in diluted condition showed same adsorption capacity at the both imprinted and nonimprinted polymers. In contrast, at the both resulting polymers which generated in concentrated condition the imprinted particles displayed slightly more adsorption capacity than the nonimprinted particles in high range of

template concentrations. This behavior can be attributed to low concentration of template in diluted prepolymerization mixture which cause the week interaction among the functional monomers and template. The poor solubility of $A\beta_{33-42}$ in aqueous media caused a considerable problem for the rebinding tests. For this reason more investigations need to address this problem and get more optimistic results.

In the last part of the work, the nano-sized surface imprinting with epitope approach in aqueous and organic media have been combined in order to recognize a hydrophilic decapeptide epitope template (T10) corresponding to the solvent exposed C-terminus of the human immunoglobulin G (IgG) heavy chain. The resulting imprinted and nonimprinted polymers in organic media revealed similar adsorption capacity towards T10 template. Two polymers were investigated in aqueous media which had different functional monomer. For polymers prepared in organic media, the resulting imprinted and nonimprinted particles revealed a similar adsorption capacity towards T10 template. When the synthesis was performed in aqueous media, the imprinted particles displayed a higher adsorption capacity than the nonimprinted particles. Compared to polymer grafted using the bisphosphonic acid monomer, polymer obtained via methacrylic acid as functional monomer showed better imprinting performance.

Our results provide a new potential for peptides and protein imprinting in aqueous media using SI-RAFT technique and it might also be transferred to epitopes of other proteins. Therefore, combining the results obtained in this work with the use of nanoparticles could result in significant improvement to the MIPs properties and applications. We believe that such synthetic MIP nanoparticles are highly promising alternatives to biological receptors with great potential in many analytical applications and other areas.

In conclusion, we have developed the promising general platform which has proved to work for different monomers and for different templates. We are currently exploiting these possibilities while applying the concept to other model systems including those of biological significance. As an alternative to the silica core particles, different nanostructured counterparts with optionally different functional properties such as magnetic or luminescent cores or labeled with probes can be used to develop the new core-shell structured MIP NPs.

Chemicals

3-Aminopropyltriethoxysilane(APTES) ≥98%	Sigma-Aldrich,Steinheim, Germany
3-Aminopropyldimethylethoxysilane(APDMES), 97%	Sigma-Aldrich,Steinheim, Germany
4-(Chloromethyl)phenyltrichlorosilane, 97%	Alfa Aesar, Karlsruhe, Germany
4-(Chloromethyl)phenyltrimethoxysilane, tech. 90%	Alfa Aesar, Karlsruhe, Germany
1-Hydroxybenzotriazole (HOBt)	Across, Geel, Belgium
4-cyanopentanoic acid dithiobenzoate(CPDB)	Strem Chemicals, Germany
N-(2-aminoethyl) methacrylamide hydrochloride	Polysciences Inc., Germany
N,N′- ethylenebisacrylamide (EBA)	Sigma-Aldrich,Steinheim, Germany
S,S'-Bis(α,α'-dimethyl-α"-acetic acid)-trithiocarbonate	Own synthesis
2,2'-Azobis(2.4-dimethyl valeronitrile),(V-65)	Wako Chemicals, Neuss, Germany
2-propanol	Sigma-Aldrich,Steinheim, Germany
2-[4-(2-hydroxyethyl)piperazin-1-yl]ethanesulfonic-acid (HEPES)	Applichem, Darmstadt, Germany
Acetic acid	Sigma-Aldrich,Steinheim, Germany
GGVVIA ($Aß_{37-42}$)	Genscript, USA
GLMVGGVVIA ($Aß_{33-42}$)	Genscript, USA
Acetone	Merck KGaA, Darmstadt, Germany
Acetonitrile (HPLC grade)	Merck KGaA, Darmstadt, Germany
Activated basic alumina	Across, Geel, Belgium
Ammonium hydroxide solution,28%	Fluka, Deisenhofen, Germany
Ammonium persulfate (APS)	Sigma-Aldrich,Steinheim, Germany
Aniline	Sigma-Aldrich,Steinheim, Germany
BOC-L-phenylalanine	Bachem, Heidelberg, Germany
Butylamine	Sigma-Aldrich,Steinheim, Germany

Carbon disulfide	Sigma-Aldrich,Steinheim, Germany
Chloroform (p.a)	Merck KGaA, Darmstadt, Germany
Colloidal silica particles, 30 wt % dispersed in methyl-ethyl ketone (MEK-ST)	Nissan Chemical, Japan
Decapeptide (T10)	GenScript, Piscataway,NJ, USA
Dichloromethane (dry)	Merck KGaA, Darmstadt, Germany
Dicyclohexyl carbodiimide (DCC)	Sigma-Aldrich,Steinheim, Germany
Dimethylformamide (dry)	Fluka, Deisenhofen, Germany
Dimethylsulphoxide (p.a.)	Merck KGaA, Darmstadt, Germany
Dipotassium phosphate	Sigma-Aldrich,Steinheim, Germany
Divinylbenzene	Sigma-Aldrich,Steinheim, Germany
D/L-phenylalanine anilide	Own synthesis
Ethylchloroformate	Sigma-Aldrich,Steinheim, Germany
Ethanol (dry)	Fluka, Deisenhofen, Germany
Ethanol(p.a.)	Merck KGaA, Darmstadt, Germany
Ethyleneglycol dimethacrylate (EDMA)	Sigma-Aldrich,Steinheim, Germany
Guanidine hydrochloride (GuHCl)	Sigma-Aldrich,Steinheim, Germany
Hexane (p.a.)	Merck KGaA, Darmstadt, Germany
Hydrochloric acid (conc.)	Merck KGaA, Darmstadt, Germany
Methacrylic acid (MAA)	Sigma-Aldrich,Steinheim, Germany
Methyl methacrylate (MMA)	Sigma-Aldrich,Steinheim, Germany
Methanol (HPLC grade)	Merck KGaA, Darmstadt, Germany
Methanol (p.a.)	Merck KGaA, Darmstadt, Germany
Methacrylamide (MAAM)	Sigma-Aldrich,Steinheim, Germany
Monopotassium phosphate	Sigma-Aldrich,Steinheim, Germany

Sodium acetate	Sigma-Aldrich,Steinheim, Germany
Silica nanoparticle, 200 nm	Own synthesis
Sodium chloride	Sigma-Aldrich,Steinheim, Germany
Sodium hydroxide	Merck KGaA, Darmstadt, Germany
Styrene (St)	Sigma-Aldrich,Steinheim, Germany
Tetrabutylammonium hydrogen sulfate	Sigma-Aldrich,Steinheim, Germany
Tetraethyl orthosilicate (TEOS) , 98%	Across, Geel, Belgium
Tetramethylethylenediamine (TEMED)	Fluka, Deisenhofen, Germany
Tetrabutylammonium hydroxide	Sigma-Aldrich,Steinheim, Germany
Tetrahydrofuran (dry)	Fluka, Deisenhofen, Germany
Tetrahydrofurane(p.a)	Merck KGaA, Darmstadt, Germany
Toluene (dry)	Fluka, Deisenhofen, Germany
Triethylamine	Sigma-Aldrich,Steinheim, Germany
Trifluoroacetic acid	Sigma-Aldrich,Steinheim, Germany

HPLC water was purified using a Milli-Q system (Millipore, Bedford, MA). Anhydrous solvents, tetrahydrofuran were stored over appropriate molecular sieves.

Methacrylic acid (MAA), ethyleneglycol dimethacrylate (EGDMA), styrene (St) and methyl methacrylate (MMA) were passed through a column of activated basic alumina to remove inhibitor and stored at -20 °C before polymerization. Methacrylamide (MAAM) was recrystallized twice from mixtures of hexane and toluene prior to use. All other reagents were used as received.

References

1. B. Sellergren, *Molecularly imprinted polymers: man-made mimics of antibodies and their application in analytical chemistry*. Vol. 23. **2001**, Amsterdam: Elsevier Science B.V.

2. C. Alexander, H.S. Andersson, L.I. Andersson, R.J. Ansell, N. Kirsch, I.A. Nicholls, J. O'Mahony,M.J. Whitcombe, Journal of Molecular Recognition, **2006**. 19(2): p. 106-180.

3. G. Wulff, Chemical reviews, **2002**. 102(1): p. 1-28.

4. K. Haupt ,K. Mosbach, Chemical reviews, **2000**. 100(7): p. 2495-2504.

5. X. Ding ,P.A. Heiden, Macromolecular Materials and Engineering, **2014**. 299(3): p. 268-282.

6. B. Sellergren ,A.J. Hall, *Molecularly Imprinted Polymers*, in *Supramolecular Chemistry*. **2012**, John Wiley & Sons, Ltd.

7. S.A. Piletsky, N.W. Turner,P. Laitenberger, Medical engineering & physics, **2006**. 28(10): p. 971-7.

8. E.L. Holthoff ,F.V. Bright, Analytica chimica acta, **2007**. 594(2): p. 147-61.

9. G. Guan, B. Liu, Z. Wang,Z. Zhang, Sensors, **2008**. 8(12): p. 8291-8320.

10. L. Ye ,K. Haupt, Analytical and bioanalytical chemistry, **2004**. 378(8): p. 1887-1897.

11. C. Alexander, L. Davidson,W. Hayes, Tetrahedron, **2003**. 59(12): p. 2025-2057.

12. M.E. Byrne, J.Z. Hilt,N.A. Peppas, Journal of Biomedical Materials Research Part A, **2008**. 84A(1): p. 137-147.

13. A. Cutivet, C. Schembri, J. Kovensky,K. Haupt, Journal of the American Chemical Society, **2009**. 131(41): p. 14699-14702.

14. Y. Hoshino, H. Koide, T. Urakami, H. Kanazawa, T. Kodama, N. Oku,K.J. Shea, Journal of the American Chemical Society, **2010**. 132(19): p. 6644-6645.

15. P. Paik, A. Gedanken,Y. Mastai, Journal of Materials Chemistry, **2010**. 20(20): p. 4085-4093.

16. B. Sellergren, *Enantiomer Separations Using Designed Imprinted Chiral Phases*, in *Chiral Separation Techniques*. **2001**, Wiley-VCH Verlag GmbH. p. 151-184.

17. V. Pichon ,K. Haupt, Journal of liquid chromatography & related technologies, **2006**. 29(7-8): p. 989-1023.

18. S. Xu, L. Chen, J. Li, W. Qin,J. Ma, Journal of Materials Chemistry, **2011**. 21(32): p. 12047.

19. X. Song, J. Li, S. Xu, R. Ying, J. Ma, C. Liao, D. Liu, J. Yu,L. Chen, Talanta, **2012**. 99(0): p. 75-82.

20. B. Sellergren ,C.J. Allender, Advanced drug delivery reviews, **2005**. 57(12): p. 1733-1741.

21. G. Wulff, A. Sarhan,K. Zabrocki, Tetrahedron letters, **1973**. 14(44): p. 4329-4332.

22. A.G. Mayes ,M.J. Whitcombe, Advanced drug delivery reviews, **2005**. 57(12): p. 1742-78.

23. R. Arshady ,K. Mosbach, Die Makromolekulare Chemie, **1981**. 182(2): p. 687-692.

24. B. Sellergren, TrAC Trends in Analytical Chemistry, **1999**. 18(3): p. 164-174.

25. O. Ramström, I.A. Nicholls,K. Mosbach, Tetrahedron: Asymmetry, **1994**. 5(4): p. 649-656.

26. R.J. Umpleby Ii, M. Bode,K.D. Shimizu, The Analyst, **2000**. 125(7): p. 1261-1265.

27. B. Sellergren ,L. Andersson, The Journal of organic chemistry, **1990**. 55(10): p. 3381-3383.

28. Y. Fujii, K. Matsutani,K. Kikuchi, Journal of the Chemical Society, Chemical Communications, **1985**. 0(7): p. 415-417.

29. D.A. Spivak, Advanced drug delivery reviews, **2005**. 57(12): p. 1779-94.

30. P.A. Cormack ,A.Z. Elorza, Journal of chromatography. B,, **2004**. 804(1): p. 173-82.

31. K. Haupt ,K. Mosbach, Trends in biotechnology, **1998**. 16(11): p. 468-475.

32. A. Katz ,M.E. Davis, Macromolecules, **1999**. 32(12): p. 4113-4121.

33. C. Lübke, M. Lübke, M.J. Whitcombe,E.N. Vulfson, Macromolecules, **2000**. 33(14): p. 5098-5105.

34. N.W. Turner, E.V. Piletska, K. Karim, M. Whitcombe, M. Malecha, N. Magan, C. Baggiani,S.A. Piletsky, Biosensors and Bioelectronics, **2004**. 20(6): p. 1060-1067.

35. E. Oral ,N.A. Peppas, Polymer, **2004**. 45(18): p. 6163-6173.

36. Z.-S. Liu, Y.-L. Xu, C. Yan,R.-Y. Gao, Journal of Chromatography A, **2005**. 1087(1–2): p. 20-28.

37. B. Sellergren, M. Lepistoe,K. Mosbach, Journal of the American Chemical Society, **1988**. 110(17): p. 5853-5860.

38. Z. Zhang, H. Liao, H. Li, L. Nie,S. Yao, Analytical biochemistry, **2005**. 336(1): p. 108-116.

39. J.-P. Lai, X.-F. Cao, X.-L. Wang,X.-W. He, Analytical and bioanalytical chemistry, **2002**. 372(2): p. 391-396.

40. J. Cederfur, Y. Pei, M. Zihui,M. Kempe, Journal of Combinatorial Chemistry, **2003**. 5(1): p. 67-72.

41. Z. Xu, D. Kuang, L. Liu,Q. Deng, Journal of pharmaceutical and biomedical analysis, **2007**. 45(1): p. 54-61.

42. H. Sanbe ,J. Haginaka, The Analyst, **2003**. 128(6): p. 593-597.

43. L. Özcan ,Y. Şahin, Sensors and Actuators B: Chemical, **2007**. 127(2): p. 362-369.

44. K. Farrington ,F. Regan, Biosensors and Bioelectronics, **2007**. 22(6): p. 1138-1146.

45. E.V. Piletska, M. Romero-Guerra, A.R. Guerreiro, K. Karim, A.P.F. Turner,S.A. Piletsky, Analytica chimica acta, **2005**. 542(1): p. 47-51.

46. J. Hantash, A. Bartlett, P. Oldfield, G. Dénès, R. O'Rielly,F. David, Analytical and bioanalytical chemistry, **2007**. 387(1): p. 351-357.

47. F.G. Tamayo, J.L. Casillas,A. Martin-Esteban, Analytical and bioanalytical chemistry, **2005**. 381(6): p. 1234-1240.

48. C. Baggiani, G. Giraudi, F. Trotta, C. Giovannoli,A. Vanni, Talanta, **2000**. 51(1): p. 71-75.

49. K. Sreenivasan, Journal of Applied Polymer Science, **1998**. 68(11): p. 1863-1866.

50. G. Wulff ,S. Schauhoff, The Journal of organic chemistry, **1991**. 56(1): p. 395-400.

51. X.-C. Liu ,J.S. Dordick, Journal of Polymer Science Part A: Polymer Chemistry, **1999**. 37(11): p. 1665-1671.

52. M. Shamsipur, J. Fasihi, A. Khanchi, R. Hassani, K. Alizadeh,H. Shamsipur, Analytica chimica acta, **2007**. 599(2): p. 294-301.

53. A.R. Koohpaei, S.J. Shahtaheri, M.R. Ganjali, A.R. Forushani,F. Golbabaei, Talanta, **2008**. 75(4): p. 978-986.

54. H. Zhang, T. Song, F. Zong, T. Chen,C. Pan, International journal of molecular sciences, **2008**. 9(1): p. 98-106.

55. Z. Sun, W. Schüssler, M. Sengl, R. Niessner,D. Knopp, Analytica chimica acta, **2008**. 620(1–2): p. 73-81.

56. L. Malosse, P. Palmas, P. Buvat, D. Adès,A. Siove, Macromolecules, **2008**. 41(21): p. 7834-7842.

57. Y.-h. Li, T. Yang, X.-l. Qi, Y.-w. Qiao,A.-p. Deng, Analytica chimica acta, **2008**. 624(2): p. 317-325.

58. W. Luo, L. Zhu, C. Yu, H. Tang, H. Yu, X. Li,X. Zhang, Analytica chimica acta, **2008**. 618(2): p. 147-156.

59. A. Molinelli, J. O'Mahony, K. Nolan, M.R. Smyth, M. Jakusch,B. Mizaikoff, Analytical chemistry, **2005**. 77(16): p. 5196-5204.

60. C. Herdes ,L. Sarkisov, Langmuir : the ACS journal of surfaces and colloids, **2009**. 25(9): p. 5352-5359.

61. W.-X. Su, J. Rick,T.-C. Chou, Microchemical Journal, **2009**. 92(2): p. 123-128.

62. K. Karim, F. Breton, R. Rouillon, E.V. Piletska, A. Guerreiro, I. Chianella,S.A. Piletsky, Advanced drug delivery reviews, **2005**. 57(12): p. 1795-808.

63. X. Feás, J.A. Seijas, M.P. Vázquez-Tato, P. Regal, A. Cepeda,C. Fente, Analytica chimica acta, **2009**. 631(2): p. 237-244.

64. F. Navarro-Villoslada, B.S. Vicente,M.a.C. Moreno-Bondi, Analytica chimica acta, **2004**. 504(1): p. 149-162.

65. X. Shi, A. Wu, G. Qu, R. Li,D. Zhang, Biomaterials, **2007**. 28(25): p. 3741-9.

66. L. Ye, R. Weiss,K. Mosbach, Macromolecules, **2000**. 33(22): p. 8239-8245.

67. K. Yoshimatsu, K. Reimhult, A. Krozer, K. Mosbach, K. Sode,L. Ye, Analytica chimica acta, **2007**. 584(1): p. 112-21.

68. O.K. Castell, C.J. Allender,D.A. Barrow, Biosensors and Bioelectronics, **2006**. 22(4): p. 526-533.

69. W.-H. Li ,H.D.H. Stöver, Journal of Polymer Science Part A: Polymer Chemistry, **1998**. 36(10): p. 1543-1551.

70. P. Ruelle ,U.W. Kesselring, Journal of Pharmaceutical Sciences, **1998**. 87(8): p. 987-997.

71. F.J. Luque, C. Alhambra,M. Orozco, The Journal of Physical Chemistry, **1995**. 99(29): p. 11344-11349.

72. W.L. Armarego ,C. Chai, *Purification of laboratory chemicals*. **2012**: Butterworth-Heinemann.

73. A. Katz ,M.E. Davis, Nature, **2000**. 403(6767): p. 286-289.

74. C.D. Ki, C. Oh, S.-G. Oh,J.Y. Chang, Journal of the American Chemical Society, **2002**. 124(50): p. 14838-14839.

75. J.-L. Gong, F.-C. Gong, Y. Kuang, G.-M. Zeng, G.-L. Shen,R.-Q. Yu, Analytical and bioanalytical chemistry, **2004**. 379(2): p. 302-307.

76. H. Asanuma, M. Kakazu, M. Shibata,T. Hishiya, Chemical communications, **1997**(20): p. 1971-1972.

77. M. Beinhoff, A.T. Appapillai, L.D. Underwood, J.E. Frommer,K.R. Carter, Langmuir : the ACS journal of surfaces and colloids, **2006**. 22(6): p. 2411-2414.

78. A. Patel, S. Fouace,J.H.G. Steinke, Chemical communications, **2003**(1): p. 88-89.

79. G. Moad ,D.H. Solomon, *The chemistry of radical polymerization*. **2006**: Gulf Professional Publishing.

80. K. Matyjaszewski ,T.P. Davis, *Handbook of Radical Polymerization*. **2002**: Wiley.

81. B. Soper, R.N. Haward,E.F.T. White, Journal of Polymer Science Part A-1: Polymer Chemistry, **1972**. 10(9): p. 2545-2564.

82. K. Ulbrich, K. Dušek, M. Ilavský,J. Kopeček, European Polymer Journal, **1978**. 14(1): p. 45-49.

83. G. Moad, E. Rizzardo,S.H. Thang, Accounts of chemical research, **2008**. 41(9): p. 1133-1142.

84. A. Beltran, R.M. Marcé, P.A.G. Cormack,F. Borrull, Journal of Chromatography A, **2009**. 1216(12): p. 2248-2253.

85. W. Sun, Dissertation Universität Duisburg-Essen, **2009**.

86. A.R. Kannurpatti, K.J. Anderson, J.W. Anseth,C.N. Bowman, Journal of Polymer Science Part B: Polymer Physics, **1997**. 35(14): p. 2297-2307.

87. T. Otsu, M. Yoshida,T. Tazaki, Die Makromolekulare Chemie, Rapid Communications, **1982**. 3(2): p. 133-140.

88. T. Otsu ,M. Yoshida, Die Makromolekulare Chemie, Rapid Communications, **1982**. 3(2): p. 127-132.

89. T. Otsu, Journal of Polymer Science Part A: Polymer Chemistry, **2000**. 38(12): p. 2121–2136.

90. H.Y. Wang, T. Kobayashi,N. Fujii, Journal of Chemical Technology & Biotechnology, **1997**. 70(4): p. 355-362.

91. B. Rückert, A.J. Hall,B. Sellergren, Journal of Materials Chemistry, **2002**. 12(8): p. 2275-2280.

92. B. Sellergren, B. Rückert,A.J. Hall, Advanced materials, **2002**. 14(17): p. 1204-1208.

93. D.H. Solomon, Rizzardo, E., Cacioli, P. , U.S. Patent **1986**. 4(581): p. 429.

94. D.H. Solomon, Rizzardo, E., Cacioli, P., Eur. Patent Appl. , **1985**. 135: p. 280.

95. G. Moad ,E. Rizzardo, Macromolecules, **1995**. 28(26): p. 8722-8728.

96. M.K. Georges, R.P.N. Veregin, P.M. Kazmaier,G.K. Hamer, Macromolecules, **1993**. 26(11): p. 2987-2988.

97. S. Boonpangrak, M.J. Whitcombe, V. Prachayasittikul, K. Mosbach,L. Ye, Biosensors and Bioelectronics, **2006**. 22(3): p. 349-354.

98. A.D. Vaughan, S.P. Sizemore,M.E. Byrne, Polymer, **2007**. 48(1): p. 74-81.

99. M. Kato, M. Kamigaito, M. Sawamoto,T. Higashimura, Macromolecules, **1995**. 28(5): p. 1721-1723.

100. J.-S. Wang ,K. Matyjaszewski, Macromolecules, **1995**. 28(23): p. 7901-7910.

101. V. Percec ,B. Barboiu, Macromolecules, **1995**. 28(23): p. 7970-7972.

102. W. He, H. Jiang, L. Zhang, Z. Cheng,X. Zhu, Polymer Chemistry, **2013**. 4(10): p. 2919-2938.

103. J.R. Adams ,S.K. Mallapragada, Macromolecular Chemistry and Physics, **2013**. 214(12): p. 1321-1325.

104. H. Zhang, B. Klumperman, W. Ming, H. Fischer,R. van der Linde, Macromolecules, **2001**. 34(18): p. 6169-6173.

105. H. Zhang, B. Klumperman,R. van der Linde, Macromolecules, **2002**. 35(6): p. 2261-2267.

106. K. Matyjaszewski ,J. Xia, Chemical reviews, **2001**. 101(9): p. 2921-2990.

107. T.E. Patten ,K. Matyjaszewski, Advanced materials, **1998**. 10(12): p. 901-915.

108. M. Teodorescu ,K. Matyjaszewski*, Macromolecular Rapid Communications, **2000**. 21(4): p. 190-194.

109. J. Xia, X. Zhang,K. Matyjaszewski, Macromolecules, **1999**. 32(10): p. 3531-3533.

110. X. Wei, X. Li,S.M. Husson, Biomacromolecules, **2005**. 6(2): p. 1113-1121.

111. R.T.A. Mayadunne, E. Rizzardo, J. Chiefari, Y.K. Chong, G. Moad,S.H. Thang, Macromolecules, **1999**. 32(21): p. 6977-6980.

112. J. Chiefari*, et al.*, Macromolecules, **1998**. 31(16): p. 5559-5562.

113. G. Moad, E. Rizzardo,S.H. Thang, Australian journal of chemistry, **2005**. 58(6): p. 379-410.

114. G. Moad, E. Rizzardo,S.H. Thang, Australian Journal of Chemistry, **2012**. 65(8): p. 985.

115. C. Gonzato, P. Pasetto, F. Bedoui, P.-E. Mazeran,K. Haupt, Polymer Chemistry, **2014**. 5: p. 1313-1322.

116. S. Perrier ,P. Takolpuckdee, Journal of Polymer Science Part A: Polymer Chemistry, **2005**. 43(22): p. 5347-5393.

117. G. Liu, H. Shi, Y. Cui, J. Tong, Y. Zhao, D. Wang,Y. Cai, Polymer Chemistry, **2013**. 4(4): p. 1176.

118. L.P.D. Ratcliffe, A.J. Ryan,S.P. Armes, Macromolecules, **2013**. 46(3): p. 769-777.

119. G. Moad, E. Rizzardo,S.H. Thang, Chemistry, an Asian journal, **2013**. 8(8): p. 1634-44.

120. D.J. Keddie, Chemical Society reviews, **2014**. 43: p. 496-505.

121. M. Milovanovic, M. Avramovic, L. Katsikas,I. Popovic, Journal of the Serbian Chemical Society, **2010**. 75(12): p. 1711-1719.

122. M. Kaupp, T. Tischer, A.F. Hirschbiel, A.P. Vogt, U. Geckle, V. Trouillet, T. Hofe, M.H. Stenzel,C. Barner-Kowollik, Macromolecules, **2013**. 46(17): p. 6858-6872.

123. G. Moad, E. Rizzardo,S.H. Thang, Polymer International, **2011**. 60(1): p. 9-25.

124. H. Willcock ,R.K. O'Reilly, Polymer Chemistry, **2010**. 1(2): p. 149-157.

125. G. Moad, E. Rizzardo,S.H. Thang, Australian Journal of Chemistry, **2006**. 59(10): p. 669-692.

126. M.-M. Titirici ,B. Sellergren, Chemistry of materials, **2006**. 18(7): p. 1773-1779.

127. S. Xu, J. Li,L. Chen, Talanta, **2011**. 85(1): p. 282-9.

128. Y. Ma, G. Pan, Y. Zhang, X. Guo,H. Zhang, Angewandte Chemie International Edition, **2013**. 52(5): p. 1511-1514.

129. Y. Hoshino, H. Koide, K. Furuya, W.W. Haberaecker, S.-H. Lee, T. Kodama, H. Kanazawa, N. Oku,K.J. Shea, Proceedings of the National Academy of Sciences, **2012**. 109(1): p. 33-38.

130. R. Barbey, L. Lavanant, D. Paripovic, N. Schüwer, C. Sugnaux, S. Tugulu,H.-A. Klok, Chemical reviews, **2009**. 109(11): p. 5437-5527.

131. B. Zhao ,W.J. Brittain, Progress in Polymer Science, **2000**. 25(5): p. 677-710.

132. N. Ayres, Polymer Chemistry, **2010**. 1(6): p. 769-777.

133. O. Azzaroni, Journal of Polymer Science Part A: Polymer Chemistry, **2012**. 50(16): p. 3225-3258.

134. Y. Hu, J.S. Li, W.T. Yang,F.J. Xu, Thin Solid Films, **2013**. 534(0): p. 325-333.

135. R.C. Advincula, W.J. Brittain, K.C. Caster,J. Rühe, *Polymer brushes: Synthesis, Characterization, Applications*. **2004**: Wiley Online Library.

136. J. Araki, Soft Matter, **2013**. 9(16): p. 4125-4141.

137. W. Xu, S. Su, P. Jiang, H. Wang, X. Dong,M. Zhang, Journal of Chromatography A, **2010**. 1217(46): p. 7198-7207.

138. R.Y. Song, X.L. Hu, J. Li,P. Guan, Advanced Materials Research, **2013**. 702: p. 68-73.

139. S. Su, M. Zhang, B. Li, H. Zhang,X. Dong, Talanta, **2008**. 76(5): p. 1141-1146.

140. F. Barahona, E. Turiel, P.A.G. Cormack,A. Martín-Esteban, Journal of Polymer Science Part A: Polymer Chemistry, **2010**. 48(5): p. 1058-1066.

141. L. Qin, X.-W. He, W. Zhang, W.-Y. Li,Y.-K. Zhang, Journal of Chromatography A, **2009**. 1216(5): p. 807-814.

142. K. Hattori, M. Hiwatari, C. Iiyama, Y. Yoshimi, F. Kohori, K. Sakai,S.A. Piletsky, Journal of Membrane Science, **2004**. 233(1–2): p. 169-173.

143. H.Y. Lee ,B. S. Kim, Biosensors and Bioelectronics, **2009**. 25(3): p. 587-591.

144. X. Huang ,M.J. Wirth, Analytical chemistry, **1997**. 69(22): p. 4577-4580.

145. C. Yoshikawa, A. Goto, Y. Tsujii, N. Ishizuka, K. Nakanishi,T. Fukuda, Journal of Polymer Science Part A: Polymer Chemistry, **2007**. 45(21): p. 4795-4803.

146. M. Czaun, M.M. Rahman, M. Takafuji,H. Ihara, Journal of Polymer Science Part A: Polymer Chemistry, **2008**. 46(19): p. 6664-6671.

147. K. Nagase, M. Kumazaki, H. Kanazawa, J. Kobayashi, A. Kikuci, Y. Akiyama, M. Annaka,T. Okano, ACS applied materials & interfaces, **2010**. 2(4): p. 1247-1253.

148. J. Ji, X. Sun, X. Tian, Z. Li,Y. Zhang, Analytical Letters, **2013**. 46(6): p. 969-981.

149. C.-H. Lu, W.-H. Zhou, B. Han, H.-H. Yang, X. Chen,X.-R. Wang, Analytical chemistry, **2007**. 79(14): p. 5457-5461.

150. A. Zengin, E. Yildirim, U. Tamer,T. Caykara, The Analyst, **2013**. 138(23): p. 7238-7245.

151. Y. Li, W.-H. Zhou, H.-H. Yang,X.-R. Wang, Talanta, **2009**. 79(2): p. 141-145.

152. Y. Li, X. Li, C. Dong, Y. Li, P. Jin,J. Qi, Biosensors and Bioelectronics, **2009**. 25(2): p. 306-312.

153. C. Gonzato, M. Courty, P. Pasetto,K. Haupt, Advanced Functional Materials, **2011**. 21(20): p. 3947-3953.

154. F.G. Tamayo, M.M. Titirici, A. Martin-Esteban,B. Sellergren, Analytica chimica acta, **2005**. 542(1): p. 38-46.

155. M.B.a.K. Haupt, Aust. J. Chem., **2009**.

156. H.-J. Wang, W.-H. Zhou, X.-F. Yin, Z.-X. Zhuang, H.-H. Yang,X.-R. Wang, Journal of the American Chemical Society, **2006**. 128(50): p. 15954-15955.

157. Y. Liu, Y. He, Y. Jin, Y. Huang, G. Liu,R. Zhao, Journal of Chromatography A, **2014**. 1323(0): p. 11-17.

158. C. Barner-Kowollik, *Handbook of RAFT polymerization*. **2008**: John Wiley & Sons.

159. M. Baum ,W.J. Brittain, Macromolecules, **2002**. 35(3): p. 610-615.

160. B. Hojjati ,P.A. Charpentier, Journal of Polymer Science Part A: Polymer Chemistry, **2008**. 46(12): p. 3926-3937.

161. Y. Tsujii, M. Ejaz, K. Sato, A. Goto,T. Fukuda, Macromolecules, **2001**. 34(26): p. 8872-8878.

162. C. Li ,B.C. Benicewicz, Macromolecules, **2005**. 38(14): p. 5929-5936.

163. C. Li, J. Han, C.Y. Ryu,B.C. Benicewicz, Macromolecules, **2006**. 39(9): p. 3175-3183.

164. C.-Y. Hong, X. Li,C.-Y. Pan, European Polymer Journal, **2007**. 43(10): p. 4114-4122.

165. C.-H. Liu ,C.-Y. Pan, Polymer, **2007**. 48(13): p. 3679-3685.

166. H. Skaff ,T. Emrick, Angewandte Chemie, **2004**. 116(40): p. 5497-5500.

167. J. Raula, J. Shan, M. Nuopponen, A. Niskanen, H. Jiang, E.I. Kauppinen,H. Tenhu, Langmuir : the ACS journal of surfaces and colloids, **2003**. 19(8): p. 3499-3504.

168. M. Beija, J.-D. Marty,M. Destarac, Progress in Polymer Science, **2011**. 36(7): p. 845-886.

169. S. Perrier, P. Takolpuckdee,C.A. Mars, Macromolecules, **2005**. 38(16): p. 6770-6774.

170. D.H. Nguyen ,P. Vana, Polymers for Advanced Technologies, **2006**. 17(9-10): p. 625-633.

171. L.-P. Wang, Y.-P. Wang, R.-M. Wang,S.-C. Zhang, Reactive and Functional Polymers, **2008**. 68(2): p. 643-648.

172. Q. Peng, D.M.Y. Lai, E.T. Kang,K.G. Neoh, Macromolecules, **2006**. 39(16): p. 5577-5582.

173. E. Unsal, E. Uguzdogan, S. Patir,A. Tuncel, Journal of separation science, **2009**. 32(11): p. 1791-1800.

174. S. Tokonami, H. Shiigi,T. Nagaoka, Analytica chimica acta, **2009**. 641(1-2): p. 7-13.

175. D. Gao, Z. Zhang, M. Wu, C. Xie, G. Guan,D. Wang, Journal of the American Chemical Society, **2007**. 129(25): p. 7859-7866.

176. C.J. Tan ,Y.W. Tong, Analytical and bioanalytical chemistry, **2007**. 389(2): p. 369-76.

177. G. Wulff, B.-O. Chong,U. Kolb, Angewandte Chemie International Edition, **2006**. 45(18): p. 2955-2958.

178. D. Vaihinger, K. Landfester, I. Kräuter, H. Brunner,G.E.M. Tovar, Macromolecular Chemistry and Physics, **2002**. 203(13): p. 1965-1973.

179. Z. Zeng, Y. Hoshino, A. Rodriguez, H. Yoo,K.J. Shea, ACS nano, **2010**. 4(1): p. 199-204.

180. X. Wang, L. Wang, X. He, Y. Zhang,L. Chen, Talanta, **2009**. 78(2): p. 327-32.

181. C. Zheng, X.-L. Zhang, W. Liu, B. Liu, H.-H. Yang, Z.-A. Lin,G.-N. Chen, Advanced materials, **2013**. 25(41): p. 5922-5927.

182. R. Suedee, Pharmaceutica Analytica Acta, **2013**. 4: p. 264.

183. C. Baggiani, L. Anfossi,C. Giovannoli, Molecular Imprinting, **2013**. 1: p. 41-54.

184. P. Pasetto, S.C. Maddock,M. Resmini, Analytica chimica acta, **2005**. 542(1): p. 66-75.

185. J. Nilsson, P. Spégel,S. Nilsson, Journal of Chromatography B, **2004**. 804(1): p. 3-12.

186. K. Reimhult, K. Yoshimatsu, K. Risveden, S. Chen, L. Ye,A. Krozer, Biosensors and Bioelectronics, **2008**. 23(12): p. 1908-1914.

187. T. de Boer, R. Mol, R.A. de Zeeuw, G.J. de Jong, D.C. Sherrington, P.A.G. Cormack,K. Ensing, ELECTROPHORESIS, **2002**. 23(9): p. 1296-1300.

188. H.-H.Y. Yong Li, Qi-Hua You , Zhi-Xia Zhuang , Xiao-Ru Wang, Anal. Chem. , **2006**. 78 (1): p. 317–320.

189. X. Yang, Z. Zhang, J. Li, X. Chen, M. Zhang, L. Luo,S. Yao, Food Chemistry, **2014**. 145(0): p. 687-693.

190. Y. Li, M. Hong, Miaomiao, Q. Bin, Z. Lin, Z. Cai,G. Chen, Journal of Materials Chemistry B, **2013**. 1(7): p. 1044-1051.

191. Y. Lu, C.-L. Yan, X.-J. Wang,G.-K. Wang, Applied Surface Science, **2009**. 256(5): p. 1341-1346.

192. G. Pan, Q. Guo, C. Cao, H. Yang,B. Li, Soft Matter, **2013**. 9(14): p. 3840.

193. D. Liu, Q. Yang, S. Jin, Y. Song, J. Gao, Y. Wang,H. Mi, Acta biomaterialia, **2014**. 10(2): p. 769-775.

194. G. Fang, C. Fan, H. Liu, M. Pan, H. Zhu,S. Wang, RSC Advances, **2014**. 4(6): p. 2764-2771.

195. T. Ishi-i ,S. Shinkai, Chemical communications, **1998**(9): p. 1047-1048.

196. S.C. Zimmerman, M.S. Wendland, N.A. Rakow, I. Zharov,K.S. Suslick, Nature, **2002**. 418(6896): p. 399-403.

197. X. Kan, Y. Zhao, Z. Geng, Z. Wang,J.-J. Zhu, The Journal of Physical Chemistry C, **2008**. 112(13): p. 4849-4854.

198. P.A. Lieberzeit, S. Gazda-Miarecka, K. Halikias, C. Schirk, J. Kauling,F.L. Dickert, Sensors and Actuators B: Chemical, **2005**. 111–112(0): p. 259-263.

199. T. Piacham, Å. Josell, H. Arwin, V. Prachayasittikul,L. Ye, Analytica chimica acta, **2005**. 536(1–2): p. 191-196.

200. M. Riskin, R. Tel-Vered,I. Willner, Advanced Functional Materials, **2007**. 17(18): p. 3858-3863.

201. A. Ersöz, A. Denizli, A. Özcan,R. Say, Biosensors and Bioelectronics, **2005**. 20(11): p. 2197-2202.

202. K. Taniwaki, A. Hyakutake, T. Aoki, M. Yoshikawa, M.D. Guiver,G.P. Robertson, Analytica chimica acta, **2003**. 489(2): p. 191-198.

203. A.D. McNaught ,A. Wilkinson, *Compendium of chemical terminology*. Vol. 1669. **1997**: Blackwell Science Oxford.

204. P. Cakir, A. Cutivet, M. Resmini, B.T. Bui,K. Haupt, Adv. Mater., **2013**. 25(7): p. 1048–1051.

205. W. Wan, M. Biyikal, R. Wagner, B. Sellergren,K. Rurack, Angewandte Chemie International Edition, **2013**. 52(27): p. 7023–7027.

206. R. Picca, C. Malitesta, R. Mohammadi, F. Ghorbani,B. Sellergren, *Novel Format of Molecularly Imprinted Polymers for the Development of Electrochemical Sensors*, in *Sensors*, F. Baldini, et al., Editors. **2014**, Springer New York. p. 165-169.

207. R. Gao, X. Mu, J. Zhang,Y. Tang, Journal of Materials Chemistry B, **2014**. 2(7): p. 783-792.

208. L. Zhu, X. Yang,Y. Cao, Analytical Letters, **2013**. 46(6): p. 982-998.

209. C. Xu ,L. Ye, Chemical communications, **2011**. 47(21): p. 6096-6098.

210. H. Chen, J. Kong, D. Yuan,G. Fu, Biosensors and Bioelectronics, **2014**. 53(0): p. 5-11.

211. D. Chen, J. Deng, J. Liang, J. Xie, K. Huang,C. Hu, Analytical Methods, **2013**. 5(3): p. 722.

212. S. Wang, R. Wang, X. Wu, Y. Wang, C. Xue, J. Wu, J. Hong, J. Liu,X. Zhou, Journal of chromatography. B,, **2012**. 905: p. 105-12.

213. U. Nenad Gajovic-Eichelmann, Chemical Sensors and Biosensors, **2013**. 14: p. 143-170.

214. M.J. Whitcombe, I. Chianella, L. Larcombe, S.A. Piletsky, J. Noble, R. Porter,A. Horgan, Chemical Society reviews, **2011**. 40(3): p. 1547-71.

215. J.L. Bowen, P. Manesiotis,C.J. Allender, Molecular Imprinting, **2013**. 1: p. 35–40.

216. D.M. Hawkins, D. Stevenson,S.M. Reddy, Analytica chimica acta, **2005**. 542(1): p. 61-65.

217. T.Y. Guo, Y.Q. Xia, G.J. Hao, M.D. Song,B.H. Zhang, Biomaterials, **2004**. 25(27): p. 5905-5912.

218. A. Bossi, S.A. Piletsky, E.V. Piletska, P.G. Righetti,A.P.F. Turner, Analytical chemistry, **2001**. 73(21): p. 5281-5286.

219. R. Schirhagl, P.A. Lieberzeit,F.L. Dickert, Advanced materials, **2010**. 22(18): p. 2078-2081.

220. T. Chen, M. Shao, H. Xu, S. Zhuo, S. Liu,S.-T. Lee, Journal of Materials Chemistry, **2012**. 22(9): p. 3990-3996.

221. A. Rachkov ,N. Minoura, Journal of Chromatography A, **2000**. 889(1–2): p. 111-118.

222. N.M. Alexandre Rachkov Biochimica et Biophysica Acta, **2001**. 1544(1-2): p. 255–266.

223. M.M. Titirici ,B. Sellergren, Analytical and bioanalytical chemistry, **2004**. 378(8): p. 1913-21.

224. H. Nishino, C.S. Huang,K.J. Shea, Angewandte Chemie, **2006**. 45(15): p. 2392-6.

225. M. Emgenbroich*, et al.*, Chemistry – A European Journal, **2008**. 14(31): p. 9516-9529.

226. Y. Lv, T. Tan,F. Svec, Biotechnology Advances, **2013**. 31(8): p. 1172-1186.

227. B.H. Stuart, *Polymer analysis*. Vol. 30. **2008**: John Wiley & Sons.

228. C. Bartholome, E. Beyou, E. Bourgeat-Lami, P. Chaumont,N. Zydowicz, Polymer, **2005**. 46(19): p. 8502-8510.

229. M.R. Halhalli, C.S.A. Aureliano, E. Schillinger, C. Sulitzky, M.M. Titirici,B. Sellergren, Polymer Chemistry, **2012**. 3(4): p. 1033-1042.

230. S.J.S.K.S.W. Gregg, Berichte der Bunsengesellschaft für physikalische Chemie, **1982**. 86(10): p. 957-957.

231. L.I. Andersson, R. Müller, G. Vlatakis,K. Mosbach, Proceedings of the National Academy of Sciences, **1995**. 92(11): p. 4788-4792.

232. S.-H. Cheong, A.E. Rachkov, J.-K. Park, K. Yano,I. Karube, Journal of Polymer Science Part A: Polymer Chemistry, **1998**. 36(11): p. 1725-1732.

233. B. Tse Sum Bui, A.-S. Belmont, H. Witters,K. Haupt, Analytical and bioanalytical chemistry, **2008**. 390(8): p. 2081-2088.

234. J.A. García-Calzón ,M.E. Díaz-García, Sensors and Actuators B: Chemical, **2007**. 123(2): p. 1180-1194.

235. Y. Chen, M. Kele, I. Quiñones, B. Sellergren,G. Guiochon, Journal of Chromatography A, **2001**. 927(1–2): p. 1-17.

236. A.M. Rampey, R.J. Umpleby, G.T. Rushton, J.C. Iseman, R.N. Shah,K.D. Shimizu, Analytical chemistry, **2004**. 76(4): p. 1123-1133.

237. H. Zou, S. Wu,J. Shen, Chem. Rev, **2008**. 108(9): p. 3893-3957.

238. B. Radhakrishnan, R. Ranjan,W.J. Brittain, Soft Matter, **2006**. 2(5): p. 386.

239. M.R. Halhalli, E. Schillinger, C.S.A. Aureliano,B. Sellergren, Chemistry of Materials, **2012**. 24(15): p. 2909-2919.

240. M.R. Halhalli ,B. Sellergren, Chemical communications, **2013**. 49(64): p. 7111-7113.

241. W. Stöber, A. Fink,E. Bohn, Journal of Colloid and Interface Science, **1968**. 26: p. 62-69.

242. W. Wang, B.H. Gu, L.Y. Liang,W. Hamilton, J. Phys. Chem. B, **2003**. 107: p. 3400-3404.

243. L. Lu, R. Capek, A. Kornowski, N. Gaponik,A. Eychmuller, Angewandte Chemie, **2005**. 44(37): p. 5997-6001.

244. X. Shen ,L. Ye, Macromolecules, **2011**. 44(14): p. 5631-5637.

245. G.H. Bogush, M.A. Tracy,C.F. Zukoski Iv, Journal of Non-Crystalline Solids, **1988**. 104(1): p. 95-106.

246. R. Scaffaro, L. Botta, G. Lo Re, R. Bertani, R. Milani,A. Sassi, Journal of Materials Chemistry, **2011**. 21(11): p. 3849.

247. M. Björklund ,M.T.W. Hearn, Journal of Chromatography A, **1996**. 728(1–2): p. 149-169.

248. J. Lin, H. Chen, Y. Yuan,Y. Ji, Applied Surface Science, **2011**. 257(21): p. 9024-9032.

249. A.B. Lowe ,C.L. McCormick, Progress in Polymer Science, **2007**. 32(3): p. 283-351.

250. A.J. Convertine, B.S. Lokitz, A.B. Lowe, C.W. Scales, L.J. Myrick,C.L. McCormick, Macromolecular Rapid Communications, **2005**. 26(10): p. 791-795.

251. D.J. Keddie, G. Moad, E. Rizzardo,S.H. Thang, Macromolecules, **2012**. 45(13): p. 5321-5342.

252. J.T. Lai, D. Filla,R. Shea, Macromolecules, **2002**. 35(18): p. 6754-6756.

253. A. Rungta, B. Natarajan, T. Neely, D. Dukes, L.S. Schadler,B.C. Benicewicz, Macromolecules, **2012**: p. 121128155433006.

254. Y. Zhao ,S. Perrier, Macromolecules, **2007**. 40(25): p. 9116-9124.

255. B.S.S. David B. Thomas, ‡ Andrew B. Lowe,§ and Charles L. McCormick, Macromolecules **2003**. 36(5): p. 1436-1439.

256. V.D. Salian, A.D. Vaughan,M.E. Byrne, Journal of molecular recognition : JMR, **2012**. 25(6): p. 361-9.

257. A.F. Tominey, J. Liese, S. Wei, K. Kowski, T. Schrader,A. Kraft, Beilstein journal of organic chemistry, **2010**. 6(66): p. 1-7.

258. C. Sulitzky, B. Rückert, A.J. Hall, F. Lanza, K. Unger,B. Sellergren, Macromolecules, **2002**. 35(1): p. 79-91.

259. M.M. Titirici, Dissertation Universität Dortmund, **2005**.

260. Y. Chen, M. Kele, P. Sajonz, B. Sellergren,G. Guiochon, Analytical chemistry, **1999**. 71(5): p. 928-938.

261. M.M. Titirici, A.J. Hall,B. Sellergren, Chemistry of Materials, **2002**. 14(1): p. 21-23.

262. A. Nematollahzadeh, W. Sun, C.S.A. Aureliano, D. Lütkemeyer, J. Stute, M.J. Abdekhodaie, A. Shojaei,B. Sellergren, Angewandte Chemie International Edition, **2011**. 50(2): p. 495-498.

263. A. Poma, A. Guerreiro, M.J. Whitcombe, E.V. Piletska, A.P.F. Turner,S.A. Piletsky, Advanced Functional Materials, **2013**. 23(22): p. 2821-2827.

264. I. Chianella, A. Guerreiro, E. Moczko, J.S. Caygill, E.V. Piletska, I.M.P. De Vargas Sansalvador, M.J. Whitcombe,S.A. Piletsky, Analytical chemistry, **2013**. 85(17): p. 8462-8468.

265. S.B. Serena Ambrosini, Karsten Haupt, Chem. Commun, **2013**. 49: p. 6746-6748.

266. A. Poma, A. Guerreiro, S. Caygill, E. Moczko,S. Piletsky, RSC Advances, **2014**. 4(8): p. 4203-4206.

267. M. Berghaus, MSc dissertation universität dortmund, **2012**.

268. M. Berghaus, R. Mohammadi,B. Sellergren, Chemical communications, **2014**.

269. Z.-Y. Ma, X.-Q. Liu, Y.-P. Guan,H.-Z. Liu, Colloids and Surfaces A: Physicochemical and Engineering Aspects, **2006**. 275(1–3): p. 87-91.

270. J.I. Taylor, C.D. Hurst, M.J. Davies, N. Sachsinger,I.J. Bruce, Journal of Chromatography A, **2000**. 890(1): p. 159-166.

271. D.K. Yi, S.S. Lee,J.Y. Ying, Chemistry of Materials, **2006**. 18(10): p. 2459-2461.

272. M. Berghaus, R. Mohammadi,B. Sellergren, submitted, **2014**.

273. A. Schmechel, H. Zentgraf, S. Scheuermann, G. Fritz, R. Pipkorn, J. Reed, K. Beyreuther, T.A. Bayer,G. Multhaup, Journal of Biological Chemistry, **2003**. 278(37): p. 35317-35324.

274. K. Halverson, P.E. Fraser, D.A. Kirschner,P.T. Lansbury, Biochemistry, **1990**. 29(11): p. 2639-2644.

275. J.L. Urraca, C.S. Aureliano, E. Schillinger, H. Esselmann, J. Wiltfang,B. Sellergren, Journal of the American Chemical Society, **2011**. 133(24): p. 9220-3.

276. A.J. Hall, P. Manesiotis, M. Emgenbroich, M. Quaglia, E. De Lorenzi,B. Sellergren, The Journal of organic chemistry, **2005**. 70(5): p. 1732-1736.

277. C. Renner, J. Piehler,T. Schrader, Journal of the American Chemical Society, **2005**. 128(2): p. 620-628.

278. L. Chen, S. Xu,J. Li, Chemical Society reviews, **2011**. 40(5): p. 2922-42.

279. Y. Zhang, D. Song, L.M. Lanni,K.D. Shimizu, Macromolecules, **2010**. 43(15): p. 6284-6294.

280. K. Wenck, S. Koch, C. Renner, W. Sun,T. Schrader, Journal of the American Chemical Society, **2007**. 129(51): p. 16015-16019.

281. D.L. Patton, M. Mullings, T. Fulghum,R.C. Advincula, Macromolecules, **2005**. 38(20): p. 8597-8602.

282. P.K. Smith*, et al.*, Analytical biochemistry, **1985**. 150(1): p. 76-85.

283. H. Xu, F. Meng,Z. Zhong, Journal of Materials Chemistry, **2009**. 19(24): p. 4183.

284. K. Yoshimatsu, B.K. Lesel, Y. Yonamine, J.M. Beierle, Y. Hoshino,K.J. Shea, Angewandte Chemie, **2012**. 51(10): p. 2405-8.

285. E. Asadi, S. Azodi-Deilami, M. Abdouss, D. Kordestani, A. Rahimi,S. Asadi, Korean Journal of Chemical Engineering, **2014**: p. 1-8.

Curriculum Vitae

Reza Mohammadi
M.Sc. (Organic Chemistry)
INFU, Faculty of Chemistry and Chemical Biology,
Technical University of Dortmund,
Otto Hahn Strasse 6,
44221 Dortmund, Germany
Tel: +49-231-7556114
Mobile: +49-152-12044267
Email: r.mohammadi@infu.uni-dortmund.de
rezamohammadi78@yahoo.com

Personal Vitae

Name:	Reza Mohammadi
Date of birth:	23rd September 1978
Place of birth:	Naghadeh, Iran
Marital status:	Married
Nationality:	Iranian
Languages known:	Turkish, Persian, English, German (basic)
Present address:	Stockumer str.158- 44225 Dortmund, Germany
Permanent address:	Mehregan st. ,No. 61, Abrasan squ., Tabriz, Iran

Educational Qualification

M. Sc. (2004 – 2007)	Organic Chemistry (Polymer field) Tabriz University(www.tabrizu.ac.ir), Tabriz, Iran
B. Sc. (1999 – 2003)	Pure Chemistry Tabriz University(www.tabrizu.ac.ir), Tabriz, Iran

Research Experience

1- INFU, Faculty of Chemistry, Technical University of Dortmund, Germany

- ❖ PhD Thesis (Oct 2010 - June 2014) *"Molecularly imprinted core-shell nanoparticles by surface initiated RAFT polymerization"* Funded by the Ministry of Science, Research and Technology of the Islamic Republic of Iran
- ❖ Project: "Synthesis and characterization of nanobeads for antibody capture"(September 2011- present)

2- Department of Organic Chemistry, Faculty of Chemistry, University of Tabriz, Tabriz

- ❖ M.Sc. Project(Sep 2004 - Feb 2007) *"Optimization of syndiotactic polystyrene preparation by titanocene catalysts (R)IndTiCl$_3$"*

Publications

1- Melanie Berghaus, Reza Mohammadi, Börje Sellergren. *"Productive encounter: Molecularly imprinted nanoparticles prepared using magnetic templates"*. **Chem.Comm. 2014,** DOI: 10.1039/c4cc01346h

2- Rosaria Anna Picca, Cosimino Malitesta, Reza Mohammadi, Fatemeh Ghorbani, Börje Sellergren. *"Novel Format of Molecularly Imprinted Polymers for the Development of Electrochemical Sensors"*. **Sensors**, Lecture Notes in Electrical Engineering, Vol. 162, **2014**, p.165-169.

3- Reza Mohammadi, Sohrab Rahmani, Ali Akbar Entezami. *"Comparison of syndiotactic polystyrene morphology obtained via heterogeneous and homogeneous polymerization with metallocene catalyst"*. **Journal of Macromol. Symp. 2008**, 274, 43–48.

4- Mojtaba Abbasian, Sohrab Rahmani, Reza Mohammadi, Ali Akbar Entezami. *"Graft copolymerization of styrene or methyl methacrylate onto syndiotactic polystyrene by ATRP technique"*. **Journal of Applied Polymer Science. 2007**, Vol. 104, p.611–619.

Oral Presentations

1- Reza Mohammadi, Börje Sellergren (2012)
"Epitope Imprinted core-shell nanoparticles by surface RAFT polymerization for IgG". AbCap Project Meeting, March 2012, university of Duisburg-Essen, Germany

2- Reza Mohammadi, Börje Sellergren (2011)
"Soluble and colloidal nano molecularly imprinted polymers by living polymerization". November 2010, TU Dortmund, Germany

3- Reza Mohammadi,Sohrab Rahmani, Mojtaba Abbasian and Ali Akbar Entezami
"Syndiotactic Polymerization of Styrene with 2-(Me) IndTiCl$_3$/MAO/SiO$_2$ Catalyst". 8th International Seminar on Polymer Science and Technology(ISPST 2007), October, 2007, Tehran, Iran.

Poster Presentations

1- Mohammadi R, Nematollahzadeh A., Wei S, Halhalli M.R., Lindemann P., Tenboll A., Chandrasekaran D., Wang Z., Berghaus M., Schillinger E., and Sellergren B. (2012). *"MIPs for antibody capture"*
7th International conference on Molecularly Imprinted Polymers-Science and technology, MIP2012 Paris, 27th-30th August 2012, Paris, France

2- Halhalli M.R., Mohammadi R, Urraca J, Kadhirvel P., Dirkmann M, Abdel Qadar A., Fritz E., Sulc R., and Sellergren B. (2012)
"A versatile method to prepare RAFT anchored thin film imprinted polymer micro and nanobeads" .7th International conference on Molecularly Imprinted Polymers-Science and technology, MIP2012 Paris, 27th-30th August 2012, Paris, France

3- Mohammadi R., Rahmani S., Abbasian M. and Entezami A. A.(2006)
"Syndiospecific polymerization of styrene with 1-(Me) IndTiCl$_3$/MAO/SiO$_2$ catalyst system".13th Iranian Seminar of Organic Chemistry, Bu-Ali Sina university, August, 2006, Hamadan, Iran.

Academic Honors and Awards

- Awarded a PhD scholarship by the Ministry of Science, Research and Technology of the Islamic Republic of Iran (2010)
- Ranked 2^{ed} among the 42 M.Sc students of chemistry with a total G.P.A 17.58 out of 20.00 (2004 -2007 Tabriz university, Tabriz, Iran)
- Third place Khwarizmi International Award (KIA) (2007)

IT Credentials

- MS Office (Word, Power Point and Excel), ISIS draw, Chem Office, Sigma plot, Graph Pad, Nano Zetasizer, TA universal analysis, Endnote.
- Literature search (SciFinder, Delphion, Scopus)

Membership to Scientific Association

- Member of Iranian Polymer Science and Engineering Society
- Member of Iranian Nano Technology Society
- Member of Molecular Imprinting Polymer Society